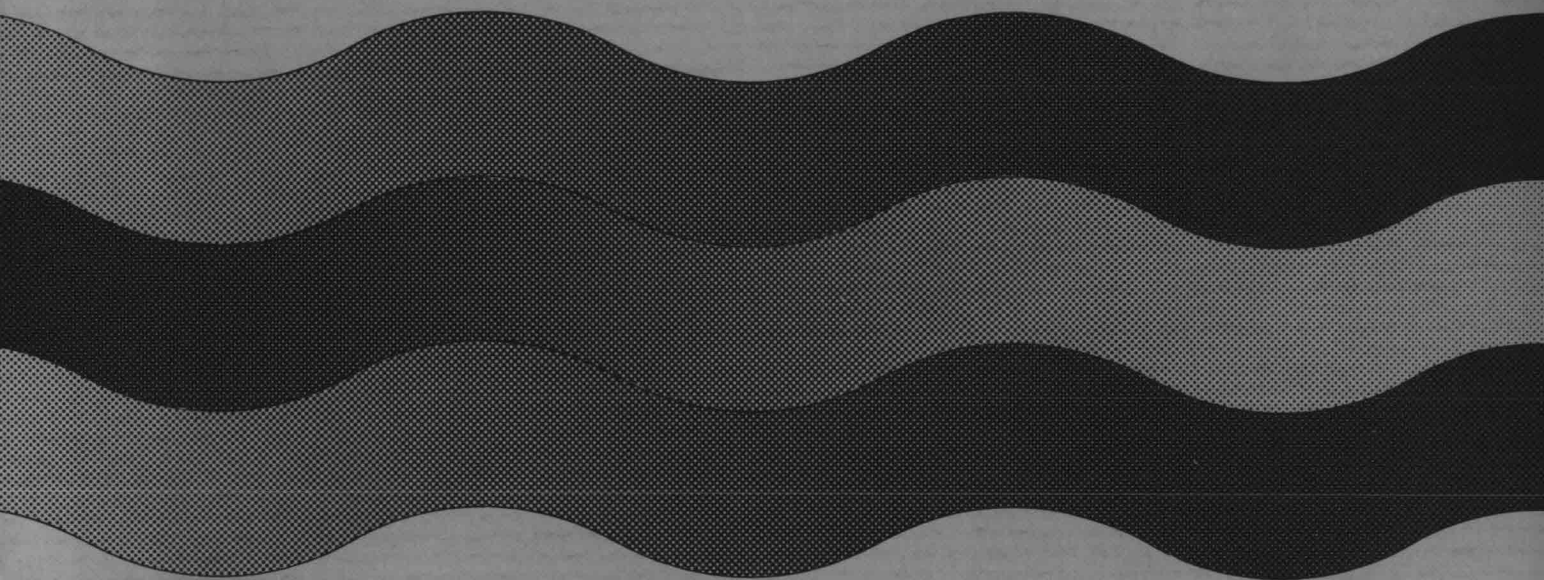


FOUNDATION ASPECTS OF COASTAL STRUCTURES



Proceedings volume *1*

International Symposium on Soil
Mechanics Research
and Foundation Design for the
Oosterschelde Storm Surge Barrier.

Delft, The Netherlands,
October 9 - 12, 1978.

FOUNDATION

ASPECTS

OF COASTAL

STRUCTURES

Proceedings volume *1*

International Symposium on Soil
Mechanics Research
and Foundation Design for the
Oosterschelde Storm Surge Barrier.

Delft, The Netherlands,
October 9 - 12, 1978.

CONTENTS

Review of the Project and History of the Design

- I. 1 Overall picture of the project
by H. Engel
- I. 2 Review of the various designs
by F. Spaargaren
- I. 3 Special geotechnical studies and their unexpected effects
by J. W. Boehmer

Stress-strain Behaviour of Oosterschelde Sands

- II. 1 Stress-strain behaviour from stress path tests
by W. A. Marr, K. Høeg
- II. 2 Stress-strain behaviour for finite element methods
by A. W. W. M. Biegstraaten, C. J. Kenter
- II. 3 Pore pressure generation
by F. P. Smits, K. H. Andersen, G. Gudehus

Predictions by Theoretical Methods

- III. 1 Probabilistic approach to determine loads and safety factors
by D. Kooman, Th. Mulder, J. K. Vrijling, L. de Quelerij
- III. 2 Computation by finite elements
by C. J. Kenter, P. A. Vermeer
- III. 3 Simple numerical methods to determine displacements and stability of piers (spring constant and Brinch Hansen)
by J. B. Sellmeijer
- III. 4 Plasticity analysis
by F. P. Smits

Predictions by Model Tests

- IV. 1 Caisson tests at Neeltje Jans, The Netherlands
by T. W. Lambe, J. W. Boehmer, W. F. Rosenbrand
- IV. 2 Model tests on piers, scale 1 : 10
by L. de Quelerij, J. J. Broeze
- IV. 3 Centrifuge tests
by P. W. Rowe

Site Investigation and Densification Studies

- V. 1a Site investigation of soils
by J. Vermeiden, P. Lubking
- V. 1b Engineering Geology: Construction of a stratigraphic model
by F. J. de Mulder, F. F. E. van Rummelen
- V. 2 Laboratory investigations regarding the artificial densification of sand and gravel materials in the Oosterschelde
by P. G. J. Davis
- V. 3 Statistical study of in-situ measurements of soil properties
by W. E. Jaworski
- V. 4 Densification in field practice - Methods and requirements
by A. A. Pladet

Soil-structure Interaction

- VI. 1 Groundwater flow and dynamic gradients
by F. B. J. Barends, R. Thabet
- VI. 2 Interaction forces between piers and sill structure
by J. D. Nieuwenhuis, J. M. van Geest, F. Molenkamp
- VI. 3 Full scale tests on elements representing the pier-sill interface
by E. P. Hudig, D. W. de Haan, C. J. van Rossen, F. Stam
- VI. 4 Sill design
by K. d'Angremond, M. R. van der Does de Bye

PREFACE

The Scientific Committee wishes to express her appreciation to the authors and co-authors of the papers presented at this International Symposium.

We know that they had only a very short time for the preparation of their contributions. Moreover, most of the authors were at the same time heavily involved in the actual design activities.

Because of the late reception the Scientific Committee was not able to study most of the papers in detail and therefore restricted her responsibility to the checking whether the content of the various contributions were in accordance with the rough directions given to the authors previously.

If necessary writers were asked to make in general minor changes for the sake of comprehension or to shorten their contribution. Nevertheless some papers exceed the desired length considerably.

The Scientific Committee did not refuse these papers. Due to the late arrival of these papers rewriting or shortening to the desired 16 pages was not always possible. Moreover, some papers present such an amount of interesting information that it was not possible to maintain the restriction.

The publications do not give a complete picture of all the work which was done for the foundation design of the storm surge barrier and related problems.

The Scientific Committee expects, however, that the participants at the Symposium will get an impression of the often very advanced methods and techniques that were applied for this purpose.

DELFT, September 13, 1978

W.J. Heijnen,

Chairman of the Scientific Committee.

SYMPOSIUM ON FOUNDATION ASPECTS OF COASTAL STRUCTURES

OVERALL PICTURE OF THE PROJECT

by:

Ir. H. Engel, Chief Engineer and Director of the Deltadienst Rijkswaterstaat
The Hague, The Netherlands

SYNOPSIS

The low lands, called the Netherlands, have alternately been a blessing and a curse for the people who lived on it. Most of it is low-lying sand, peat and clay along a North Sea that is and has been one of the busiest navigation areas of the world but can also produce floods when northwestern storms raise the waterlevel in the cone shaped southern part. The Dutch prefer to enjoy the prosperity that the shipping on the North Sea and the Rhine brings them behind dikes or barriers that are able to keep the stormsurges out. The stormsurge of February 1953 that killed nearly 2.000 people and disorganized an area in the southwest where 150.000 people were living gave the impulse to the Deltaplan, a project primarily aiming at the protection of the southwestern part of the Netherlands. The Deltaplan as it was conceived in 1956 consisted of the closure of 4 estuaries, 3 by dams and 1 by a dam and a number of sluiceways that could take care of high Rhine discharges. Several secondary dams were necessary for the execution of the plan. The last of the closures, the damming of the Oosterschelde estuary would be finished in 1978. Around 1970, when 3 of the 4 estuaries were closed, the closure of the biggest estuary, the Oosterschelde, got strong opposition, not only from the oyster- and mussel fisheries that were threatened by the plan but also from nature conservancy committees and biologists. They pleaded for keeping the Oosterschelde open and accept more risk as to safety against flooding and advocated heightening the 145 km stretch of dikes around the estuary. In 1976 the government decided on a compromise consisting of a stormsurge barrier, which normally allows the water to flow in and out of the basin but would be closed under storm conditions. As the barrier would need a total aperture of 14.000 m², had to be build in a sandy bottom and under open sea conditions it demanded for co-operation of all experts in the coastal engineering field.

In an early stage the Rijkswaterstaat (part of the Ministry of Transport, Water Control and Public Works) responsible for the design and the execution of the project has sought co-operation with a selected consortium of contractors to work out a design that was feasible, that could be realised in 1985 and for price limited by the government to 3000 million 1976 guilders. A great number of consultants are involved; the Delft Hydraulic Laboratory and the Delft Soil Mechanics Geotechnical Laboratory play a leading part among them.

Due to the great number of experts in many fields that are involved in the project, the main problem for management seems to be communications.

LOCATION

The Netherlands are situated at cross roads of navigation traffic, the southern part of the North Sea and the main inland shipping artery of Europe, the Rhine.

From a point of view of economy this location has big advantages, from a point of view of security against flooding, the location is not so well chosen.

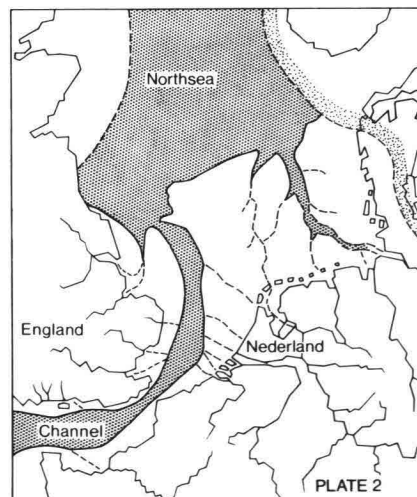
Since the prevailing winds in West Europe come from south-west to north-west directions and the North Sea is relatively shallow, it is obvious that during long lasting storms the sea will raise considerably in the cone shaped basin of the southern North Sea. A raised sea level combined with high waves can mean a disaster for the low lying lands around the North Sea.

Flood disasters form part of our history and occurred as often as three times in a century. In former ages the defense has always been to dam off small creeks and to heighten the dikes.

Only this century, big plans have been executed to shorten our coast line. This began by the closing of the Zuiderzee in 1932, launched by the severe flood of 1916 and the Deltaplan that followed the disastrous flood of February 1953.

The Deltaplan was based on ideas of Dutch engineers which were formed during and after the war of 1940-1945. The Deltaplan reduced the coast line of the southern part of the Netherlands with 700 kilometer. Only two estuaries would be left open: The Western Scheldt, the connection between the Antwerp sea port and the North Sea and the entrance to Rotterdam, The Rotterdam Waterway. These estuaries will be protected by higher dikes. The Deltaplan was approved in the Dutch Parliament in 1958. It offered not only a better protection against the sea, it had also advantages for the fresh water management and it would connect the isles in the south west with the main land.

The south western part of the Netherlands form a delta of the rivers Rhine, Meuse and Scheldt; by nature such an area is flat and low. Geologically speaking the Netherlands are formed very recently and its soils are composed of sediments of the rivers: sand, silt and clay. Often interspaced by peat layers formed in the recent interglacial epoch. Solid rock in the western parts of the Netherlands can only be found at depths of one kilometer and more. In some parts of the world such a type of soil is considered unsuitable for heavy structures. The Dutch geotechnical engineers owe their positions to the fact that the Dutch have always been building on this soils. It seems strange that we praise ourselves lucky that the sub soil at the location of the storm surge barrier consists mostly of fine sands.



The Northsea abt.17000 years ago.

THE DELTAPLAN AND ITS RECENT CHANGES

The period in which the 1953 disaster occurred, was favourable for the undertaking of great improvements. The reconstruction of the post war period came to an end, the increase of the population and the expanding industrialisation raised questions concerning our environment. Questions not only on how to protect the country against the stormsurges from the North Sea, but also questions on how to use the water of the Rhine and the not very accessible archipelago in the south west.

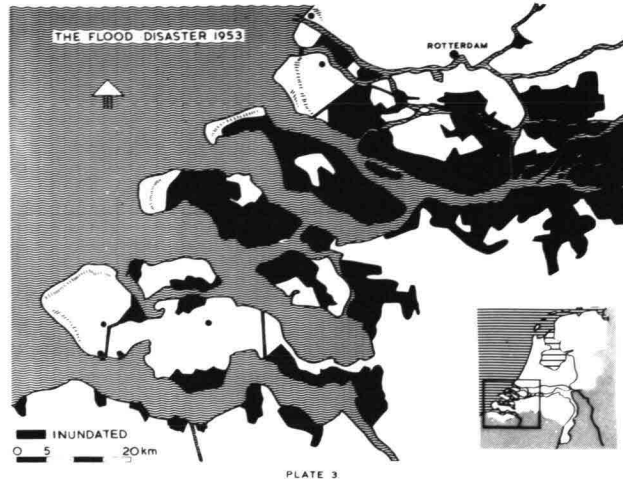


PLATE 3

The Deltaplan, in the first place conceived to enhance the security of the Dutch people, brought more than protection alone. In the fifties the main extra aims of the Deltaplan beside protection were seen in the area of the water management and the extra planning possibilities around the fast growing harbour of Rotterdam, while much attention was given to the problem of leaving the main shipping arteries through the Delta undisturbed. The total plan seemed daring enough and logically the execution started with the defence of the most vulnerable spots of the country around Rotterdam and with the closures on the smallest scale. So in 1958 the barrier in the Hollandse IJssel near Rotterdam was finished and at the same time work was started at the closure of the Veerse Meer that got its dams in 1961. The most important construction of the Deltaplan was the big discharge-sluiques complex in the Haringvliet; this was finished in the mid sixties and the closure came in 1971. In 1965 and 1970 the closure of the Grevelingen and the Volkerak were finished and in 1972 the closure of the Brouwershavensche Gat was a fact. The original time schedule was closely followed and the development of new methods for bottom protection, for dike construction and for closing operation seemed to indicate that the biggest estuary, the Oosterschelde could be closed in 1978 by an impervious dam. Behind that dam a brackish lake turning gradually into a fresh water lake would give extra possibilities for the agriculture in the surrounding areas. In the meantime the port of Rotterdam was enlarged in such a way that it became one of the world's most important harbours. In the growth philosophy of that time still other big extensions were designed. Towards the end of the sixties many people became aware that the extension of ports and industries not only brought wealth but also brought air pollution, water pollution and a general deterioration of the environment. As the Dutch were already prosperous, more prosperity could not be the only goal. The people became more interested in the environment and the preservation of the landscape and more or less natural areas. The Oosterschelde basin with its big tidal differences, its tidal flats and banks became more and more interesting not only for the oyster and mussel fisheries but also for the biologist who found in it an area where very interesting ecological processes take place. It proved to be an estuary with a big bio-mass production and probably one of the cradles of

the Marine life in the North Sea.

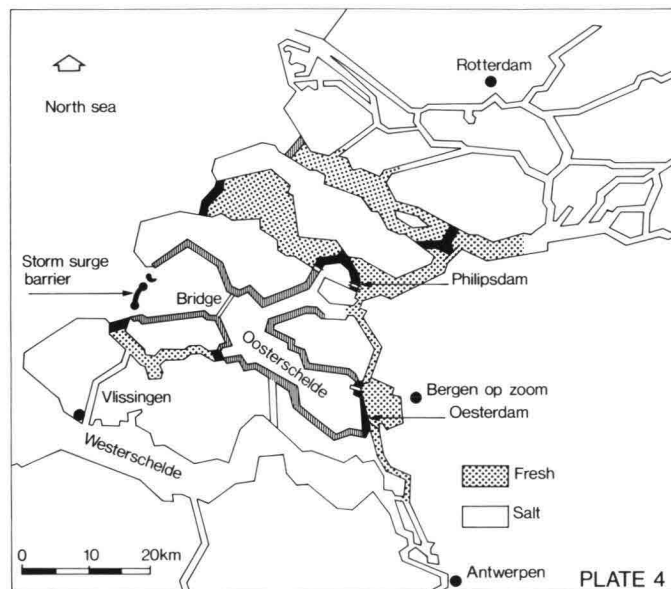
Reevaluation of the Oosterschelde closure was necessary and it certainly did not take place in a serene atmosphere. On the one side the people who asked for the promised protection at the earliest possible date, on the other side action groups which considered the engineers as barbarians, only interested in the building of dams and the killing of nature. In november 1974 the government decided that the work on the closure dam would be stopped and in a one and a half year period the feasibility, the price and the construction time of a barrier in the Oosterschelde should be assessed. If a barrier could be built before 1985 and the extra costs would not exceed two billion guilders than a barrier would be built but, if the engineers could not meet one of these requirements, the original plan for damming the Oosterschelde would be executed.

In the period following this decision a great number of plans for the construction of the barrier was designed and analysed on the aspects of feasibility, cost, execution time. At the same time plans for the necessary secondary dams were worked out. And finally a policy analysis was executed which compared three possible solutions for the protection of the Oosterschelde

area: closing of the estuary with a dam, closing of the estuary with a storm surge barrier and the heightening of the 140 kilometers dike around the estuary.

Rijkswaterstaat, being the agency responsible for the execution of the Deltaplan was in charge of these studies. The fact that the storm-surge barrier with its opening of ten to twenty thousand square meters had to be built on a sandy bottom in open sea conditions made it a very complex project that asked for the most in advanced tech-

niques of coastal engineering. For this reason Rijkswaterstaat proposed a cooperation with a consortium of Dutch contractors with great experience in the execution of works at sea or in the coastal areas. Besides a great number of consultants the Delft hydraulic laboratory and the Delft geotechnical laboratory were involved and played a very important role. The conditions under which the feasibility study had to be executed were not very favourable. The time to do such an important study was extremely short, pressure groups doubted the integrity of the engineers and the engineers between themselves had to come out with a plan they all could support.



The policy analysis tried to give a qualitative and if possible a quantitative assesment of the impact of the three alternatives in the fields of security, ecology, fishery, cost and time schedules, socio-economic effects like: manpower required and houses disowned, shipping, water management and recreation. Especially enlightening for civil engineers was the ecological study. A closed and open estuary kept about the same amount of animal life but big changes occurred in the population. The unique character of the tidal system could only be conserved without a dam and security could only be gained within a reasonable periode of time by building a barrier or a dam. In 1976 the government decided that a barrier should be built; the parliament approved and the design was completed.

THE COOPERATION BETWEEN RIJKSWATERSTAAT, CONTRACTOR AND MAIN CONSULTANTS

Rijkswaterstaat is the government organisation responsible for the main dikes and other sea defense works, for the main navigation channels and canals, the motor ways and the water management. As a part of the Ministry of transport, water control and public works Rijkswaterstaat consists of 26 departments totalling 11.000 persons. In the building of the storm surge barrier 3 departments are greatly involved:

- Deltadienst, the Delta Department, coordinator, general designer for all projects in the Delta area
- Directie Bruggen, Department of Bridges, acting as designer for all steel structures
- Directie Sluizen en Stuwen, Department of Locks and Weirs, acting as designer for all concrete structures.

Usually a project is designed by Rijkswaterstaat and consequently tendered.

Supervision during the construction fase remains Rijkswaterstaats responsibility. Because of the complexity, size and duration of the main closures in the Deltaplan, a different approach is followed. In an early stage several groups of contractors are invited to take part in a tendering procedure and compared by general criteria concerning their ability, the cost of their equipment, the overhead etc. To one of the groups an overall project contract is given wich lays out the criteria for the subcontracts which are to be defined in a later stage and the way in which the price of such subcontract will be settled.

This method has been beneficial both for the contractors and for the government.

As the project takes usually several years of construction new techniques are developed in cooperation with the contractor. The contract form makes it possible that both contractor and government profit by this new developments. Progress in the field of hydraulic engineering and constructions techniques are a must for the execution of the Deltaplan. With the hydraulic knowledge of the fifties the closure of the Oosterschelde would have been too big an adventure. The development of the hydraulic modelling techniques, the mathematic tidal models and the construction techniques for the bottom protection, for closure operation and dam construction were necessary to render the projects feasible and to keep them within the financial limits.

Of course the described method of dividing the project in subcontracts and coming to terms with a contractor chosen beforehand asks for a good knowledge of construction techniques on the side of the government and makes a careful and informed price calculating group essential.

For the Oosterschelde storm surge barrier no tendering was done as the main Dutch contractors in the field were already involved in the

feasibility study. However in the same way as the earlier closures were executed a general contract has been agreed to and the total project is subdivided in parts which will be agreed to as soon as the design permits.

The progress in the hydraulic field and in the geotechnical field were greatly enhanced by the work of the Delft Hydraulics Laboratory and the Delft Soil Mechanics Laboratory. These institutes were created about fifty years ago when the Zuiderzee works asked for advanced knowledge in these fields. Both contractors and laboratories have profited from the knowledge gained during the Zuiderzee works and the Delta works.

Around six hundred highly qualified scientists and engineers worked together on the design and the related studies of the storm surge barrier. The design is subdivided in a number of substudies, executed by project groups of scientists, designers and builders. The integration of the result of the project groups is a difficult work. From time to time all partial results had to be put together in a total design. New elements came up which resulted in changes in the design of the constituents.

Changes which required the reprogramming of the work in a great number of project groups. As one can understand the communication between all

concerned asks for a lot of attention. A communication system with a strict formal basis could hamper severely the flexibility to react on new ideas and solutions. Too little and haphazard communication leads to big time losses in the groups while they are working without sufficient knowledge of the state of the design.

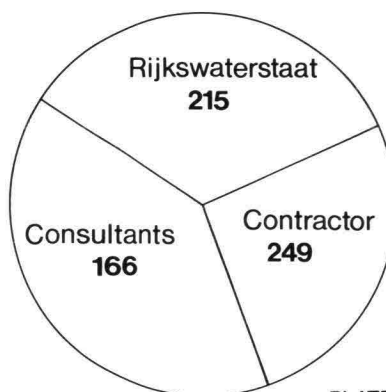


PLATE 5

Manpower involved in the barrier design.

SYMPOSIUM ON FOUNDATION ASPECTS OF COASTAL STRUCTURES

REVIEW OF THE VARIOUS DESIGNS.

by:

. Frank Spaargaren, Rijkswaterstaat
Engineering Division of the Delta department
Burghsluis The Netherlands

SYNOPSIS

The designers of the Oosterschelde storm surge barrier had to deal with a number of widely differing aims and criteria. On the one hand hard political limits were imposed regarding the allowable construction time and the costs. On the other hand natural criteria specific to the site of construction were present.

Special hydraulic, morphological and soil mechanical conditions are met by construction works in the mouth of the tidal Oosterschelde estuary which opens into the North Sea. With this data as starting point a design philosophy has been developed and will be described.

The barrier should allow the tides to penetrate the estuary under normal conditions and at the same time it should prevent the penetration of extremely high waters during storm conditions. To fulfil the conflicting requirements several solutions were studied for their technical and economic feasibility.

In these studies special attention was paid to the foundation technique, the method of construction, the design of filters and scour protection.

The paper shows the development of the design, from caisson-type structures via piers on a cell foundation to a monolithic pier design.

Ultimately in 1985 a heavy civil engineering construction, known as the "storm surge barrier", has to be completed in the month of the Oosterschelde estuary. The barrier consists essentially of a number of concrete elements between which the openings can be closed by means of sliding gates.

During normal weather conditions the gates are held open to allow tidal flow in and out of the estuary. In this way the aquatic environment of the Oosterschelde can be preserved. During storms the barrier can be closed, thus effectuating the shortening of the coast desired in the Delta Act, and protecting the terrestrial environment against storm flooding.

The present design of the storm surge barrier is a result of extensive studies carried out both in The Netherlands and abroad, by the Dutch Public Works Authority (Rijkswaterstaat), laboratories, engineering contractors, institutes and advising consultants. A mobilisation of scientific knowledge was, and still is, necessary because the study of the design and construction method is a problem of integration of the first order- an integration problem because the barrier must be constructed in a dynamic situation of physical factors; air, water and soil, of wind and storm, of waves and tides, and of a shifting sandy sea bed. Moreover, the barrier must be adjusted to the ecological dynamics of the Oosterschelde estuary.

The study of this dynamic environment, together with the conditions stipulated by the government with respect to the technical feasibility, costs and construction duration, have led to a large number of boundary conditions and design criteria.

The first boundary condition is defined by the present topography at the mouth of the estuary, (see fig. 1) the desired environmental circumstances and the execution of the works. The barrier must be built on the site originally approved for the dam in the Oosterschelde, thus in the three 25 to 35 m. deep channels, the Roompot, the Schaar van Roggenplaat, and the Hammen, which together give a total breadth of approximately 4 km (see fig. 2).

It is not possible to apply a dry method of construction since the necessary temporary works would dam the Oosterschelde and damage the natural environment. In addition it is desirable to limit the on-site construction activities in the open sea as far as possible. And so the study was directed on the prefabrication possibilities of the structure.

Another boundary condition is the one concerning the ultimate total area of the flow openings in the barrier. And this condition is defined on the one hand by the fact that the barrier may not be too expensive and on the other hand by the ecological requirement that the tidal flow in the Oosterschelde must be preserved as much as possible. In the study of the flow openings

the assumption was made that in any case 65% of the present tidal amplitude, corresponding with a mean amplitude of 2.30 m. at Yerseke, was to be maintained. A rough check has been made of the design consequences should 90% of the mean amplitude, corresponding to 3.1 m. and for approx 100% corresponding to 3.50 m. mean tidal amplitude at Yerseke, be maintained. The reduction in the area of the Oosterschelde estuary due to the compartment dams was taken into consideration during these studies (see fig. 3 and fig. 4).

The barrier must further be able to withstand any storm surge with a waterlevel that occurs with a mean frequency of at least 2.5×10^{-4} times per year.

Other boundary conditions are the following:

- the flow division over the barrier must correspond by approximation to the present flow division over the channels.
- it must be possible to close the barrier at the low water turn of the tide preceding a storm, and also by tidal currents in both directions.
- the stability of the barrier must remain ensured should one or more of the gates refuse to work during the closing operation.

From these boundary conditions for the design and construction, and also the effect of the storm surge barrier on the environment, other aspects and requirements are derived concerning both the form of the barrier as a whole and its component parts. During the studies carried out between 1974 and 1976 tens of widely differing preliminary designs were tested on their merits. After early selection the remaining designs evolved in three serious alternatives. These designs differed both in the foundation method and in the choice of the main structure.

The three alternatives are;

1. Caissons founded on a sill
2. Columns on foundation-caissons
3. Caissons on foundation-caissons

Comparative cost estimates and construction schedule have been compiled for each of the alternatives. In each case the reduction in the flow opening from 70,000 m² in the channels to 14,000 m² in the barrier is achieved with a sill construction in or under the barrier and further with large concrete box-beams in the barrier, thus reducing the open profile in the vertical sense (see fig. 5). The form of the open profile is furthermore such that optimum hydraulic conditions are obtained in the barrier.

Further the configuration of the three alternatives is defined for the following main elements (see fig. 6):

- the foundation: the base which delivers the reaction to the own weight of the barrier and the forces working upon it.

- the scour protection: measures against erosion of the sand under and at both sides of the barrier.
- the construction: the concrete frame in which the sluice gates are able to move and through which the forces acting on the gates are transmitted to the foundation.
- the sluice gates: the means by which the barrier can be opened and shut.

In the alternative "caissons founded on a sill" (see fig. 7) the sill is a filter construction, built up in layers of stone which, during execution, are compacted and levelled. The caissons, placed on this sill, are concrete structures consisting of a lower box-section, two end-walls, two intermediary walls and an upper box-section. The traffic road is visualised on top of the upper box-section. The flow opening is further reduced by means of box-beams (stop logs) which rest on the lower box-section. The scour protection at both sides of the barrier consists of scour protection matting and shoulders of concrete blocks.

In the alternative "columns on foundation-caissons" (see fig. 8) the sill consists again of a compacted and levelled filter construction made of stone layers. The foundation caissons are large, open (at both ends), reinforced concrete elements which are sunk and then buried in the sea bottom. The columns are reinforced concrete walls which are placed on top of the foundation caissons. Their function is to bear the water pressure and wave loads and to transmit them through the foundation caissons to the lower bearing soil layers. Again, the same erosion protection and box-beams (for the reduction of the flow openings) are applied in this alternative.

In the alternative "caissons on foundation-caissons" (see fig. 9) a combination of the above described elements is used.

The concrete elements such as foundation caissons, caissons, columns, box-beams etc. are all prefabricated, either in construction docks or on construction sites, and from there are transported and placed with specially designed floating equipment. The sluice gates are prefabricated steel structures operated by a lifting mechanism.

By these studies a large number of alternative configurations and elements for the barrier have been considered and investigated with respect to the most favourable form of the flow opening - in other words, with respect to the flow coefficient of the opening. Another aspect of the studies concerns the compaction of the loose soils under the barrier in order to reduce the risk of internal instability under the influence of the cyclic wave loading, and also the compaction of the sea bed along the edges of the scour protection in order to reduce the risk of settlement gradients, as a result of scour holes, to an acceptable

minimum (see fig. 10).

And so these three alternatives were comparatively judged, whereby ultimately the preference was given to the design alternative "columns on foundation caissons" because:

- it was thought, even though there is very little experience with the construction of such structures, that a solution could be found to the design and construction problems connected to this alternative. The uncertainties in the construction of the alternative "caissons founded on a sill" were considered too large in connection with the problem of sand deposits during construction.
- the barrier could be operational in 1985.
- the estimated costs were within the imposed limits.

Moreover, the application of a single set of sluice gates was worthy of serious consideration, since the design was such that, should one of the gates refuse, the stability of the barrier would not be endangered, and also the waterlevel in the estuary would still remain within acceptable limits.

Meanwhile, the column-foundation caissons idea has been subjected to continuous reappraisal and has evolved in a storm surge barrier comprising monolithic piers, a barrier with a total length of about 3.2 km. and with 70 openings (see fig. 11). With this design the on-site construction time for one pier has been reduced from 13 weeks to 3 days. Expected high construction phase loading by the foundation caisson solution was also reason for this reconsideration.

In the three channels, and at a centreline distance of 45 m., piers will be placed with a height of 35 to 45 m. and footplates measuring 25 x 50 m. Between the piers the sill will be heightened and box-beams will be placed in order to achieve the desired effective flow opening of 14,000 m². A single set of steel sluice gates will be installed between the piers. The electro-mechanical installation serving the gates will be housed in the reinforced concrete box-section bridge elements to be placed above the piers. Along the centre-line of the barrier the sea bed will be dredged deeper and will be consolidated at the pier locations.

The prefabrication of the piers will take place in a drained construction dock measuring 800 x 1200 m. and which is subdivided into 4 compartments. As soon as the piers in a compartment have been completed, it will be flooded and the ring dyke will be opened. By means of a special transport-pontoon the piers will be brought to their locations in the channels, and there they will be lowered onto the prepared sill of stone.

At this moment the construction dock for the piers is dry, and in March next year the construction of the piers is scheduled

to commence. In order to transport labour and materials to the construction dock, which is situated on a work island in the middle of the Oosterschelde, is, at this moment, a temporary bridge being built between Schouwen-Duiveland and the work island. It will be ready early in December of this year. Meanwhile the existing and - in the revised design - redundant scour protection matting is being removed and the new protection is being laid. Further, a work harbour is being built.

The design activities which now take place concern, amongst others, the transport pontoon (see fig. 12) for the transport and placing of the piers, and the compaction pontoon for the soil improvement works in the sea bed.

It is of importance for the successful completion of the storm surge barrier that all the activities which have to be carried out between now and 1985 take place in careful accordance with the time and cost schedules.

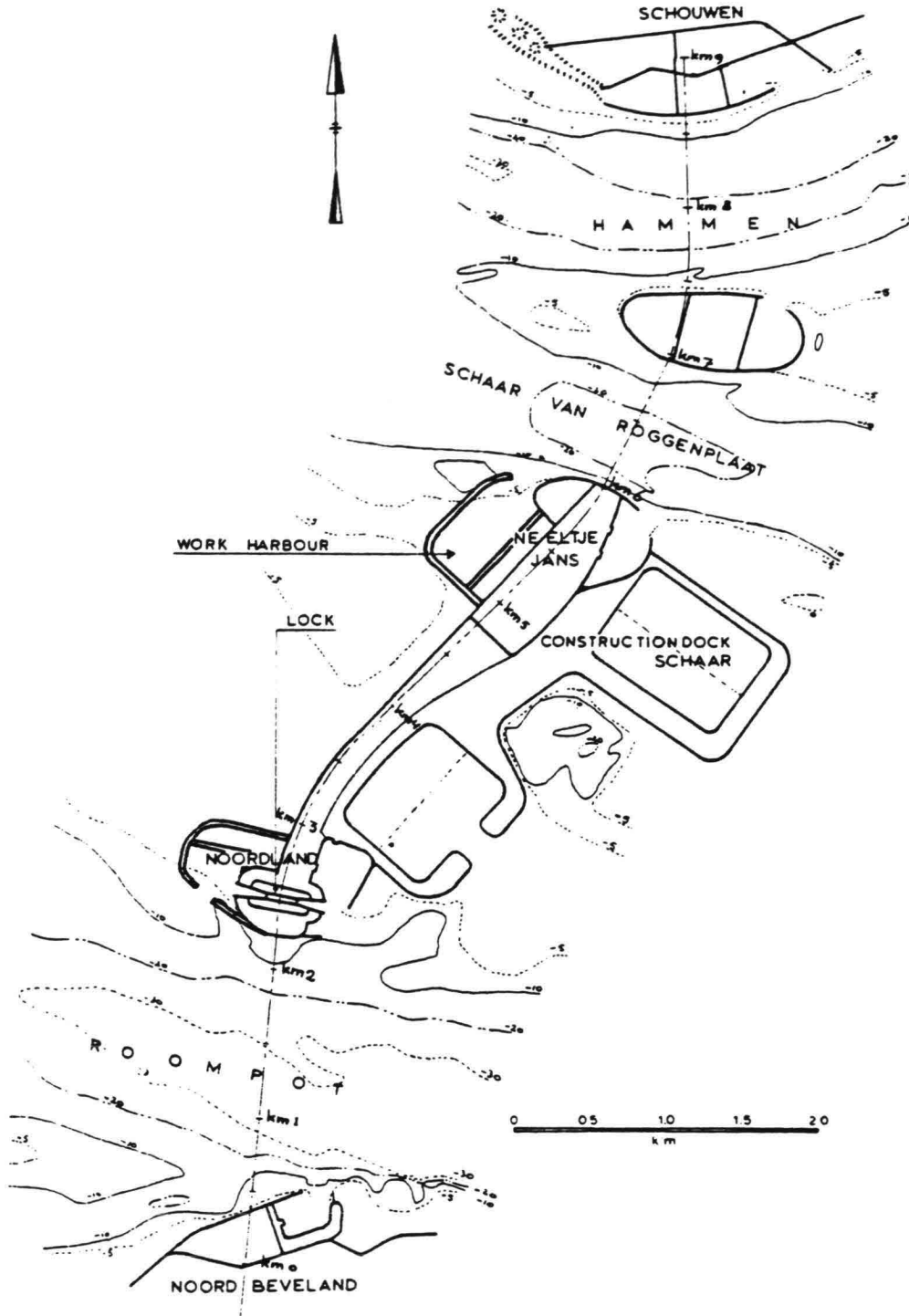


Fig.1 Present situation:
The mouth of the Oosterschelde with workislands



Fig.2 Long-section at the site of the Oosterschelde dam

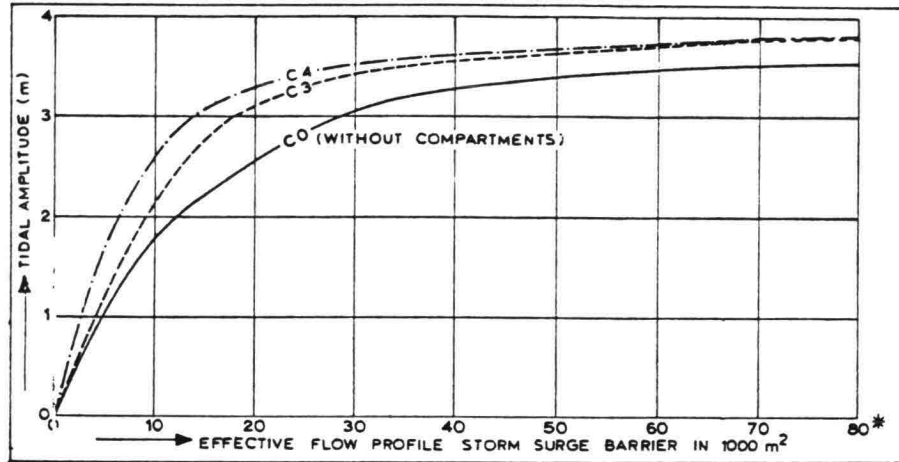


Fig. 3 Relation between flow profile and tidal amplitude for a mean tide. (For C0 and C3: at Yerseke, for C4: at Wemeldinge). *Flow profile corresponding to the present situation.

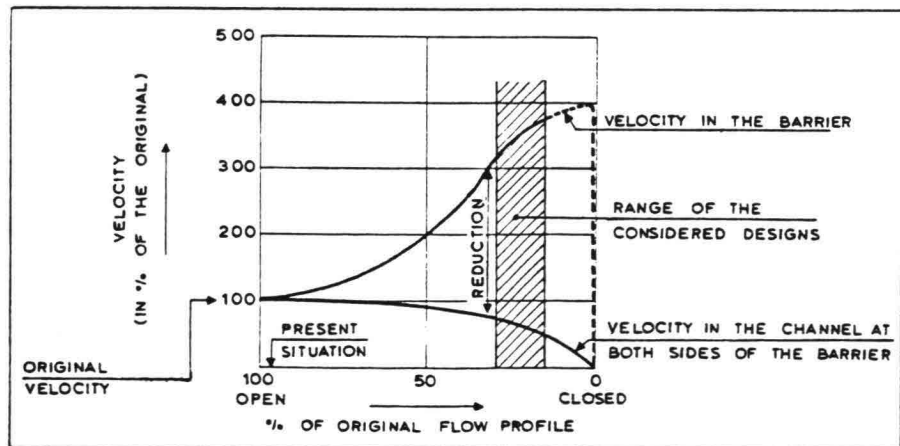


Fig.4 Relation between the current velocity in and behind the storm surge barrier and the flow profile restriction.

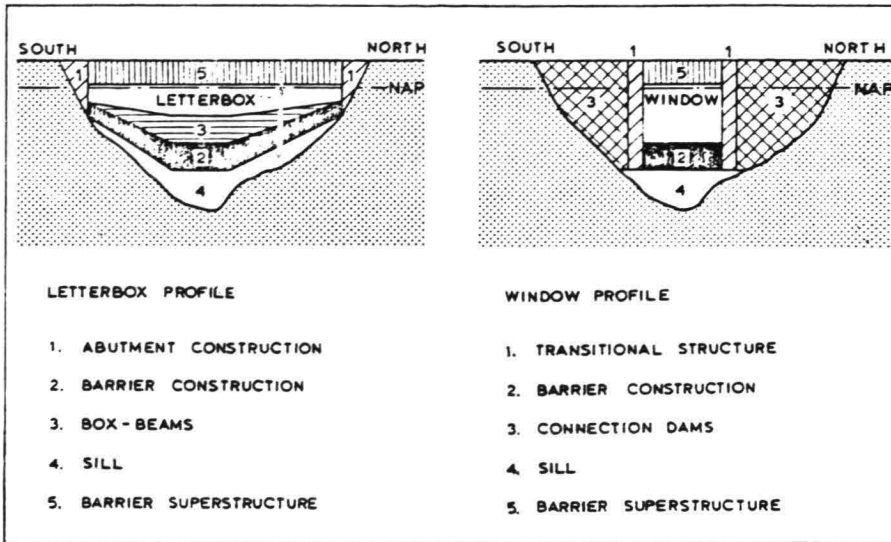


Fig. 5 Alternatives for restricting the flow profile.

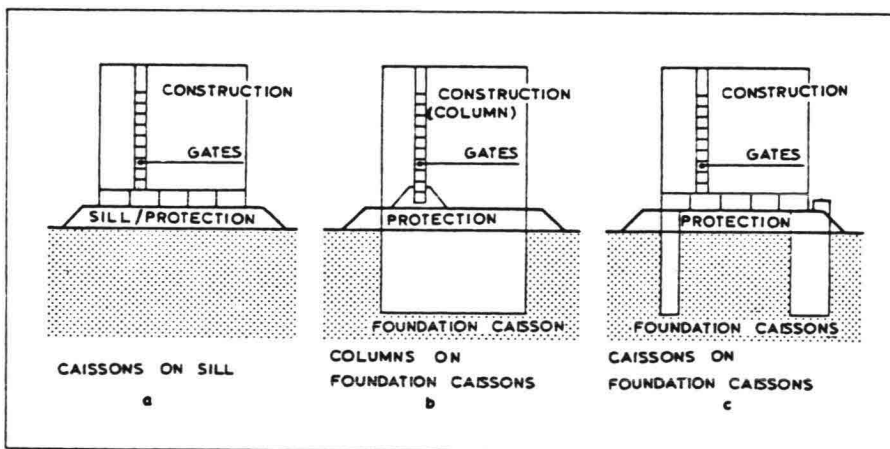


Fig. 6 Foundation methods

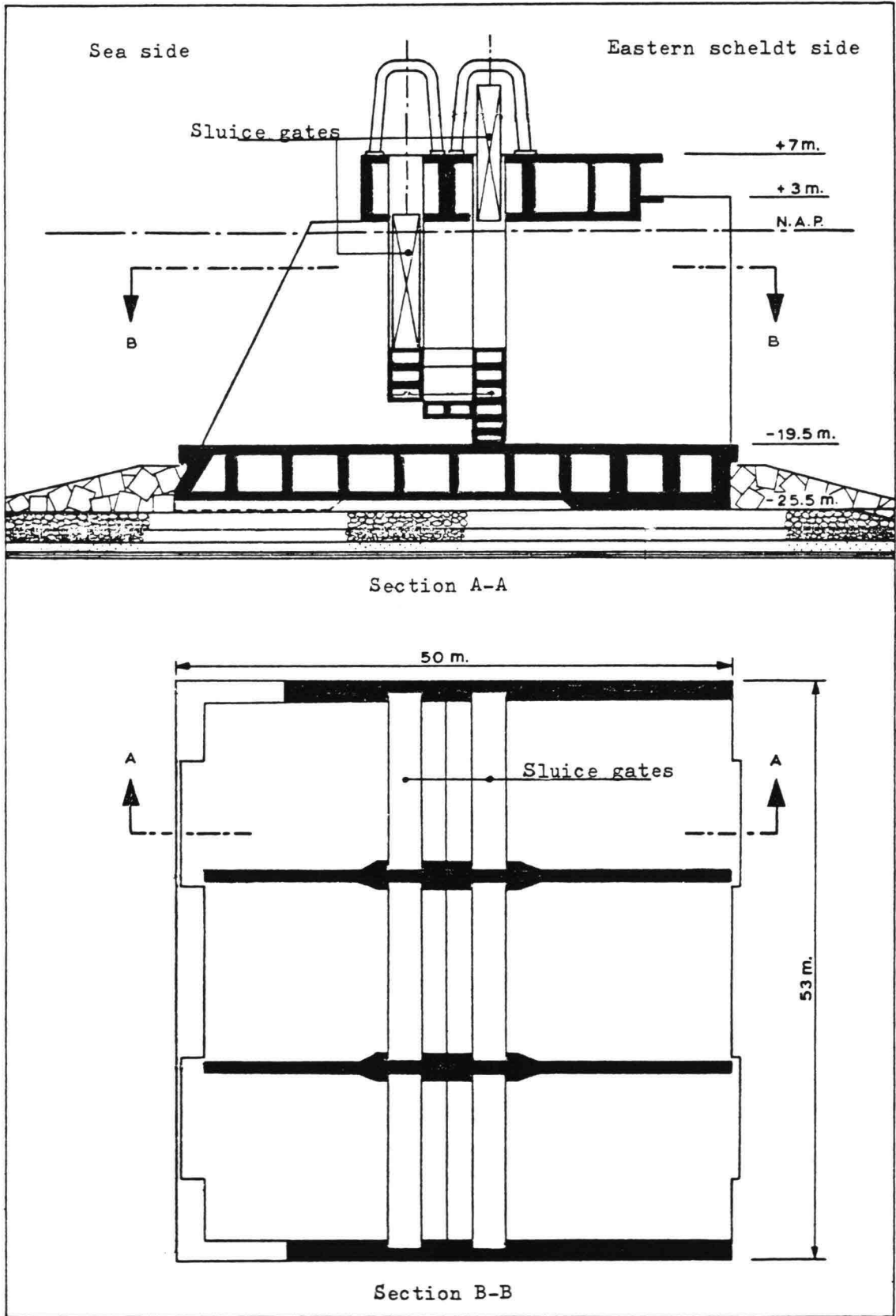


Fig. 7 Caissons on sill.

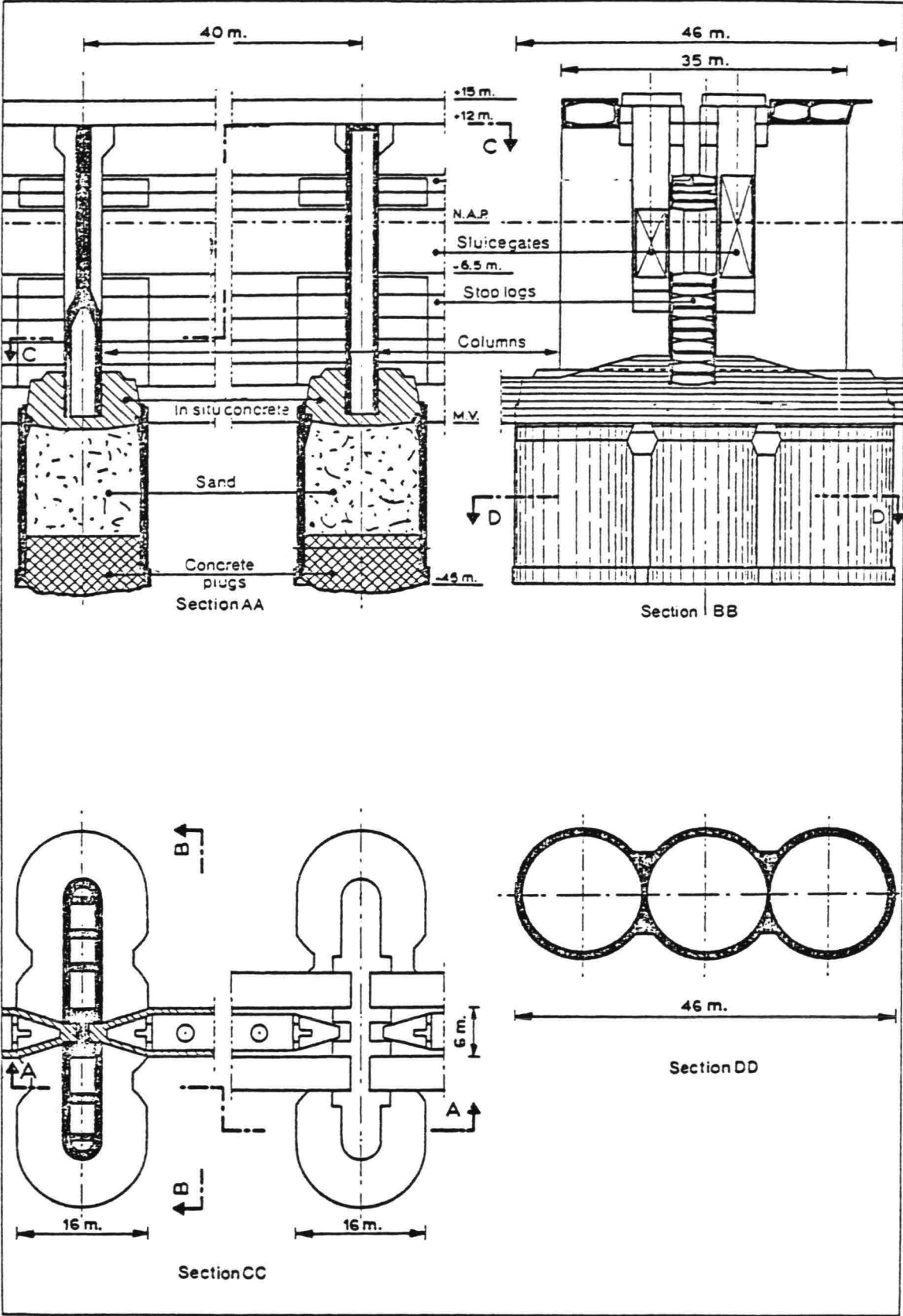


Fig. 8 Columns on foundation caissons

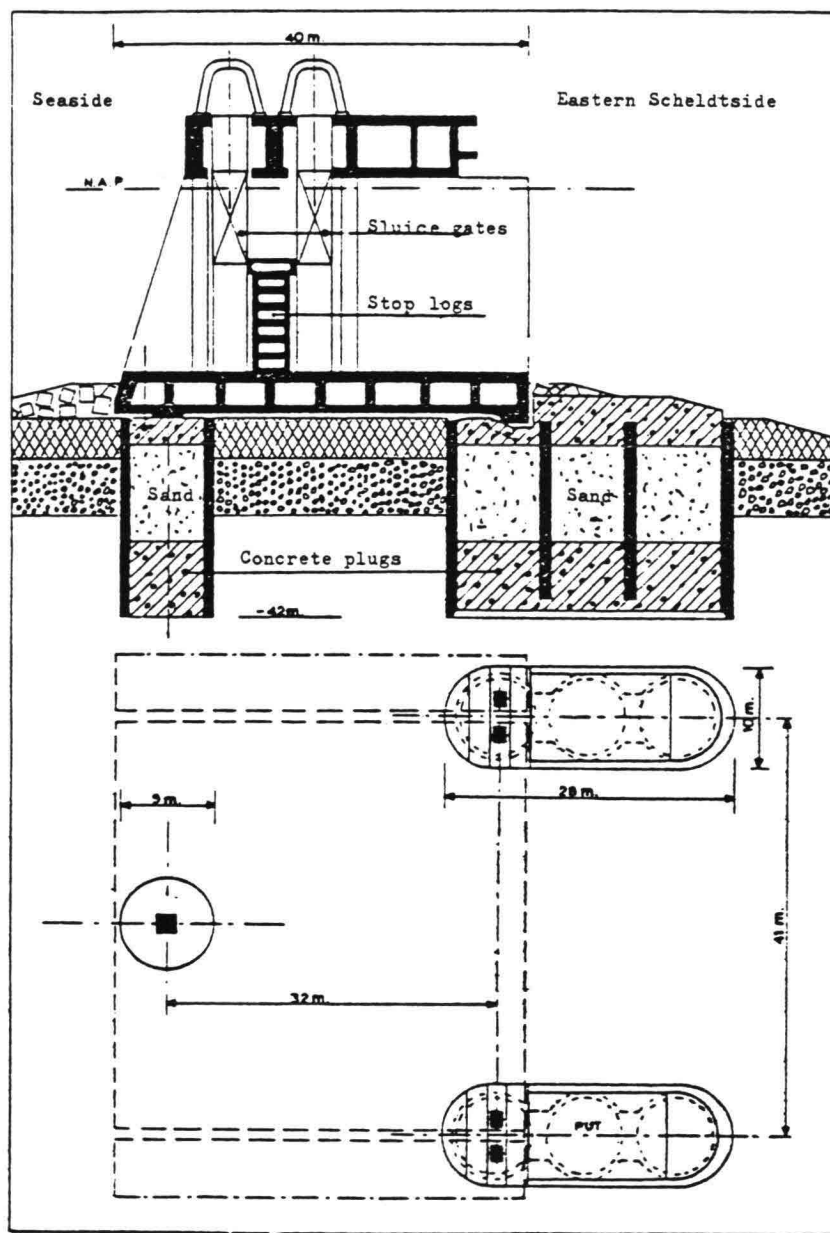


Fig. 9 Caissons on foundation caissons.

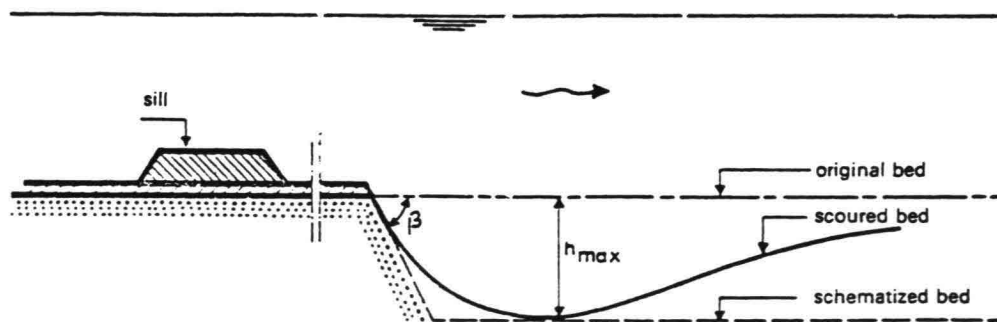


Fig. 10 Scour holes.

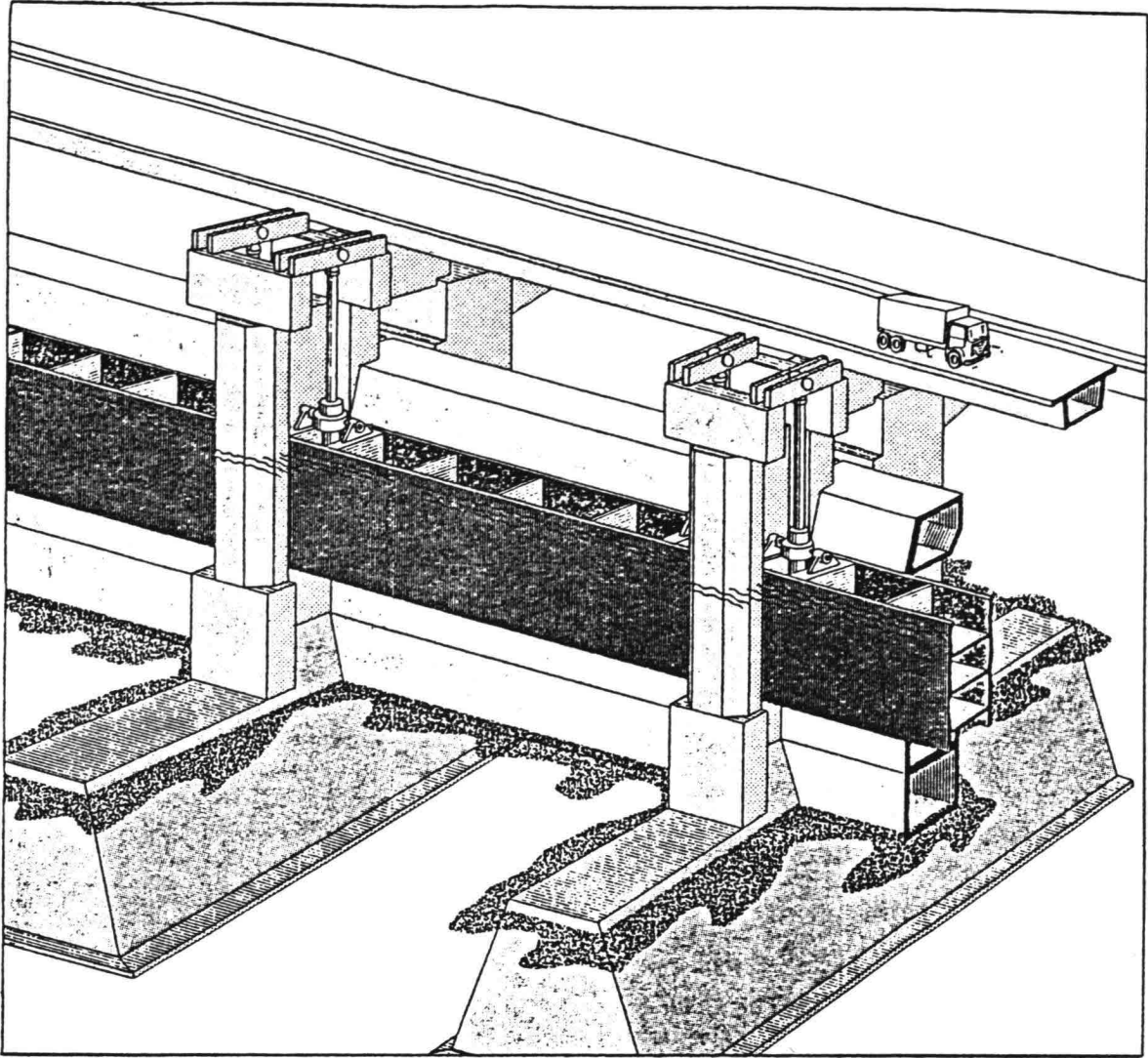


Fig. 11 Piers with sill, box beams and sluice gates.

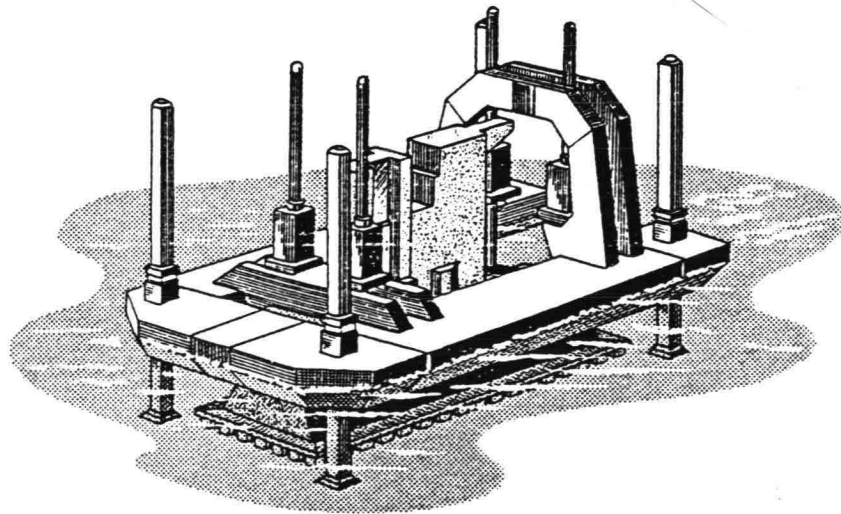


Fig. 12 Preliminary design of the new pier transport equipment.

FOUNDATION ASPECTS OF COASTAL STRUCTURES

GEOTECHNICAL OOSTERSCHELDE STUDIES
and
SOME UNEXPECTED ASPECTS

by:

Jan Willem Boehmer,
Senior engineer in science and engineering analysis at
Rijkswaterstaat Deltadienst, a department in the Dutch Public Work Service

PART (I)

on the interaction between the designer and the geotechnical engineer.

1. SUMMARY

The scope of this paper is to start a presentation of the basis for past and future design-oriented studies and to give an overview of them at the same time. The present paper is focussed on the interaction between the geotechnical engineer and the "designer" of which examples are given. Some key aspects in this interaction process like field tests, modeltest studies, parametric studies with analytical models, site work and geological interpretation are highlighted. Some initial conclusions are added, just as far as they could be of interest to the designer.

2. INTRODUCTION

2.1. Key questions

One of the key problems in the interaction between the "designer" and the geotechnical engineer is, "how to ask the really important questions". Experience in Rijkswaterstaat is, that these questions should be design-oriented. We learned that, by this, the researcher eventually reduces the unsafe feelings of the designer. Also the researcher then seems to do a better job than if he treats the subject from just an academic point of view. The first step in an efficient design process seems to be that the designer and the researchers should gradually refine the "design criteria" which determine this work. Appropriate studies of mechanisms, field evidence and possible malfunctioning are needed to help develop these criteria. Extensive evaluation of field evidence and of the observed mechanism in the past is an important first step in this process, as will be shown.

2.1. Request for criteria

Rijkswaterstaat has a continuous interest in a systematic documentation on how we arrived at the performance criteria which now support the design. Priority were to be given to the criteria for barrier. Table I shows in concept a checklist for the design criteria of the barrier. Tables II and III show how in concept the same sort of criteria can be summarized for the dikes and flow slides. I added these "criteria checklists" to invite discussion and improve on them, in later discussion paper. Also shown are "criteria charts" and the "criteria profiles", which can be used to set criteria for construction control as during densification and for barrier control.

This sort of checklists, charts and profiles need further refinement before actual application on design. Time is short however to do so. Such an integrated study of criteria is in agreement with the recommendations from a study by the Rand corporation. They recommend to apply "safety programs" to the overall "system".

Table IV gives the recommendations from Rand studies, for a

POTENTIAL WEAKNESSES	MULTI-MEDIA - FIELD EVIDENCE	CRITERIA
<ul style="list-style-type: none"> 1. Poor design 2. Poor construction 3. Poor materials 4. Poor workmanship 5. Poor maintenance 6. Poor operation 7. Poor inspection 		<ul style="list-style-type: none"> 1. Adequate design 2. Adequate construction 3. Adequate materials 4. Adequate workmanship 5. Adequate maintenance 6. Adequate operation 7. Adequate inspection

Table I CRITERIA-CHECKLIST FOR STORMSURGE BARRIER

POTENTIAL WEAKNESSES	MULTI-MEDIA - FIELD EVIDENCE	CRITERIA
<ul style="list-style-type: none"> 1. Retained flow level 2. Over toppling waves 3. Drop in water level 4. Wave attack 5. Flow slide attack 		<ul style="list-style-type: none"> 1. Adequate design 2. Adequate construction 3. Adequate materials 4. Adequate workmanship 5. Adequate maintenance 6. Adequate operation 7. Adequate inspection

Table III CRITERIA CHECKLIST FOR DIKES

POTENTIAL WEAKNESSES	MULTI-MEDIA - FIELD EVIDENCE	CRITERIA
<ul style="list-style-type: none"> 1. Poor design 2. Poor construction 3. Poor materials 4. Poor workmanship 5. Poor maintenance 6. Poor operation 7. Poor inspection 		<ul style="list-style-type: none"> 1. Adequate design 2. Adequate construction 3. Adequate materials 4. Adequate workmanship 5. Adequate maintenance 6. Adequate operation 7. Adequate inspection

Table II CRITERIA CHECKLIST FOR BORDER-PROTECTION

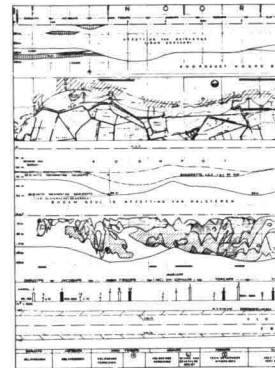


Fig. 2 CRITERIA PROFILE FOR BORDER PROTECTION NEAR BARRIER

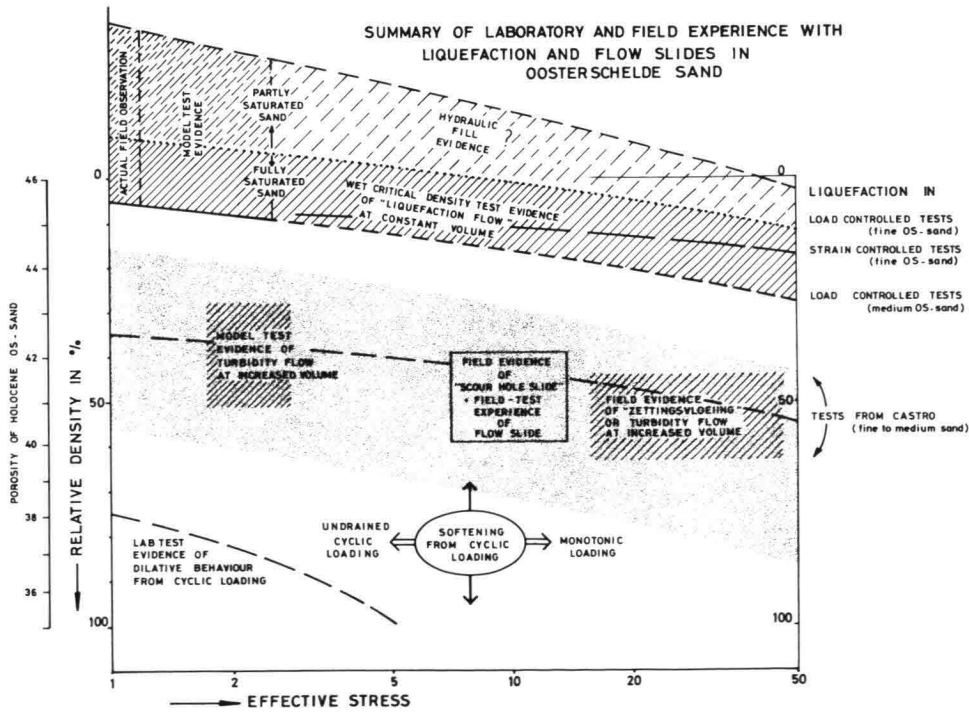


Fig. 1 CRITERIA CHART FOR LIQUEFACTION SUSCEPTIBILITY IN OOSTERSCHELDE SANDS

comparison of geotechnical problems in three alternative plans for the Oosterschelde closure.

Table V applies some judgement to the safety of various aspects in the three closure systems. However criteria on which these judgements are based should be improved. Since the improvement of these criteria depend on evaluation of past experience and a good interaction between the designer and the geotechnical engineer, we will first proceed on these two aspects.

3. INTERACTION BETWEEN RESEARCH AND DESIGN IN THE PAST



Fig. 3 HOLLAND WAS FLOODED



Fig. 4 HOLLAND WAS PROTECTED STONE BY STONE

After twenty five years hydraulic studies became so integrated into design, construction and watermanagement, that we cannot imagine to do without them any more. Some examples are:

- the hydraulic model studies for the initial design of the Deltaplan (see paper by Engel)
- the hydraulic studies to obtain loads on the barrier i.e. the probabilistic loads in particular (see paper by Kooman)
- the hydraulic studies for the future operation and closing strategies of the barrier.

Hydraulic studies served construction control of Oosterschelde borders since 1868. From that time on, the regular soundings of the borders provided enough data on stability against flow slides. As a result flow slide statistics could be started and used successfully in border protection.

POLAND	DESIGNS	GEOTECHNICAL STUDIES
CLOSED DAM	SURFACE CAISSON ON SILL	TEMPORARY INFLUENCE OF CYCLIC LOADING FROM SUMMER STORMS + HEADLOSSE TEMPORARY RISK OF FLOW SLIDES OVER 4 KM
	BLOCKFILL DAMS ON SILL	
SLICE BARRIER	SURFACE CAISSONS ON SILL	LONG TERM INFLUENCE OF CYCLIC LOADING + HEADLOSS FROM WINTER STORMS LONG TERM RISKS OF FLOW SLIDES OVER 4 KM
	EMBEDDED CAISSONS - a. deep in subsoil - b. undeep in subsoil - c. undeep in sill	
OPEN DIKES	HYDROFILL DIKES WITH RESISTIVE CORE ON OUTSIDE	LONGTERM RISKS OF FLOW SLIDES OVER 150 KM
	HYDROFILL DIKES WITH RESISTIVE CORE ON INSIDE	

NOTE: ADDITIONAL COMPARTMENT WORKS FOR WATER MANAGEMENT AND NAVIGATION

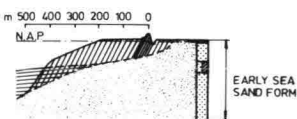
Table IV SUMMARY OF GEOTECHNICAL PROBLEMS FOR THREE CLOSURE STRATEGIES

alternative	CLOSED DAM	SLICE BARRIER	OPEN DIKES
CONSTRUCTION TIME	1980	1995	1994
BARRIER LENGTH	9 KM	9 KM	145 KM
BARRIER SAFETY	+	+	+
DIKE SAFETY	0	0	0
SCOURTHREAT EFFECT			
REDESIGNED DIKES	+	-	+
BARRIER FOUNDATION	++	+	+
GATES FAIL TO CLOSE			
SCOUR HOLES DEVELOP			
BARRIER TIPS			
DEEP RITS			
CONSTRUCTION ERROR			

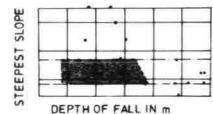
PM: IMPACTS ON SECURITY OF PEOPLE, FINANCIAL COSTS, ECONOMY, ECOLOGY, WATER SUPPLY, SOCIAL ASPECTS
From SAND Report/Analysis of Oosterschelde Alternatives

Table V ASSESSMENT OF SAFETY FOR THREE CLOSURE STRATEGIES

(a) field evidence of the influence of geology on flow slide



(b) last measured slopes just before flow slides



(c) influence of stormtypes on flow slide occurrence

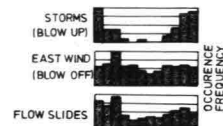


Fig. 5 FLOW SLIDE STATISTICS FOR OOSTERSHELDE BORDERS NEAR BARRIER

Geotechnical experience has not been as extensive. In the thirties and forties there was considerable cooperation with LGM in making borings, defining "critical densities" and discussing flow slide mechanisms (Koppejan, van Wamelen, Weinberg 1948).

Integrated foundation research really started in the late sixties. Some specific examples are described in the following.

3.1. Safety program on surface caissons

In 1966 prototype measurements of pore pressure were made to check the stability of the caissons under a cableway tower in the Grevelingen. In fact this was the first test which was meant to check a prediction method for pore pressure generation (Koning and Loof, 1966). Then in 1970 two full scale model tests were executed with Brouwersdam caissons. One test - at Zonnemaire - served to test predictions of pore pressures during installation of the caisson and to set a criterium for the maximum rate of loading. The other test, at the worst part of the site, in "the Kous" served as construction control in the site itself.

Aspects like installation procedures, field instrumentation, construction control, and performance evaluation became part of this action.

In particular the goals of this test were:

- to check prediction methods for consolidation in sands
- to obtain a criterium for the maximum excess pore pressure

Predictions were performed by LGM (Koning, 1971), and by Rijkswaterstaat using CONSOL. Special interest existed in checking the results of parametric studies as described by Christian and Boehmer (1971) and of the effect of time dependent loading (Segaar, 1973).

Both caisson tests in the Grevelingen and in the "Kous" were in fact early tests with cyclic loading, and had as a goal, to check pore pressure generation in the field as a result of static and cyclic loading.

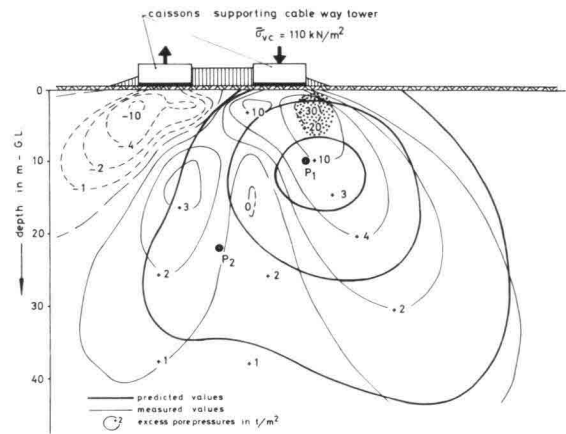
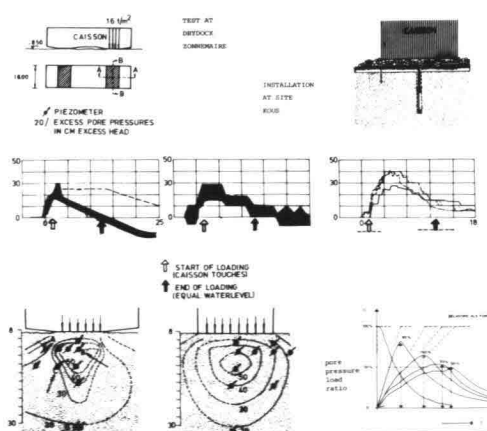


Fig. 6 Predicted and measured excess pore pressures under Grevelingen caissons just after passage of 3 cable way cars.

Note: shaded zone indicates unacceptable shear stresses from elastic analysis.

IN SITU CAISSON TESTS FOR BROUWERSDAM CLOSURE



"Unfortunately" no summer storm occurred in the "Kous" before the caissons were buried in the sand. So no results were obtained.

Results of the Grevelingen test indicated no danger of generation.

An other more recent test in which the effect of cyclic loading was tested in situ was with a large diameter pile in the Oosterschelde. This was meant to check the prediction of deformations from slow cyclic horizontal loading as a result of cableway-car passing.

Fig. 7 Predicted and measured excess pore pressures under Brouwersdam caissons (a) tests in drydock "Zonnemaire" (b) tests in closure gap "Kous".

3.2. Safety program for dikes

A similar prediction evaluation procedure was applied in 1971 to check the safety of dikes along the Schelde-Rijn-Canal. A full scale dike was forced to failure. Specific goals were:

- to check the rate of consolidation in the foundation
- to check the effectiveness of drainage of the dike crests, in case consolidation would not occur fast enough
- to check the "failure factor" for Bishop's method after correct account for excess pore pressures and slab surfaces
- to check other prediction methods as well, like CONSOL
- to check the "critical depth after a flow slide"; this is the depth beneath which a dike will undergo a complete failure instead of a progressive type of failure (page 10). In the latter case consolidation occurs fast enough, for the dike to fail in slices.

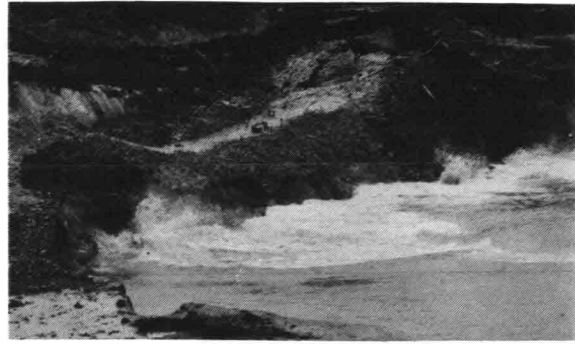


Fig.8a Dike slide in a forced failure of an existing dike at Auvergne polder

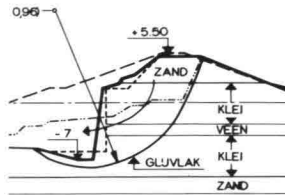


Fig.8b Profile before and after sliding

3.3. Safety program for flow slides, including flow slide statistics

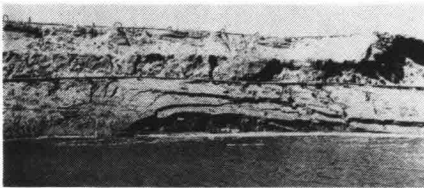


Fig. 9 Dike sliding in a forced failure of an existing dike at Noordland dry dock.

Fig. 10 Sand-water boils during unexpected flow slide in a border protected by pumping.



First densification tests were executed with blasting and vibroflotation, to obtain densities below "critical". Also a test was set up in 1973 - in the Noordland harbour to check the safety of dikes against flow slides. Goals were now:

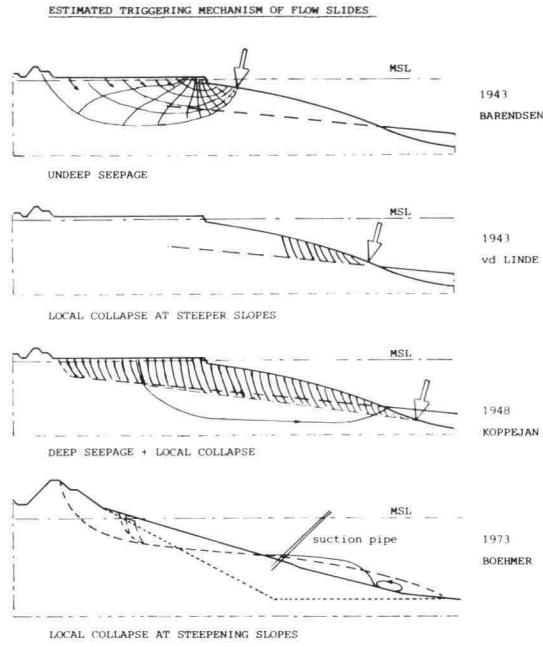
- to check the mechanism of flow slides
- to check the rate of sliding of a sand dike, when it fails in slices. Observed mechanisms in this test were so unexpected, that it was decided to proceed with flow slide tests in a large flume at the hydraulic laboratory. The problem with the tests in the large flumes is that we have artificial soil conditions, i.e. the variability of the soil in the field cannot be reproduced. Also the geometry is so much different, that:
 - stress level differences influences the initial liquefaction
 - consolidation and turbidity currents are difficult to scale
 - the load which controls the flow slide in the field cannot be simulated.

At the same time a program "Flow Slide Statistics" has been started to produce "criteria Charts" and "criteria profiles" which are used to judge the safety of broader slopes. (See page 2). The activities are meant as well to obtain more insight in the flow slide mechanism and to predict where the next flow slide will fall.

If successful, we hope to instrument a test section, where a slide is forced or just waited for.

Fig. 11 PREDICTED AND OBSERVED FLOW SLIDE MECHANISMS

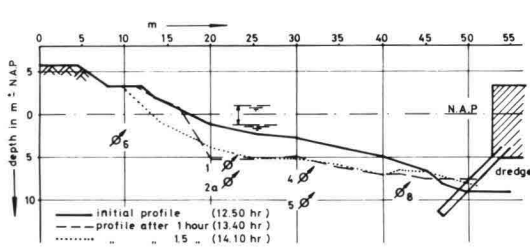
(a) History of prediction.



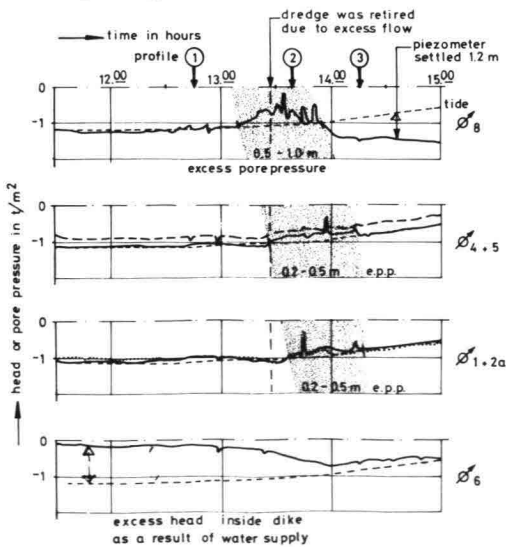
(b) Detail of mechanism.



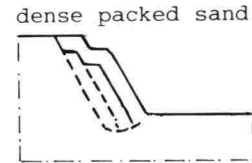
(c) Measurements at Noordland.
c.1 profile with piezometers.



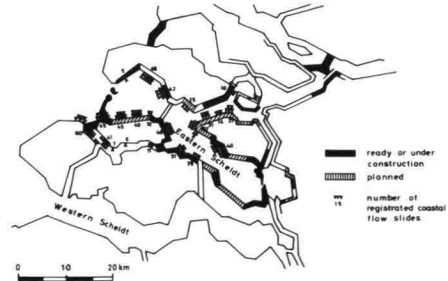
c.2 measurements of excess pore pressure vs time



(d) Measured flow slide in dredge flumes.



(e) Flow slide occurrence in Oosterschelde area.



(f) Predicted scour and sedimentation after 1985

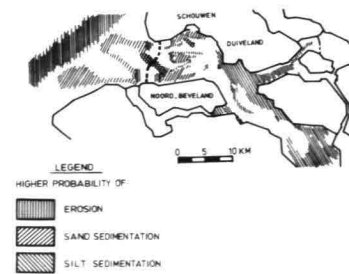
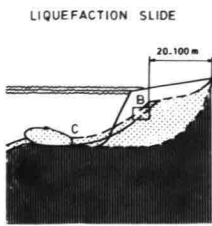


Fig.12 PREDICTED AND OBSERVED LIQUEFACTION SLIDE MECHANISMS

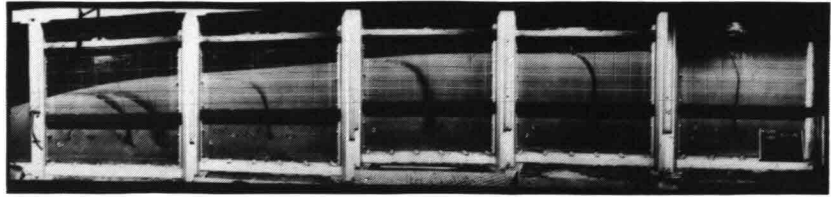
(a) Detail of mechanism.



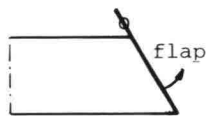
LEGEND

- SAND IN EQUILIBRIUM
- LIQUEFIED SAND AFTER COLLAPSE
- FLOWING SAND AFTER DILATANCY AND CONSOLIDATION

(b) Observed liquefaction slide in large scale flume.



(c) Test set up in large flume.



(d) Sandrain in large flume.



(e) Liquefaction slide in dredge flume.

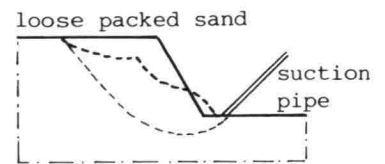
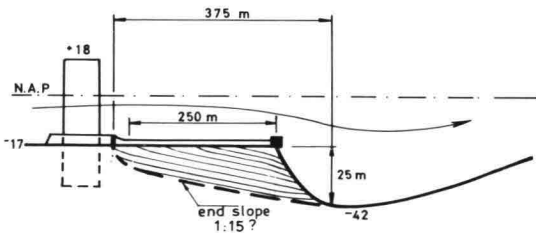


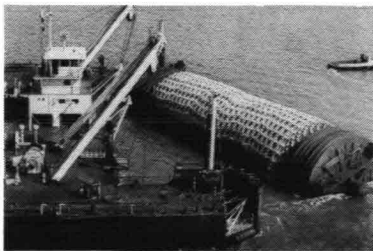
Fig.13 SCOURHOLE SLIDES

(a) Impression of mechanism.

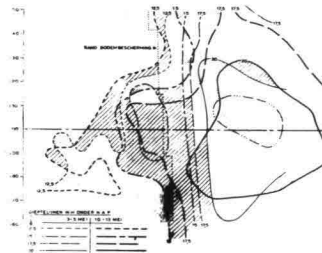
FLOW SLIDE FOLLOWED BY BARRIER SLIDE
progressive failure mechanism altered bottom protection?



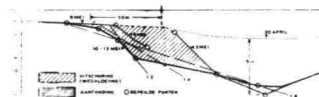
(b) Impression of damage and backward erosion.



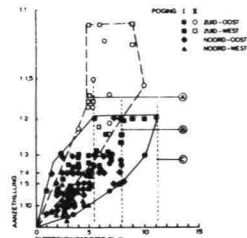
(c) Brouwersdamslide situation.



(d) Profile of sliding and backward erosion.



(e) Experience with slope development versus depth of scour hole.



I feel more field (test) information is needed before continuing an expensive laboratory program in still larger flumes. This is motivated in table IX. The above described examples are design oriented activities, namely to design the extent of new slope protection in front of the raised dikes.

4. INTERACTION BETWEEN RESEARCH AND DESIGN IN THE BARRIER STUDIES



Fig.14 HOLLAND IS SAFE AGAIN

It is not difficult to recall our hesitation when, in 1974, we were asked whether a storm surge barrier of surface caissons on a sill would be feasible. Although caissonlike structures in the past temporarily have been subjected to the cyclic loading of relatively mild summer storms, this barrier will be subjected to heavy winterstorm conditions for a number of years.

Fortunately the described experience was of great help to set up an integrated program of civil- and geotechnical engineering, when the barrier studies started.

4.1. Problem description

From the moment, the storm surge barrier was proposed, the geotechnical engineers were faced with two problems areas in which experience was missing in order to answer the designer's questions, both in and outside Holland. One area included the behaviour of a caisson type structure under winter storm conditions. In particular non symmetric loading conditions were faced, i.e. a combination of cyclic loading, as a result of waves and of static loading as a result of headloss. A second area was the stability of slopes of scour holes which become more than 10 meter deep.

For the prediction of caisson behaviour, little use could be made of existing offshore and earthquake experience, since long term accumulation of horizontal movement had to become an object of study as important as the short term generation of excess pore pressures. Methods to predict such movements caused by non symmetric loading were not well developed.

In addition experience show that settlements of caissons under static loading are big if the sill is not densified. The winterstorm conditions would make these settlements only bigger.

As a result of the loose conditions and the application of compressible sills, settlement estimates or "shake downs", were up to 1 meter initially. No comparable experience existed in offshore practice.

Effective densification of the sill was considered especially difficult since sand might move in the pores between stones before densification and move out afterwards.

An additional soil structure interaction problem was that originally a heavy deformation criterium was set on the caissons, in the order of several centimeters. This criterium was derived from the Haringvlietbarrier, the only 'comparable' structure around, where differential settlements of only centimeters were allowed to avoid cracking of the floor. This was the consequence of the application of a pile foundation. In the case of the barrier loads were to be transferred by a caisson floor. Since the caissons were to be independent units, each with its own gates, they allowed for more deformations as long as the cais-

son floor would be strong enough to withstand pressure differences. For the time being it was requested to limit deformation to less than 20 cm.

4.2 Scour slide research and site conditions

Predicted depths and slopes of scour holes at the end of a bottom protection on both sides of the structure, exceed the scale of past experience. Especially since the Oosterschelde sands are known for their potential to liquefy and to cause flow slides.

Figure 15 shows soil conditions at the Oosterschelde site at the start of the barrier project.

The site is located in an area which is known for its flow slides. Most of these flow slides occurred right near the southern abutment of the dam. Some of them -even recent ones- would cause dike failures overnight.

They always occur in the Holocene sand layer with relative densities as low as 35% or porosities as high as 40-40% locally. Since this layer will reach until 15 meter under the future sill, flow slides can develop, which can cause backward erosion in the bottom protection. They eventually can create the same sort of damage as erosion of the sill might do.

As we saw from past flow slide research the mechanism of the flow slides is not yet fully known. Therefore it will be difficult to predict the damage and the rate of backward erosion when a scour slide occurs. A research program for it cannot be carried out in the course of 1,5 years, which is the time which we were allowed to spend to investigate the feasibility. Therefore an early decision was taken to densify the Oosterschelde bottom, both at the site of the barrier itself and at the site of the scour holes.

An extensive program of soil exploration and densification tests was undertaken to investigate the feasibility of densification, as is discussed in the papers of session V.

4.3. Model tests in field, laboratory and computer

Meanwhile two field model tests were set up in the Neeltje Jans harbour.

An as large as possible test caisson was subjected to cyclic loading including a headloss component. The tests were set up to check the effectiveness of densification and to check prediction methods. Just as was the case in the Zonne-maire and Kous tests one test was instrumented without a sill to check the prediction models, if possible until failure conditions.

In the other test a sill was included to check the behaviour of both drainage under the caisson and the influence of densification. This sill was included in order to satisfy the designer's request for a representative model test. A procedure with stepwise improving predictions was adapted to set up a successful loading program, and to give the designer updated estimates of the deformations.

Important to know is that the designer felt convinced the necessity to test the effect of the variability of the subsoil in the field and to see how successful densification could be, despite the difficulties with earlier in situ tests.

4.4 Shift to embedded caissons after the Neeltje Jans field tests

One outcome of the test was that loose zones directly under the caisson could cause large movements to occur at small ratios of h/v (order 0,3). This was alarming to the designer, since he had still not solved his problem how to keep the loose zones of sand out of his soil before densification would start.

Also problems arose with designing a soil-structure interaction which would allow for an h/v design ratio of 0,45 (0,6 at failure). The designer therefore shifted to an embedded caisson design. Since the pressure on the project became big due to this shift, the work on the evaluation of the field test was frozen. That is the reason that not much yet is published on these tests.

STRATIFICATION OFF STIFF AND WEAK LAYERS
AS RECOVERED IN MAY 1976

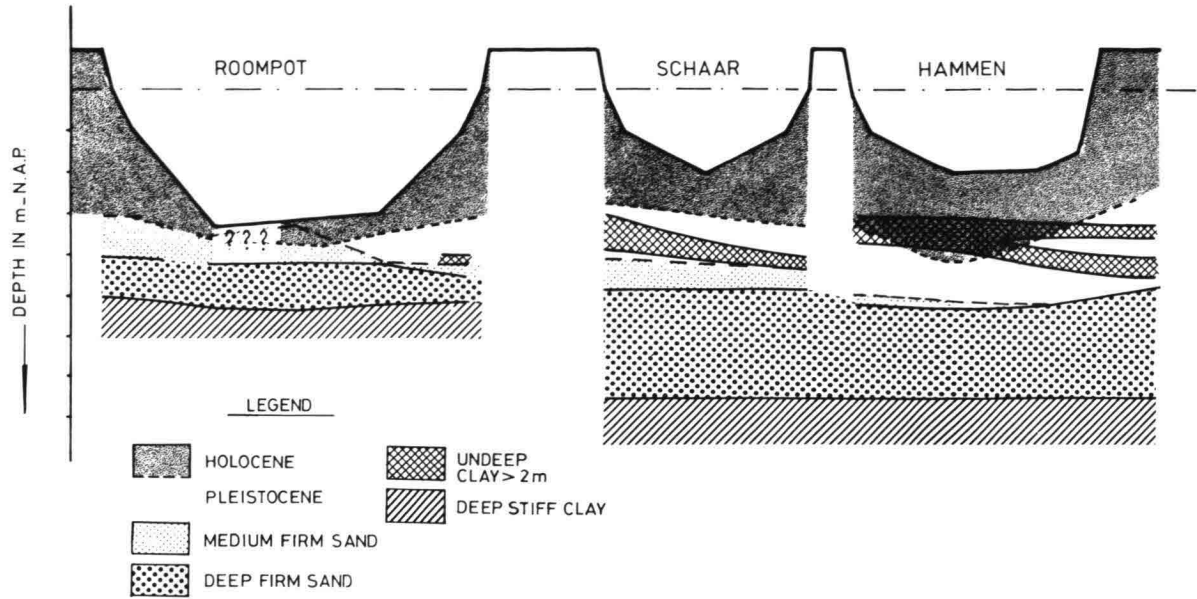


Fig. 16 Results of site investigation medio 1976

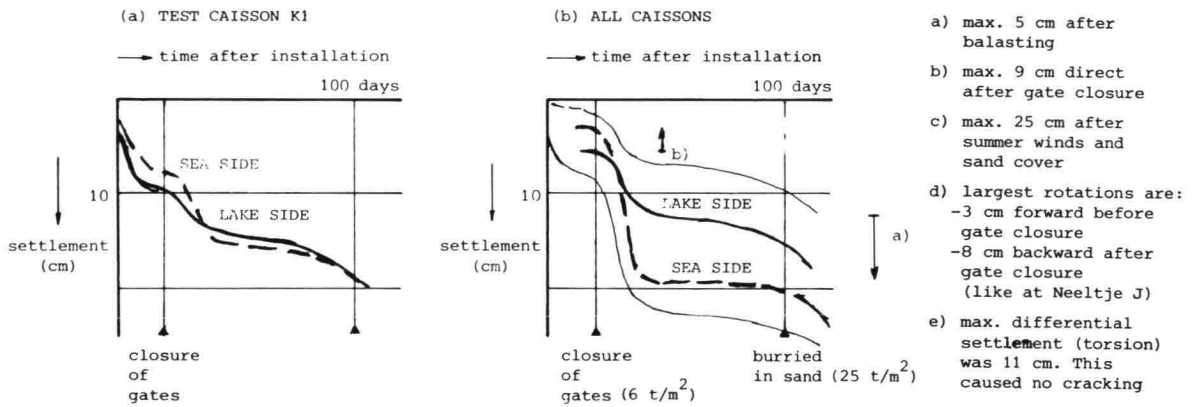


Fig. 17 Settlements of Kous caisson after installation at site

The little evaluation which was done showed one very important aspect, namely that if gradually increasing (storm) loads would be applied to the caisson, excess pore pressures would remain low as a result of 'preshear effects'. (paper by Smits) Therefore it was assumed that if the caisson solution was to be maintained and if such loose zones could not be avoided during construction, that the gates should be controlled in a test period after construction.

This would impose a constraint on the future barrier control services. Since that was not acceptable and since an alternative design was available, namely the embedded caisson design, a shift was made towards this design.

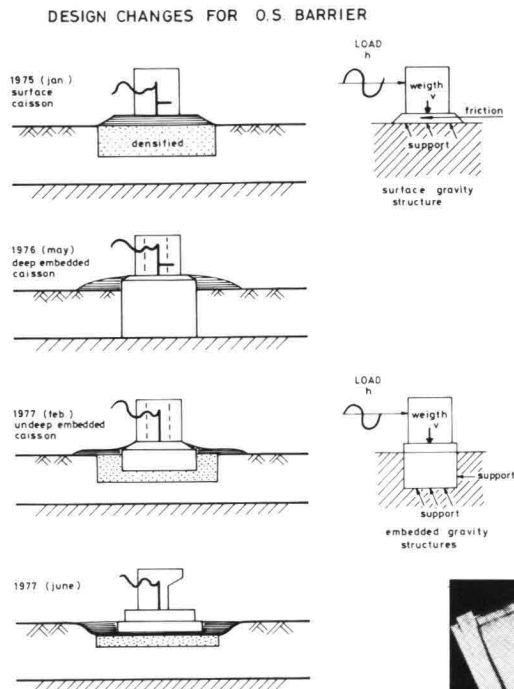


Fig. 18 DESIGN CHANGES FOR OOSTERSCHELDE BARRIER

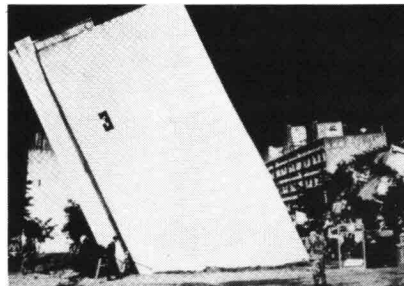


Fig. 19 FAILURE OF HIGHRISE BUILDING AFTER EARTH QUAKE



Fig. 20 INCLINED BUILDING

The shift in design had side effects. Because of the difficult mechanisms involved in the Neeltje Jans tests, like the pre-shear effects, the shift in design was misinterpreted by outside observers.

Although the policy makers explained their decision to shift as above, a weekly journal commented:

- that this test period for the barrier seemed to make no sense to them, since high rise buildings do not need a test period as well

Obviously there seems to be a limit to "interact" on difficult mechanisms.

The media should know however that earth quakes experience has shown how high rise buildings can tipover if the subsoil is not densified (see fig.19). On the contrary when the foundation consists of fine rock inclined buildings are feasible (see fig.20).

4.5. Parametric design studies of embedded caissons

After the Neeltje Jans field test was over, the following was concluded with respect to the continuation of model test studies:

- a good soil structure interface which includes densification is a must both in the field and in the model tests,
- no more field model tests are needed, once good soil structure interface is designed properly,
- laboratory model test facilities and analytical models in combination with stress path tests are sufficient tools to optimize the design.

The laboratory test papers describe how successful several models were used for parametric studies of various design (Rowe, de Quellerij and Broeze).

Other papers (Nieuwenhuis-Molenkamp, Biegstraaten-Kenter, Kenter-Vermeer) show

how succesful CONSOL was used in these parametric studies as well. Still there were numerous unexpected effects.

I recall:

- (1) The deep embedded caisson moving more than the undeeep embedded caisson, regardless whether or not the base stiffness would be the same.
- (2) The foundation layer under the deep caissons turned out to be more silty than expected, after soil exploration was finished at sufficient depth. This is especially the case in the so called 'blind spot', which could only be explored recently, because of the existing sill from the former closure design. One can see from this too how dangerous it is to start construction of a design without adequate site exploration. (See fig 16) This causes a change towards an undeeep embedded caisson. At first it was still buried. Later on a more caissonlike pier was proposed which is placed on a foundation bed.
- (3) During the course of the studies the "design h/v " went up to 0,6 (failure values close to 0,8 base friction + 0,3 side support for buried caissons and 0,7 + 0,2 for the present piers).
- (4) Temporarily low friction factors (0.45) resulted from 1:1 scale "element tests" at Schelphoek (Hudig e.a.). This was the result of adding a nylon mat with sandlayers above and beneath the it to the foundation bed. Improvement of foundation bed design did this factor rise again to 0.68.
- (5) "Cyclic gradients" at h/v ratio's of 0.45 (112 MN/252 MN) would be larger than early designs of the foundation bed would allow for. Therefore a two layered foundation bed was proposed (D'Angremond e.a.)
- (6) The maximum load went down by 30% (112 MN versus 160 MN)

Especially point (6) shows how useful a flexible design approach can be even after design dimensions have been fixed. For example when h/v becomes still lower, or when filter research on effect of stress level and time results higher critical gradients (see table I) "densification and filterbed construction" becomes more flexible.

More study on the crtiteria in table I might resolve more flexibility in other construction items as well.

4.6 Evolution in the foundation design approach

From the geotechnical point of view the approach of producing a foundation design went through a new phase of evolution. My feeling is that -more than was expected- our approach of considering the subsoil as a 'boundary condition' changed towards an approach in which the top layer of the foundation is considered a construction material. Quality standards or criteria should be developed as part of the overall design. Criteria for design options like densification and soil replacement should be given priority as well.

This is different from past experience in the Delta in which the top-layer was left as it was and either used to serve as a shallow foundation for a caisson type closure, or bypassed, by driving piles through them as in case of the Haringvliet barrier.

The parametric studies gave birth to new developments in the interaction process. First the researcher started to find out that in the long run he does not only improve the 'safe-feelings' of the designer, but that he will be able to save cost by making appropriate optimisation studies. By that time het wants a voice in the design process. Fortunately a project organisation was set up which allowed for that.

Further improvement of safety and optimisation of cost is of course attractive. Political pressure on the costs of the project stimulates this process more than ever. However, pressure to work on schedule and pressure to keep the cost of studies limited work against it.

Looking back, we must say that the project improved on its design strategy since strategies for construction control and barrier operation control are under development.

Table VI illustrates how these strategies evolved towards more interaction between the researcher and the organisation.

Some remarks should be made on this table:

- (1) We went from common sense designing towards a semi-probabilistic approach today and aim to end at a full probabilistic design later on.
- (2) The researcher greatly contributed in establishing design criteria, where past experience or 'field evidence' did not provide these.
- (3) 'Function analysis' and extra model studies proved useful to define the desired criteria.
- (4) 'Fault trees' and acceptable maintenance requirements were developed to refine the description of 'malfunctioning' and relevant criteria (paper by Kooman et al).
- (5) An early set up for the Barrier operation control was started in order to establish these acceptable maintenance requirements (BARCON studies).

Table VII shows how criteria improved when the researcher got more reliable predictions. No need to say, that model tests in laboratory and the field played a keyrole in this process.

Table VIII shows how priorities can be analyzed for future model tests on the basis of the probability that the design and barrier operation benefits from it (cost benefit analysis) and of the probability of improved understanding after the test (on malfunctioning mechanisms and design criteria).

In view of this it seems desirable to make a further analysis of past and future benefits in the barrier project as a function of the level of effort in the studies. That would make it easier to decide on a reasonable budget for the studies, now four years of intensive studies -two more than was planned for- put great pressure on the costs of the studies. The set up of a graph like in figure 21 might help us to make a reasonable decision

EVOLUTION OF PERFORMANCE CRITERIA					
design alternative	1974	1976	1978		1985?
	surface caisson placed on sill	embedded caisson buried in subsoil	embedded caisson (placed on foundation bed)		
Possible malfunction			construct. phase	end phase	
STABILITY (at max load endphase) - overall safety factor - base friction - side support	2 & 3 1,5 ¹⁾ end of constr.	1,15 ²⁾ end of constr.	longit/ transv. 1,35	1,5	updated performance ⁴⁾ criteria, on the basis of substitution of construction control experience into the probabilistic approach. Further of inclusion of maintenance as a function of freedom of operation.
DEFORMATION - horizontal deflection from translation + rotation - relative movements between piers - settlement	20 cm 10 cm	10cm	3) longit/ transv. 5 + 10 / 5 + 20	(transl. + rot) 7,5+3,5 / 1,3+1,2	
FLOW - hor. static gradients - hor. cyclic grad. -seagravel - coarse sand -subsoil - vert. cyclic gradients	max. static gradient 0.15	same	0,15 2 & 2,5 3,5 & 4	5) <0,08> <2,2> <2,2> <3,4>	
SOIL STRUCTURE INTERACTION - max/min (°/min) - mobilized passive - relative movements between sill and pier for lower gate beam	undensified 2 (0,1) densified 1,5(0,2)	undensified 1,5(0,4)	1,5	1,5 1,1-1,5	
DEMONIFICATION - subsoil - sill	→ →	→ →	CPT 150 pores: 39% upper part densified lower part demafied		

1) Criteria did not increase despite less conservative soil parameters and improved understanding of mechanisms and improved analysis (parametric studies) as a result of geotechnical research and the semi probabilistic approach.
 2) Brinc's Hansen was too optimistic as compared to centrifuge and Kate test.
 3) Here criteria depend on the probability of malfunctioning of the gates and comprised deformation components (dc) and tolerances (tc) during construction.
 4) Design criteria change gradually into performance criteria.
 5) Values in () are estimated 'failure' values < > are predicted values

Tabel VI Design strategy for Oosterschelde barrier

BEFORE 1975 COMMON SENSE APPROACH	1975-1977 DETERMINISTIC AND FLEXIBLE	1977 e.v. SEMI- AND FULLY PROBABLISTIC
phase I (1) ESTIMATE FEASIBILITY from past experience and model tests set scedule for time+cost	← ESTABLISH CRITERIA (for needs, functions, performance, cost, construction time) assuming no maintainance	(1) DETERMINE POSSIBLE MALFUNCTIONS on basis of function analysis and model tests (2) ESTABLISH PERFORMANCE CRITERIA on the basis of ACCEPTABLE MAINTAINANCE to prevent malfunctioning
phase II (1) DESIGN (2) PREDICT PERFORMANCE (stability, deformations, flow) (3) COMPARE PREDICTIONS WITH CRITERIA (4) IMPROVE DESIGN if necessary	include ← PARAMETRIC STUDIES with more performance aspects ← EVALUATIONS of PREDICTIONS on basis of model tests ← ALTERING of DESIGN AND CONSTRUCTION if necessary or desirable on basis of parametric studies and evaluation	include ← PROBABLISTIC STUDIES OF LOADS AND STRENGTHS on basis of model tests ← TRANSLATION OF BASIC DESIGN CRITERIA IN CONSTRUCTION CRITERIA ← REFINE DESIGN on basis of feasible construction criteria ← LEAVE FLEXIBLE DESIGN OPTIONS OPEN within practical (optim- and pessim guess)
phase III CONSTRUCTION on basis of FIXED CONTRACTS	CONSTRUCTION on basis of flexible framework of contracts "RAAM-CONTRACT"	I ASSESS PERFORMANCE II ASSESS DESIGN III INSTRUMENT FIELD IV EVALUATE AND DOCUMENT CONSTRUCTION V APPLY SURRVEILLANCE VI EVALUATE PERFORMANCE VII ADJUST BARRIER CONTROL if necessary
phase IV	BARRIER CONTROL during end of construction and start of operation	FLEXIBLE DESIGN STRATEGY + CONDITION CONTROL (SAFETY PROGRAM)

Tabel VII Improvement in design criteria for Oosterschelde barrier

I PERFORMANCE CRITERIA	start of project (update yearly)	statement of: possible malfunctions, mechanisms, field evidence, criteria updating on the basis of new modeltest studies and maintainance policy
II DESIGN ASSESSMENT evaluation and documentation	end of fixed design options (yearly)	conditions on which design based predictions made & implied by design { evaluation and comparison of predictions and criteria } documentation definition of key aspects for instrumentation, construction control and future evaluation
III FIELD INSTRUMENTATION	before and during construction	install instruments to measure key aspects of performance portray predictions for instruments interpretate and compare with "predicted" behaviour
IV CONSTRUCTION ASSESSMENT EVALUATION DOCUMENTATION	during construction	document (with text, photos, movies) key aspects of construction - especially where construction deviates from design evaluate deviations (by adjusting predictions)
V SURVEILLANCE	monthly	visual inspection obtain & portray field measurements obtain information - data on mechanisms, (for check with predicted mechanisms)
VI PERFORMANCE EVALUATION	yearly	compare { actual performance - predicted performance } criteria of performance explain differences adjust construction procedured and barrier - control procedures on the basis of updated predictions

Tabel VIII Sequence of foundation studies for design assessment, construction control and barrier operation control.

TYPE OF MODELTEST AND APPLICATION	RISK OF UNEXPECTED BEHAVIOUR (level of unsafety)		PROBABILITY OF UNEXPECTED BEHAVIOUR (or incorrect prediction) (on the basis of field- and lab. tests experience)	CONSEQUENCE OF UNEXPECTED BEHAVIOUR in terms of repair and maintainance
	test	priority		
single barrier ¹⁾	2	2	medium-large	medium-large
field flow slide ²⁾	1	1	large	large
test dike ³⁾	2	2	medium	small
single barrier	3-2	2	medium	medium
model flow slide	3	3	small?	large
test dike	3	3	large	small
parametric barrier	2	2	large	medium
modeltest flow slide	3-2	2	small-medium	large
study dike	3	3	large	small

1) Movement of particles in base contact at wave side of caisson
 2) Mechanism which shows how bottom protection is destroyed or stops the slide
 3) Fatigue mechanism of dike protection at stagnant water level

Tabel IX Possible procedure for priority determination in large scale model test and field test studies

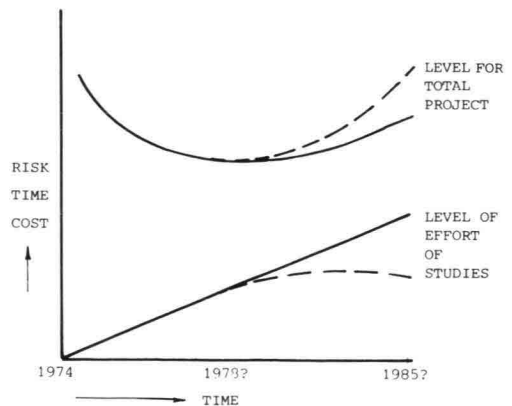


fig. 21 Cost - benefit analysis in the project versus level of study effort

5. CONCLUSIONS

- (1) Safety of the project is served by a continued long term interaction of the client, the designer and his advisors. This helps the designer to define key questions and to translate the advisor's answer in design terminology. Geotechnical contributions can still improve on these aspects.
- (2) Priority in the foundation design studies should be given to assessment of criteria and mechanism as shown in the CRITERIA TABLES 1, 2 and 3. Then attention should be given to CRITERIA-CHARTS and CRITERIA-MAPS. Like in figure 1 and 2.
- (3) A thorough evaluation of the research studies should be undertaken to help to set priorities, for future criteria research.
- (4) Priorities for further model tests should be based on both
 - a) cost benefit analysis for design and construction
 - b) probability of improved understanding
- (5) It is desirable to analyse past and future benefits in the barrier project as a function of the level of effort in the studies in order to decide on a reasonable research budget.

6. ACKNOWLEDGEMENT

I am grateful to my colleagues in the project organisation for their invitation to prepare this summary paper on foundation aspects of coastal structures, the geotechnical studies in particular.

It is a great compliment to many colleagues and friends, at Rijkswaterstaat, at the Delft Soil Mechanics Laboratory, at DOSbouw and to our consultants, to be invited for this first symposium on Oosterschelde related problems. Through their original ideas, cooperation and critiques they have helped to raise the state of the knowledge in this field.

In a matter of years they raised it to a level of confidence, which is as high as in earthquake and offshore engineering.

I remember the conflicting discussions on subsoil densification and on the set up of two Neeltje Jans in situ caisson tests, in order to study the effect of densification on the expected deformations of the structure. That was the event, which more than anything else, stimulated geotechnical engineering, studies of pore pressures and deformations under these structures.

Hopefully many experienced colleagues and friends, I referred to, will remain inspired enough to stay around this project through its completion.

After all, the geotechnical profession is scarcely populated in this hydraulic designer's environment, while continuity in attention and past experience is required to face the problems still ahead in this project.

I thank Smits, Lubking, Segaar, Lambe and Houweling for their critical review and their help in assembling this paper.

SYMPOSIUM ON FOUNDATION ASPECTS OF COASTAL STRUCTURES

STRESS-STRAIN BEHAVIOR FROM STRESS PATH TESTS

by:

W. Allen Marr, Research Associate, Massachusetts Institute of Technology
Cambridge, Massachusetts, U.S.A.

Kaare Hoeg, Director, Norwegian Geotechnical Institute, Oslo, Norway

S Y N O P S I S

Stress-strain behavior of a soil element depends greatly on the past, present and imposed state of stress, in particular the effective stress path. This paper demonstrates this fact for static and cyclic loading using stress path tests obtained with simple shear and triaxial equipment. Using measurements of stress-strain behavior from stress path tests, one can obtain insight into the fundamental aspects of behavior of the pier foundation, develop parameters for use in analytical and numerical models, and help guide and interpret model tests.

I N T R O D U C T I O N

This paper illustrates to the civil engineer the important influence of stress path on parameters for predicting stress-strain behavior of soil. A stress path consists of a line drawn through points on a plot of stresses. This line indicates how stresses change. Stress paths constitute an effective way to portray the past, present and future stresses acting on a soil element.

Lambe (1967) proposed the Stress Path Method as an approach to solve geotechnical problems. Lambe and Marr (1978) describe further developments of the approach and illustrate some aspects of its use. The stress path approach builds from the principle that soil behavior depends primarily on the past, present and imposed effective stresses, i.e. total stresses minus pore water pressure.

Ideally, soil deformations under structures like the piers for the storm surge barrier should come from analyses using constitutive stress-strain models formulated for the soil in three dimensions. However, realistic mathematical models for soil behavior are extremely difficult to formulate and use without considerable simplification.

The stress path approach constitutes an alternate approach to obtain soil deformations. Representative soil elements are subjected to stresses in the laboratory predicted for the corresponding elements in the field, and the resulting strains and pore water pressures are recorded. One obtains soil deformations by integrating strains for appropriate elements over the associated lengths. In practice, one must use laboratory devices which impose, as closely as possible, the correct stress paths on the soil.

Figure 1 lists some of the factors which influence stress path. Past stresses are generally referred to as "stress history", present stresses as "initial stresses" and future or imposed stresses as "changes in stress". All of the factors listed in Figure 1 influence the behavior of soil. Most times, the effect of stress history on a lab sample is built in by testing a soil element which has undergone a stress history comparable in effect to the stress history in the field.

Geotechnical engineers have devised equipment to test along the more common stress paths encountered in design. Woods (1978) describes some of the common equipment and use of the results. Figure 2 lists some of the more familiar types available, the key features of each, and the major limitation to widespread

use of each. Today, engineers rely primarily on results from triaxial and simple shear tests complemented with information from field tests. Plane strain and true triaxial equipment are primarily research tools.

Figure 3 illustrates total stress paths achieved in common tests with triaxial and simple shear equipment and indicates the types of facilities to which these stress paths are relevant. Stress paths differing from those illustrated can be achieved with the triaxial equipment, provided rotation of principal stresses and the intermediate principal stress are not important for the situation being considered.

The next section of this paper demonstrates the effect of stress path on stress-strain behavior of Oosterschelde sand for static loading (single application and retention of a load). This is followed by a section which considers similar stress paths but changes in stress which are cycled to determine the influence of wave loading on the pier.

The sand used for these tests come from the Neeltje Jans harbor in the Oosterschelde. They have a uniform gradation with a mean grain size of 0.17 to 0.28 mm with less than 0.5% of the sample, by weight, smaller than the #200 sieve. The sand consists mainly of subrounded to rounded, quartz grains with some feldspars and small amounts of mica, shell fragments and calcite. A minimum dry density of 1.43 t/m^3 and a maximum dry density of 1.73 t/m^3 resulted using ASTM D2049-69 procedures.

Simple shear samples were prepared by controlled pluviation of dry sand into the membrane followed by assembly of the equipment and saturation of the sample with flowing water. Triaxial samples were prepared by tamping moist sand in layers, followed by assembly of the equipment and saturation with carbon dioxide followed by flowing water.

STRESS PATHS FOR THE OOSTERSCHELDE PIER

Figure 4 shows stress paths for three elements in the foundation of the pier. These paths result from using a lateral effective stress coefficient of 1.0 to obtain initial effective stresses and linearly elastic theory to obtain changes in stress resulting from the weight of the pier, the static tide difference and the peak wave.

Comparison of the actual stress paths for typical elements in Figure 4 with those obtainable in conventional laboratory equipment shown in Figure 3 shows that Element A has a stress path similar to that in a triaxial compression test, Element B compares with a simple shear test and Element C compares with a triaxial extension unloading test. These examples indicate the nature of stress paths one should examine for the stress-strain behavior of the pier foundation.

STRESS-STRAIN BEHAVIOR FOR STATIC LOADING

Figure 5 shows test results for a stress path like that for Element A in Figure 4. Test D has full drainage so that no excess pore pressures develop. This compares to loading in the field at a slow rate compared with drainage time. With no excess pore pressures, the effective stress path and the total stress path (minus initial pore pressures) are the same. In the undrained test, U, excess pore pressures develop with shearing, altering the effective stress path. Even though the two tests D and U have the same total stress path, their stress-strain behavior is quite different. The drained test has a strength more than two times that of the undrained test.

Figure 5 contains two additional tests, u and d, identical to the first two, except the stress magnitudes are reduced to 1/5 of that of U and D. This stress reduction duplicates the effect of a scale model of the prototype pier.

The sand samples for the four tests in Figure 5 were for practical purposes identical. At the lowered stress level the undrained test, u, gives more than twice the ultimate strength of the drained test, d, a result exactly the opposite of that found with tests U and D. The modulus data show that reducing the stress level by a factor of five results in a reduction of initial modulus by a factor of only 1.2 to 1.5 in these tests.

A comparison between the results from tests U and u shows completely different pore pressure behavior. The samples have the same initial void ratio. For sample U with the high initial effective stress level, this void ratio is above the critical void ratio, and the sample experienced positive excess pore pressures throughout the test. However, for sample u at the low initial effective stress level, undrained shearing created a tendency to dilation, and significant negative excess pore pressures developed with a corresponding increase in the effective stress level. Therefore, when interpreting the results of model tests on sand, an uncritical extrapolation of results from the model to prototype predictions may be misleading. A basic understanding of the effective stress-strain behavior of the soil foundation is a prerequisite for such extrapolation.

These tests demonstrate that drainage and stress level, components which affect effective stress path, have a profound effect on stress-strain behavior. Figures 6 and 7 summarize considerable data from triaxial compression tests giving the effect of stress level on modulus and friction angle. Figure 6 gives moduli as a function of consolidation stress level from undrained tests. Moduli values are secant moduli for a stress difference one-half that at failure. Figure 7 shows friction angles determined from triaxial tests on specimens at different porosities and stress conditions. Figure 7a shows that for any one porosity there exists considerable scatter in the strength data. Figure 7b shows that much of this scatter at a porosity of 41% results from differences in stress path, principally from differences in effective stress at failure, as indicated by \bar{p}_f . Data shown in Figure 7a include tests with various consolidation stresses, drainage and effective stress paths which accounts for the remaining scatter.

Another parameter affecting present state of stress, and therefore stress path, is the coefficient of lateral stress, K. K depends on stress history and soil type. Its value is difficult to determine, especially in sands like those of the Oosterschelde, yet its influence may be considerable. Figure 8 shows drained triaxial results for tests consolidated to the same $\bar{\sigma}_v$ but different $\bar{\sigma}_h = K \cdot \bar{\sigma}_v$. K has a substantial effect on strain and strength.^V

Finally, consider the influence of the inclination of the total stress path on stress-strain behavior. Figure 9 shows test results for undrained conditions from triaxial compression loading and triaxial compression unloading. The effective stress paths and the resulting stress-strain behavior are essentially identical. Considering the same total stress path, however with complete drainage, produces a radically different result. The drained unloading test has a much smaller strength than does the drained loading test.

Figures 5 through 9 demonstrate for static loading that stress-strain behavior is highly dependent on effective stress path. Since stress history, coefficient of lateral stress - K, changes in stress produced by construction, and drainage influence the effective stress path, they have an important influence on stress-strain behavior.

STRESS-STRAIN BEHAVIOR FOR CYCLIC LOADING

Waves occur in irregular patterns producing an irregular stress path in each element in the foundation of an offshore facility. For laboratory testing, one commonly simplifies the train of waves of random magnitude produced by a storm to a train of equivalent waves of one magnitude. Andersen et al. (1978) describe one method to obtain an equivalent storm of uniform waves from the real storm and cyclic tests on the soil.

This discussion considers only cyclic stress path testing using triaxial and simple shear apparatus, although research has been conducted with many other types of equipment (Woods, 1978).

For cyclic loading, consider stress paths like those given in Figure 4 except now the stresses resulting from the wave are repeated. If the period of the wave is short compared to the time for drainage of the foundation, undrained conditions may prevail. Figure 10 shows data for cyclic tests with undrained conditions performed in triaxial and simple shear equipment. The stresses for the simple shear test are similar to those given in Figure 4 for the center of the pier foundation. The stresses for the triaxial test are similar to those given in Figure 4 for Element A at the edge of the pier foundation. Data from the simple shear test show permanent or residual shear strains develop which lead to a permanent horizontal displacement in the field. Data from the triaxial test show residual axial strains which result in a permanent vertical displacement in the field. Residual strains in both tests increase with each additional cycle of load. Additionally, residual excess pore water pressures develop with each cycle which reduce the effective stresses towards the failure envelope. Figure 10 illustrates the build-up of residual pore pressure with the normalized parameter, $\Delta u / \Delta u_f$, where Δu is the residual excess pore pressure at the end of a cycle and Δu_f is the final residual excess pore pressure. In this paper Δu_f is taken as the residual excess pore pressure at 1% residual axial strain in triaxial tests and 1% residual shear strain in simple shear tests.

Figure 10 defines a modulus, E_Σ , which relates stresses to the residual strains that develop in cyclic loading. A second modulus, E_{sec} , defines the slope of the stress-strain curve in a particular cycle. Figure 10 shows how these two parameters change with cycling. The main point of Figure 10 is to illustrate that the stress-strain behavior at each point in the foundation depends on the stresses existing at that point in a rather complicated way. Furthermore, with cyclic loading, one is concerned not only with the stress-strain behavior within any one load cycle but also with the more important long-term development of residual strains with cycling.

With a wave period which is long compared to the time required for drainage, cyclic loading occurs with drained conditions. Figure 11 compares cyclic triaxial tests with equal conditions except one is drained and one is undrained. In the first few cycles, the drained test deforms more than the undrained test, presumably due to volume changes. In later cycles the trend reverses as the effective stresses in U decrease and the shear distortions continue. The drained test eventually comes to a state where essentially no further strain accumulates; whereas, the undrained test continues to strain with additional cycles.

The lower part of Figure 11 shows for a fixed number of cycles both samples have similar E_{sec} but considerably different E_Σ (log scale). The undrained sample reaches 1% permanent axial strain in 200 cycles, but the drained sample requires over 1000 cycles to reach the same strain. For other stresses and other densities the effects of drainage on stress-strain may differ considerably from that shown.

Figure 12 shows the effect of stress level in undrained cyclic triaxial tests. All test variables except \bar{p}_0 are the same for all samples. For the conditions of the tests, and at a selected number of cycles, a field element at a stress level of 53 t/m² might undergo a strain over 20 times that of the comparable element in a scale model at a stress level of 8 t/m². A partial explanation of such behavior parallels the discussion accompanying Figure 5 and the results in Figure 7b.

Figure 13 illustrates the important effect of K on cyclic behavior. K affects not only the magnitude but also the type of strains that develop. The three triaxial tests in Figure 13 have the same initial $\bar{\sigma}_v$ but different $\bar{\sigma}_h = K \cdot \bar{\sigma}_v$.

The cyclic shear stress is the same for all three tests. The test with K of 1 develops only cyclic and no residual strains. Figure 13 shows that a triaxial element with K of 0.5 develops compressive residual axial strains while the element with K of 2 develops large extensive axial strains. (The sample increases in length.) Recall that K is a quantity which is difficult to assess in practice.

Figure 14 illustrates the importance of inclination of the effective stress path using drained triaxial results. Cycling the lateral stress in a drained triaxial test, Test 135, gives much larger residual strains than cycling the axial stress, Test 45, with equal magnitude. As was shown with static tests, altering the inclination of the total stress path with undrained conditions has no significant effect on stress-strain behavior.

Figure 15 gives simple shear data to show the effect of magnitude of cyclic shear stress superimposed on an average shear stress, in this case 2.5 t/m^2 . The residual strains that develop for a fixed average shear stress are highly dependent on the magnitude of the superimposed cyclic shear stress.

Figures 10 through 15 demonstrate that stress-strain behavior of Oosterschelde sand for cyclic loading is highly dependent on factors which affect the effective stress path. As with static loading, stress history, K, changes in stress produced by construction and drainage influence the effective stress path. Therefore these factors have an important influence on the cyclic stress-strain behavior of soil. We do not yet know enough about the complex stress-strain behavior of soil to use a few simple tests to develop parameters to define general constitutive laws. One approach as described above is to perform laboratory tests with stress paths similar to those in the field from which the engineer obtains parameters to use in his method to predict performance.

S U M M A R Y

Stress path testing consists of subjecting a representative soil element in the laboratory to the past, present and imposed stresses predicted for that element in the field and measuring the resulting strains and pore water pressures. Practical testing considerations limit the cyclic testing of the Oosterschelde sands in the laboratory to stress paths obtainable in triaxial and simple shear equipment. The paper demonstrated for elements at the center and edge of the pier foundation how these tests could be used to approximately duplicate the *in situ* stress path and obtain the resulting stress-strain behavior. Behavior for other elements in the foundation can be obtained by combining results from simple shear and triaxial stress path tests. Because stress-strain behavior of soil is so dependent on effective stress path, such stress path tests are essential to determining relevant soil parameters.

Difficulties one faces in using stress path tests to predict prototype performance of the pier include:

1. It is extremely difficult to take good "undisturbed" samples of sand in the field, and one can not obtain a laboratory sample identical to the sand soils existing in the Oosterschelde before and after densification.
2. Prediction of amount of drainage in the field and duplication of that amount in a laboratory element is difficult.
3. Triaxial equipment cannot duplicate the rotation of principal stresses that occurs in the pier foundation. We do not know the relative importance of this limitation for cyclic loading.
4. The strain condition in the simple shear sample is well defined but not the horizontal stresses. This uncertainty complicates interpretation of the test.

These difficulties primarily affect the accuracy with which one can predict field performance. Despite these difficulties, we conclude that stress path tests are essential to define the complex stress-strain behavior that occurs in the foundation of the pier. The results of stress path tests allow the engineer to (1) grasp the fundamental aspects of the stress-strain behavior of the pier foundation, (2) develop parameters for use in analytical and numerical models, and (3) help guide and interpret model tests.

R E F E R E N C E S

- Andersen, K.H., Hansteen, O.E., Hoeg, K. and Prevost, J.H. (1978) "Soil Deformations Due to Cyclic Loads on Offshore Structures", Chapter 13 in Numerical Methods in Offshore Engineering, Wiley.
- Lambe, T.W. (1967) "The Stress Path Method", Proceedings of ASCE, Journal of Soil Mechanics and Foundations Division, Vol.93, SM6, November.
- Lambe, T.W. and Marr, W.A. (1978) "Stress Path Method - Second Edition", to be published.
- Woods, R.D. (1978) "Measurement of Dynamic Soil Properties", Proceedings of ASCE Geotechnical Engineering Division Specialty Conference, Vol.1, pp. 91-178.

STRESS	REQUIRED INFORMATION
PAST "stress history"	<ul style="list-style-type: none"> * Geologic past - gravity, chemical, temperature, strain, time, climate. * <i>Key question - Largest past effective stresses?</i>
PRESENT "initial stress"	<ul style="list-style-type: none"> * gravity, pore water pressure, horizontal stress. * <i>Values obtained from measurements.</i>
FUTURE-IMPOSED "changes in stress"	<ul style="list-style-type: none"> * changes due to construction and flow of water. * <i>Magnitude depends on stress-strain relation of soil.</i>

FIGURE 1: Factors Influencing Stress Path

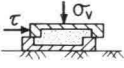
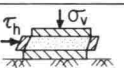
DEVICE	CAPABILITY	DIFFICULTY
DIRECT SHEAR 	alter τ , σ_v to measure strength	complex displacement pattern imposed; cannot obtain strain
TRIAXIAL 	alter σ_v , σ_r measure ϵ_{axial} , ϵ_{volume}	two of three principal stresses always equal
SIMPLE SHEAR 	alter σ_v , τ_h ; $\epsilon_r = 0$ measure δ	difficult to determine horizontal stress
PLANE STRAIN 	alter σ_v , σ_x ; $\epsilon_y = 0$ measure ϵ_{axial} , ϵ_{volume}	sophisticated equipment not commonly available, friction problems
TRUE TRIAXIAL 	alter σ_v , σ_x , σ_y , τ_{vx} , τ_{xy} , τ_{yv} measure ϵ_v , ϵ_x , ϵ_y , δ	complex test to run, no data for cyclic loads
TORSIONAL SHEAR 	alter τ_{θ} measure δ	non-uniform strains
SHAKE TABLE 	alter τ_h measure δ	limited stress states

FIGURE 2: Laboratory Devices to Obtain Stress-Strain Behavior

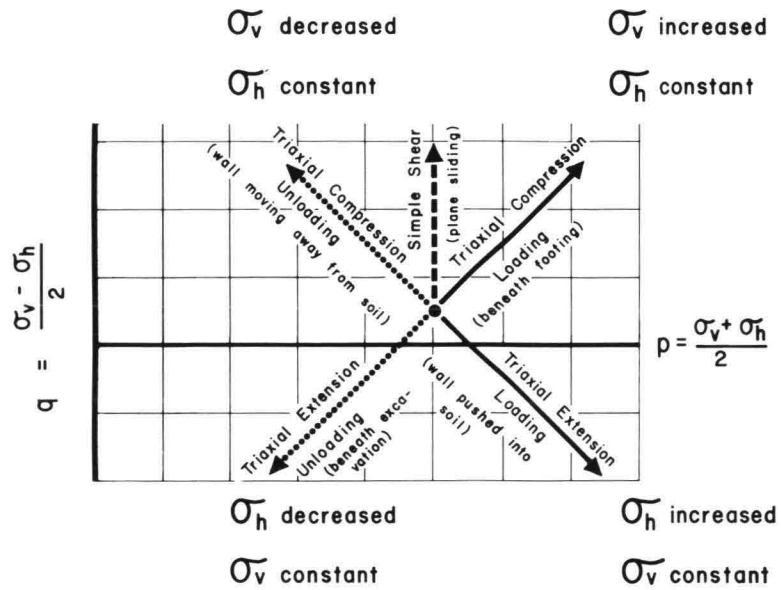
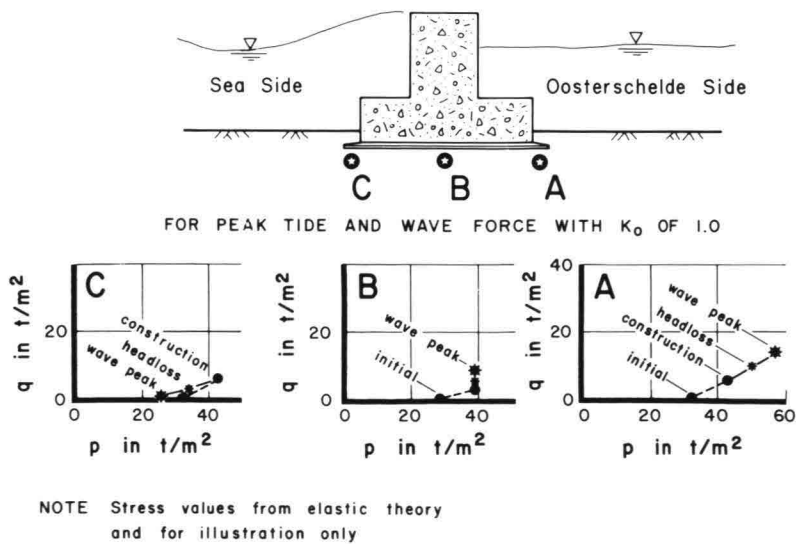


FIGURE 3: Typical Total Stress Paths



NOTE Stress values from elastic theory and for illustration only

FIGURE 4: Stress Paths in Pier Foundation

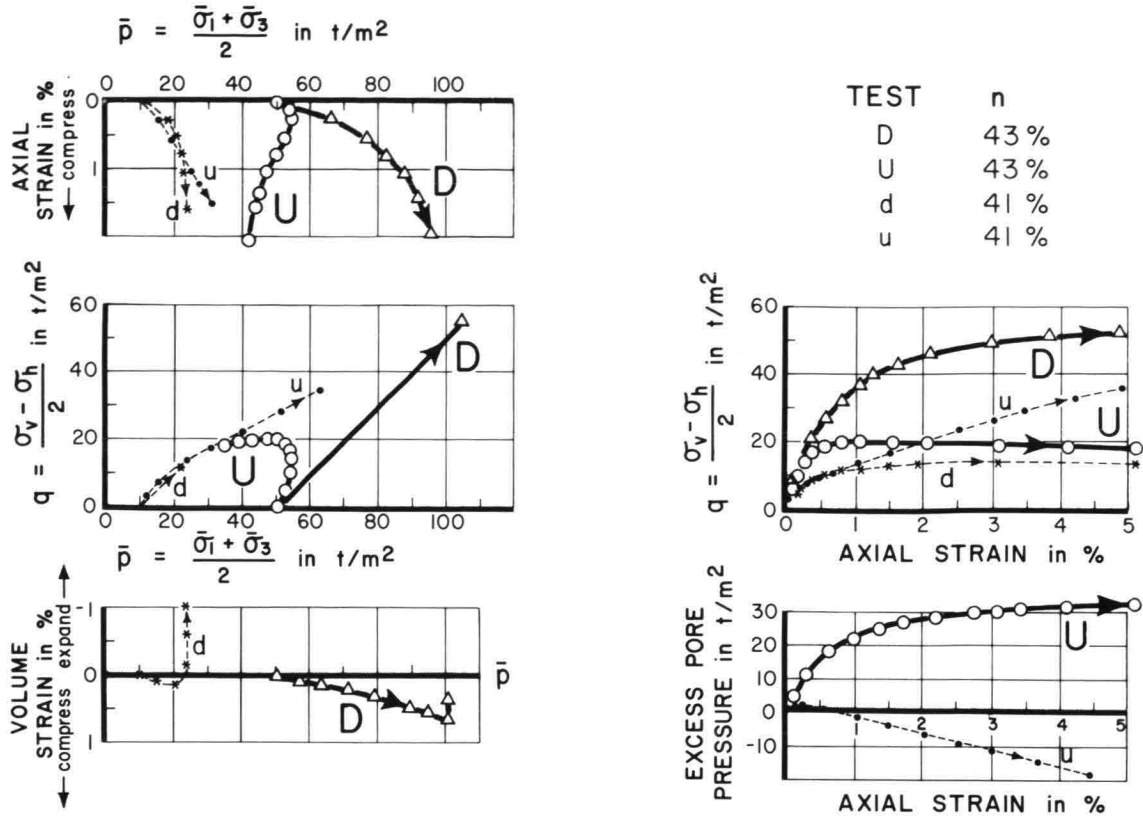


FIGURE 5: Drained and Undrained Triaxial Tests

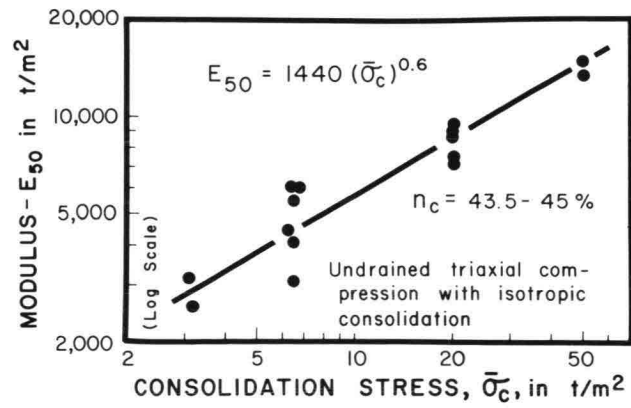


FIGURE 6: Modulus for Oosterschelde Sand

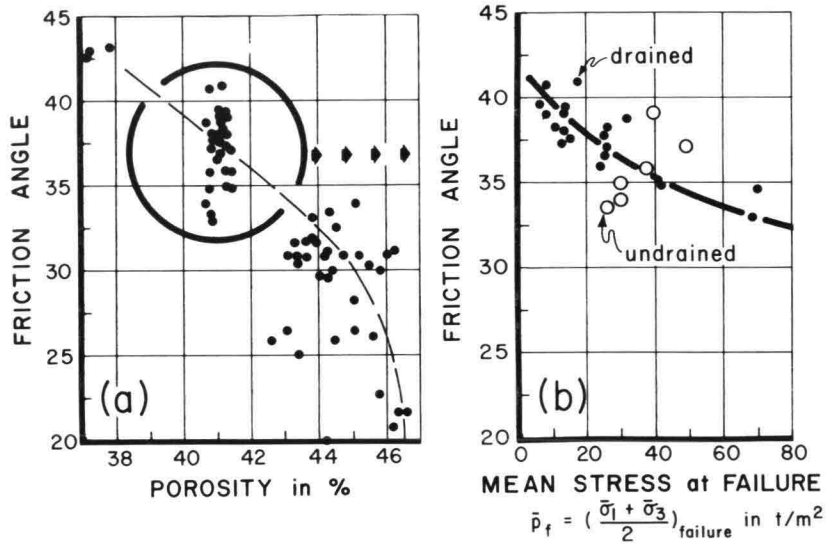


FIGURE 7: Friction Angle for Oosterschelde Sand

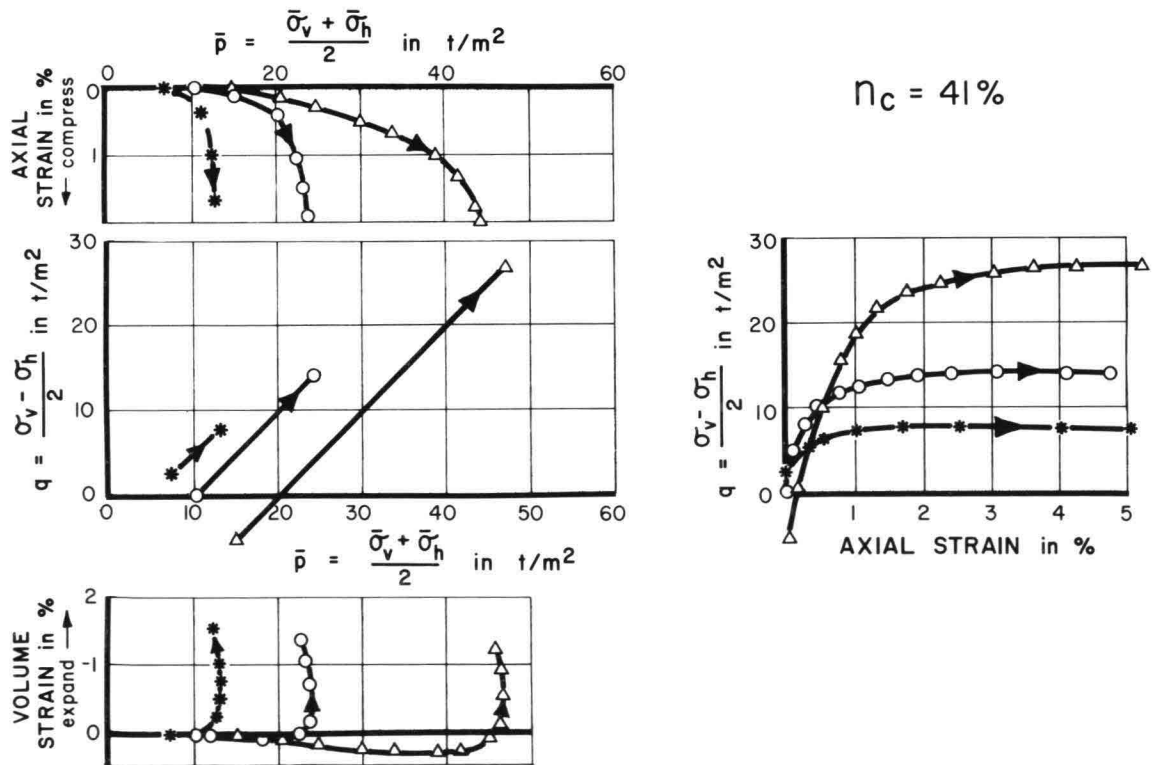


FIGURE 8: Static Triaxial Tests for Different Initial Stresses

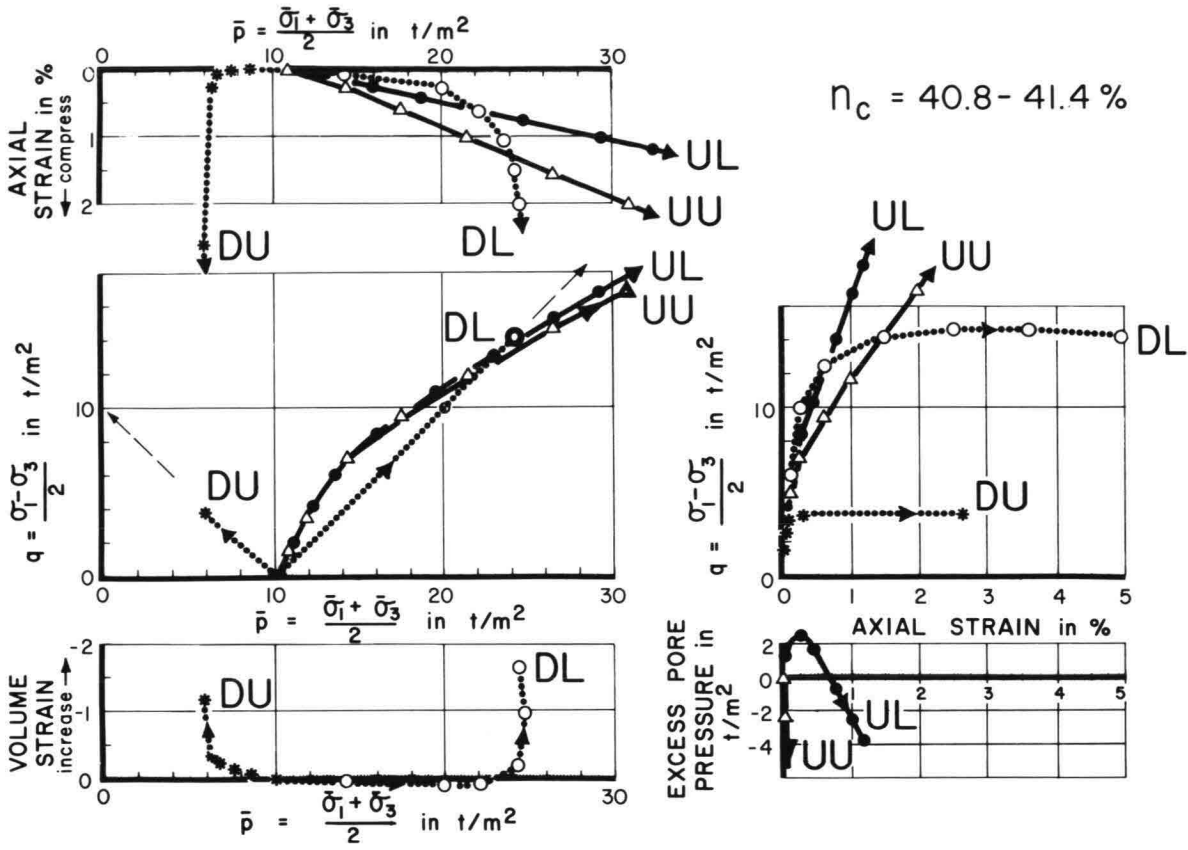


FIGURE 9: Static Triaxial Tests for Different Total Stress Paths

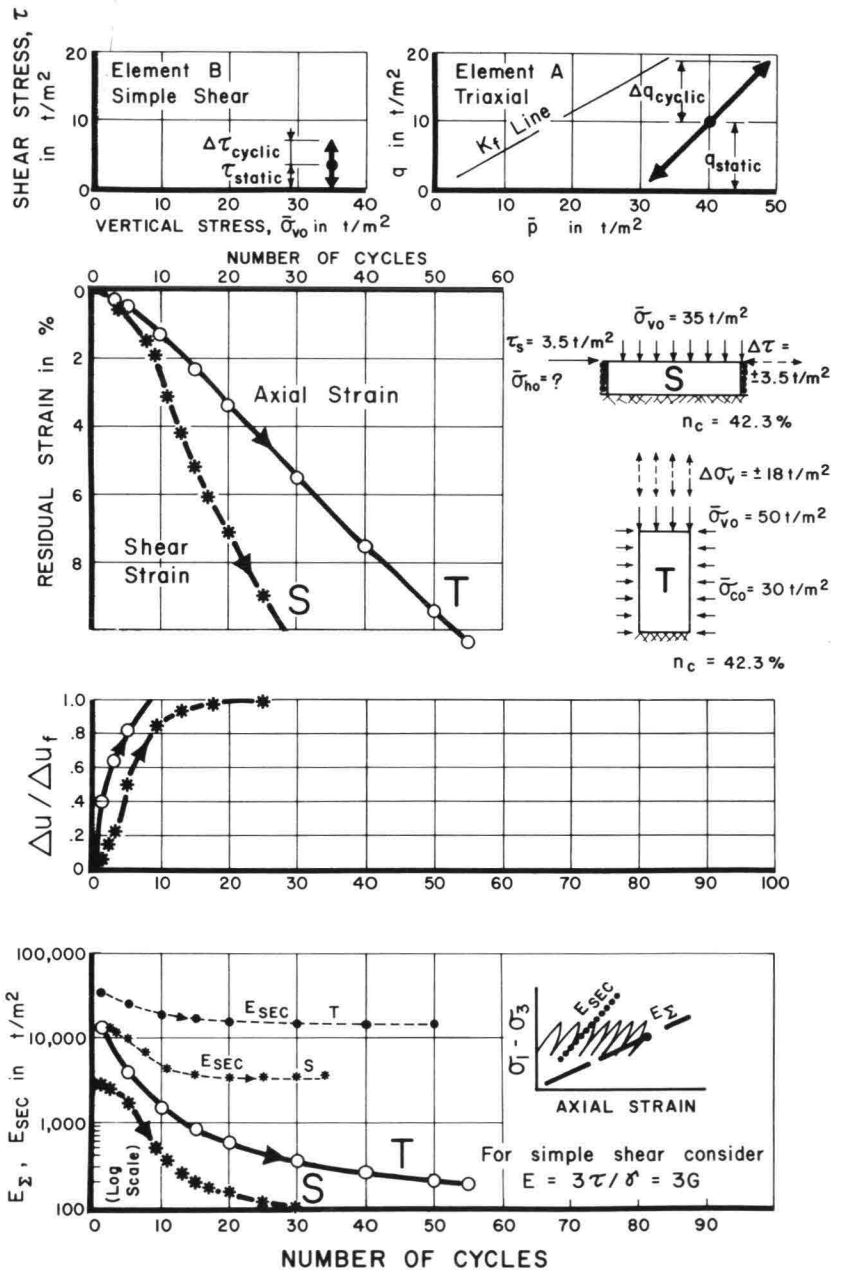


FIGURE 10; Undrained Cyclic Simple Shear and Triaxial Tests

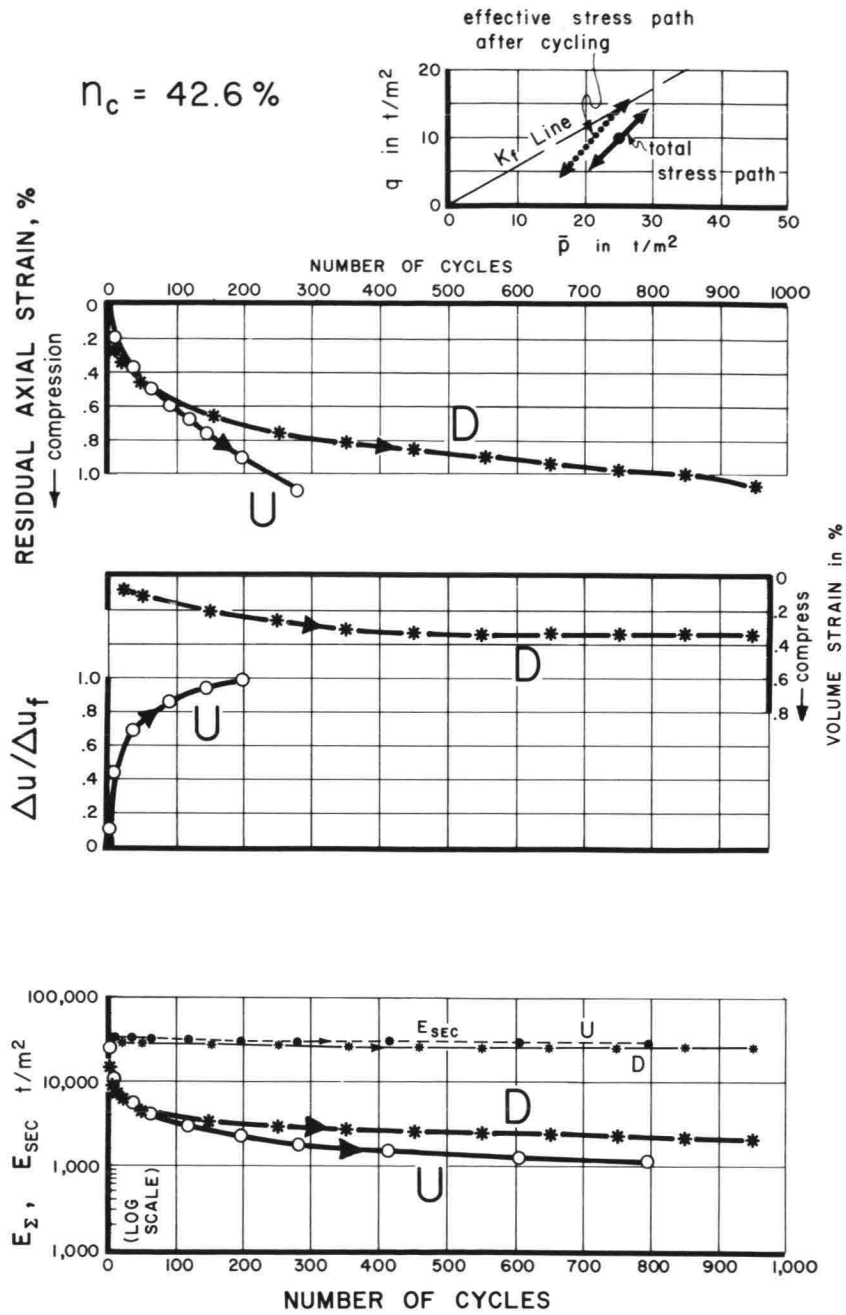


FIGURE 11: Comparison Between Drained and Undrained Cyclic Triaxial Tests

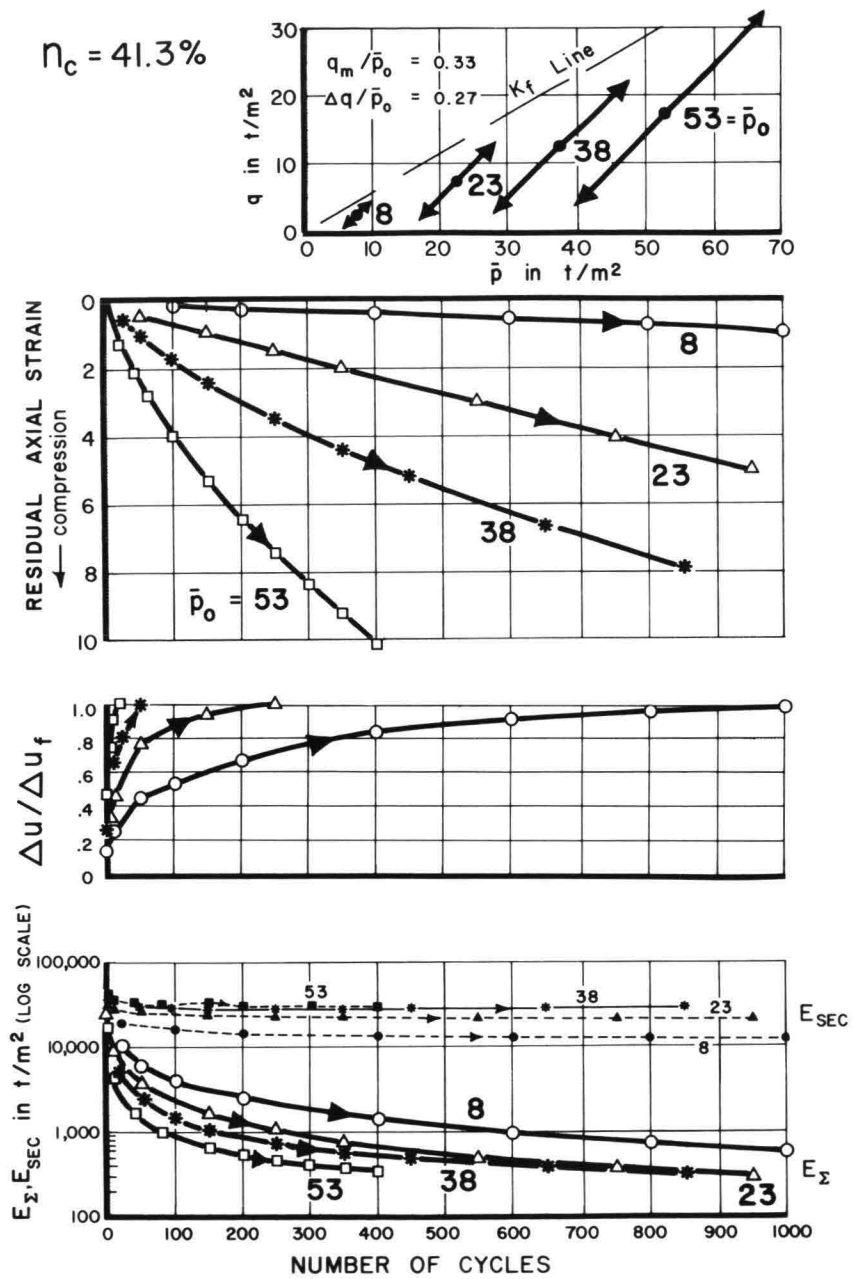


FIGURE 12: Effect of Stress Level in Cyclic Triaxial Tests

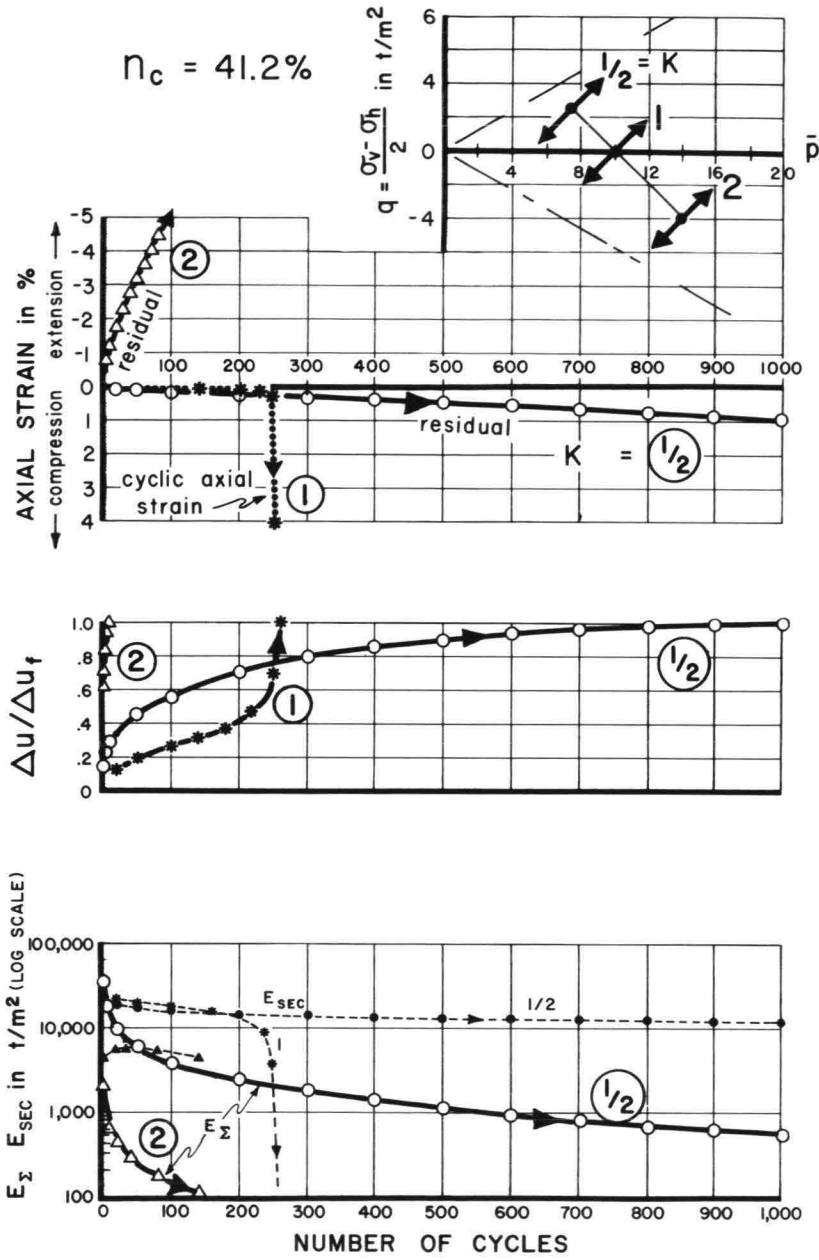


FIGURE 13: Effect of Initial Stresses in Cyclic Triaxial Tests

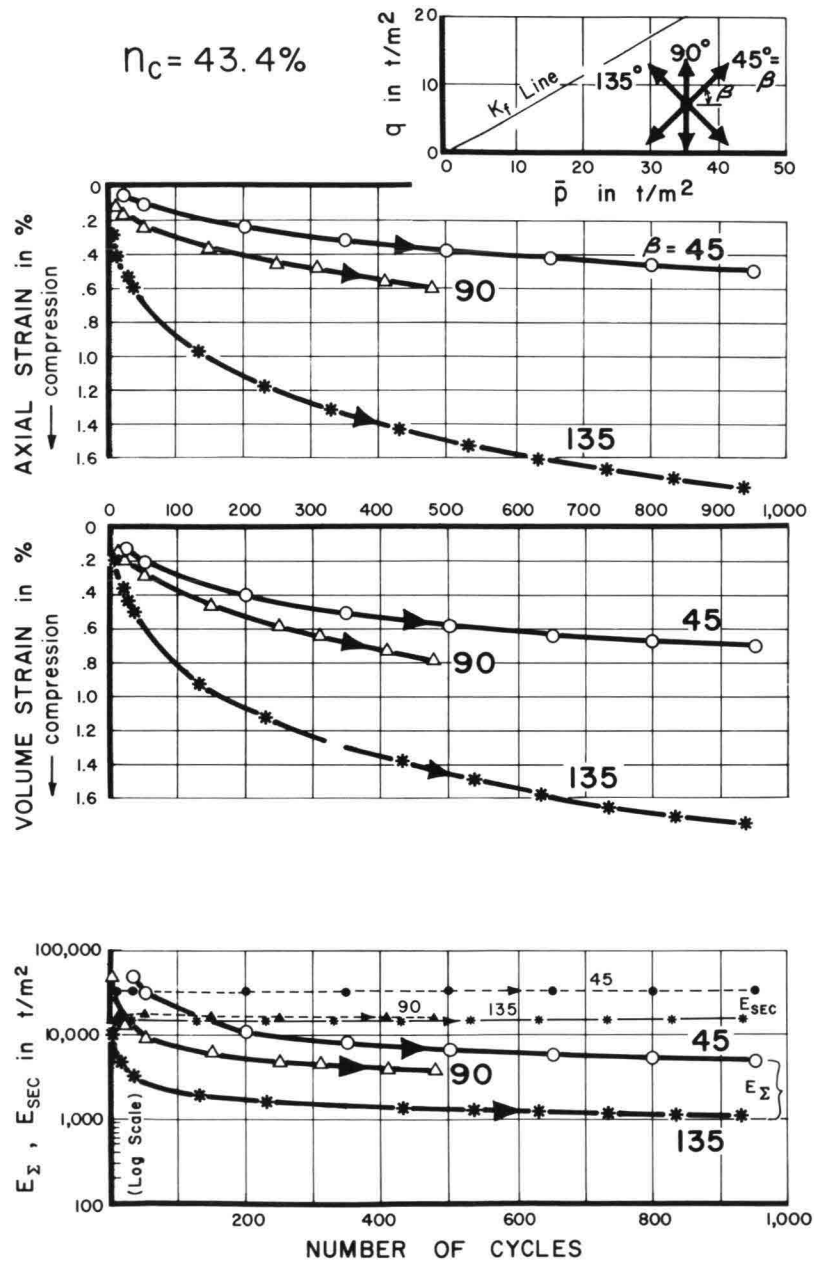


FIGURE 14: Inclination of Stress Path in Drained Cyclic Triaxial Tests

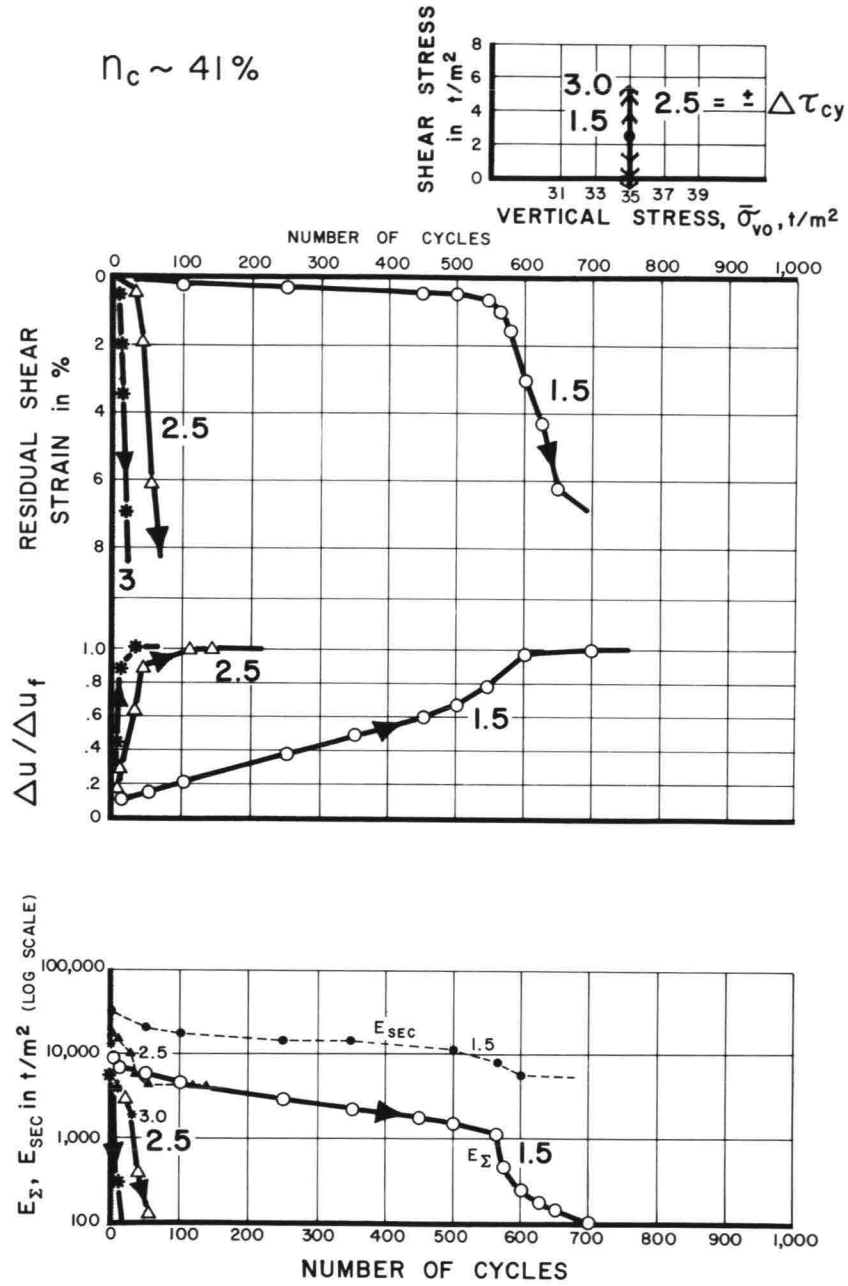


FIGURE 15: Cyclic Shearing in Simple Shear Tests

SYMPOSIUM ON FOUNDATION ASPECTS OF COASTAL STRUCTURES

STRESS-STRAIN BEHAVIOUR FOR FINITE ELEMENTS

by:

Ton Biegstraaten, Rijkswaterstaat Deltadienst
Den Haag, The Netherlands

Cor Kenter, Delft Soil Mechanics Laboratory
Delft, The Netherlands

SUMMARY

In this paper a description is given of the development of the stress-strain model of Consol. Consol is the finite element program that is used for most of the computations for the foundation of the Oosterschelde storm surge barrier. The development leading to the final stress-strain model is described together with investigations for the solution method of the non-linear equations. The resulting model is compared with data of parametric triaxial stress path tests. A method is given to include the influence of drained load cycles on stress-strain behaviour. The frame work for present and future work will be outlined.

I. HISTORY

Consol was originally developed at M.I.T. by Christian and Boehmer in 1969 [1] as a linear elastic consolidation program. After introduction at Rijkswaterstaat in 1970 it was further developed to include other types of boundary conditions.

For a better description of the stress and displacement patterns a simple non-linear version was made. A bi-linear shear relation solved by a secant one step approach was used.

In 1974 a linear relation between the shear stress level and resulting volume change was included [2].

In 1975 an incremental version was made in order to cope with multistep loading. This version was based on the approach used by Duncan [3] and later by Christian [4] and is the basic version of the present stress-strain model. It will be described and then followed by a description of adjustments and investigations concerning the accuracy of the model.

II. THE BASIC STRESS-STRAIN RELATIONII.1. Shear relation

Shear loading ($\tau/\tau_p > (\tau/\tau_p)_{\max}$)

$$\tau = \frac{\gamma}{a+b\gamma} \quad \text{when } \tau \leq \tau_p \quad (1)$$

τ = maximum shear stress
 γ = maximum shear strain
 a, b = parameters ($\frac{1}{a}$ initial tangent modulus, $\frac{1}{b}$ asymptatic value for τ)
 τ_p = the peak value for τ at the present isotropic stress
 $(\tau/\tau_p)_{\max}$ = the maximum shear stress ratio value previously reached

The relation resembles the one given by Kondner [5] and used by Duncan [3]
The tangent modulus is equal to:

$$G_T = \frac{d\tau}{d\gamma} = \frac{1}{a} (1-b\tau)^2 \quad (2)$$

a depends on $\bar{\sigma} = \frac{1}{2}(\bar{\sigma}_x + \sigma_y)$ analogous to [3] , [4]

$$\frac{1}{a} = H_\ell p_a \left(-\frac{\bar{\sigma}}{p_a}\right)^N \quad (3)$$

$H_\ell, N = \text{constants}$

$p_a = \text{atmospheric pressure (pressure reference value)}$

$$b = \frac{R_f}{\tau_p} \quad (4)$$

$R_f = \text{constant describing the difference between the asymptotic value of}$

$\tau (= \frac{1}{b}) \text{ and } \tau_p.$

τ_p follows from the Mohr-Coulomb failure criterion.

$$\tau_p = -\bar{\sigma} \sin \phi + c \cos \phi \quad (5)$$

$\phi = \text{angle of internal friction}$

$c = \text{cohesion}$

Shear unloading ($\tau/\tau_p \leq (\tau/\tau_p)_{\max}$)

$$G_T = H_u p_a \left(-\frac{\bar{\sigma}}{p_a}\right)^N \quad (6)$$

$H_u = \text{constant}$

$p_a, N = \text{identical to loading values}$

$H_\ell, H_u, N, p_a, \phi, R_f, c \text{ are input parameters}$

II.2. Compression relation

Compression loading ($\bar{\sigma}_{\text{vol}} < \bar{\sigma}_{\text{vol max}}$)

$$\bar{\sigma}_{\text{vol}} = \frac{K_i}{A} (e^A \epsilon_{\text{vol}} - 1) \quad (7)$$

$$\bar{\sigma}_{\text{vol}} = \frac{1}{3} (\bar{\sigma}_x + \bar{\sigma}_y + \bar{\sigma}_z)$$

$$\epsilon_{\text{vol}} = \epsilon_x + \epsilon_y + \epsilon_z$$

$K_i, A = \text{constants}$

Relation (7) is based on Terzaghi's one dimensional compression law extended to more general stress-strain components.

The tangent modulus K_T is equal to:

$$K_T = \frac{d\bar{\sigma}_{\text{vol}}}{d\epsilon_{\text{vol}}} = K_i + A \cdot \bar{\sigma}_{\text{vol}} \quad (8)$$

Unloading ($\bar{\sigma}_{\text{vol max}} \leq \bar{\sigma}_{\text{vol}} < 0$)

$$K_T = K_u$$

$K_u = \text{constant}$

Tension ($\sigma_{vol} \geq 0$)

$$K_T = K_{ten}$$

$$K_{ten} = \text{constant}$$

K_i, A, K_u, K_{ten} are input parameters.

II.3. Dilatancy

The term dilatancy is used for the volume change due to shear strain change. This distinguishes it from volume change due to compression. The basic law can be expressed in differential form:

$$d \epsilon_{vol}^d = D d\gamma \quad (9)$$

$d \epsilon_{vol}^d$ = the volume change from dilatancy

D = the dilatancy modulus

Two cases are distinguished:

a. Dilatancy during shear loading.

In this case $d\gamma$ is the non-elastic shear strain change of the difference between the shear strains when using loading and unloading parameters.

$$D = \frac{\sin \phi_t + \tau/\bar{\sigma}}{1 + \sin \phi_t \tau/\bar{\sigma}} \quad (10)$$

This formula is based on Rowe's stress-dilatancy concept [6]

ϕ_t = an input parameter.

- b. Dilatancy during shear unloading.

$d\gamma$ = the shear strain change

D = constant (input parameter)

II.4. Solution procedure

The solution procedure is often referred to as the tangent stiffness method. It is an Eulerian type of integration procedure in which the total load to be applied is divided into a number of steps. At the end of each step the tangent moduli (K_T, G_T and D) are determined which are kept constant during the next step.

For the stiffness terms Hooke's law is used, in tensor notation:

$$\Delta \sigma_{ij} = (K_T - \frac{2}{3} G_T) \delta_{ij} \Delta \epsilon_{kk} + 2G_T \Delta \sigma_{ij}$$

δ_{ij} is the Kronecker delta, $\Delta \sigma_{ij}, \Delta \epsilon_{ij}$ are the stress and strain increment tensors.

Dilatancy is included by means of a load vector iteration procedure (initial strain method [7]).

III. ORIENTATION OF THE STRAIN TENSOR INCREMENT

When the model described in II was applied to the problem of horizontally loaded caissons the computed failure load was lower than the expected failure load. The caisson was sliding over the upper layer of the soil with very small influence on the deeper layers.

The program seemed to "forget" the weight of the caisson and the previous loading path had only a slight influence.

Looking at the model this becomes clear because each step is basically an elastic computation in which the incremental strain tensor is co-axial with the incremental stress tensor. Tests done in Cambridge [8] however, have shown that for shear loading it is a better approximation to assume co-axiality between the incremental strain tensor and the total stress tensor while the co-axiality between stress and strain increment tensor during unloading can be maintained. The assumption now made is to have co-axiality between the elastic incremental strain tensor and the incremental stress-tensor and co-axiality between the non-elastic incremental strain tensor and the total stress tensor.

The necessary correction can be applied by using the same iteration method as used for dilatancy. The initial strain term is computed as follows.

The computed strain increment is coaxial with the stress increment. From unloading parameters the elastic strain increment can be computed, which can be subtracted from the strain increment resulting in the plastic strain increment. This is also coaxial with the stress increment. Because the solution procedure is based on the stress situation at the end of the previous load increment, the orientation of the state of stress is also taken at the same situation. The plastic strain tensor must be rotated over the angle difference between the state of stress and the stress increment orientation, which keeps the shear strain and volumetric strain the same. The difference between the rotated and original tensor is the initial strain tensor which must be added to the computed strains.

IV. ACCURACY OF THE SOLUTION METHOD

Apart from the finite element method which will not be discussed here the convergence of the solution method can be investigated. This can be done by assuming a very simple equilibrium situation e.g. an idealized plane strain test. The tangent stiffness method can be programmed very easily for such a case. Because the shear and compression relations (1), (7) relate to total values, results for the idealized plane strain tests can be known exactly when excluding dilatancy and the strain orientation correction.

Three types of stress-path's were checked:

Type A ($\sigma_x + \sigma_y$) constant, τ increasing

Type B σ_x constant, σ_y decreasing

Type C τ constant, ($\sigma_x + \sigma_y$) decreasing

Two types of material were used, a weak and a stiff material (M1 and M2)

	ϕ	N	p_a	R_f	H	N_i	A	K_u	Stresses in kN/m^2
M1	38°	0.5	100	0.9	65	3600	-180	$5 \cdot 10^4$	
M2	42°	0.5	100	0.9	254	8780	-400	$14 \cdot 10^4$	$\nu = 0.4$ (assumed constant)

All stress path's start at a value of 100 kN/m^2 for $\bar{\sigma}$ and 0 for τ except the type C path, which starts with $\tau = 25 \text{ kN/m}^2$.

Each path was computed with the Euler type of approach using 10, 20 and 40 increments.

The results were checked against the exact solution but also against a higher order type integration method which includes not only the starting values of the stresses but also the final values of the stresses^{*)}. Because the tests are stress controlled, the integration rule is the trapezoid rule. All computed ϵ_{vol} values were accurate or nearly accurate and it is not worthwhile to reproduce the figures. The shear strain behaviour was more interesting. While the type A path gives approximately the exact values, the type B path deviates significantly and the type C path shows no shear strain at all, thus indicating a rather serious error in the derivation of the equations.

The error is contained in the derivation of the tangent shear modulus in which first a and b were assumed constant and later after determining the tangent shear modulus were made a function of $\bar{\sigma}$.

The derivation of the correct equations is given in appendix 1, together with the description of the solution procedure for both the integration methods.

The description of the results can be divided into two parts:

- 1) Comparison of the correct and incorrect method.
- 2) Comparison of the two integration methods with the exact results.

ad 1. Comparison of the correct and incorrect method.

When looking at the resulting equations in appendix 1 the difference between the correctly and incorrectly derived equations is caused by the interdependency of the shear strain and the isotropic stress.

The shear strain change is both a function of the change of the shear stress and the isotropic stress.

The result of the test computations agrees with this. The type A path gives no difference between both methods. The type B path gives a difference of up to 80% for the strains and 10% for the stresses.

The type C path gives no shear strain at all for the incorrect method. The stiff material is a little bit more sensitive for using the correct equations.

When 40 increments are used the integration error for the type B path is smaller than the formulation error.

Some results for the weak material can be found in fig. 1, 2, 3 using 40 steps.

Conclusion: For specific stress paths it can be very important to use the correct method, especially for paths between the type B and C path. Such paths can be found on the sea side of the Oosterschelde structure.

ad 2. Comparison of the two integration methods with the exact results.

All paths show the same behaviour for both materials. For material M1 the results for the type C path are given in fig. 4. For material 2 the results for the type A path are given in fig. 5. Both using 10 and 40 increments for the Euler method and 10 for Heun's method.

Euler 40 or Heun 10 are accurate enough. It is interesting to note that one Heun step has about the same execution time as two Euler steps, so for the present tests Heun's method is more efficient.

Also considering the larger stability region when using a higher order method makes the Heun method become more favourable than the Euler method.

Considering these results the program Consol should be changed. It will become more efficient when using a Heun integration scheme. This however was too difficult to do in Consol.

It seems necessary however to use the correct solution method. It was programmed, adding a third initial strain iteration. For the not too complicated problems the results were better than expected. Stress paths were following the failure line in stead of crossing it.

*) (a Heun type of approach)

It made results worse than they were only when reaching the origin of the τ - σ diagram. This happens at the tension side of the Oosterschelde constructions. This primarily numerical problem was never solved properly, the integration-iteration scheme was too unstable. So most computations were still made with the incorrect solution method. There is however one justification (though only a practical one) for doing so. When computing stress paths with both increasing τ and σ the integration and formulation errors have opposite signs and counteract each other. These stress paths are fortunately important ones. From the mathematical point of view it is just wrong.

V. ELASTO PLASTICITY

When examining the resulting equations and the behaviour of the model one can see a great similarity with the so called elastoplastic formulation in which a yield surface moves as a function of the stresses and a hardening parameter in the stress space. At the time of building the mechanism to change the orientation of the strains it was possible to switch to an elasto plastic formulation. The required result could then be obtained in a more straight forward way. Some changes would have been necessary. These were:

- a) The shear-stress shear strain relation now determines the total shear strain in the new model it would be the plastic shear-strain.
- b) The same applies to the compression relation.
- c) The unloading criterion for shear would be different, this will be discussed later.
- d) Unloading dilatancy does not fit in the model and additional methods are still necessary.
- e) The resulting equations will be non symmetric so a different solution procedure must be implemented.

The reasons for not doing so, were:

- a) There was no experience with elastoplastic models.
- b) Consol is a production program, not a research project.
- c) Changing the existing model was very simple.
- d) Evaluation of model parameters is more simple for the existing model because the elastic strains need not be subtracted from the total strains.

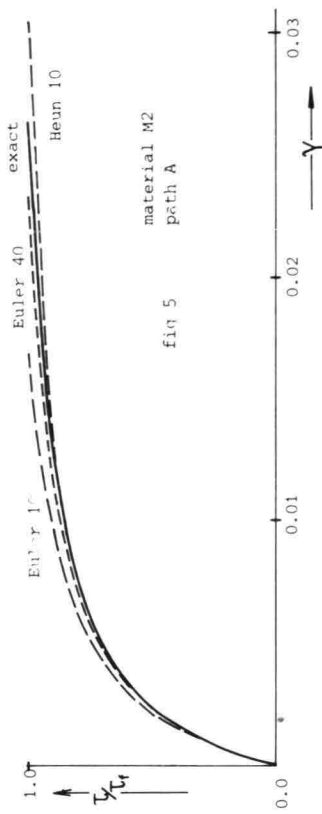
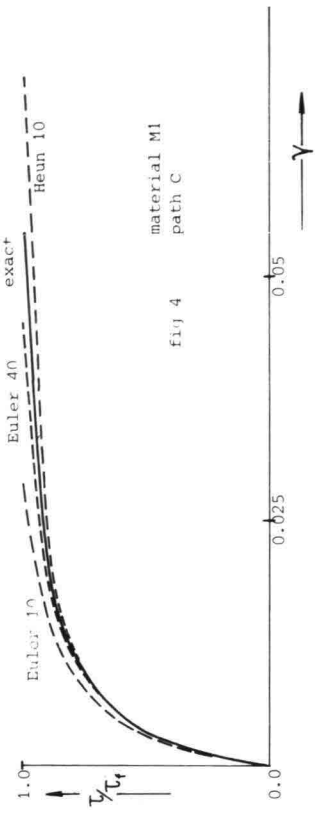
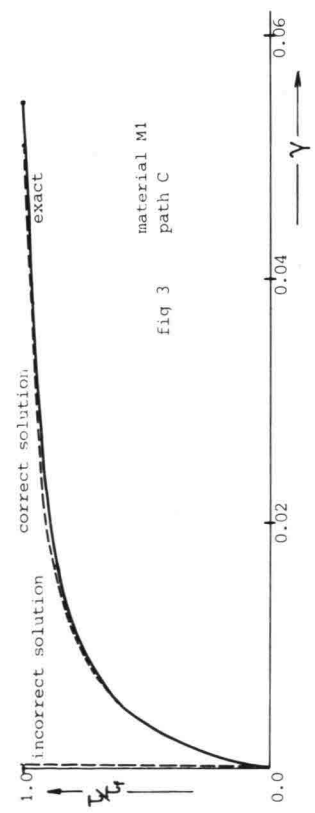
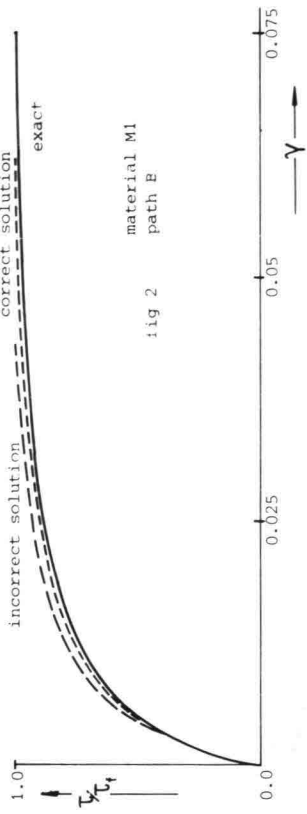
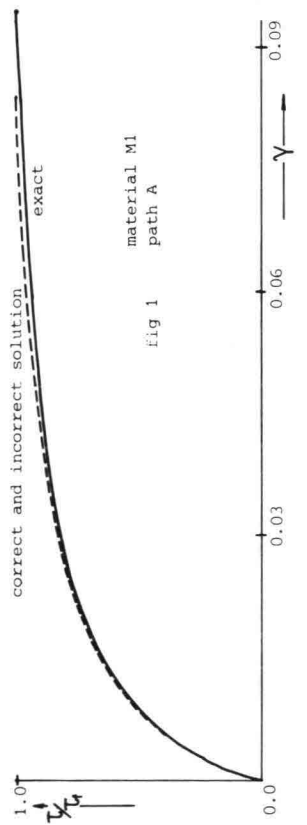
At the Delft University of Technology a project was being developed which turned out to be an elastoplastic variant based on the same type of equations. The model, called ELPLAST, developed by Vermeer is described in [9]. The most important difference is the unloading criterion. It is not based on the stresses (chapt. II) but on the plastic shear strain (γ_p). Based on the equations given here (1, 2, 4):

$$\gamma^p = \frac{\tau}{H_0 \cdot p_a \cdot \left(-\frac{\sigma}{p}\right)^N (1-R_f \cdot \frac{\tau}{\tau_p})} \quad (11)$$

ELPLAST can use other equations e.g. a cubic spline function for the shear relation.

Drawn in the τ , $\bar{\sigma}$ diagram the lines resulting for each value of γ_p are not straight as in Consol but curved. So for K_0 paths Vermeer's model predicts plastic strains while Consol only gives elastic-strains. Laboratory tests (referred to in [9]) are in favour of Vermeer's model.

At the end of chapter IV a problem was mentioned which occurred when the stresses reached the origin of the τ , σ diagram. This could not be avoided in Consol.



CONSOL MODEL ACCURACY OF SOLUTION METHOD.

It was also met in ELPLAST. An extra vertical yield surface at low pressure topping the Mohr Coulomb cone, and the use of interface elements was sufficient for solving the problem.

Both programs, Consol and ELPLAST have been used for computations for the storm surge barrier. Results will be given in another paper by Kenter and Vermeer.

VI. DETERMINATION OF PARAMETERS

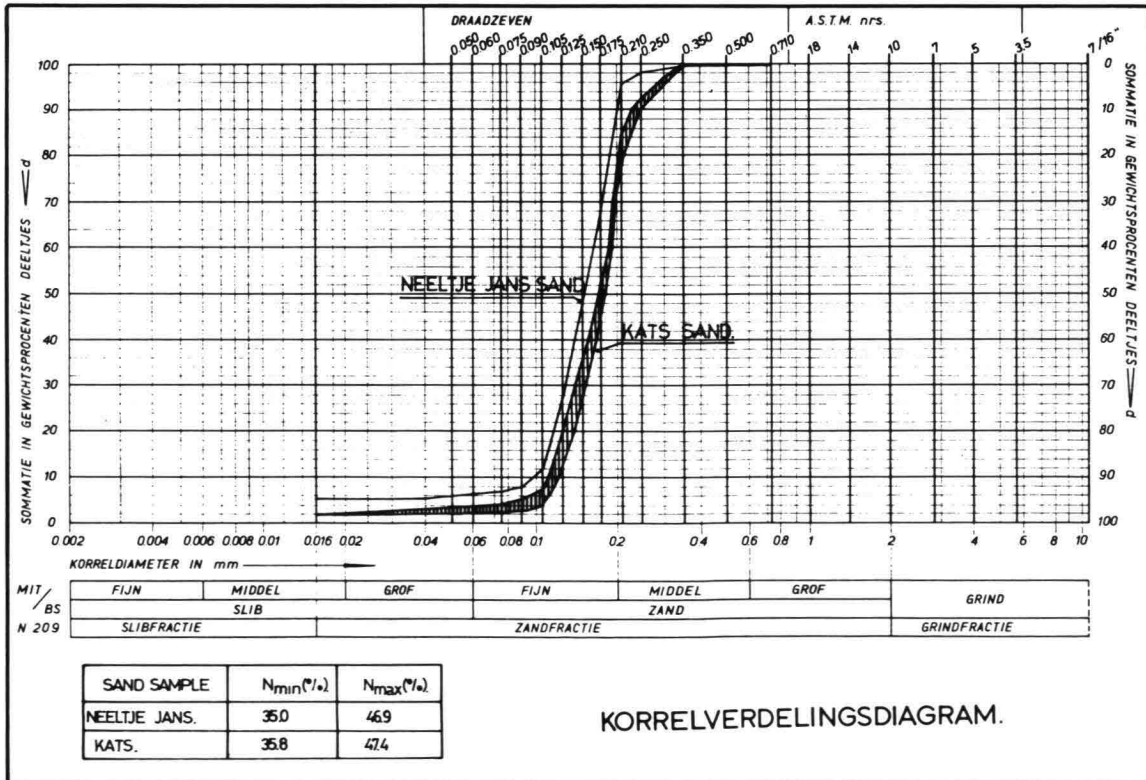
VI.1. Static parameters for sand

Quality of the stress-strain model

The quality of a Kondner-Duncan type stress-strain model as described in the previous chapters, was tested by a great number of drained, static triaxial tests on sand.

A rather defective model will only give correct results for stress-paths of the type the parameters were determined from. In that case for each type of stress- path that is found in prototype conditions, a rather complicated stress path test is required. On the other hand a correct stress-strain model only needs a few simple laboratory tests for the determination of the parameters and various more complicated prototype stress-strain conditions can be described. Because of the great number of piers and different soil conditions associated with them, a thorough study of the correctness of the stress-strain model was of economical importance.

The test program was conducted on fine ($d_{50} = 175 \mu$) rather uniform sand, which had little angularity. The sand is very similar to the Neeltje Jans sand and characteristic for the Oosterschelde.



27 Triaxial tests were run, apart from rehearsals. All tests were drained and mainly static. One load cycle was included in the consolidation stage as well as the shear stage, in order to examine the unloading and reloading behaviour. The samples were remoulded.

The test parameters were:

- porosity ($n = 39\%, 43\%$)
- consolidation stress ($p = 50, 100, 200, 500 \text{ kN/m}^2$)
- anisotropy during consolidation ($K_o = 0.33, 0.5, 1.0, 2.5$)

- shear mode (extension $\frac{\Delta\sigma_H}{\Delta\sigma_V} = -1, \infty$, compression $\frac{\Delta\sigma_H}{\Delta\sigma_V} = 0, -1$)

A more detailed description of the tests is given in [11] and [12].

By trial and error the CONSOL-material parameters which gave the best fitting curves were determined. Some characteristic curves are given in fig. 6.11, together with the results of the respective triaxial tests. Because strains and displacements due to the dead weight of the soil (consolidation-stage) are set zero in CONSOL-calculations, the CONSOL-curves and triaxialtest-curves coincide after the consolidation-stage. Moreover, this skips the rather indefinite stress-strain behaviour at lower stress levels. In general a good agreement was found between the theoretical and empirical curves, even for widely differing stress paths.

This means that for Oosterschelde sand a wide range of stress paths, which are found in prototype conditions, can be represented by one rather simple stress path for determining the stiffness parameters.

E.g. a good and simple test to determine the stiffness-parameters for sand underneath the pier foundation may be the following very common triaxial test:

- isotropic consolidation to a characteristic stress level, unloading and reloading (one cycle)
- shearing with constant confining pressure, unloading and reloading till failure.

Defects of the stress model and possible improvements

The main defects that were found in the CONSOL stress-strain relation are:

- The angle of internal friction ϕ and the unloading modulus for compression K_u are dependent on σ_{vol} according to the tests ($\frac{d\phi}{d\sigma_{vol}} \approx 10^{-2} \text{ o/kN/m}^2$). This is not the case in CONSOL.

This error is not serious, if the values are determined at characteristic stress-levels.

- Dilatancy is described poorly by one parameter ϕ_{tp} , indicating the turning point in dilatancy. Another parameter is required to define the magnitude. Besides, dependancy on σ_{vol} is not included. However, in drained conditions these defects will not have great influence.
- Anisotropy is not included in the CONSOL stress-strain model. The Oosterschelde sediments possess mainly a fabric with an n-fold ax. The stiffness in vertical direction is greater than in horizontal direction; the difference equals the difference due to about 2% decrease in porosity. If the rotation of the principal stresses is considerable, anisotropy may not be neglected.

A rather simple and practical way to include anisotropy in the stress-strain relation might be as follows:

1. determine from a triaxial compression and extension test $S_{\alpha=90^\circ}$ and $S_{\alpha=0^\circ}$ respectively. ($\alpha =$ angle between greatest principal stress and horizontal, $S =$ some stiffness parameter).
2. Adapt the tangent stiffness-parameters according to:

$$S_\alpha = S_{\alpha=90^\circ} - \frac{\alpha}{90} (S_{\alpha=90} - S_{\alpha=0})$$

α being determined at the end of the previous increment. Since α is not very sensitive for S , an iterative procedure may be omitted at small load increments.

Value of the parameters

The values of the stress-strain parameters which produce the curves best fitting on the test results were:

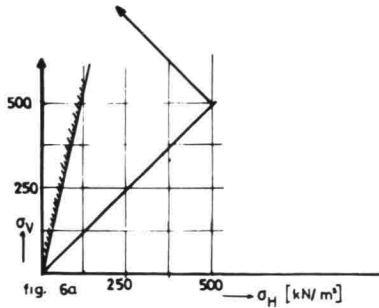


fig. 6a

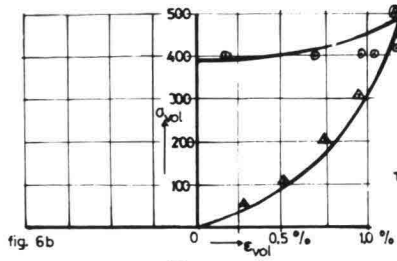


fig. 6b

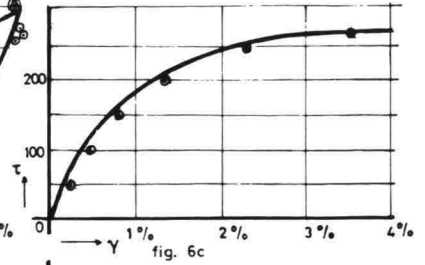


fig. 6c

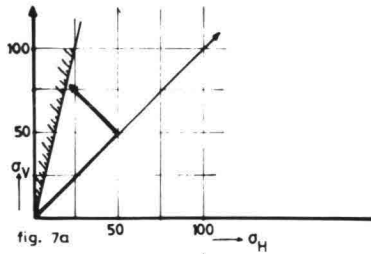


fig. 7a

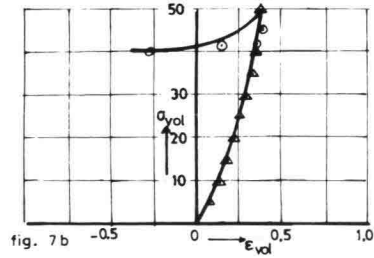


fig. 7b

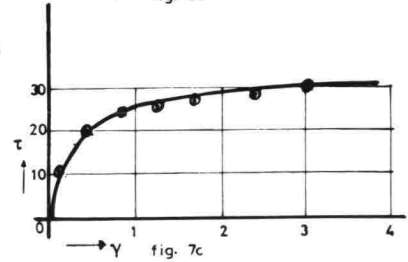


fig. 7c

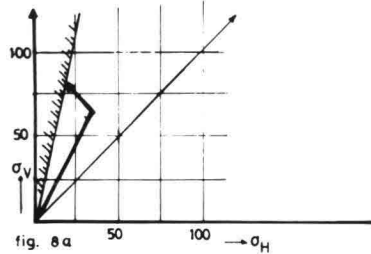


fig. 8a

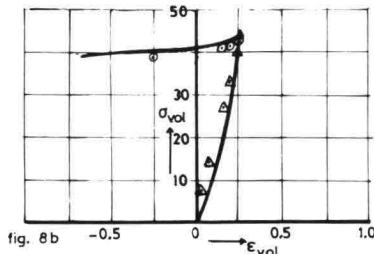


fig. 8b

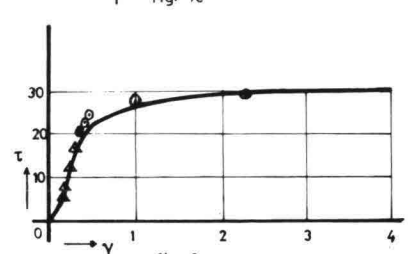


fig. 8c

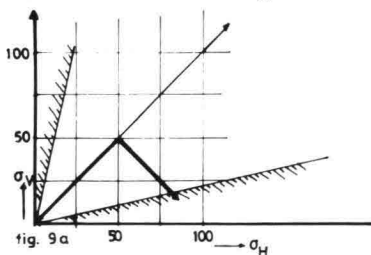


fig. 9a

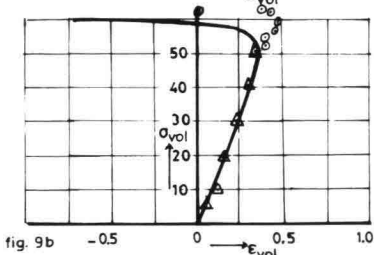


fig. 9b

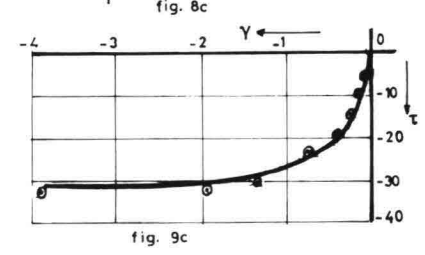


fig. 9c

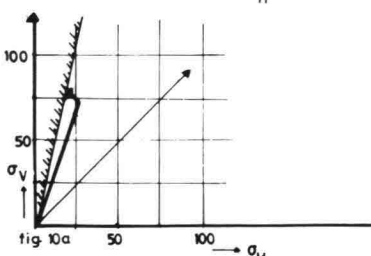


fig. 10a

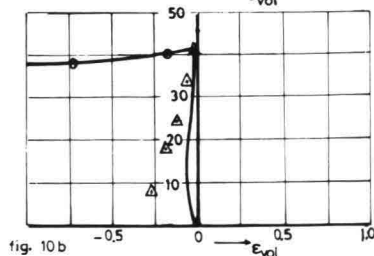


fig. 10b

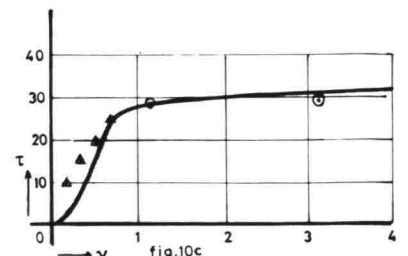


fig. 10c

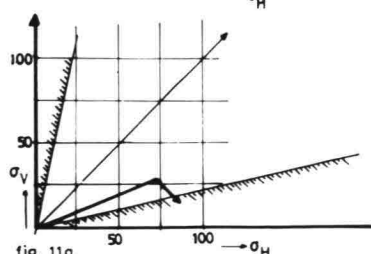


fig. 11a

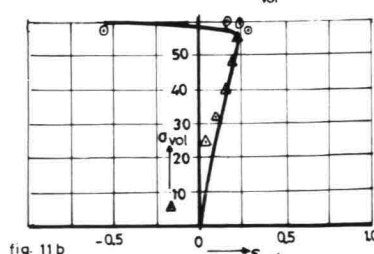


fig. 11b

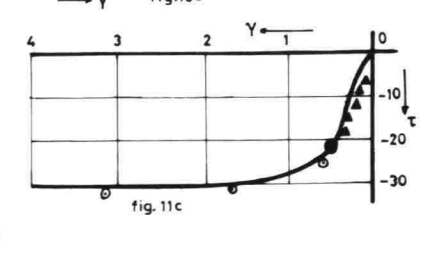


fig. 11c

<p>OOSTERSCHELDE FINE SAND STATIC DRAINED TRIAXIAL TESTS COMPARISON BETWEEN CONSOL AND TESTDIAGRAMS</p>	<p><u>SYMBOLS</u> ▲ TESTRESULT; CONSOLIDATION STAGE ⊙ TESTRESULT; SHEARSTAGE</p>
---	--

n = 39% (compaction by vibrating needles)	n = 43% (undensified)
$\phi = 40^\circ$	$\phi = 35^\circ$
$\phi_{tp} = 0^\circ$	$\phi_{tp} = 20^\circ$
A = 225	A = 150
Ki = 8500 kN/m ²	Ki = 7000 kN/m ²
Ku = 28000 kN/m ²	Ku = 14000 kN/m ²
H _l = 200	H _l = 150
Hu = 275	Hu = 150
N = 0.5	N = 0.5
R _f = 0.95	R _f = 0.95

These values may be looked upon as representative of the sand described above under drained, static conditions.

VI.2. Drained cyclic parameters for seagravel and slags

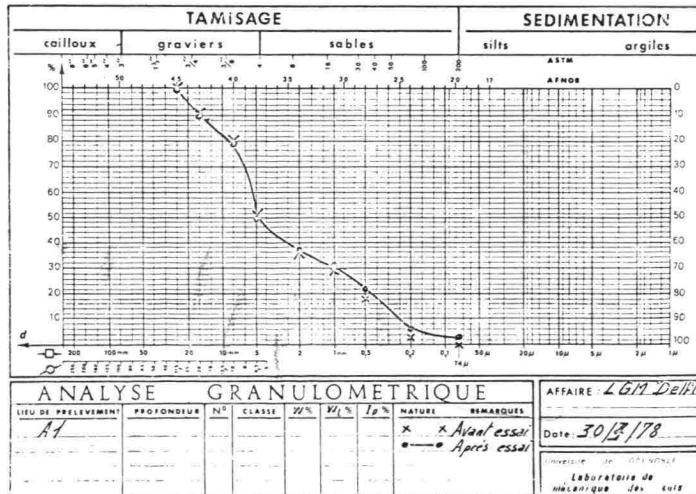
Testprogram

Seagravel or slags will be used immediately under the piers. It therefore has to endure a larger cyclic loading component than sand. Besides, it is more sensitive for cyclic deformation, because of the greater difference between maximal and minimal density. Determination of only static parameters therefore seems to be inadequate for seagravel.

A cyclic test program was set up, in which the following parameters were incorporated:

- relative density ($R_D = 0.3, 0.5, 0.6, 0.7, 0.8$)
- confining pressure ($\sigma_H =$ after consolidation)
- sand inclusion
- shearmode ($\frac{\Delta\sigma_H}{\Delta\sigma_V} = \infty, 0$, representing foundation bed and sill respectively)
- long time performance.

The tests were performed on 3 types of seagravel, one kind of slags and two types of quarry-stone, all with Fuller-type-grain-size distributions (fig. 12). Use was made of the big triaxial devices of the Universities of Karlsruhe (h = 2 m, $\phi = 1$ m) and Grenoble (h = 1 m, $\phi = 0.4$ m). Stress control on these apparatus has to be done by hand. This limits the possible cyclic stress paths to either increasing σ_H or σ_V , for practical reasons. Results of these tests are given in [14], [15].



Description of the method

In figure 13 several stresspaths are drawn, these were calculated with CONSOL for elements underneath the pier at the Oosterschelde-side. The consolidation stage of the stress-path for the triaxial test is determined so that it averages the calculated stress paths for deadweight and head-logs. The first five cycles of the cyclic load are run along the consolidation path ($\frac{\Delta\sigma_H}{\Delta\sigma_V} = K_0$). For practical reasons the other cycles are run along a $\sigma_H = \text{constant}$ path ($\frac{\Delta\sigma_H}{\Delta\sigma_V} = 0$), with the same amplitudes, being

$$\sqrt{(\Delta\sigma_H)^2 + (\Delta\sigma_V)^2}$$

In this way deformations are determined for two values of $\frac{\Delta\sigma_H}{\Delta\sigma_V}$ at the same amplitude (see figure 14):

These are:

$$\epsilon_K \text{ for } \frac{\Delta\sigma_H}{\Delta\sigma_V} = K_0 \quad (0 < K < 1)$$

and

$$\epsilon_0 \text{ for } \frac{\Delta\sigma_H}{\Delta\sigma_V} = 0$$

Deformations for values of

$$\frac{\Delta\sigma_H}{\Delta\sigma_V} = p \quad (0 < p < K_0) \text{ may be found}$$

by linear interpolation:

$$\epsilon_p = (1 + \frac{\epsilon_{K_0} - \epsilon_0}{K_0} \times \frac{p}{K_0}) \times \epsilon_0 = \alpha_p \times \epsilon_0$$

Because of the high safety coefficients and therefore rather linear behaviour of the construction, it is assumed that the factor α_p still holds for greater amplitudes.

Using these correction factors α_p , one can derive the strains ϵ_p^* belonging to an arbitrary stress path out of the strains ϵ_0^* belonging to a stress path with

$$\frac{\Delta\sigma_H}{\Delta\sigma_V} = 0, \text{ accordingly:}$$

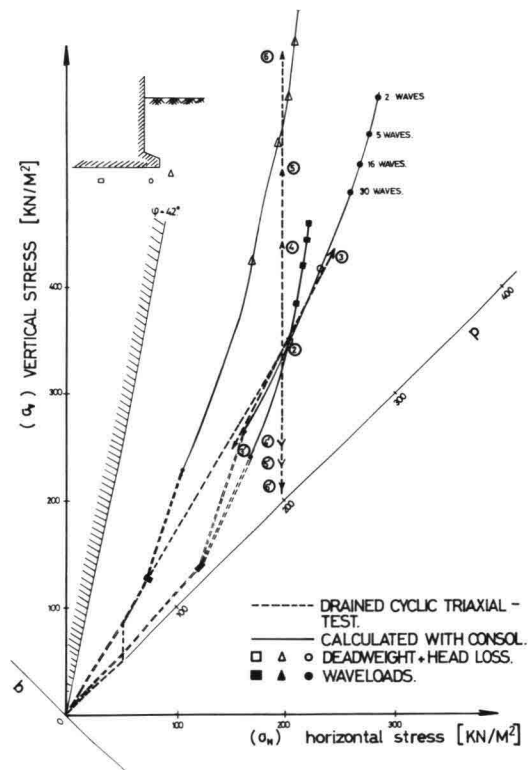
$$\epsilon_p^* = \alpha_p \times \epsilon_0^*$$

if the amplitude

$$\sqrt{(\Delta\sigma_H)^2 + (\Delta\sigma_V)^2} \text{ along both paths}$$

is the same. Three different amplitudes were applied in the triaxial tests, the smaller two counting 50 cycles, the largest counting 10 cycles.

The strains at amplitudes in between may be found by linear interpolation (see figure 15). The effects of a greater number of cycles was determined by logarithmic extrapolation (see figure 16).



STRESSPATHS SEAGRAVEL - FOUNDATION BED.
DUE TO KATSSTORM M2.

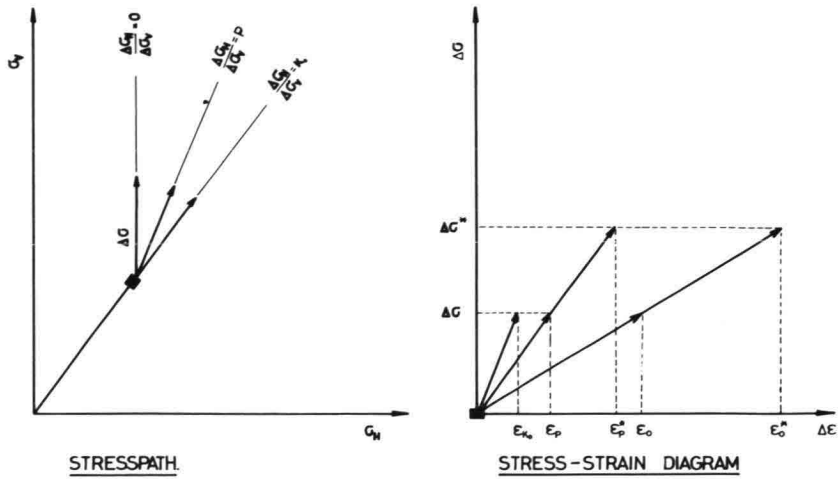
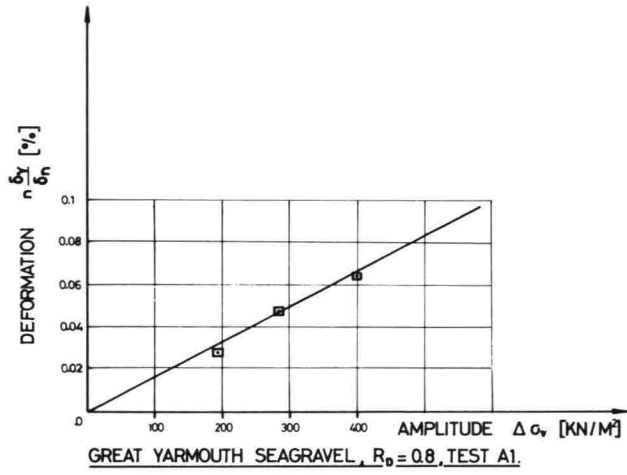


FIG 14.



GREAT YARMOUTH SEAGRAVEL, $R_0 = 0.8$, TEST A1.

FIG 15.

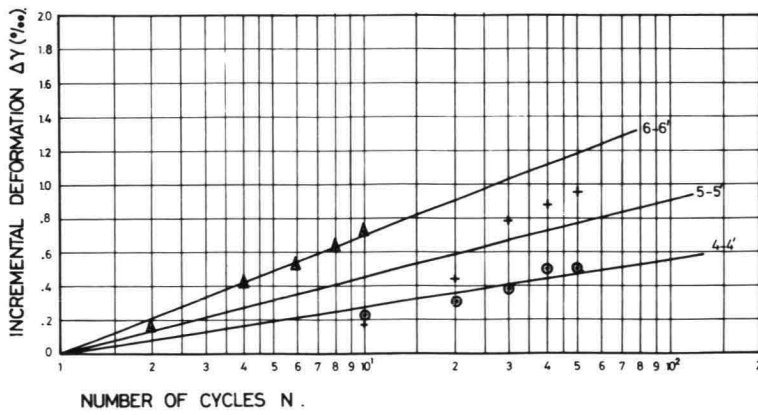
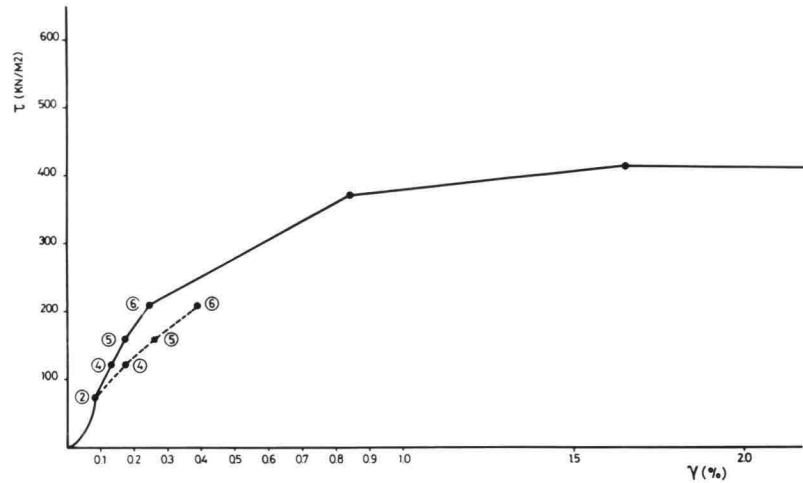


FIG 16.

Results

Using the method described above, all materials are present for constructing the stress-curves for an arbitrary storm. In figure 17 this was done for the storm that was simulated in Kats-test M₂ |13|. The material considered is seagravel from Great Yarmouth, a rather angular material with a grain size distribution shown in fig. 12.

About 50% increase of shear deformation was found due to cyclic loading. The "static" curve was constructed out of the test results by skipping reloading and unloading deformations. A similar increase could be derived out of the modeltests in Kats |13| .



GREAT YARMOUTH SEAGRAVEL $R_D = 0.8$, TEST A1.
DRAINED CYCLIC TESTS.

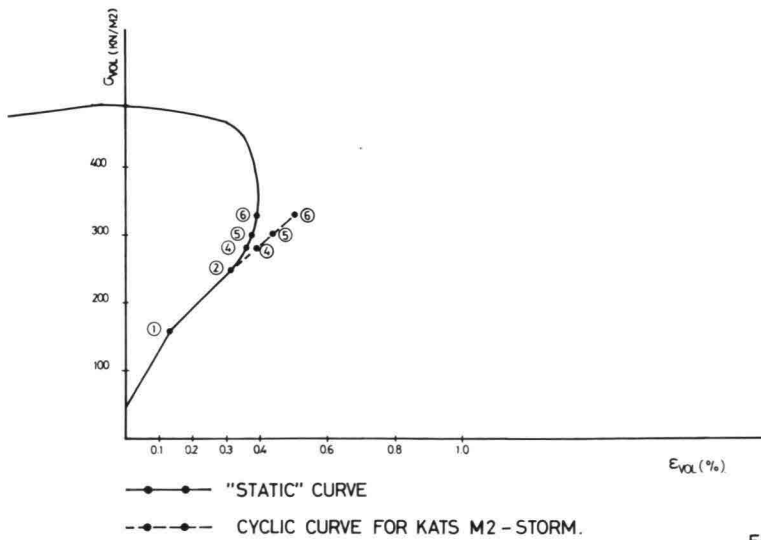


FIG 17.

The following parameters of the CONSOL-stress-strain model gave the best fitting curves:

- | | |
|--------------|--------------------------------|
| $R_D = 0.8$ | $K_i = 32000 \text{ kN/m}^2$ |
| $H = 1700$ | $A = 270$ |
| $H_u = 2500$ | $K_u = 200.000 \text{ kN/m}^2$ |
| $N = 0.5$ | $\phi = 42^\circ$ |
| $R_f = 1$ | $\phi_{tp} = 38^\circ$ |

VII. FUTURE DEVELOPMENTS

Three directions can be discerned:

- a) the development of stress-strain models
- b) determination of model parameters and checking of the models
- c) using the models for complicated computations

ad a) The CONSOL project is primarily aimed at production work. Some study on the subject is necessary, but that will be mainly literature study. Some development could be necessary when the presented models must be adjusted to cope with the problems which occur.

ad b) Far more important is how to determine model parameters and to check the validity range of a model.

A computer model is being developed which supplies the frame work for these tasks.

All types of laboratory tests involving only the three main stresses and strains can be stored and retrieved by simple commands.

Implementation of new models should become as easy as possible and determination of model parameters should be based on a great number of laboratory tests. As well as the result the accuracy of the parameters must also be estimated. Graphical representation of the results can be given. Models can be checked and compared.

The program must be easily extendable to conform to the users wishes.

ad c) When a suitable model has been found and its parameters can be determined, it can be used for more complicated computations. One of the tools is a finite element program. For a couple of years now a new program has been under development from the integrated system GENESYS. When the stress-strain model is correct, there are still all sorts of boundary conditions which must be properly specified e.g. interfaces between soil and structure. The program is built very systematically so these extensions can easily be made. At the moment a critical state model is built in. Differences from the usual models are:

- 1) The usual models have a fixed shape of the ellipse, while the model developed here is flexible. The basic input is the amount of volumetric strain along e.g. a K_0 path. Because the ellipse is flexible the shear strain along such a path can also be specified and this determines the shape change of the ellipse.
- 2) Usually fixed formulas combine two or more qualities e.g. the failure shear stress and the isotropic stress by Mohr Coulomb criterion [5]. It is also possible to assume a relation between those quantities and to specify the nature of such a relation when solving a problem. The derivation of the equations is more complex but the result is more flexible. The user can choose between a number of preformulated formulas or specify data points for interpolation.

Integration of the relation will be done by a mixed method. Integration is carried out for each element separately and the final result will be checked for equilibrium by an initial stress method.

The program contains wall elements and a very general set of possible boundary conditions. It will be extended to contain consolidation according to methods of the type described by Smith [10]. At the moment the system is partially finished and not yet fully operational.

APPENDIX 1

Derivation of the solution procedure.

Relations for the shear strain

$$\frac{d\tau}{d\gamma} = \frac{\partial\tau}{\partial\gamma} + \frac{\partial\tau}{\partial\bar{\sigma}} \cdot \frac{d\bar{\sigma}}{d\gamma} \tag{12}$$

when it is assumed that τ is both a function of γ and $\bar{\sigma}$.

$\frac{\partial\tau}{\partial\gamma}$ is given by (2)

$$\frac{\partial\tau}{\partial\gamma} = G_T = \frac{1}{a}(1-b\tau)^2$$

$\frac{\partial\tau}{\partial\bar{\sigma}}$ is obtained by differentiating (1), which gives

$$\frac{\partial\tau}{\partial\bar{\sigma}} = \frac{\gamma}{(a+b\gamma)^2} \left\{ \frac{\partial a}{\partial\bar{\sigma}} + \gamma \frac{\partial b}{\partial\bar{\sigma}} \right\} \tag{13}$$

a and b are given by (3), (4), (5) so

$$\frac{\partial a}{\partial\bar{\sigma}} = -\frac{a \cdot n}{\bar{\sigma}} \quad \text{and} \quad \frac{\partial b}{\partial\bar{\sigma}} = -\frac{b}{\bar{\sigma}} \tag{14}, (15)$$

eliminating γ by substituting (1) gives

$$\frac{\partial\tau}{\partial\bar{\sigma}} = \frac{\tau}{\bar{\sigma}} (1-b\tau) \cdot n + \frac{\tau^2}{\bar{\sigma}} \cdot b \tag{16}$$

(2), (16) in (12) gives

$$\frac{d\tau}{d\gamma} = \frac{1}{a}(1-b\tau)^2 + \left\{ \frac{\tau}{\bar{\sigma}}(1-b\tau) \cdot n + \frac{\tau^2}{\bar{\sigma}} \cdot b \right\} \frac{d\bar{\sigma}}{d\gamma} \tag{17}$$

(17) can be written in integral form.

$$\Delta\gamma = \int_{\Delta\tau, \Delta\sigma} \frac{a}{(1-b\tau)^2} \left\{ d\tau - \left\{ \frac{\tau}{\bar{\sigma}} (1-b\tau) \cdot n + \frac{\tau^2}{\bar{\sigma}} \cdot b \right\} d\bar{\sigma} \right\} \tag{18}$$

This is the correct equation to be integrated. The original incorrect equation assumes no relation between γ and $\bar{\sigma}$ and so assumes $d\bar{\sigma} = 0$ resulting in

$$\Delta\gamma = \int_{\Delta\tau, \Delta\sigma} \frac{a}{(1-b\tau)^2} d\tau \tag{19}$$

When τ_0 and $\bar{\sigma}_0$ are the stresses at the beginning of the step and τ_1 and $\bar{\sigma}_1$ at the end the Euler and Heun type integration formulas can be written as follows:

(18) can be written more briefly as:

$$\Delta\gamma = \int_{\Delta\tau \Delta\sigma} (P \cdot d\tau - Q \cdot d\bar{\sigma}) \quad \text{with } P \text{ and } Q \text{ stress functions} \tag{20}$$

Because the effective stresses are the input parameters, the Euler and Heun integration rules are given by:

$$\Delta\gamma = \Delta\tau \cdot P(\tau_0, \bar{\sigma}_0) - \Delta\bar{\sigma} \cdot Q(\tau_0, \bar{\sigma}_0) \quad \text{for Euler integration} \quad (21)$$

and

$$\Delta\gamma = \frac{1}{2}\Delta\tau \{P(\tau_0, \bar{\sigma}_0) + P(\tau_1, \bar{\sigma}_1)\} - \frac{1}{2}\Delta\bar{\sigma} \{Q(\tau_0, \bar{\sigma}_0) + Q(\tau_1, \bar{\sigma}_1)\} \quad (22)$$

for the Heun integration method.

When τ_1 and $\bar{\sigma}_1$ are not input values they must be estimated from $\Delta\gamma$ computed by the Euler integration method.

2. Relation for the volumetric strain.

Using (8) gives

$$\Delta \varepsilon_{vol} = \int_{\Delta\bar{\sigma}_{vol}} \frac{1}{K_i + A \cdot \bar{\sigma}_{vol}} d \bar{\sigma}_{vol} \quad (23)$$

according to Hooke's law for plane strain, it follows that

$$\bar{\sigma}_{vol} = (1+\nu) \cdot (\sigma_x + \sigma_y)/2 = (1+\nu)\bar{\sigma} \quad (24)$$

When it is assumed that the third direction has no influence on the non linear behaviour, $(1+\nu)$ can be assumed constant, ν being an input parameter.

(24) and (23) give:

$$\Delta\varepsilon_{vol} = \int_{\Delta\bar{\sigma}} \frac{1+\nu}{K_i + A \cdot (1+\nu)\bar{\sigma}} \cdot d\bar{\sigma} \quad \text{or} \quad = \int_{\Delta\bar{\sigma}} R \cdot d\bar{\sigma} \quad (25)$$

(25) can be solved by the same formulas as (20) which gives

$$\Delta\varepsilon_{vol} = R(\bar{\sigma}_0) \cdot \Delta\bar{\sigma} \quad \text{for the Euler integration} \quad (26)$$

and

$$\Delta\varepsilon_{vol} = \frac{1}{2}\Delta\bar{\sigma} \{R(\bar{\sigma}_0) + R(\bar{\sigma}_1)\} \quad \text{for the Heun integration} \quad (27)$$

Formulas 21, 22, 26, 27 can be programmed and the results may be checked with the original formulas (1) and (7).

BIBLIOGRAPHY

1. Boehmer, J.W.
Christian, J.T. Plane strain consolidation by finite elements,
M.I.T. R 69-60, Soil Mechanics Publication no.
243, August 1969.
2. Biegstraaten, A.W.W.M.
Kenter, C.J. Dilatancy in Consol, Report CO-40.5.81-0/11,
Soil Mechanics Laboratory Delft
3. Duncan, J.C.
Chang, C.Y. Non-linear analysis of stress and strain in soils,
Proc., ASCE, JSMFD vol. 96, no.SM5 p.p.1629-1653.
4. Christian, J.T.
Molina Fernandez, R. Finite element analysis of large strains in soils,
M.I.T. R71-37, Soils publication no.289 Sept.1971
5. Kondner, R.L.
Zelasko, J.S. A hyperbolic stress strain formulation for sands,
Proc. 2nd. Pan Am.Conf.Soil Mech., Brazil II (1963)
p.p. 289-324
6. Rowe, P.W. The stress dilatancy relation for static equilibrium
of an assembly of particles in contact, Proc. Royal
Soc. A 269 (1962) p.p. 500-527.
7. Zienkiewicz, O.C. The finite element method in structural and con-
tinuum mechanics, Me.Graw Hill, 1968.
8. Roscoe, K.H. The influence of strains in soil mechanics, Géo-
technique 20, no. 2, p.p. 129-170 (1970)
9. Vermeer, P.A. A double hardening model for sand, Delft Progr.
Rep. 2 (1977) p.p. 303-320
10. Smith, I.M. Some time-dependent soil-structure interaction
problems, F. Finite Elements in geomechanics p.p.
251-293, Wiley (1975)
11. Heemstra, J.
Kenter, C.J. Triaxial tests on Kats-sand, Delft Soil Mechanics
Laboratory, report CO-406102/39 part A and B
(1977) (Dutch)
12. Heusdens, J.J.
Kenter, C.J. Parametric comparison of static triaxialtests on
Kats-sand, Delft Soil Mechanics Laboratory, report
CO-406102/40 (1978) (Dutch)
13. De Quelerij, L.
Broeze, J.J. Modeltest on piers, scale 1 : 10. Proceedings of
International Symposium in Soil Mechanics and
foundation design for the Oosterschelde Storm
Surge Barrier, ch. IV.2. (1978)
14. Bösinger, Ing. E.
Meissner,Dr.Ing.H. Bericht über die Durchführung von Dreiaxialver-
suchen an Seekies, Institut für Bodenmechanik
und Felsmechanik, Universität Karlsruhe (1977).
15. Biguenet, G. Des essais triaxiaux exécutés sur les matériaux
de l'Escaut Oriental, Institut de Mécanique
(IMG), Université de Grenoble (1978)

SYMPOSIUM ON FOUNDATION ASPECTS OF COASTAL STRUCTURES

PORE PRESSURE GENERATION

by:

Frans P. Smits, Research Engineer, Delft Soil Mechanics Laboratory
Delft, The Netherlands

Knut H. Andersen, Civil Engineer, Norwegian Geotechnical Institute
Oslo, Norway

Gerd Gudehus, Professor of Soil Mechanics, University of Karlsruhe
Karlsruhe, Germany

SUMMARY

Major problems with the design of sea structures are caused by the repeated loading effect due to wave action. Cyclic shear stresses with amplitudes far below the undrained strength in monotonic loading tend to develop excess pore pressures, causing a reduction of the stiffness and the residual undrained strength, which may lead to inadmissible displacements or loss of stability.

The present paper deals with the cyclic loading behaviour of cohesionless soils. The mechanism of cyclic loading is discussed on the basis of constitutive parameters which govern the pore pressure generation. Selected topics of laboratory investigation are presented, like the effect of average versus cyclic shear stress ratio, β^*/k_D -determination, preshearing behaviour and interpretation of stormloading tests. Solution methods to boundary value problems are reviewed. Two methods which have been applied in connection with the Oosterschelde caisson tests are briefly described.

INTRODUCTION

Although at present the phenomenon of cyclic loading and its implications for cohesionless soils are fairly well understood, quantifying its effects is still a serious task. Pore pressures would not be so much a matter of concern if we were not used to express structural safety through stability against failure in terms of effective stresses. Separate consideration of pore pressure is necessary as we are yet unable to carry out calculations based on the simultaneous equilibrium of soil skeleton and pore fluid storage equations. However, effective stress strain relations in case of alternating stresses are extremely difficult and computer time involved in tracking individual load cycles is very large. On the contrary, experience has been obtained with considering the pore pressure generation within individual cycles as induced by an external agency and calculating the response of the soil by following peak cycle loading. In this concept pore pressure production is made a function of the initial stress condition and the stress variations in successive cycles. Both the determination of these stresses and the calculation of the response to the generated pore pressures in terms of displacements require adequate stress strain relations, which preferably may be obtained from cyclic laboratory tests. Stress strain relations are subject of the contributions to this symposium by Marr and Høeg and by Biegstraaten and Kenter. The present paper deals with the determination of pore pressures only.

1. THE MECHANISM OF CYCLIC LOADING1.1. Undrained versus drained cyclic loading

The most commonly used method to study cyclic loading behaviour of sand is by

undrained cyclic triaxial and simple shear testing. This originates from the similarity with in situ wave or earthquake loading, which is virtually undrained in a single load cycle, but also from the comparative simplicity of solving the field problem by an uncoupled method.

A main information obtained from cyclic laboratory tests is pore pressure generation in undrained loading and volume change in drained loading. To interpret the basic mechanism let us compare a drained and an undrained cyclic triaxial test with octahedral effective stress, σ' , respectively total stress, σ , kept constant. Figure 1 shows the volume change in the drained test and figure 2 the pore pressure change in the undrained test for the first few cycles. Figure 3 shows the decrease of volume and figure 4 the increase of pore pressure as a function of number of cycles for two cyclic stress ratios τ_c/σ'_0 . Subscripts c and o denote the cyclic and initial static components respectively.

In a drained test there is a volume increase at the end of the loading stage of the first cycle if the sand is denser than critical (figure 1), however, a volume decrease if the density is below critical. After the first full cycle there is always a net volume decrease even for the densest sand (at least according to the authors tests). During subsequent cycles the volume decrease per cycle decreases rapidly and finally approaches zero as shown by figure 3 for both low and high cyclic stress ratios. In the undrained test there is a pore pressure decrease in the loading stage of the first cycle for densities above critical and always a positive excess pore pressure after completion of the first cycle (figure 2). The pore pressure generation per cycle usually decreases during the first few cycles, whereafter it tends to stabilize. With increasing number of cycles the generation may approach zero at low cyclic stress ratios; however, at high cyclic stress ratios pore pressure will be produced at an increased rate again until it approaches the octahedral total stress (figure 4).

The plastic volume decrease per cycle in a drained test is recovered in an undrained test by elastic expansion of the soil skeleton, causing a pore pressure rise to the extent of the elastic unloading. This is the conventional elastic-plastic explanation of pore pressure generation, which is not quite correct in detail. In an undrained test with constant cyclic shear stress amplitude several factors govern the local concavity or convexity of the generation curve of figure 4. The normalized pore pressure generation per cycle, termed β -coefficient, tends to decrease with number of cycles due to the non-linearity of the recompression curve and due to the decay of plastic volume decrease per cycle in a drained test. However, it tends to increase due to a growing effective cyclic stress ratio after each undrained cycle. Such influencing factors may be recognized in an analytical expression for β as given in the next section. In a first approximation β may be considered as a constant for practical analysis, in which case it is frequently defined as the tangent to the linear section of the generation curve.

1.2. Factors influencing pore pressure in a soil element

Consider a saturated sand element under cyclic load and a fixed simple mode of deformation, i.e. the direction of stress and strain increments may be constant except for cyclic changes of signs. The pore pressure generation in one cycle, Δu , can formally be calculated (Gudehus, 1978) as:

$$\beta^* = \frac{\Delta u}{\tau_c} = \left| - \left(\frac{D}{M} \sin \nu \right)_{\text{load}} - \left(\frac{D}{M} \sin \nu \right)_{\text{unload}} \right| \quad (1)$$

and Bjerrum's parameter β is expressed:

$$\beta = \beta^* \frac{\tau_c}{\sigma'_0} \quad (2)$$

Relevant are three constitutive parameters of the grain skeleton, in general different for loading and unloading, viz.

D, an incremental elastic bulk modulus, $\Delta\sigma' = D\Delta\epsilon^e$,
M, an incremental distortional stiffness modulus, representing plastic shear behaviour, $\Delta\tau = M\Delta\gamma^p$,
 $\sin \nu$, a factor of dilatancy, relating incremental plastic volume strains and distortions, $\Delta\epsilon^p = \Delta\gamma^p \cdot \sin \nu$.

Equ. (1) does not serve to calculate Δu from elastic-plastic parameters but to outline some factors of influence, based on the present knowledge on constitutive parameters. Assuming rate independence of the above parameters, Equ. (1) demonstrates that frequency and shape of stress-time oscillation curves have no influence, which seems in agreement with experimental evidence. It also shows that the octahedral component of the cyclic stress variation does not influence pore pressure generation. For simplicity's sake the parameters D, M and $\sin \nu$ are discussed separately, although they are not independent.

Dilatancy is the most important factor. Taking D/M as constant for this instant (which will be acceptable after a certain number of cycles within the same mode), we can conclude from Equ. (1): For having a net pore pressure increase $\sin \nu$ must be negative for unloading and of bigger amount than the possible $\sin \nu$ for loading. Goldscheider (1976) has in fact found that the amount of contractancy upon load reversal always exceeds the one of dilatancy, and that the biggest difference occurs for loose sand. Thus two things seem to be justified: the liquefaction potential is non-zero for all densities, and maximum for low density.

D and M both depend on mean stress level σ' in a similar manner, whereas $\sin \nu$ does not. Thus, in first approximation, $\Delta u/\tau_c$ may be stress-level independent. Otherwise D may be constant, but M is certainly not. M is different for loading and unloading ($M_{load} < M_{unload}$), increasing with the number of cycles for a constant effective mean stress, which is referred to as the "preshearing" effect (cf. Sec. 2 of this paper), and decreasing with the effective cyclic stress ratio or mobilized strength (Darve, 1976). Most of these factors have been studied by comprehensive LGM tests (LGM, 1975).

Any interpretation is far more complicated if the direction of stress and strain increments changes. Dilatancy and stiffness undergo extreme variations for such changes (Goldscheider, 1976, and Darve, 1976), and the same holds for $\Delta u/\tau_c$ by Equ. (1). This effect is often referred to as "directional effect" and was repeatedly verified in liquefaction tests (e.g. Mori et al, 1978). Note that preparation of samples can also produce such a directional effect.

2. SELECTED TOPICS FROM CYCLIC LABORATORY TESTS

2.1. General

Several hundreds of cyclic loading tests have been carried out during the years of 1974 till 1978 at Delft Soil Mechanics Laboratory (LGM), Massachusetts Institute of Technology (MIT), Norwegian Geotechnical Institute (NGI), Instituut voor Grondmechanica en Funderingstechniek (IGF) and the University of Karlsruhe to assist the design of the Oosterschelde Storm Surge Barrier. The majority of these tests, communicated by internal reports, LGM (1975), Lambe (1977), NGI (1977), IGF (1976), Goldscheider and Winter (1977), have served as an aid to predict the behaviour of large scale model tests.

Some of the parameters investigated are:

- cyclic shear stress amplitude, τ_c ;
- average shear stress, τ_a ;
- consolidation pressure, σ'_0 ;
- cyclic stress path;
- overconsolidation (isotropic and anisotropic);
- cyclic frequency;
- shape of stress-time pulse;
- β^*/kD -determination;
- initial porosity;
- preshearing;
- drained versus undrained cyclic loading;
- variable cyclic shear stress ("storm-loading");
- undisturbed versus reconstituted sampling;
- preparation method of reconstituted samples;
- sand type;
- strain-controlled cyclic loading;
- simple shear versus triaxial testing.

It is outside the scope of this report to discuss all these parameters, some of them have been reviewed excellently in recent literature (Seed, 1976), and discussed by Lambe (1977) in connection to the Oosterschelde closure. The following sections deal with some special topics which seem to have attracted less attention in literature.

2.2. Effect of average and cyclic shear stress ratios

The actual stress paths experienced by elements of the foundation soil within a full load cycle have a complex shape and vary from one point to another. In addition rotation of principal axes may occur, and if so, as for instance for elements below the central section of a symmetrically loaded structure, simple shear tests may be more representative than triaxial tests. Simplified stress paths for a number of significant elements must be selected to be studied by laboratory tests. As cyclic shear stress variation is evidently the primary parameter governing pore pressure generation, such paths may be chosen as the straight paths connecting the stress points with maximum and minimum shear stress. Simulating them in laboratory tests may involve the variation of mean stress depending on the capability of the testing equipment, but certainly must satisfy the shear stress variation between $\tau_a \pm \tau_c$. Cyclic shear stress variations with a pronounced average static component may occur below the edges of a structure due to a rocking action superimposed on the permanent load, but also below the center of a structure if it is subjected to static tidal forces.

Figures 5a and 5b show typical pore pressure generation and cyclic strain curves versus number of cycles in undrained simple shear tests for samples subjected to the same cyclic shear stress τ_c but with different average shear stress τ_a : symmetric loading with $\tau_a = 0$ and asymmetric loading with $\tau_a = \tau_c$. The difference in average shear stress causes a more rapid pore pressure generation and a smaller number of cycles to "failure" (large strains) in asymmetric loading. It is also interesting to observe that the excess pore pressure starts to increase from the very beginning of cyclic loading. The increase of shear strains, on the other hand, is relatively modest until it suddenly starts to increase significantly as failure is approached. This is especially true for symmetric loading. It indicates that excess pore pressure is a more sensitive parameter to work with than strains for cohesionless soils.

Results of simple tests with different cyclic shear stress ratios are summarized in contour diagrams as shown by figures 6a, b and c for an average shear stress of 25 kN/m^2 , expressing the number of cycles required to reach equal levels of pore pressure and cyclic strain by different cyclic shear stress ratios. This kind of diagrams have proven to be useful as summaries of test results and also for further use and interpretation of the test results.

Figures 7a and 7b show the number of cycles to reach an excess pore pressure 50% of vertical consolidation pressure and to reach a cyclic shear strain of 3% as a function of cyclic stress ratio τ_c/σ_{V0}' for different average shear stress ratios. These plots indicate that the ratio of average versus cyclic shear stress is a significant parameter to characterize pore pressure generation and deformation in cyclic loading: At equal cyclic stress ratios both pore pressures and cyclic strains develop at a higher rate with increasing ratio τ_a/τ_c . Similar behaviour has been observed in cyclic triaxial tests.

2.3. Determination of β^*/kD

Goldscheider and Winter (1977) have developed a triaxial device for directly measuring β^*/kD , parameter required for estimating upper bounds of pore pressures in earth bodies (Gudehus, 1978). This is briefly described here.

A cylindrical sample ($h = 18 \text{ cm}$, $d = 10 \text{ cm}$) is saturated with glycerine encapsulated in a latex membrane and drained on one end. The sample is loaded in a triaxial cell by $\sigma_{10}' \pm \Delta\sigma_1$ and $\sigma_{30}' \pm \Delta\sigma_3$. The cyclic stress components $\Delta\sigma_1$ and $\Delta\sigma_3$ can have different magnitudes and signs, but their frequencies are equal. The reference stress values σ_{10}' and σ_{30}' can be fixed at will. Only tests with $\sigma_1' > \sigma_3'$ are possible as yet. The pore pressures on both ends and in midheight of the sample are measured and evaluated.

Saturating the sample requires some care as any inclusion of air and any access of water must be avoided. This is achieved by first saturating the sample with deaired water and then replacing the water by flowing through the sample with glycerine. The sample is preconsolidated under σ_{10}' and σ_{30}' to produce a well-defined initial state. Cyclic loading is executed until the pore pressure becomes stationary. β^*/kD is calculated on the basis of the linear theory of pore pressure production and dissipation with special allowance for the viscosity of glycerine.

Contrary to other liquefaction tests, the sample is not brought to failure (at least not intentionally), and there is no problem of rubber mould penetration.

Figure 8 shows the measured pore pressures versus the number of cycles N . The sample was fine Oosterschelde sand with $n = 0.36$. The stresses varied between $\sigma_1' = 300 \text{ kN/m}^2$, $\sigma_3' = 300 \text{ kN/m}^2$ and $\sigma_1' = 450 \text{ kN/m}^2$, $\sigma_3' = 300 \text{ kN/m}^2$. Quite typically, there is a marked pore pressure production in the first few cycles, followed by a reduction due to drainage up to a certain almost stationary final value.

This process is somewhat similar to the pore pressure development in the first Oosterschelde large caisson test (De Leeuw, 1976 and Heijnen, 1976). It appears that preshearing reduces β^*/kD considerably.

2.4. Preshearing

In a real storm generally much more cycles occur than can be applied in an undrained laboratory test without causing failure in cyclic loading. This is due to partial drainage in the field (higher effective stresses) and due to a decreasing response of the soil to shear stress reversals with number of cycles. The latter is the so-called preshearing effect. This effect is here considered for certain fixed modes of shearing as simple shear or triaxial. It has been reported by Finn, e.a. (1970) and later by Bjerrum (1973) as the influence of prior strain history on the liquefaction characteristics of sand, and it has been referred to in this paper as being reflected by an increase of the distortional stiffness

modulus M (cf Sect. 1.2). It is hypothesized that the accumulated plastic volume strain may be a measure for the increase of distortional stiffness M and by this for the decreasing liquefaction potential. The decay of plastic volume decrease per cycle, however, is an effect of a decreasing modulus M , which reveals itself through the relation between distortional and volumetric plastic strain increments. The accumulated plastic volume strain by preshearing remains very small and has no direct relation to the strain increments per cycle.

An attempt has been made to evaluate the preshearing effect by studying undrained cyclic triaxial tests with intermittent drainage stages. The pore pressure generation per cycle at the end of each undrained stage has been plotted against the accumulated volume or porosity change produced in previous drainage stages for different values of the cyclic stress level as shown by figure 9. As the cyclic stress ratio is normalized with respect to the initial consolidation stress, τ_c/σ'_0 , the undrained stages should be continued to a constant pore pressure level $\Delta u/\sigma'_0$ for the β versus Δn curves to be related to a constant effective cyclic stress ratio as well and to a constant value of the incremental recompression modulus D . This condition has not been met in the present tests, which may have contributed to the scatter of β -values at the higher cyclic stress ratios. The β versus Δn relations, shown in figure 9, have been obtained by staged tests with increasing cyclic stress ratios in subsequent undrained stages. The question arises to what extent these relations depend on how the accumulated volume change has been reached. This has not yet been investigated thoroughly, although the present tests seem to indicate that pore pressure generation is somewhat higher if a particular volume change has been reached by a few cycles with high stress ratios than if it had been reached by a larger number of small stress ratio cycles. Sets of β versus Δn curves for different preshearing histories may therefore be required.

In view of the dependency of pore pressure generation on effective cyclic stress ratio sets of β versus Δn curves may have to be established also for different excess pore pressure levels $\Delta u/\sigma'_0$.

2.5. Interpretation of varying cyclic shear stresses ("storm-loading")

Storms are composed of waves with different heights, and the cyclic shear stresses in an element will change from one cycle to another. A procedure for taking the effect of varying cyclic stresses into account in calculations has therefore been developed.

The procedure is based on the results from stress-controlled tests with constant shear stress amplitude (figure 6). It predicts generated pore pressure and development of average and cyclic shear strains for soil elements subjected to varying cyclic shear stresses under undrained conditions. The procedure is based on the assumption that the generated excess pore pressure accumulates during the storm. For a wave at any time in the storm, the soil starts out with a pore pressure which is equal to the pore pressure at the end of the previous wave. This is valid irrespective of whether the cyclic stress ratios are different or not for the new and the previous waves. This means that an element subjected to varying cyclic shear stresses will follow a pattern in the pore pressure contour diagram as shown in figure 10a. It may be seen from the figure that the pore pressure generated during one cycle will depend on the previous cyclic stress history. This pore pressure accumulation procedure is based on the same ideas and principles as the strain-accumulation procedure described by Andersen (1976) and Andersen, Hansteen, Høeg and Prévost (1978).

From the predicted pore pressure pattern in figure 10a a cyclic stress history may be transformed into an equivalent number of cycles with constant cyclic stress

amplitudes. This can be done at any stage of the storm. For the example in figure 10a, the complete cyclic stress history is equivalent to 975 cycles at a cyclic shear stress of $\pm 15 \text{ kN/m}^2$ ($\frac{\tau_c}{\sigma'_{vc}} = \pm 0.043$). Earlier in the storm, at point A, the stress history is equivalent to 24 cycles at a cyclic shear stress of $\pm 25 \text{ kN/m}^2$ ($\frac{\tau_c}{\sigma'_{vc}} = \pm 0.071$).

The predicted pore pressure pattern defines the equivalent number of cycles and the corresponding cyclic shear stress ratio at any stage during a storm. This can be used to find the corresponding average and cyclic shear strains which develop. As an example, for point A with an equivalent number of cycles of 24 at a cyclic stress level, $\frac{\tau_c}{\sigma'_{vc}} = \pm 0.071$, the strain contour diagrams in figure 10b and 10c show that the average and cyclic shear strains will be 0.3% and $\pm 0.06\%$ respectively.

The procedure described above has been used to calculate the behaviour of simple shear tests which were run with varying cyclic shear stress. A comparison between calculated and measured values of pore pressure and average and cyclic shear strains is presented in figure 11. The agreement between calculations and measurements is reasonably good.

3. METHODS TO SOLVE BOUNDARY VALUE PROBLEMS

3.1. Survey of boundary value problems

As outlined above, the building of pore pressure in a homogeneously strained undrained sand element depends on many factors in a very complicated manner. This is even more so for a sand body with non-homogeneous stresses and strains. The boundary condition of forces, displacements and drainage must be given. In addition, the initial stress field is needed.

It is helpful to consider three groups of solution methods (Gudehus, 1978). The fully coupled methods try to observe all conservation laws (mass, linear momentum) and constitutive laws (grain skeleton, pore fluid) with an assumed relationship for the exchange of linear momentum between the two phases. It is possible to write down these conditions as linear equations in the respective increments of effective stress, strain and pore pressure. Transposed into a suitable finite element form, this is a set of equations with a non-symmetric matrix, causing some well-known numerical problems.

The real problem, however, is the strong dependence of incremental stiffness on effective stress, direction of increments, and previous cycles (cf. Sec. 2.4 of this Report). Effective stress is, on principle, given by updating previous calculation steps. This procedure may appear as trivial, but it implies an accumulation of incomplete knowledge concerning initial stress field and sequence of incremental stiffness matrices. The directional dependence of incremental stiffness renders the problem incrementally non-linear. This non-linearity is necessary, cf. Kolymbas (1978) and Darve (1976). Even if the directional dependence may be given, almost nothing is known about convergence and uniqueness of the iterative procedure required to solve the system of non-linear equations. Actually the directional dependence of incremental stiffness is rather well understood only for the first cycle (Kolymbas, 1978, Goldscheider, 1976, Darve, 1976), but not for a big number of cycles.

Thus the fully coupled numerical methods are as yet outside of the range of applicability. Semi-coupled may be called those methods that satisfy conservation and constitutive laws only for certain groups ('bunches') of cycles. Only the cumulative stresses and strains within each 'bunch' are correlated. Typical simplified constitutive laws of this type correlate stress, strain and pore pressure with the number of cycles. The conservation laws of momentum and mass are satisfied after each 'bunch'. This method is certainly simpler than the fully coupled methods, but the inherent errors can scarcely be judged. Note that conservation and constitutive laws within each cycle will generally be violated. It would be desirable to have at least a few correct solutions of the fully coupled methods to check the validity of semi-coupled methods. Without these it can only be conjectured that the errors are the bigger the more important the influence of kinematical constraints is.

Even cruder, but also simpler, are the uncoupled methods. The effective stress fields (average and cyclic) are determined in advance. Then only the production and dissipation of pore pressures have to be calculated. This procedure leads to simplified estimates of pore pressure generation (Gudehus, 1978). It is also possible to work with updated effective stresses, which is necessary in case of a relatively strong pore pressure generation (cf. Sec. 2.4). In the uncoupled methods the constitutive law of the grain skeleton is not considered in detail. In other words the system is, in a sense, assumed as statically determinate.

Model tests are an attractive alternative, but are not considered here (Smits, 1977).

3.2. Pore pressure calculation with updating of cyclic response

A procedure is described to calculate pore pressure generation by actual storm loading, which allows for the capacity of the soil to improve its resistance against liquefaction by preshearing during the rise time of a major storm or during prior moderate storms. It has been applied for the first time to predict the Neeltje Jans tests by a simplified uncoupled analysis (Smits, 1976), which is reported in a contribution to this symposium. Considering preshearing will also reduce the dependency of calculated excess pore pressure on sample formation techniques.

Suppose a storm being divided into a number of parcels, which are of sufficient duration that a probability distribution of wave heights may serve to assess the number of individual wave heights, but otherwise with the shortest possible duration to allow maximum sensitivity of the calculation procedure to the rise time of the storm. Within each parcel the production of pore pressure is calculated as if loading by individual cycles was undrained, keeping track of simultaneous dissipation by operating a consolidation equation which contains the rate of generation as an added pumping term \dot{w} ,

$$\nabla^2 u = \frac{\gamma_w}{kD} \left(\frac{\partial u}{\partial t} - \dot{w} \right) \quad (3)$$

with

$$\dot{w} = \sigma'_o \cdot f \cdot \beta \left(\frac{\tau_c}{\sigma'_c}, \frac{\tau_a}{\tau_c}, n_o, n_o - \Delta n \right) \quad (4)$$

where f is wave frequency

The parcel is divided into a number of small time intervals Δt , for which Equ. (3) is solved. After each interval the pumping term is updated.

The first step in the analysis is to determine cyclic shear stress ratios for individual elements or zones of the foundation soil due to boundary loading by the maximum wave. In a first approximation it is then assumed that cyclic stress ratios due to smaller waves are proportional to the wave forces. The cyclic stress ratios required are the actual shear stresses τ_c and τ_a normalized with respect to the mean or octahedral consolidation stresses σ'_0 . In the present case these are obtained by closed-form plasticity solutions, assuming constant mobilization of strength. However, they may as well be obtained from a suitable finite element calculation. At the start of a new parcel and of subsequent updating steps stresses σ'_0 are determined by allowing an actually non-existing full dissipation of pore pressures under the action of the weight of the structure and the instantaneous tidal force. The average shear stresses, τ_a , are determined in drained loading by the weight of the structure and the instantaneous tidal force at the field stress condition resulting from the previous parcel or time step Δt . The cyclic shear stresses, τ_c , are obtained by undrained application of the maximum wave load within the parcel at the field stress condition resulting from the previous parcel or the previous time step Δt . Having determined the cyclic stress field, the rate of pore pressure generation for the elements is obtained by calculating the production per cycle, using β versus τ_c/σ'_0 relations, accumulating over the number of cycles at individual wave heights and dividing by the parcel duration. This is a valid procedure only if a random sequence of wave heights within a parcel may be assumed.

Due to simultaneous dissipation the above procedure would lead to stationary pore pressures eventually if not the rate of generation would decrease due to pre-shearing. Keeping the rate of generation constant over a time interval Δt , it is adjusted for the next time step by selecting new β -values according to the redistributed stress field and the accumulated plastic volume strains produced by previous cycles (using β versus Δn relations of figure 9). Consolidation proceeds with updated pumping term and initial excess pore pressure condition. The accumulated plastic volume strains are calculated from the consolidation process. For this reason the stiffness modulus D in Equ. (3) is to be obtained preferably from the intermittent drainage stages in cyclic laboratory tests. Actual excess pore pressures in certain cases may decrease after having reached a maximum within a parcel (Smits, 1976). This has been verified by model tests and has also been observed in the β/kD tests (Smits, 1977, Goldscheider and Winter, 1977).

3.3. Pore pressure calculation using contours to evaluate storm-loading

A procedure is described to calculate the excess pore pressure due to a rise of tide and due to a subsequent storm, which has been applied to predict the behaviour of the Hammen 17 caisson (NGI, 1977). The caisson is embedded 9 m into the soil and 46 m wide as shown in figure 12. The tide difference is assumed to rise to a maximum of 7 m on the sea side in the course of 5 hours. It is assumed that the storm loading occurs after the tide has reached its maximum height. The waves which are of significance for the pore pressure generation are listed in the table in figure 12 in the order they occur.

The tide will cause a horizontal force on the caisson and a vertical pressure equal to the tide difference on the seafloor at the sea side, which introduces seepage forces in the soil. The excess pore pressure which will be generated by the tide is a function of the octahedral normal stress changes, the shear stress changes (dilatancy effect) and the drainage boundary conditions. For simplicity the dilatancy component is disregarded in this example. If the soil were undrained, the pore pressure changes would thus be equal to the octahedral normal stress changes. These may be calculated with a finite element method using a material model according to Duncan and Chang (1970).

The effect of drainage has been evaluated by means of a finite element analysis for uncoupled consolidation, with the computer program FECON 2 (Martin and Schiffman, 1977), assuming that the pore pressures are generated with a constant rate. The calculated excess pore pressure distribution after 5 hours, when the tide has reached its maximum value, is presented in figure 13.

The pore pressure generation in the soil beneath and around the caisson at the end of the storm is found by first calculating the pore pressure which could have been generated if no drainage were taking place. It is then assumed that this pore pressure is building up with a constant rate during the storm, and the simultaneous pore pressure dissipation during the storm and the remaining excess pore pressure at the end of the storm are calculated. (A varying rate of generation could also have been analysed.) The excess pore pressures from the tide, figure 13, are input as initial pore pressures.

To start calculation of pore pressure production cyclic shear stress ratios τ_c/σ'_0 , have been determined by a finite element analysis with a material model based on Duncan and Chang (1970) and Hardin and Drnevich (1972). Other improved material models may be used. Figure 14 shows a distribution of the calculated stress ratios for the maximum wave, whereas stress ratios for smaller waves are assumed to be proportional to the wave forces. Each element will thus be subjected to a storm-loading composed as shown in the table in figure 14.

In section 2.5 on interpretation of varying cyclic shear stresses, it was shown that the excess pore pressure generation can be determined by accumulating pore pressure in a contour diagram as the one of figure 10a. In this way the excess pore pressure has been determined for all elements in the soil. The results is presented in figure 15a which shows the excess pore pressure generated by cyclic storm loading under undrained conditions at the time the maximum wave attacks.

The pore pressure dissipation occurring simultaneously with the generation has been calculated by the same program for uncoupled consolidation as used for the dissipation of the pore pressures generated by the tide. Since there will be a reloading of effective stresses during the pore pressure dissipation, the unloading/reloading compressibility was used.

The calculated development of excess pore pressures with time is presented in figure 16 for 4 different points in the soil. The pore pressure generations under undrained conditions are included for comparisons. The distribution of excess pore pressure at the end of pore pressure generation including the effect of drainage, is presented in figure 15b.

As mentioned in section 2.4, cyclic loading accompanied by preshearing will reduce the tendency for excess pore pressure generation. This effect is disregarded in these calculations. For the Oosterschelde soil conditions, this will be conservative, in the sense that the calculated pore pressures in figure 15b will be

upper limits. Instead of analysing the entire storm period the storm may be divided into smaller time intervals. The procedure may then be used to analyse each time interval and update the soil properties from one time interval to another.

ACKNOWLEDGEMENT

Many persons within the organisation of the authors have contributed to the work described herein, and the authors would in particular like to express their thanks to mr. W. Rosenbrand and mr. F. Schenkeveld of LGM to Dr. P.B. Selnes, mr. P. Stenhamar and mr. S. Kildalen of NGI, to Prof. R. Schiffman of the University of Colorado and to Dr. M. Goldscheider and mr. H. Winter of the University of Karlsruhe.

REFERENCES

- Andersen, K.H., 1976, Behaviour of clay subjected to undrained cyclic loading, International Conference on Behaviour of Offshore Structures, Boss'76, Trondheim, Vol. I, pp. 392-403. Also published in NGI Publication 114.
- Andersen, Hansteen, Høeg and Prevast, 1978, Soil deformations due to cyclic loads on offshore structures, Chapter 13 in Numerical Methods in Offshore Engineering, Wiley, 1978.
- Bjerrum, L., 1973, Geotechnical problems involved in foundations of structures in the North Sea, Geotechnique, Vol. 23, No. 3, pp. 319-358.
- Darve, F. et al., 1976, Incremental stress-strain relationship for cohesionless soil; Numerical Methods in Geomechanics, Vol. I, pp. 264-269.
- De Leeuw, E.H., 1976, Results of large scale liquefaction tests, International Conference on Behaviour of Offshore Structures, Boss'76, Trondheim, Vol. II, pp. 65-84.
- Delft Soil Mechanics Laboratory (LGM), 1975, Internal reports CO-227760 and CO-401260.
- Duncan, J.M. and C.Y. Chang, 1970, Nonlinear analysis of stress and strain in soils, ASCE, Proceedings, Vol. 96, No. SM5, pp. 1629-1653.
- Finn, W.D. Liam, P.L. Bransby and D.J. Pickering, 1970, Effect of strain history on liquefaction of sands, Journ. on Soil Mech. and Found. Div., ASCE, Vol. 96, No. SM6, pp. 1917-1934.
- Goldscheider, M., 1976, Dilatanzverhalten von Sand bei geknickten Verformungswegen, Mech. Res. Comm. 2, pp. 143-148.
- Goldscheider, M. and H. Winter, 1977, Triaxial test for determination of combined liquefaction parameter β / kD , Karlsruhe, International Report for LGM.
- Gudehus, G., 1978, Stability of saturated granular bodies under cyclic load, Proc. Int. Symp. on Dynamic Methods in Soil and Rock Mechanics, Vol. III, Karlsruhe, 1977, Balkema, Rotterdam.
- Hardin, B.C. and V.P. Drnevich, 1972, Shear modulus and damping in soils; design equations and curves, ASCE, Proceedings, Vol. 98, No. SM7, pp. 667-692.
- Heijnen, W.J., 1976, Ergebnisse einiger bodenmechanischer Studien und Versuche im Rahmen der Absperrung der Oosterschelde in den Niederlanden mit einem Caissondam, Verträge Baugrundtagung, Dtsch. Ges. f. Erd- und Grundbau, Essen.

Kolymbas, D., 1978, Ein nicht-lineares viscoplastisches Stoffgesetz für Böden, Veröff. Inst. Bodenmech. Felsmech., Heft 77, Karlsruhe.

Lambe, T.W., 1977, Prediction of strain and pore pressure from cyclic triaxial tests, Document L-40, Rijkswaterstaat Deltadienst, Den Haag.

Martin, H.L. and R.L. Schiffman, 1977, FECON 2 - a computer program for two-dimensional uncoupled consolidation, user's manual, Norwegian Geotechnical Institute, Internal Report 51405-8.

Mori, K. et al., 1978, Influence of sample disturbance on sand response to cyclic loading, Journ. Geot. Eng. Div., Proc. ASCE, Vol. 104, GT3, pp. 341-356.

Norwegian Geotechnical Institute, 1977, Calculated pore pressure generation and cyclic and permanent displacements of the Hammen 17 caisson, Contract report 77302-4.

Norwegian Geotechnical Institute, 1977, Undrained simple shear tests on Oosterschelde sand, Contract report 77302-3.

Seed, H.B., 1976, Evaluation of soil liquefaction effects on level ground during earthquakes. Spec. Session on Liquefaction Problems in Geotechnical Engineering, pp. 3-104, ASCE National Convention, Philadelphia.

Smits, F.P., 1976, Predictions of in-situ caisson test I by analytical plasticity analysis and by 1-g modelling, LGM, Delft.

Smits, F.P., 1977, Similitude studies on offshore structures at $n_g = 1$ scale, Proc. 9th Int. Conf. on Soil Mech. and Found. Eng., Tokyo, Vol. 2, pp. 401-405.

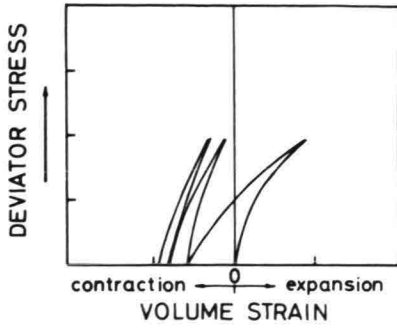


Fig. 1: Volume change in a drained cyclic triaxial test

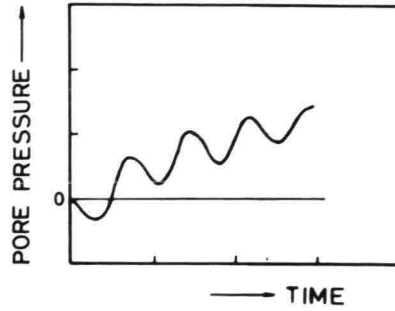


Fig. 2: Pore pressure change in an undrained cyclic triaxial test

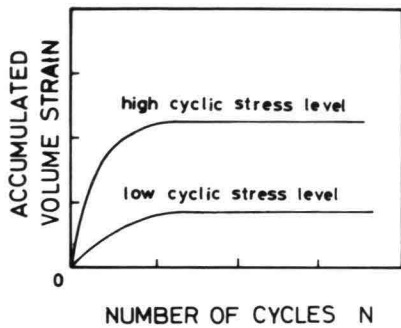


Fig. 3: Decrease of volume with number of cycles in a drained triaxial test

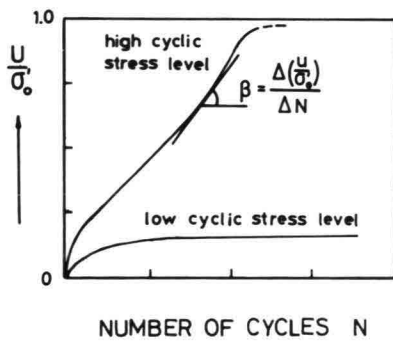


Fig. 4: Increase of pore pressure with number of cycles in an undrained triaxial test

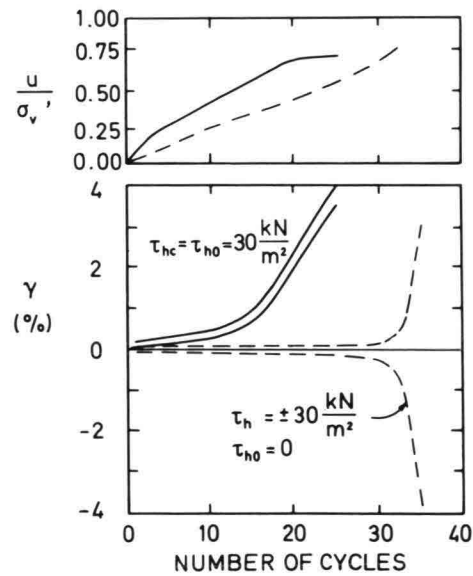


Fig. 5: Typical results from two simple shear tests with undrained cyclic loading.
 a) Zero static shear stress
 b) Static shear stress of 30 kN/m^2

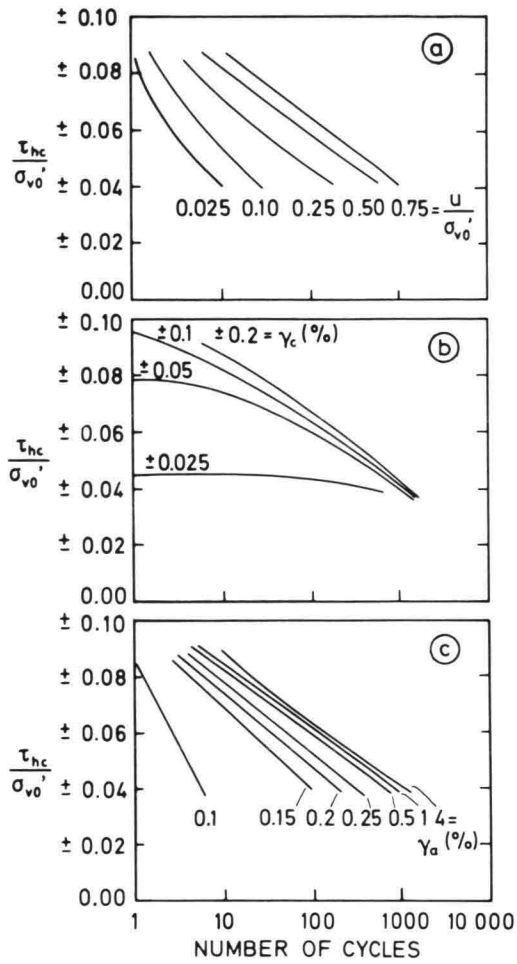


Fig. 6: Summaries of results from un-drained stress-controlled cyclic simple shear tests with a static shear stress of 25 kN/m²

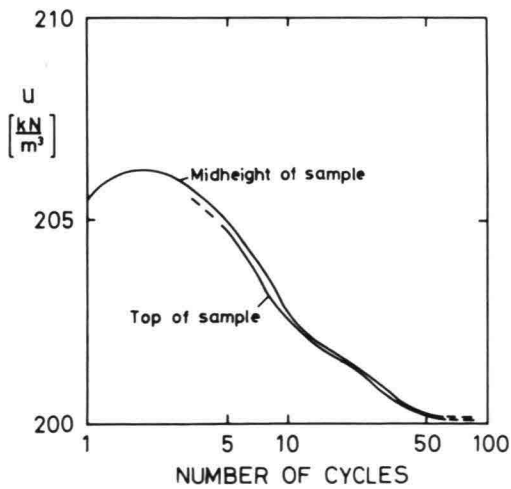


Fig. 8: Pore pressure versus number of cycles in β^*/kD -test

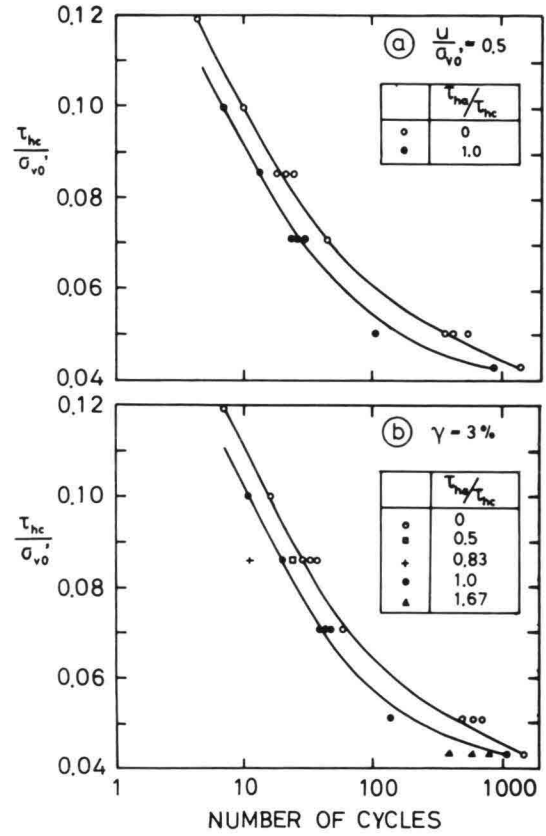


Fig. 7: Effect of average and cyclic shear stress ratios in simple shear tests

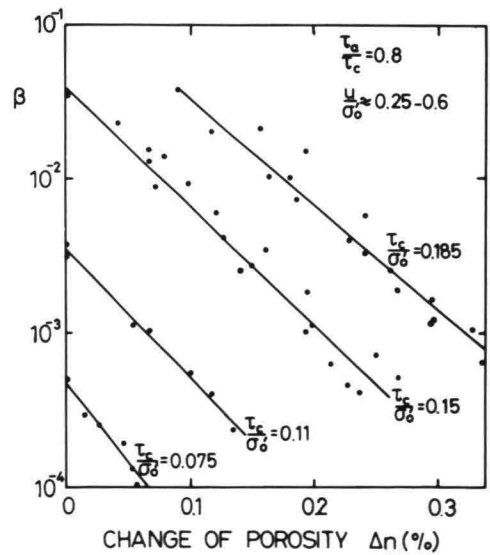


Fig. 9: Effect of preshearing: reduction of β with decreasing porosity by cyclic loading

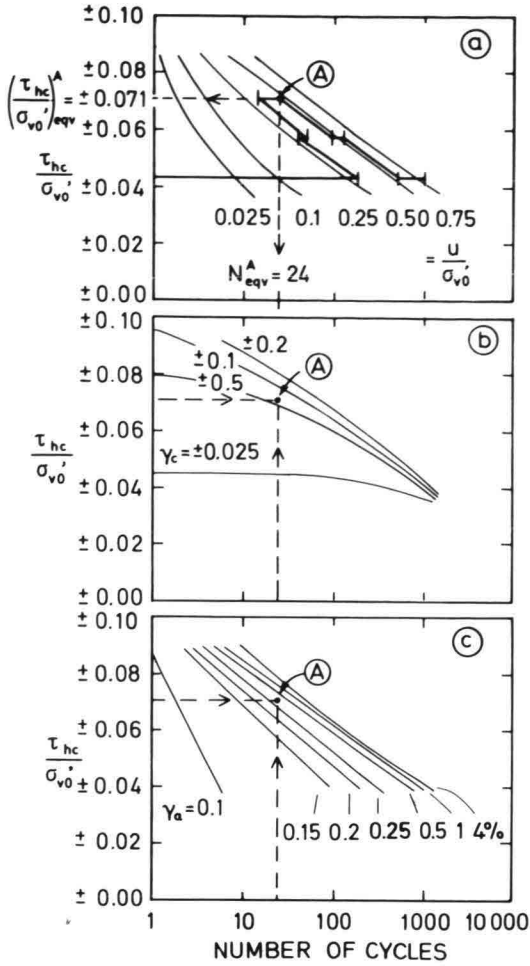


Fig. 10: Prediction of excess pore pressure and average and cyclic shear strains with varying cyclic shear stresses.
 a) Development of excess pore pressure and determination of equivalent number of cycles.
 b) Determination of cyclic shear strain.
 c) Determination of average shear strain

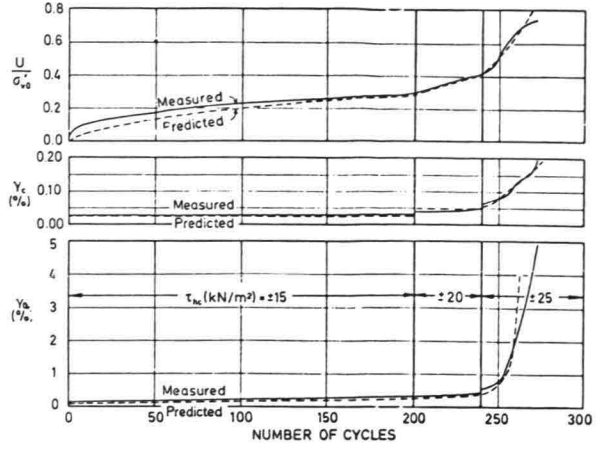


Fig. 11: Comparisons between calculated and measured excess pore pressure and strains for a simple shear test with varying cyclic shear stress amplitudes.

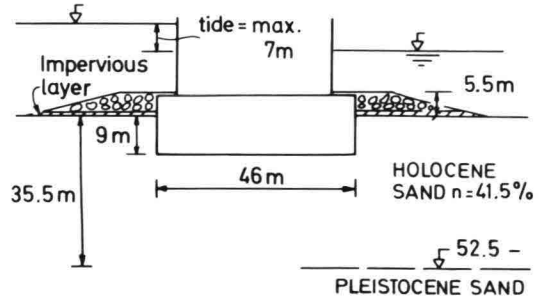


Fig. 12: Example problem.

STORM LOADING SCHEME:

No. of waves	Horizontal force (kN)	Moment (kNm)	$\frac{\tau_c / \sigma'_c}{(\tau_c / \sigma'_c)_{max}}$
49	+ 24600	+ 509000 / -381000	0.43
24	+ 32800	+ 668000 / -501000	0.57
4	+ 41500	+ 835000 / -626000	0.71
1	+ 49300	+ 989000 / -742000	0.86
1	+ 58700	+1202000 / -901000	1.00

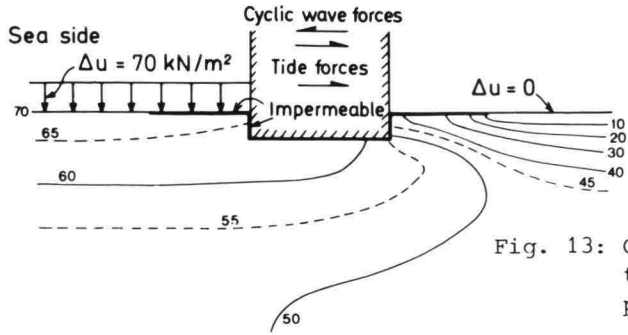


Fig. 13: Calculated excess pressure due to the tide. Numbers give excess pore pressure in kN/m².

No of waves	$\frac{\tau_c}{\sigma'_o} / (\frac{\tau_c}{\sigma'_o})_{max}$
49	0.43
24	0.57
4	0.71
1	0.86
1	1.00

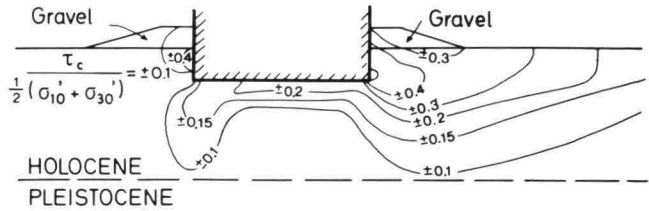
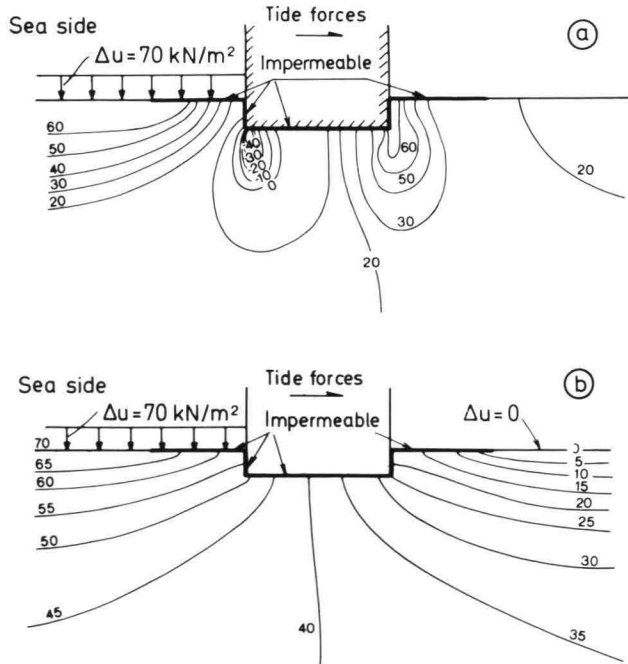


Fig. 14: Calculated cyclic shear stress ratios τ_c / σ'_o , for the maximum wave.



Numbers give excess pore pressures in kN/m²

Fig. 15: Calculated excess pore pressure due to cyclic storm loading.
a) Undrained conditions
b) Drained conditions

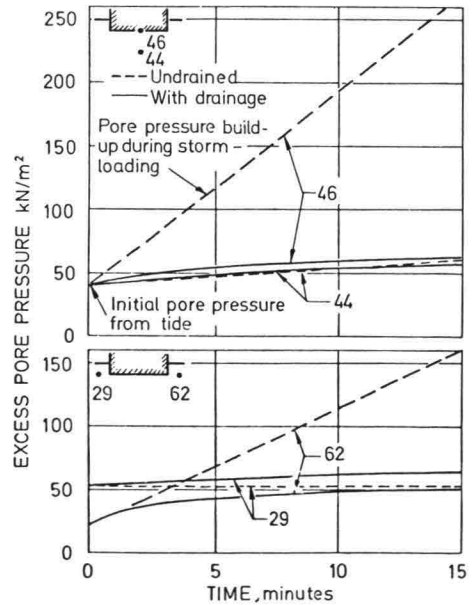


Fig. 16: Development of excess pore pressure at various points in the soil during the storm.

SYMPOSIUM ON FOUNDATION ASPECTS OF COASTAL STRUCTURES

PROBABILISTIC APPROACH TO DETERMINE LOADS AND SAFETY FACTORS.

By: D. Kooman, project engineer Rijkswaterstaat, Deltadienst,
Den Haag, Nederland

J.K. Vrijling, project engineer DOSBOUW v.o.f., Burghsluis,
Nederland

T. Mulder, project engineer DOSBOUW v.o.f., Burghsluis,
Nederland

L. de Quelerij, project engineer, Rijkswaterstaat, Deltadienst,
Den Haag, Nederland.

SYNOPSIS

The designcriteria of the Stormsurgebarrier Oosterschelde are related to the designcriteria of sea-retaining dikes, which are postulated in statistical terms by the former Deltacommittee.

Both loads on and strength of the SSB-structural elements are determined in statistical terms in order to check the semi-probalilistic design and the stipulated probability of failure. The probability of failure is derived by means of probabilistic calculations. Described are transformation of boundary conditions into a probability distribution of loadings. The principle of the probabilistic computation and the determining of the basic variables of the foundation structure is indicated. The calculated probability of failure is discussed in relation with the partial safety factors of the semi-probabilistic method. The effects of varying the statistical parameters on failure probability is shown.

1. GENERAL ASPECTS

The stormsurgebarrier (SSB) across the mouth of the Oosterschelde, has been planned, to permit the closure of this estuary during stormfloods. Under normal circumstances, the reduction of the vertical tidal movement, due to the open barrier is not allowed to be more than about 20%. Because the SSB will be closed when a high sealevel occurs, enormous forces will be exerted during extreme stormfloods. This paper gives some information about the probabilistic approach of both the loading on and the design of the SSB.

After the stormflooddisaster of February 1st, 1953, the Netherlands Delta Committee stipulated that primary sea-retaining structures have to provide full protection against stormsurgelevels with an excess-frequency of $2,5 \cdot 10^{-4}$ per year. In the case of conventional defences, such as dikes, an extreme waterlevel may be used as a designcriterion, because overtopping is the most important threat to dikes. However, this differs in the SSB case. This construction consists of concrete pillars, steel gates, a sill, bottomprotection and a foundation. These components have to be designed on the basis of loadingcombina-tions which will give the most dangerous threat to the structural stability. These loading combinations originate from waves and headloss and are threfore only partially dependent on the seawaterlevel. This means, that the direct link with the Deltacommittee stipulation has been lost. Therefore, the design highwaterexcessfrequency is considered to be the excess-frequency of the "potential threat" to a sea-defense, whatever the construc-tion appearance maybe. This means a research programme which has to result in a probability density function (p.d.f.) of loadings (forces, moments, pressures), derived from the multi-dimensional p.d.f. of the natural boundary conditions (waves, seawaterlevels, inside waterlevels), and of the responsfunction of the construction.

Using the p.d.f. of the loadings, there are several design levels on which a design-process can be carried out. In the different levels is expressed how far the stochastic character of the construction itself is taken into account. The more stochastic aspects are incorporated into the designprocess, the more complex the designprocedure will be. The following scheme (fig.1) gives the various levels, with increasing complexity, on which a construction can be designed.

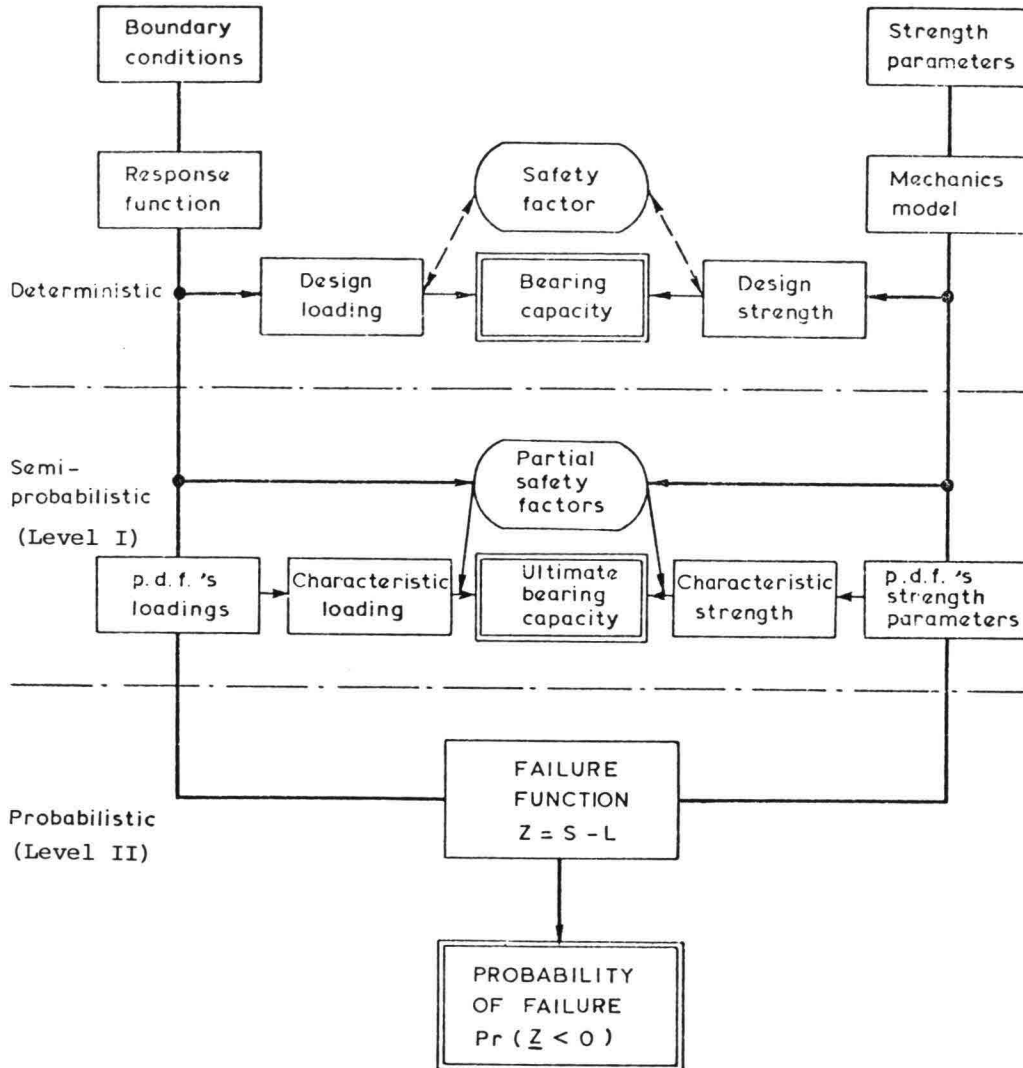


fig. 1 Designlevelscheme

In the deterministic method, attention is hardly paid to the stochastic aspects of the designprocess. All uncertainties are considered to be covered by one, overall, safety factor. In the semi-probabilistic method, a deterministic choice is made with regard to the design load. In this case: the load with the probability of exceedance of $2,5 \cdot 10^{-4}$ per year, the so-called "extreme load" is chosen. By means of a set of safetycoefficients, the stochastic character of the parameters, involved in the bearing capacity of the construction (e.g. strength, dimensions, model-results) is incorporated. With the help of these safety-coefficients, the design-load and the characteristic strength (the strength, having a defined lefttail probability) are separated. Information is given in more detail in par. 4.

Reference to the probabilistic method is made, when both the p.d.f.'s of the loadings and the strength-parameters are taken into account in the mechanical calculations to evaluate the failure probability of a structural element.

The SSB is a construction, consisting of various components. The failure probability of these components is calculated by means of the probabilistic calculations. One of the aims of the probabilistic approach is to obtain knowledge about the failure probability of the complete construction. Therefore the relation between the failure of the components and the complete construction must be known. Also knowledge about other failure-influencing aspects such as mis-management have to be known. Instruments to demonstrate the interactions between these aspects are the "event- and faulttrees".

As the SSB is a complex structure and the probabilistic method a new technique, the policy will be that the construction is designed by the semi-probabilistic method and checked as much as possible by the probabilistic method. This has the advantage, that on the one hand the safety coefficients used can be tested and on the other hand effects of variations in the p.d.f.'s of construction properties can be made clear quantitatively. This will provide information for the set-up of testing-systems and control programmes.

The formation and use of fault-trees will be discussed in par. 2. The way in which the p.d.f.'s of the loadings, based on the p.d.f. of the natural boundary conditions have been determined, will be discussed in par. 3. In par. 4, is explained how the p.d.f. of the strength was achieved and the use of the p.d.f. in both the semi-probabilistic and the probabilistic method. Finally par. 5 discusses how the failure probability has been calculated for the various ultimate bearing-capacity models of the foundation.

2. FAULTTREES

A faulttree is a very useful instrument for analysing the failure behaviour of a complex system. It can be defined as a scheme of the causal relationships between a well-defined undesired situation and all the possible causes. Information, necessary for the formation of a faulttree is obtained from "event-trees". An event-tree is a scheme of the causal relationship between a well-defined undesired event (= one of the causes of the faulttree) and all possible effects. Concentrating on faulttrees, it is stated that an undesired situation can be caused by:

- technical failure of structural elements
- management faults
- aggressive human action (sabotage, war, etc.)
- Acts of God (meteorstrike, planecrash, etc.)

In the SSB case, the undesired situation is the inundation of parts of Zeeland caused by an extreme discharge through the barrier.

The engineering responsibility is mainly limited to the technical failure of SSB-parts or the complete SSB.

The failuresystem of the SSB consists of 3 main elements:

- M: management system
 - malfunctioning without structural failure
 - failure of structural elements
- T: technical system
 - exceedance of loading
 - shortage of bearing capacity

} of construction elements
- C: causalities
 - causal relationship between malfunctioning and failure of construction elements

These 3 elements contribute tot the failure probability of a certain construction element.

In principle, a faulttree can be shown as follows:

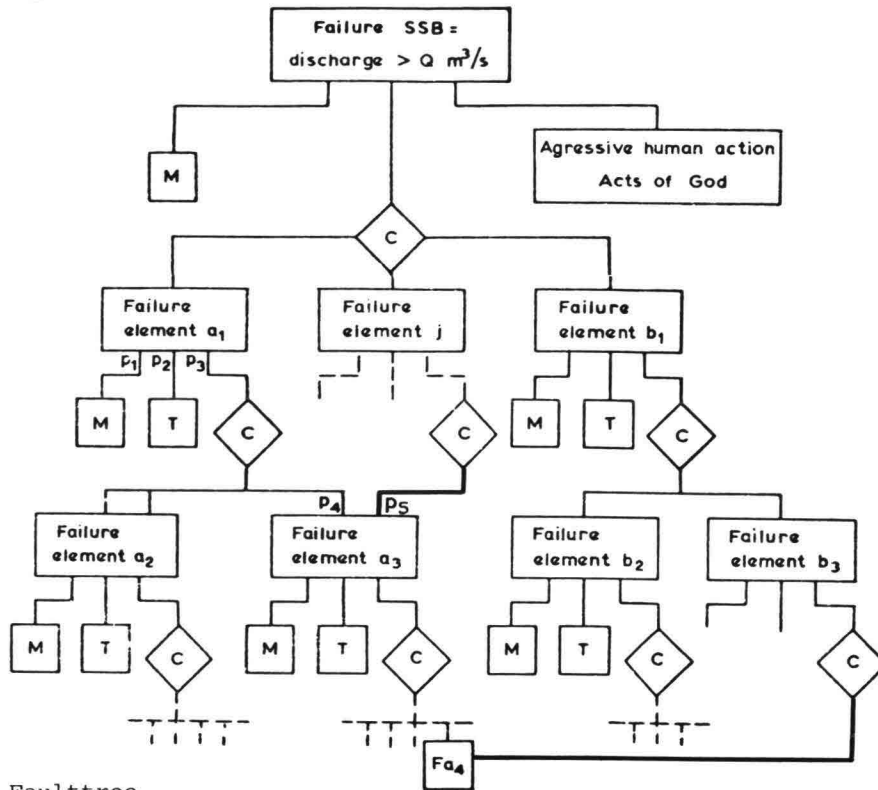


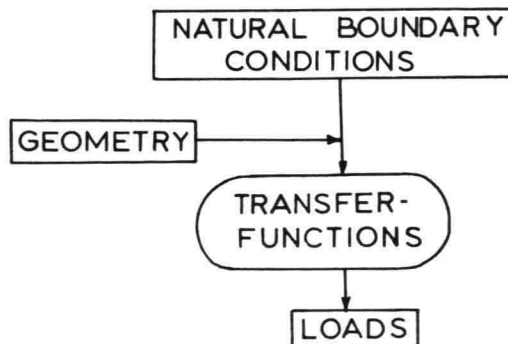
fig. 2 Faulttree

The influence of M is the most difficult to estimate, but can be limited by reducing the influence of human error e.g. by using computer processing. Important parts of M can be transferred to T, which can be more objectively quantified. The probabilities of T and C can be evaluated by means of the probabilistic calculations. The correlation factors P_1, P_2 , etc., which indicate the individual contribution of M, T and C to the next undesired event, are also necessary. However, there is often a lack of statistical information about these correlations. Then, "engineering judgement" has to contribute. With the help of the described analysis, the effect of the failure probability of for example element a3 on the failure probability of the SSB can be made clear. Also the effect of improvements of the foundation (e.g. by better compaction) on the SSB-failure probability can be quantitatively judged. Furthermore, the effect of measures in the management sphere can be traced.

3. PROBABILITY FUNCTION OF LOADINGS

In the case of the storm surge barrier it is obvious that loads exerted by the natural boundary conditions mainly by waves and headloss play a dominant role.

The following scheme tries to show, that not only knowledge of these boundary conditions is necessary, but that some transfer functions have to be available to transform these natural boundary conditions - given a certain geometry - in loads acting on the barrier.



- 5 -

These transferfunctions can be the result both of mathematical and scale models.

By considering the natural boundary conditions as stochastic elements with their probability density functions it is possible to determine a statistical description of the total load acting on the barrier (being a combination of wave and headloss-loads) following the above-mentioned scheme.

For the determination of the loadings the most important boundary conditions are:

1. the stormsurge level at sea
2. the waterlevel on the Oosterschelde
3. the prevailing seastate.

For the headloss 1 and 2 are decisive; 1 and 3 for the wave-load on the barrier. The stochastic properties of these parameters will now be discussed.

For the distribution of the stormsurge level on the sea the already well-known excess frequency curve for stormlevels for Burghsluis and Vlietepolder (corrected on influences due to the Delta Works, inclusive of the SSB) has been used as a starting point. This frequency curve has been based on many years of statistics.

$$F(\underline{HW} > HW) = \exp\left(-2.3 \frac{HW - 2.94}{0.696}\right)$$

The distribution of the waterlevels on the Oosterschelde has been based on the distribution of low-waterlevels which precede stormsurgelevels, which will lead to the close the barrier. Next, consideration was given to the effects of the Oosterschelde-waterlevels caused by the closed barrier, such as wind setdown, translation waves, fluctuations etc.

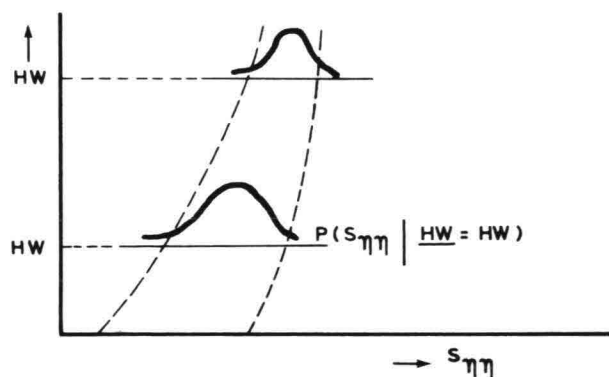
Based on the central limit theorem a normal distribution is chosen for the waterlevels on the Oosterschelde with

$$\mu_{IWL} = \text{NAP} - 0,25 \text{ m and } \sigma_{IWL} = 0,65 \text{ m.}$$

By studying on the one hand the physical background of the phenomena of the wind set-up and the wave-generation and on the other hand the observations during recent stormfloods, it has been possible to determine the probability density function of wavespectra as a function of the stormsurgelevel.

fig. 4

wave-spectra -
stormsurgelevel -
relationship



$$P(S_{\eta\eta} | \underline{HW} = HW)$$

Now the joint probability density function of wave spectra and stormsurgelevels can be determined.

$$P(S_{\eta\eta}, HW) = p(HW) \times P(S_{\eta\eta} | \underline{HW} = HW)$$

Starting from hydrostatic pressure-distributions on both sides of the barrier and a potential profile in the sill around the base of the pillar, the headloss-load (HL) can simply be indicated as a function of the geometry of the structure,

the storm surge level and inner waterlevel.

$$HL = f (H W ; I W L, \text{ geometry})$$

For linear systems the transition from waves to waveloads takes place with the aid of the "spectral method". To this end the irregular surface of the sea is described by means of a "variance spectrum", to be called wave-spectrum from now on ($S_{\eta\eta}(f)$)

As in this case the wave-spectra are relatively narrow the traditional parameters $H_z 1/3$ (significant wave height) and T_z (mean wave period) can be obtained by means of the following relations.

$$H_z 1/3 = 4\sqrt{m_0} \qquad T_z = 2\sqrt{\frac{m_0}{m_2}}$$

$$m_{11} = \int_0^{\infty} f^n \times S_{\eta\eta}(f) df$$

As, by approximation, the transition from waves to wave-loads is a linear phenomenon, we can find for the wave-load a similar spectrum:

"wave-load spectrum" $S_{bb}(f)$

Starting from a transferfunction $O(f)$ which is defined as:

"the wave-load (o-top) per unit of wave-amplitude as function of the wave frequency", the following relationship exists between the wavespectrum and the wave-load spectrum.

$$S_{bb}(f) = O^2(f) \times S_{\eta\eta}(f)$$

For the SSB these transferfunctions for the waveload have been determined with the aid of mathematical models based on linear wave-theories. Checks on linearity and magnitude were made by means of scale models in the Hydraulics Laboratory at Delft.

The waveload spectrum, determined in the above mentioned way, contains the statistical information needed to establish in a simple way the probability distribution of the individual wave loads WL, namely:

$$P(WL > WL) = \exp\left(-\frac{(WL)^2}{2m_0}\right) \qquad \dots\dots\dots \text{Rayleigh-distribution}$$

Depending on the limit-state one wishes to consider, it is possible now to use this probability distribution in various manners.

In the case of increasing deformations, where all waveload amplitudes are in principle important one will use the Rayleigh-distribution and the probability density function to be deduced from this

$$p(WL) = \frac{\partial}{\partial WL} \{P(WL > WL)\} = \frac{WL}{m_0} \exp\left(-\frac{(WL)^2}{2m_0}\right)$$

if, on the other hand, a model is considered where a one time exceedance of the load leads to collapse, then one ought to find the probability distribution of the waveloads, which are exceeded at least once. Starting from N independent waveloads within the duration of a seastate, according to the Binomial-distribution, the chance, that none of the wave-loads will exceed a level WL, equals

$$\{1 - P(WL > WL)\}^N$$

The probability that the level WL is exceeded at least once, equals:

$$1 - \{1 - P(WL > WL)\}^N$$

- 7 -

The related probability density function then reads:

$$p(WL) = \frac{WL \times N}{m_0} \{1 - P(WL > WL)\}^{N-1} \times P(WL > WL)$$

Finally we can still view another model, where collapse only occurs when a load-level is exceeded several times (dynamic pore pressure generation). Based on the Binomial-distribution we find for the probability distribution of a load, which exceeds a given level WL m times:

$$1 \left[\sum_{k=0}^{k=m-1} \frac{N!}{k!(N-k)!} \times P(WL > WL)^k \times \{1 - P(WL > WL)\}^{N-k} \right]$$

Based on the probability density function $p(HW)$ of the storm surge levels and the conditional probability density functions of the wavespectra $p(S_{\eta\eta} | \underline{HW} = HW)$ and the inner waterlevels $p(IWL | \underline{HW} = HW)$ it is possible to determine the probability of occurrence of a combination of a storm surge level class, a wavespectrum class and an inner water level class:

$$\begin{aligned} & P(HW_i \leq \underline{HW} < HW_i + \Delta HW \text{ and } S_j \leq \underline{S} < S_j + \Delta S \text{ and} \\ & IWL_k \leq \underline{IWL} < IWL_k + \Delta IWL) \\ & = \int_{HW_i}^{HW_i + \Delta HW} P(HW) dHW \times \int_{S_j}^{S_j + \Delta S} P(S_{\eta\eta} | \underline{HW} = HW) dS_{\eta\eta} \times \int_{IWL_k}^{IWL_k + \Delta IWL} P(IWL | \underline{HW} = HW) dIWL \end{aligned}$$

(as $S_{\eta\eta}$ and IWL are independent)

By using transfer functions for the waves and the headloss the probability of occurrence of the waveload spectrum and the headlossload belonging to that combination of natural boundary conditions is known. By doing this for each possible combination of boundary conditions, a joint probability density function of the waveload spectra and the headlossload can be found.

Introducing the probability density function of the individual wave loads (depending on the type of limit-state under study) this joint p.d.f. of waveload spectra and headlossload can be transformed in a p.d.f. of individual wave-load and headlossload.

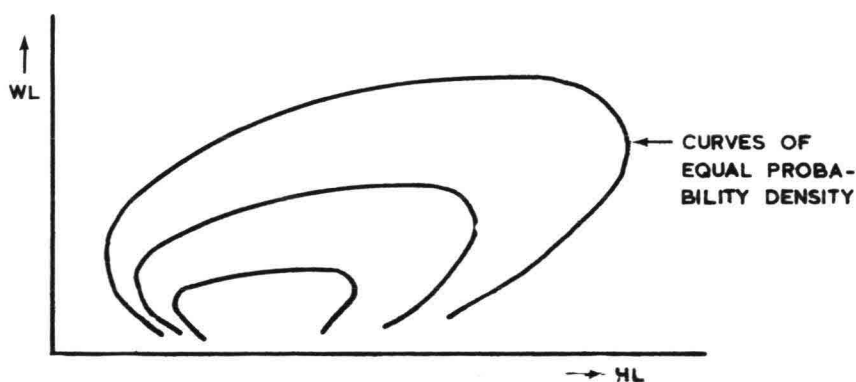


fig. 5

To arrive at a probability distribution of a total load TL for a specific limit-state, based on the joint p.d.f. of individual waveload and headlossload (e.g. load perpendicular on the SSB, moment at foundation level etc.) it has to be known in what ratio the wave and headlossload contribute to this limit-state.

In general this can be defined as follows:

$$TL = \alpha \times HL + \beta \times WL$$

Now the probability of exceedance of a specified total load can be determined per limit-state by integrating the bi-dimensional probability density function $p(HL, WL)$ over the area for which $\underline{TL} > TL$, applies.

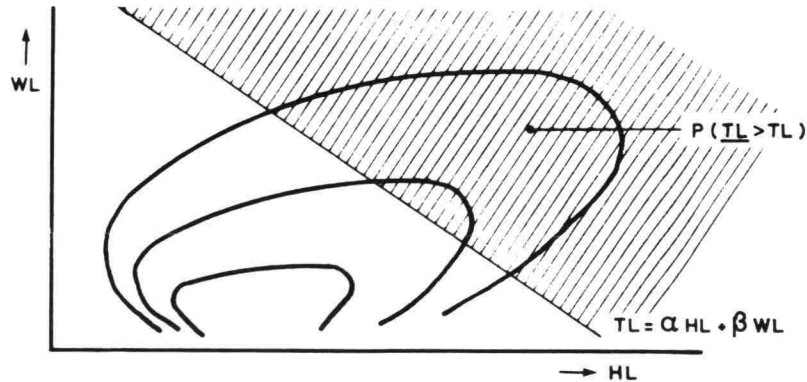


Fig. 6

$$P(\underline{TL} > TL) = \int_{\underline{TL} > TL} p(HL, WL) dHL dWL$$

With regard to the soil mechanical part of the design we can distinguish a few specific cases concerning the composition of the total, namely:

1. Sliding-model, where the headlossload and the quasi-static waveload share an equal part : $\alpha = 1$; $\beta = 1$
2. Ultimate bearing capacity model, according to Brinch-Hansen, where the wave load is halved: $\alpha = 1$; $\beta = \frac{1}{2}$
3. Pore pressure generation, whereby the influence of the static headloss load is negligible with respect to the cyclic waveload : $\alpha = 0$; $\beta = 1$

4. DESIGN APPROACH

4.1. Semi probabilistic approach.

Traditionally the parameters used in structural design have been thought of as specified constants, but in reality they are at random which implies that their exact magnitude is not known with certainty in the design stage and in the case of the hydraulic loads, as shown above, not even after construction.

For an advanced analysis, that takes account of this random character.

It is necessary to specify a set of basic variables. These are normally the fundamental parameters which play a role in the theoretical relationships, on which the design of a particular structure is based.

The main categories of basic variables are resistance and loading (see fig. 4.).

The p.d.f. of the resistance is mainly determined by variations of the strength of material, geometric deviations and uncertainties in theoretical relationships.

In the field of mechanical properties of materials large quantities of test data are available which have been analysed to obtain means, standard deviations and distribution types. It is found that the strength of ductile materials including prestressed concrete is well represented by a log-normal distribution.

Data for brittle materials fits a Weibull distribution.

For permanent loads, which are assumed to be constant during the life of the distribution function is assumed to be normal. The probability of maximum hydraulic loads is examined in paragraph 3. The structure of the barrier is

rather insensitive to geometrical imperfections; therefore the variability of structural dimensions and geometry is less important than the variations in load and strength parameters.

The uncertainties in theoretical relationships should be quantified by verifying theoretical solutions in comparison with a sufficient number of tests on full scale or representative models. The number of tests should be adequate to determine the mean value and the standard deviation of the ratio X_m , which is assumed to be normally distributed.

$$X_m = \frac{\text{Actual behaviour}}{\text{Predicted behaviour}}$$

For design purposes it is too cumbersome to take account of the probability distribution of the basic variables.

The introduction of the "characteristic value" concept simplifies the work without losing all statistical information.

The characteristic value of strength parameters is normally specified as a small percentage (5%) of the strength distribution.

The characteristic values of loads are as a rule defined as those having a probability of excess of 5% during the life of the structure.

For normal design purposes a code of practice specifies the use of design equations in which sufficient reliability is achieved by the use of a number of partial safety factors:

In the design of the storm surge barrier the definitions and purposes of the partial safety factors as described in ISO standard 2394 are used.

For the sake of completeness they are summarised below:

γ_{s1} takes into account the possibility of unfavourable deviation of the loads from the characteristic external loads,

γ_{s2} takes into account the reduced probability that various loadings acting together will all be simultaneous at their characteristic value,

γ_{s3} is intended to allow for possible adverse modification of the load effects due to incorrect design assumptions and constructional discrepancies,

γ_{m1} is intended to cover possible reductions in the strength of the materials in the structure as a whole as compared with the characteristic value obtained from specimen control tests,

γ_{m2} is intended to cover possible weaknesses of the structure arising from any other cause than the reduction in the strength of the materials allowed for in γ_{m1} , including manufacturing tolerances,

γ_{c1} is intended to take account of the nature of the structure and its behaviour: for example progressive collapse,

γ_{c2} is intended to take account the seriousness of attaining a limit state from other points of view for example economic consequences, danger to community.

The performance requirements to be met with regard to any limit state are then

ULTIMATE LOAD \leq ULTIMATE RESISTANCE

FUNCTION ($\gamma_{c1} \times \gamma_{c1} \times \gamma_{s1} \times \gamma_{s2} \times \gamma_{s3}$ x Effects of F_k)

$$\leq \text{FUNCTION} \frac{f_k}{\gamma_{m1} \cdot \gamma_{m2}}$$

where F_k represents characteristic loads

and f_k " " strength

In practical design safety factors are mostly prescribed by national codes. The difficulties encountered with the design of the foundation to the (O.S.) stormsurgebarrier made a special assessment of the appropriate safety factors necessary. Led by engineering judgement the designers decided on the form as given below.

- $\gamma_{s1} = 1.0$ The design have a probability of exceedance of 2.5×10^{-4} per annum. Therefore no allowance is made for unfavourable deviations.
- $\gamma_{s2} = 1.0$ Wave and head loads are combined in a sophisticated manner taking account of their stochastical correlation.
- $\gamma_{s3} = 1.1$ Uncertainties in the theoretical models for the prediction of waves and wave loads could amount to 10% higher loads.
- $\gamma_{m1} = 1.1$ Besides a reduction of the friction angle measured in laboratory tests an allowance is made for the heterogeneous character of the soil layers which form the foundation.
- $\gamma_{m2} = 1.1$ Although the limit state of the foundation is mainly described by a simple friction model as will be shown below, a safety factor seemed necessary to allow for unexpected sand deposits between the construction and the foundation layers.
- $\gamma_{c1} = 1.0$ The possibilities for redistribution of forces between sill and construction are very uncertain so no allowance is made.
- $\gamma_{c2} = 1.15$ This factor takes into account the fact that before the equilibrium between loads and resistance is lost, the deformation becomes unacceptable.

Substitution of the factors in the limit state equation gives

$$\text{function} (1.26 \times \text{effects of } F_k) \frac{f_k}{1.2} \leq \text{function} (\frac{f_k}{1.2})$$

4.2. Probabilistic approach

After having established a set of safety factors for the foundation it is rational to execute a reliability analysis to find the failure probability of the structure under design. This probability should be in line with the reliability of the other parts of the barrier such as the steel and the concrete structure. The reliability of the foundation is determined by means of an advanced first order second moment method.

The starting point of this method is the reliability function:

$$Z = \text{RESISTANCE} - \text{LOADING} \geq 0$$

which may be expressed as a function of the basic variables essential to the problem

$$Z = g(X_1, X_2, X_3, \dots, X_n) \geq 0 \quad \dots (1)$$

Z should be considerably in excess of zero. The standard deviation of Z, σ_Z , is influenced by the variability of each of the basic variables X_i which are at

random by nature around their mean values m_i , as shown in the previous paragraph. The probability of failure is the probability that $Z < 0$. If Z is assumed to be normally distributed the index β , defined as

$$\beta = \frac{m_Z}{\sigma_Z}, \quad \dots (2)$$

determines the probability of failure.

If Z is approximated by a linearised form of the reliability function.

$$Z = g(x_1^*, x_2^*, \dots, x_n^*) + \sum_{i=1}^n (x_i - x_i^*) \cdot g_i(x^*) \quad \dots (3)$$

where $g_i(x^*) = \frac{\delta g}{\delta x_i}$ at the point $x^* = (x_1^*, x_2^*, \dots, x_n^*)$

$$\text{then } m_Z = g(x_1^*, x_2^*, \dots, x_n^*) + \sum_{i=1}^n (m_i - x_i^*) g_i(x^*) \quad \dots (4)$$

$$\text{and } \sigma_Z = \left(\sum_{i=1}^n (g_i(x^*) \cdot \sigma_i)^2 \right)^{\frac{1}{2}} \quad \dots (5)$$

In accordance with Lind σ_Z may now be expressed as a linear combination of the individual standard deviations

$$\sigma_Z = \left(\sum_{i=1}^n \alpha_i \cdot g_i(x^*) \cdot \sigma_i \right) \quad \dots (6)$$

$$\text{where } \alpha_i = \frac{g_i(x^*) \cdot \sigma_i}{\left(\sum_{j=1}^n (g_j(x^*) \cdot \sigma_j)^2 \right)^{\frac{1}{2}}} \quad \dots (7)$$

$$\beta = \frac{\sum_{i=1}^n (m_i - x_i^*) g_i(x^*)}{\sum_{i=1}^n \alpha_i \cdot g_i(x^*) \cdot \sigma_i} \quad \dots (8)$$

and by rearranging

$$\sum_{i=1}^n g_i(x^*) (m_i - x_i^* - \alpha_i \cdot \beta \cdot \sigma_i) = 0 \quad \dots (9)$$

The solution to this equations is therefore

$$x_i^* = m_i - \alpha_i \cdot \beta \cdot \sigma_i \text{ for all } i$$

which defines the linearisation point x^* generally known as design point.

If m_i , σ_i and β are given the design point may be found by solving equation (9) in conjunction with (7). An iterative procedure leads to the result; (Rackwitz) the failure probability.

A special problem is encountered one of the basic variables is not normally distributed. Then the original distribution will be replaced by a normal distribution. The mean and the standard deviation of the latter are chosen so that at the design point the probability density and the cumulative probability in the approximately normal and the original distribution are equivalent.

As stated above the starting point of a reliability analysis is the formulation of a reliability function in terms of the basic variables.

$$Z = \text{RESISTANCE} - \text{LOADING} \geq 0$$

But in some fields of civil engineering no theoretical description of the studied phenomena is available. This is especially true for scour problems which govern the design of the top layer of the sill. Neither transfer functions to transform waves and head difference into forces exerted on stones, nor a theoretical model for the stability of the stones are known. To overcome these problems a scheme to simulate all possible combinations of wave attack and head difference in a scale model of the sill will be executed. By integration of the joint probability function of the boundary conditions (waves, inner- and outer waterlevels) over the area where serious damage at the sill is found in the model tests, a failure probability can be determined.

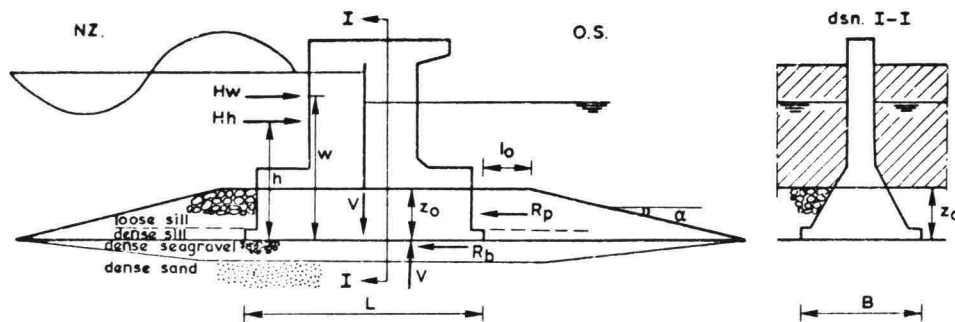
In paragraph 5 the reliability function for the foundation will be derived from the widely known theoretical models for foundation failure.

5.0 RELIABILITY ANALYSIS OF THE FOUNDATION.

5.1 Description of the theoretical failure models

The pillar, with an effective weight v , is placed on a foundation bed of compacted sea-gravel with dense sand underneath. The pillar is surrounded by a sill of coarse material (see fig.7).

fig. 7. Foundation construction of the stormsurge barrier.



geometry: L = pier length (50 m)	load: H_w , w = wave force-arm
B = pier width (25 m)	H_h , h = headloss force-arm
Z = embedment (11 m)	V = effective weight pier
l_0 = sill bank (10 m)	R_p = passive resistance
α = inclination (1:4)	R_b = horizontal base resistance.

The construction is subjected to a cyclic wave-force component and a static head-loss force as previously explained.

The resistance R of the foundation consists of two parts:

- the passive earthpressure of the sill material at the backwall of the pillar,
- the sliding resistance at the base of the pillar.

(NB. In this paper the consequences of the cyclic generation of excess pore pressure generation will not be considered).

The theoretical model for the passive resistance of the sill which is derived from the Kötter-equations is a function of the construction geometry and the soil-parameters (litt.2).

- γ_s = unit weight of sill, submerged
- ϕ_s = internal friction angle sill
- δ_s = friction angle sill - concrete backwall.

$$R_p = \frac{1}{2} \gamma_s \cdot z_o \cdot B \cdot \frac{1 + \sin \phi_s \sqrt{1 - (\tan \alpha / \tan \phi_s)^2}}{1 - \sin \phi_s \sqrt{1 - (\tan \alpha / \tan \phi_s)^2}} \cdot \exp \left[\left\{ \delta_s - \alpha + \arcsin \left(\frac{\sin \delta_s}{\sin \phi_s} \right) - \arcsin \left(\frac{\sin \alpha}{\sin \phi_s} \right) \right\} \tan \phi_s \right]$$

For the sliding resistance at the base two different slide planes have to be examined;

- a curvilinear slide plane which passes through the various layers of the subsoil,
- a straight slide plane that develops in the boundary layer between the concrete base and the seagravel bed.

The first possibility is modelled by the Brinch Hansen equations for the ultimate bearing capacity of excentrically loaded shallow foundations for drained conditions (litt. 1).

$$Q/BL' = \frac{1}{2} \gamma_b \cdot B \cdot N_\gamma \cdot i_\gamma \cdot s_\gamma + q \cdot N_q \cdot s_q \cdot i_q$$

Q = vertical ultimate bearing capacity

γ_b = submerged unit weight of subsoil

$$q = z_o \cdot \gamma_s$$

N_γ, N_q : bearing capacity factors

$$N_q = e^{\pi \tan \phi_b} \cdot \tan^2(45 + \phi_b/2); N_\gamma = 1,5 (N_q - 1) \tan \phi_b$$

ϕ_b = internal friction angle of subsoil.

$s_\gamma, s_q; i_\gamma, i_q$: shape and inclination factors

$$s_\gamma = 1 - 0,4 B/L'; s_q = 1 + \sin \phi_b \cdot B/L'$$

$$i_\gamma = \sqrt[5]{1 - 0,7 R_b/V}; i_q = \sqrt[5]{1 - 0,5 R_b/V}$$

$$L' = L - 2e \quad (\text{effective length})$$

$$e = \text{excentricity} = \frac{\text{base moment } M}{V}$$

The combinations of horizontal force and vertical bearing capacity, that fulfil the condition given by the Brinch Hansen equation, (plotted in fig.8) from a curve in the $Q - R_b$ plane (see fig.8).

Some attention should be paid to the calculation of the drained moment on the base area, which determines the excentricity e .

First, the moment caused by the passive resistance at the backwall (R_p) has to be subtracted from the external moment.

Secondly, only half of the wave moment has been taken into account, because the other half will be carried by the pore pressures in the subsoil, as modeltests at Kats and offshore experience have shown.

This yields for the excentricity

$$e = (M_h + \frac{1}{2} M_w - R_p \cdot \frac{1}{3} z_o) \cdot \frac{1}{V}$$

The possibility that a straight slide plane develops in the boundary layer between concrete base and foundation bed, is modelled by a simple friction law (base sliding model)

$$R_b = \tan \phi_b \cdot V.$$

A number of full scale tests have been executed on the boundary layer to assess

the friction co-efficient $\tan \delta_b$.
 In the $Q - R_b$ plane (see fig. 8) the base sliding model is given by a straight line. It is easily seen that for some combinations of horizontal and vertical forces the base sliding model forms the limit state as for other combinations the Brinch Hansen model is the limiting condition.
 So two reliability functions can be formulated:

1. $Z = R_{\text{passive}} + R_{\text{base}} - H_h - H_w$
2. $Z = R_{\text{passive}} + \tan \delta_b * V - H_h - H_w$

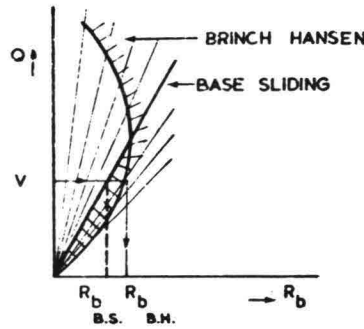


fig. 8 comparison of the two limit state models for the foundation.

5.2. Determination of the basic variables.

The basic variables X_i which play a role in the two reliability functions derived in the preceding paragraph are resumed in the table below.

	Base sliding model	Brinch Hansen Model
Geometry	$L, B, z_o, 1_o,$	$L, B, z_o, 1_o,$
Soil strength	$\gamma_b, \gamma_s, \phi_s, \delta_s, \delta_b$	$\gamma_b, \gamma_s, \phi_s, \delta_s, \phi_b$
Model factor	X_m	X_m
Load	$V, H_h + H_w$	$V, H_h + H_w, M_h + \frac{1}{2} M_w$

All parameters except the loading will be assumed to be normally distributed. First a global estimate was made for the mean and the standard deviation of the basic variables. Then estimate was refined for the parameters which the probability of failure.

The variation in the dimensions of the concrete structure (L, B) can be ignored with regard to this problem, because they will be recognised more accurately during construction. The sill-dimensions ($z_o, 1_o, \alpha$) on the other hand are sensitive to small changes in the construction method and to settlements afterwards. Therefore a standard deviation is specified for these parameters.

For the determination of the stochastic properties of the soil parameters only a very restricted number of measurements were available. So some engineering judgement had to be brought in.

The submerged unit weight γ_b, γ_s that is a function of the unit weight of the solids and the porosity is stable against large variations (5%) in porosity. For this reason the standard deviation is small.

The most complicated problem is the determination of the friction angle (ϕ_s) of the sill. Here the friction properties of a four layer system, partially compacted and with grain sizes increasing with height from gravel to stones of 1000-3000 kg, have to be expressed by one parameter. Because no test on the coarse materials was available the estimate has been based on tri-axial tests on sandfree loose seagravel. The lowest value (33°) of these tests is considered as a characteristic value for the four layer system of the sill.

A mean value $\mu(\phi_s) = 36^\circ$ is derived from the tests as a conservative value for the sill material.

According to Lambe and Whitman (Litt. 3) the friction angle between loose material

and a rough concrete surface is equivalent to the friction angle of the material itself.

However, with respect to the large grain-size of the sill material a pessimistic assumption was made.

$$\begin{aligned} \mu(\delta_s) &= \frac{2}{3} \cdot \mu(\phi_s) \\ \sigma(\delta_s) &= \sigma(\phi_s) \end{aligned}$$

The friction angle ϕ_b is a representative value for the twolayer system under the bottom of the pillar (see fig. 7). As however the slide planes pass mainly through the subsoil consisting of dense holocene sand, the friction properties of this material are taken as being decisive.

Because ϕ_b is mainly a function of the sand porosity great care will be taken to compact the subsoil and to check if the required relative density of 70% and a maximum porosity of 39% is reached.

Therefore drained tri-axial tests were carried out on samples with a density corresponding to this requirement.

For a mean prototype stress level equal to 200 kN/m^2 the stochastic properties of ϕ_b were determined:

$$\mu(\phi_b) = 36^\circ$$

$$\sigma(\phi_b) = 2^\circ$$

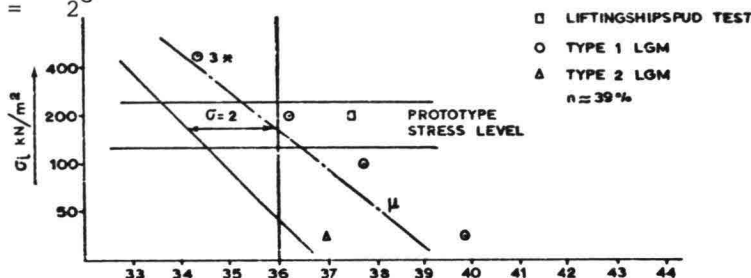


fig. 9. Standard deviation ϕ_b .

However some correction has to be made because the Brinch Hansen model is based on plain strain values, which can be approximated by 1.1. $\times \phi_{\text{triax}}$. this:

$$\mu(\phi_b) = 40^\circ$$

$$\sigma(\phi_b) = 2^\circ.$$

N.B. The small standard deviation reflects the result of careful compaction and extensive checking of the subsoil.

The essential parameter in the base-sliding model is obviously the friction factor $\tan \delta_b$.

Moreover this parameter is not easily assessed because it strongly depends on the construction of the boundary layer between concrete and gravel, the stress level and the loading condition (static or cyclic).

Therefore a number of scale tests were carried out on a 7 m^2 large copy of the scale 1:1 boundary layer construction including the foundation layer of gravel. The loading condition was also simulated at prototype scale as far as the frequency, the amplitude of the cyclic part and the static mean level were concerned. From a series of 5 tests results at different stress-levels were selected and translated to the prototype values given in the diagram below

$$\begin{aligned} \mu(\tan \delta_b) &= 0,67 \\ \sigma(\tan \delta_b) &= 0,05. \end{aligned}$$

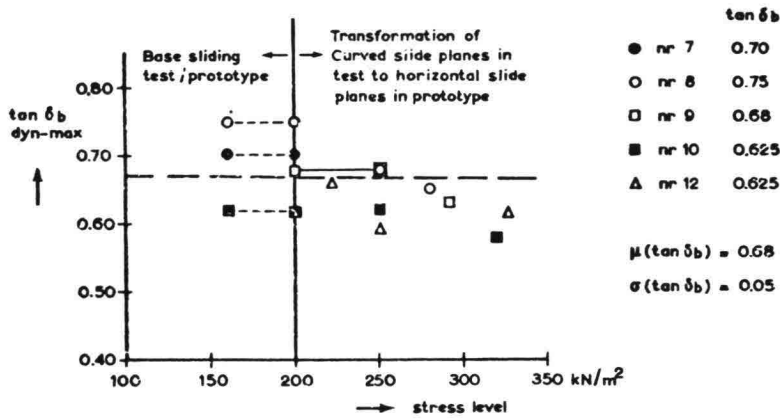


fig. 10. Standard deviation $\tan \delta_b$.

For the uncertainties in the theoretical models the parameter X_m has been introduced.

Although experiments and experiences seem to prove that Brinch Hansen is a conservative description of reality a mean value of 1.0 for X_m has been introduced. The same applies for the Kötter-equations which form the model for the passive resistance R_p .

The base sliding model needs no mean correction because the essential parameter $\tan \delta_b$ has been derived from tests under the presumed validity of the model. For the random uncertainty of all models a standard deviation of 6% is assumed. The derivation of the probability of exceedance function of the loads is dealt with in paragraph 3, but reference should be made to the difference in loading assumptions for the Brinch Hansen model and the base sliding model. This difference is accounted for by the choice of α and β in paragraph 3.

5.3. Results

According to the theory of paragraph 4 the probability of failure of the two reliability functions specified above has been evaluated.

Besides that the contribution of each basic variable to the variance of the reliability function is calculated.

table 2. Reliability analysis.

Basic variables X_i	Dimension $\overline{X_i}$	Mean values $\mu(X_i)$	Standard deviation (X_i)	Contribution X_i to the variance of Z ($\sigma^2(Z)$) in %	
				B.H.	B.S.
z_0	m	11.	0.25	.7	.7
α	degr.	14.	1.5	.5	.5
γ_s	MN/m^3	10.	0.7	.7	.8
V_0	MN	202	5.1	.6	.5
$H_h + H_w$	MN	103.6	5.22	76.2	78.4
ϕ_s	degr.	36	1.8	1.3	1.5
δ_s	degr.	24	1.8	0.1	.1
ϕ_b	degr.	40	2	8.1	-
$\tan \delta_b$	-	0.67	0.05	-	8.0
X_m	-	1.0	0.06	11.9	9.4

- 17 -

	B.H.	B.S.
\bar{Z} (MN) :	2.41×10^4	1.95×10^4
$\sigma(Z)$ (MN) :	$.42 \times 10^4$	$.40 \times 10^4$
β :	5.73	4.83
Failure probability :	5.3×10^{-9}	6.9×10^{-7}

It is evident that the probability of failure of the base sliding model is 100 times greater than the probability of failure of the Brinch Hansen model, because for the combinations of R_b and V under study the base sliding model forms the limiting factor (see fig. 8).

From the table the following conclusions can be drawn:

The construction is insensitive to geometrical imperfections.

In both models, despite their differences the main contribution to the variance of the reliability function is caused by the distribution function of the loading. The most important soil parameters in respectively the Brinch Hansen and the Base sliding model are ϕ_b and $\tan \delta_b$.

In the next paragraph all attention will be devoted to the Base sliding model. The influence of a change in the stochastic properties of the most important soil mechanical parameters, the friction co-efficient $\tan \delta_b$ and the model reliability factor X_m has been investigated.

An increase of the standard deviation of $\tan \delta_b$ or X_m causes a sharp rise in the probability of failure and the contribution of these parameters to the variance of Z (see fig. 11).

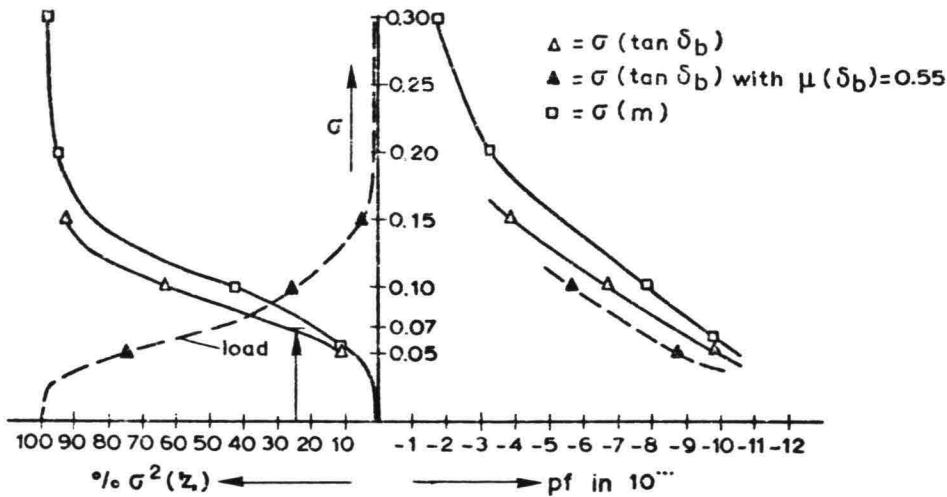


fig. 11. The relation between $\sigma(X_1)$, the probability of failure and $\sigma^2(Z)$.

It can be strikingly seen that an increase of the standard deviation of $\tan \delta_b$ from 0,05 to 0.10 multiplies the probability of failure by a factor 10^3 .

On the other hand a decrease of the mean value of $\tan \delta_b$ from 0.67 to 0.55 causes only a ten fold increase of the failure probability.

From these results some conclusions can be drawn with regard to priorities in soil mechanical investigation and quality control.

5.4. Correlation with safety factors.

As previously stated, an aim of the probabilistic calculation was an objective appraisal of the choice of partial safety co-efficients (see 4) based on engineering judgement.

For this purpose a level of risk acceptable to society has to be defined.

Although this problem is still the subject of extensive discussions, some reference can be made to the Delta-report on the one hand and to social acceptance of human risk that can be derived from fatality statistics on the other hand (see litt. 4). Because a thorough analysis of the socially acceptable risk is not yet available and the probabilistic method itself is a new and developing technique, it was decided to postulate a target-level for the probability of failure of the storm surge barrier to stimulate further studies.⁻⁷ The acceptable risk level for the barrier as a whole is set at 10^{-7} per annum which implies a probability of failure for the components of less than 10^{-7} per annum in order to facilitate the calibration of the safety factors in the different fields of engineering. As already explained in 4.1 the semi-probabilistic design equation is

$$R_k \geq 1,5 \times L_k$$

where

L_k load with a probability of exceedance of $2,5 \times 10^{-4}$ per annum.
 R_k characteristic strength(5%) of the foundation.

For normal design purposes the characteristic strength is approximated by substituting the characteristic values of the basic variables in the theoretical model. The exact method however requires the derivation of the probability density function of the foundation strength taking account of the probability density functions of the basic variables.

In the case of the foundation the small difference between the approximate and the exact method (see fig. 13) shows the accuracy of the approximate practical design method.

The probability density function of the strength has been exactly evaluated for various embedment depths $z_0 = 4, 8, 11$ m (see fig. 12) to find the characteristic strength as a function of z_0 . At the same time the probability of failure has been calculated for the three alternatives to find the relation between the safety co-efficient and this risk (see fig. 13).

$$\gamma = 0,11 \log (pf) + 0,55.$$

From this equation the conclusion can be drawn that a safety co-efficient $\gamma > 1,32$ is sufficient to reach the target risk level as specified above. However it must be realised that the value of $\gamma = 1.5$ incorporates a factor to prevent excessive deformation under working loads.

($\gamma_c = 1,15$ see 4.1.).

In fig. 8 it is shown once again that great attention should be paid to the co-efficient of variation of the foundation resistance.

A rise in the variation from 5% to 12,5% necessitates an increase in safety co-efficient from 1.4 to 1.9 to keep the probability of failure at 10^{-8} .

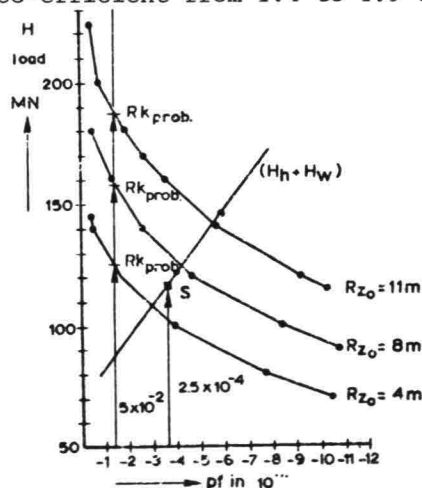


fig. 12, R and $H_h + H_w$ exceedance frequency

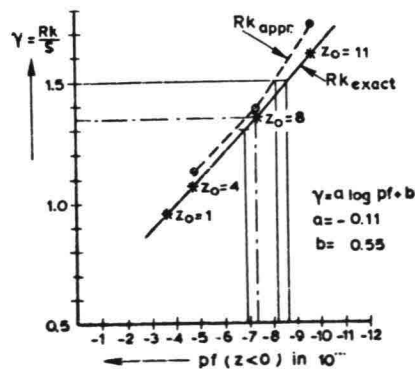


fig.13, Relation $pf \rightarrow \gamma$ for different z_0

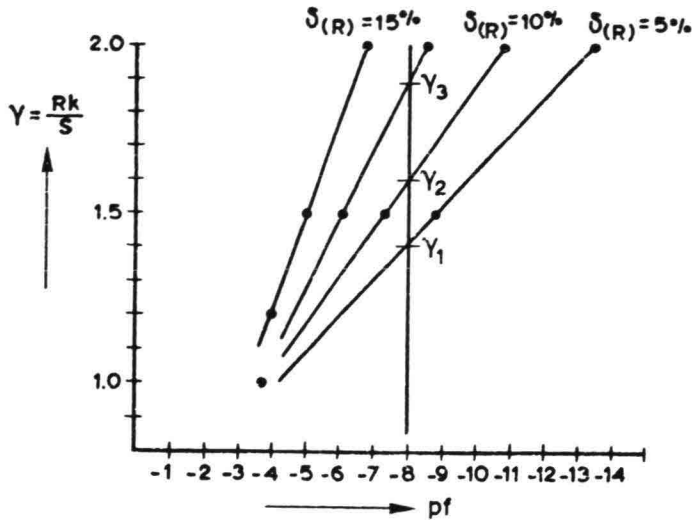


fig. 14 Relation $pf \rightarrow \gamma$ for different $\delta(R)$.

5.5. Conclusion

The application of probabilistic reliability calculations provides a quantitative insight into the influence of the stochastic uncertainty of the basic parameters. Thus it forms an important tool in assigning priorities in study or quality control to specific parameters of theoretical models. Besides this it is possible to bring the probability of failure of the different components of the storm surge barrier in line and to estimate the overall reliability of the system.

6. Litterature

1. J. Brinch Hansen. A Revised and Extended Formula for Bearing Capacity. Danish Geotechnical Inst. Bull. 28, 1970.
2. H. Sellmeyer. Description Spring Constant Method, to be published in Proc. Symp. on Foundation Aspects of Coastal Structures, Delft, 1978.
3. T.W. Lamb; R.V. Whitman. Soil Mechanics, chapter 2. J. Wiley & Sons, New York 1969.
4. C.H. Buschmann. "Maximum voorstelbaar ongeval" Ingenieur nr. 44, 1975.
5. Rationalisation of safety and serviceability factors in structural codes. CIRIA report 63, 1976.
6. Inleidende probabilistische berekeningen. Rapport TNO-IBBC B-78-30 maart 1978.

List of symbols

B	-	pierwidth
B.H	-	Brinch Hansen model
B.S	-	Base Sliding model
C	-	causalities
F_k	-	characteristic Load
HW	-	Stormsurge Level
Hw	-	Horizontal wave force

$H_h; HL$	-	Headloss Load
$H_z, 1/3$	-	Significant wave height
IWL	-	Innerwaterlevel (Oosterschelde)
L	-	pier length
L^1	-	effective pier length
L_k	-	load with probability of exceedance of $2,5 \cdot 10^{-4}/\text{year}$
M	-	moment; management system
N.S	-	North Sea
N	-	bearing capacity factors
O	-	transferfunction
O.S	-	Oosterschelde
P()	-	probability
Q	-	vertical ultimate bearing capacity
R	-	Resistance
R_b	-	horizontal base resistance
R_p	-	passive resistance
$S_{\eta\eta}; S_j S_j$	-	Wave spectrum
S_{bb}	-	waveload spectrum
SSB	-	Storm Surge Barrier
$S\gamma, q$	-	Shape factors
T	-	technical system
TL	-	total Load
\bar{T}_z	-	mean wave period
V	-	pier weight
WL	-	wave Load
X_i	-	basic variable
X_i^*	-	basic variable at design point
X_m	-	model factor
b	-	suffix, indicating base
e	-	excentricity
f	-	wave frequency
fk	-	characteristic strength function
h	-	suffix, indicating headloss; headloss arm
i	-	shapefactors
l_o	-	sill bank
m_n	-	constants to characterize the wave spectrum
m_i	-	mean value of variable X_i
p;pdf	-	probability density function
pf	-	probability of failure
P_i	-	correlation factor
w	-	wave force arm

- 21 -

z_0	-	depth of embedment
α	-	contribution factor of healoss force; inclination
β	-	" " " wave force; reliability index
γ	-	safety coefficient; submerged unit weight
γ_{ci}	-	partial safety factor concerning structural aspects
γ_{mi}	-	" " " " material properties
γ_{si}	-	" " " " stochastic load character
δ	-	friction angle; coefficient of variation
σ	-	standard deviation
μ	-	mean value
ϕ	-	internal friction angle

SYMPOSIUM ON FOUNDATION ASPECTS OF COASTAL STRUCTURES

COMPUTATION BY FINITE ELEMENTS

C.J. Kenter, Research Engineer, Delft Soil Mechanics Laboratory

P.A. Vermeer, Research Engineer, Delft University of Technology

SUMMARY

During the evolution of the design - from a two dimensional caissonbarrier without embedment via three dimensional caisson foundation with deep embedment to a pier foundation with shallow embedment - a great number of F.E. computations have been made. The following computer programs were used:

- SEEP (Barends) for ground-water flow
- CONSOL (Christian, Boehmer, Biegstraaten) elasto-plasticity without consolidation
- SPONS (V. Bijsterveld) for linear elastic consolidation
- CASCO (Verruijt) for non linear elastic consolidation
- ELPLAST (Vermeer) for elasto-plastic consolidation

The validity of the results of the F.E.-computations was studied by means of various large scale model tests, such as Neeltje Jans, Oregon and Kats. In this paper the more relevant results of these evaluation-studies will be submitted. The value of certain schematizations, which were made to save money and time, will be discussed. The use of triaxial stress path tests for the determination of inputparameters in a Kondner-Duncan stress-strain relation (CONSOL) was examined and recommendations in this respect will be given.

1. COMPUTATION BY ELPLAST

The computer program Elplast has been used for the prediction of model tests in which plane strain conditions were approached. Two such tests were performed in the Oosterschelde area (Neeltje Jans) and another in a wave tank (Oregon). In this part of the paper the basic equations which are used in Elplast will be presented. The features of the material behaviour which are taken into account and those which are ignored will be discussed. Also included is a presentation of computational results and relevant measurements for the test mentioned above.

1.1. Basic equations in Elplast

In this section the equations for the coupled behaviour of the soil skeleton and the pore fluid will be described briefly. The behaviour of the soil skeleton depends on the effective stress

$$\underline{\sigma}' = \underline{\sigma} - \underline{m} w, \quad \underline{m}^T = (1, 1, 1, 0, 0, 0) \quad (1)$$

where $\underline{\sigma}$ is the total stress and w the stress in the pore fluid. The components of the stress vector are $\sigma_x, \sigma_y, \sigma_z, \sigma_{xy}, \sigma_{yz}$ and σ_{zx} respectively. The constitutive law for the soil skeleton is of the form

$$\underline{\dot{\sigma}}' = C \underline{\dot{\epsilon}} \quad (2)$$

where $\underline{\dot{\sigma}}'$ and $\underline{\dot{\epsilon}}$ are stress and strain rates respectively. The matrix C is based on an elastoplastic constitutive model which will be discussed in a special section of this paper.

Within the finite element discretisation the strains and the pore stresses at a point are related linearly to a set of nodal displacements and nodal stresses. This is expressed by the equations $\underline{\dot{\epsilon}} = B \underline{\dot{u}}$ and $\dot{w} = N \underline{\dot{w}}$; the nodal displacements are assembled in the vector \underline{u} and the stresses in the vector \underline{w} ; a dot is used to indicate a time derivative. The computer program Elplast is based on simple constant strain elements and this means that the matrix B is constant within an element. The equilibrium conditions for a composition of finite elements can be written as $\int B^T \underline{\dot{\sigma}}' dV = \underline{\dot{f}}$, where V is the volume of the region analysed and \underline{f} a

vector in which all external nodal forces are assembled. Substitution of the equations $\dot{\underline{q}} = \underline{\dot{q}}' + \underline{m} \dot{\underline{w}}, \dot{\underline{q}} = C \dot{\underline{\epsilon}}, \dot{\underline{\epsilon}} = B \dot{\underline{u}}$ and $\dot{\underline{w}} = N \dot{\underline{w}}$ gives an equation of the form

$$K \dot{\underline{u}} + L \dot{\underline{w}} = \dot{\underline{f}} \quad (3)$$

The above matrix equation is not sufficient for determining the solution of the problem; an additional condition must be imposed on the pore stress \underline{w} . This condition is obtained by considering the flow of the water in the soil skeleton. The pore water equation is

$$\underline{m}^T \dot{\underline{\epsilon}} - \frac{n}{K_p} \dot{\underline{w}} + k_x \frac{\delta^2 \underline{w}}{\delta x^2} + k_y \frac{\delta^2 \underline{w}}{\delta y^2} + k_z \frac{\delta^2 \underline{w}}{\delta z^2} = 0 \quad (4)$$

where k_x , k_y and k_z are coefficients of permeability; the Cartesian x, y, z -frame is chosen coaxial to the principal directions of permeability. The incorporation of an anisotropic permeable soil is important for the Oosterschelde estuary; thin, more or less horizontal clay bands are for instance present at the Neeltje Jans site.

The symbols n and K_p in equation (4) stand for the porosity of the soil and the compression modulus of the pore fluid respectively. The incorporation of K_p is important for a not completely saturated soil. The compression modulus can then be computed from

$$\frac{1}{K_p} = \frac{1-a}{K_w} + \frac{a}{K_a} \approx \frac{a}{K_a} = \frac{a}{p_a} \quad (5)$$

where a is the fraction of air in the pores. K_w and K_a are the tangential moduli for water and air respectively and p_a the absolute pressure in the pores. The identity $K_a = p_a$ follows from Boyle's Law. The quantity $(1-a)/K_w$ can usually be disregarded with respect to a/K_a . For a composition of finite elements equation (4) can be replaced by an algebraic equation of the form

$$L^T \dot{\underline{u}} + S \dot{\underline{w}} = H \underline{w} \quad (6)$$

The problem is described by the differential equations (3) and (6). The integration of equation (3) is hampered by the fact that the matrix K is not constant, i.e. $K = K_0$ at the beginning of a time step but at the end it yields $K \neq K_0$. As usual in elastoplastic analyses a pseudo force vector $\underline{\Delta g}$ is used and equation (3) is replaced by

$$K_0 \underline{\Delta u} + L \underline{\Delta w} = \underline{\Delta f} + \underline{\Delta g} \quad (7)$$

where $\underline{\Delta g}$ depends on $\underline{\Delta u}$, making the problem non linear. The symbol Δ is used to denote finite increments. In equation (6) the matrices L , S and H can be considered to be constant, but integration of that equation in time requires an interpolation rule for the pore pressures \underline{w} . This problem is solved by applying the numerical integration rule $\int \underline{w} dt = \Delta t \underline{w}_0 + \alpha^* \Delta t \underline{\Delta w}$, where the subscript 0 is used to denote values at the beginning of the time step. A value $\alpha^* = 0.5$ would correspond to trapezoidal integration. However we often used $\alpha^* = 0.6$ for reason of numerical stability². Equation (6) is now integrated to obtain

$$L^T \underline{\Delta u} + (S - \alpha^* \Delta t H) \underline{\Delta w} = \Delta t H \underline{w}_0 \quad (8)$$

The equations (7) and (8) are solved in the computer program Elplast. It is primarily due to the non linearity of $\underline{\Delta g}$ that this is done iteratively for each step.

1.2. On the constitutive Law

The program Elplast is based on the so-called Double Hardening Model for sand. A description of this model under triaxial stress and strain conditions is given in reference 3. General stress and strain conditions are treated in ref. 4. and it is shown that the general model is greatly simplified by the assumption $\sigma'_2 = \lambda (\sigma'_1 + \sigma'_3)$, where σ'_2 is the intermediate principal stress and λ a proportionality constant. Stroud⁵ showed that this assumption is more or less realistic for plane strained soil; he observed for a specific sand $\lambda = 0.37$. This assumption is used in Elplast to eliminate the intermediate stress in plane strain problems. The two most important equations in the "simplified" double hardening model will be presented here.

The equations incorporate the plane strain stresses

$$s = \frac{1}{2} |\sigma'_1 + \sigma'_3| \quad , \quad t = \frac{1}{2} |\sigma'_1 - \sigma'_3| \tag{9}$$

where σ'_1 and σ'_3 are the major and minor principal stress respectively. The plastic yielding of sand is described by the equations

$$Y_1 = \frac{t}{s} - F \left(\frac{s_0^\beta}{s^\beta} \int d\gamma^P \right) = 0 \quad , \quad Y_2 = \alpha \frac{s^\beta}{s_0^\beta} - |\epsilon_1^P + \epsilon_3^P| = 0$$

where the plastic shear strain increment $d\gamma^P$ is defined as $|d\epsilon_1^P - d\epsilon_3^P|$. The yield functions Y_1 and Y_2 contain the experimental constants α and β and the experimental function F . The reference stress s_0 may be chosen arbitrarily. An impression of the function F is given in figure 1.

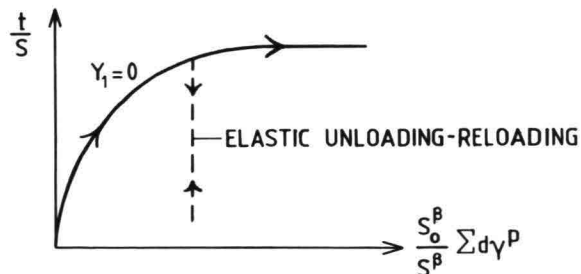


Fig. 1. Yield condition.

The equation $Y_1 = 0$ describes a curved yield locus in s,t -plane which approaches a straight failure line as $\sum d\gamma^P$ increases (figure 2). No curvature would be obtained for $\beta = 0$ but values close to 0.5 are usually measured. The shape of this so-called shear yield locus corresponds closely to yield loci determined experimentally^{3,4,5}.

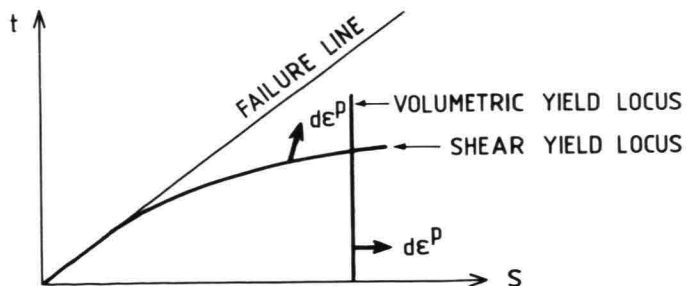


Fig. 2. Yield loci

A non-associated flow rule is assigned to the shear yield locus. This flow rule is largely based on Rowe's stress-dilatancy theory⁶.

The equation $Y_2 = 0$ describes a volumetric yield locus as indicated in figure 2; the corresponding flow rule is assumed to be associated. The plastic volume strain for a stress path with $t = 0$ is described by the volumetric yield locus.

The Double Hardening Model is based on the salient features of sand in initial loading and in a single unload-reload cycle. The model is accurate enough as long as the rotation of the major principal stress remains limited to an angle of about 45° . This type of loading will be referred to as one-way loading. It comprises for example triaxial compression conditions as well as triaxial extension conditions. However a combination of the two is excluded because of the extreme jump in the direction of σ_1' when passing from compression to extension conditions. For cyclic one-way loading (many cycles) it cannot a priori be stated that the model is accurate enough; an additional condition has to be satisfied. This additional condition will be discussed later; the major condition of one-way loading will be discussed first.

The constitutive model is restricted to one-way loading since it does not incorporate hysteresis and accumulation of strain which are particularly observed in two-way cyclic loading. The hysteretic behaviour of sand is usually unimportant in an unload-reload cycle of one-way loading. Furthermore, the plastic strains hardly change in such a stress cycle. The above statements are based on test results as presented in figure 3; it concerns a drained, cyclic, triaxial compression test. In this test we measured a shear strain of 3.4% in initial loading and 4.5% after 60 unload-reload cycles. A boundary problem with comparable stress variations and an equivalent number of cycles can be solved, within engineering accuracy, using Elplast, since the final strains have the same order of magnitude as the strains due to initial loading.

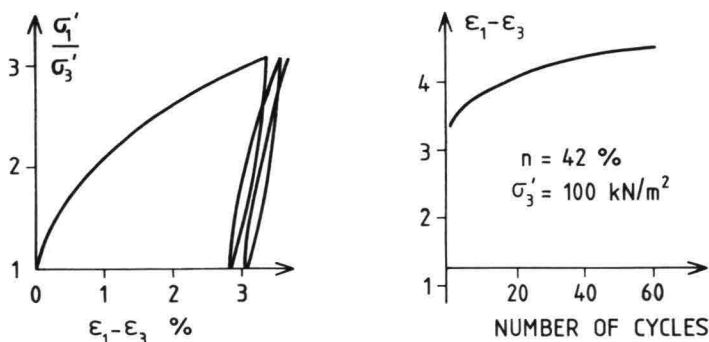


Fig. 3. Drained cyclic triaxial test on a loose sample.

It is recalled that the model is not accurate enough for all one-way loading problems. Although very small for cyclic one-way loading, the tendency of contraction in unloading (being neglected in the model), may lead to large deviatoric strains and even to complete liquefaction of an undrained element of sand. Thus the drainage capacity of the soil determines whether or not the accumulation of volume strain due to cyclic loading can be neglected. An Elplast computation should therefore be checked by analysing the stress cycles computed (at selected points in the subsoil) and the corresponding amount of volume strain neglected. The cyclic triaxial test mentioned above (figure 3) was in fact performed in the context of such an analysis. Such an analysis does not only provide a check on the volume strains but also on the magnitudes of the shear strains that have been computed in typical soil elements.

1.3. The Neeltje Jans tests

Two in situ test were analysed by Vermeer en Calle^{7,8} using the computer program Elplast. The tests will not be described completely in the present paper since this is done in reference 9. The first test concerns a caisson being directly placed upon an undensified subsoil; the second one concerns a caisson on a sill of coarse material and a densified subsoil.

The prediction for the first test was based upon an elastoplastic model which was different from the present one. Moreover contraction of the soil due to pure cyclic loading was incorporated by assuming

$$\underline{\epsilon} = \underline{\epsilon}^e + \underline{\epsilon}^p + \underline{\epsilon}^{pc} \quad , \quad \underline{\epsilon}^{pc} = \underline{\epsilon}^{pc}(\tau^a, N)$$

where $\underline{\epsilon}^e$ and $\underline{\epsilon}^p$ are the elastic and plastic strain components respectively, as defined in each elastoplastic model. The strain $\underline{\epsilon}^{pc}$ is purely volumetric and linked to the shear stress amplitude τ^a and the number of stress cycles N . We used a relation for $\underline{\epsilon}^{pc}$ which was hardly based on experimental evidence, since test results providing detailed information were scarce. The prediction of the first test was unsuccessful. Unexpected displacements occurred which might have been caused by a poor initial caisson-soil contact or by a small but very loose layer of sand underneath the caisson. Comparing the measured and predicted pore water pressures it was concluded that $\underline{\epsilon}^{pc}$ had been overestimated in the calculations. It had already been concluded on the basis of laboratory tests that the plastic strains $\underline{\epsilon}^p$ were described very poorly by the single yield surface that was incorporated on the model.

The time between the first and the second in situ test was used to develop the model. The "cyclic strain" $\underline{\epsilon}^{pc}$ was removed from the model and the plastic strain $\underline{\epsilon}^p$ was described by two yield surfaces as indicated in the previous section. The loading scheme and both the measured and predicted displacements for test II are shown in figure 4. The ratios of the total loads to the length of the caisson (27.7 m) were used in the plane strain analysis. This is on the safe side with respect to the magnitudes of the displacements; they tend to be underestimated for cyclic loading due to the present constitutive model but tend to be overestimated due to the above plane strain simplification. A brief description of the computational procedure will be given.

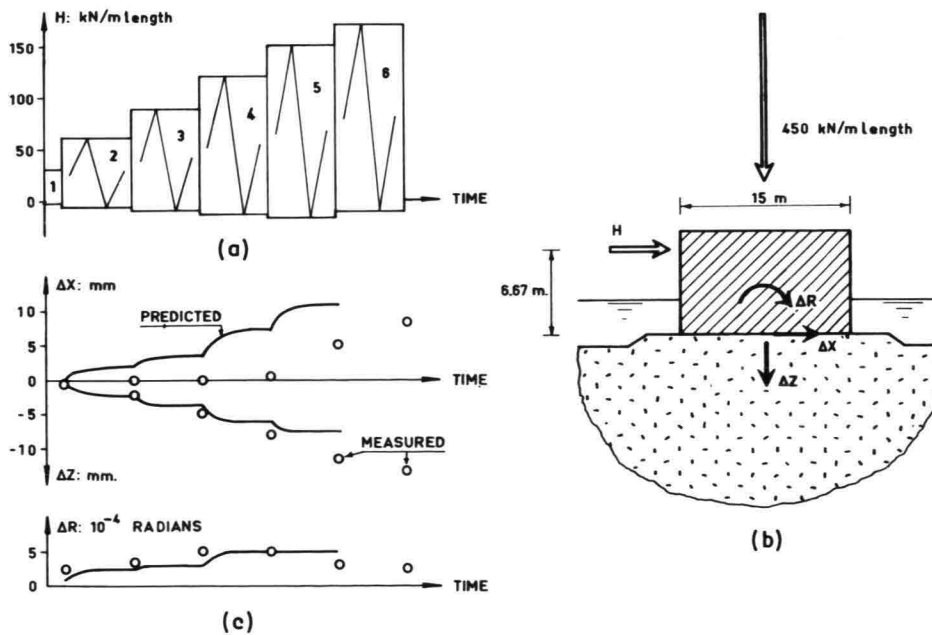


Fig. 4. Caisson test II at Neeltje Jans: (a) loading scheme; (b) cross section; (c) displacements and rotation.

The initial stress state in the soil was assumed to be geostatic with the horizontal effective stresses equal to 0.5 the vertical effective stresses. Starting from this initial state the additional stresses due to the weight of the sill and the caisson were calculated. All displacements for the prediction were measured from this stage.

The first part of the loading scheme (the parcels 0 and 1) was considered to be unimportant and the horizontal force was therefore directly increased to the average value in the second part (parcel 2). It should be noted that all loads were applied incrementally. Starting from the average value of the horizontal force three loading cycles were followed. More loading cycles of the second part of the loading scheme were not followed since the plastic displacements hardly increased in the third cycle computed (shakedown). In this manner a prediction for the displacements at the end of the second part of the loading scheme was obtained, including the variations of the pore water pressures in a loading cycle.

Starting from the state of stress and strain at the "end" of the second part of the loading scheme, the horizontal force was increased up to a new average value and three cycles from the third part of the scheme were followed. Further cycles were not followed since the plastic displacements would have increased only a little. A prediction for the displacements of pore water pressures and displacements in the third part of the loading scheme had thus been obtained. The computations for the other stages of loading were performed in analogy with the one for the third part of the loading scheme.

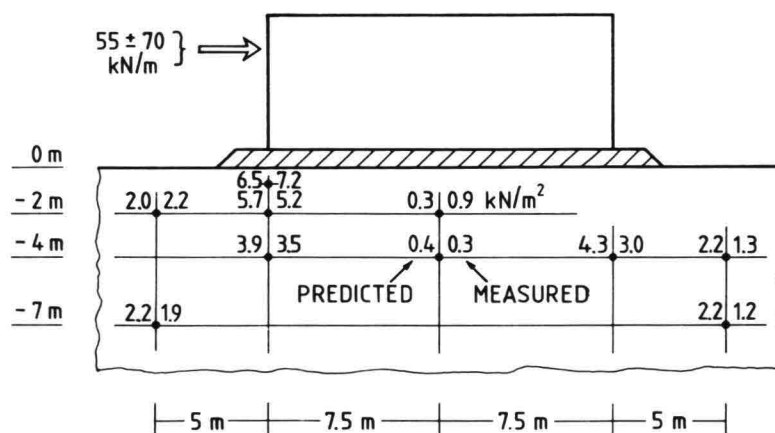


Fig. 5. Predicted and measured pore pressure amplitudes for the fourth part of the loading scheme.

Both the measured and the predicted amplitudes of the cyclic pore water pressures are shown in figure 5. These pressures refer to the fourth part of the loading scheme. Amplitudes for other parts need not be shown since both the measured and predicted pressures were proportional to the amplitude of the horizontal force.

It follows from the figures 4 and 5 that the results of the 2nd in situ test have been predicted reasonably well. It should be noted that the prediction of the pore water pressures was based upon a completely saturated soil, i.e. an incompressible pore fluid. The assumption of a not completely saturated soil would lead to somewhat smaller pressures.

1.4. Caisson performance in a wave tank

A prediction for a model test in a wave tank has been given by Vermeer & van Dongen¹⁰ using the computerprogram Elplast . This test was carried out in a wave tank at Oregon State University (U.S.A.). A schematic longitudinal cross-section of a part of the tank is shown in figure 6. The caisson was loaded by waves coming from a wave board. This type of loading (a few heavy waves) had been translated into a horizontal force varying between 16 kN/m and -4kN/m with a non constant point of application as indicated in figure 6. Furthermore the pore pressure along the top of the sandbed in front of the caisson varied in time due to the wave action. In spite of these complexities the boundary conditions were followed fairly accurately in the computations. This was at least supposed when performing the calculations.

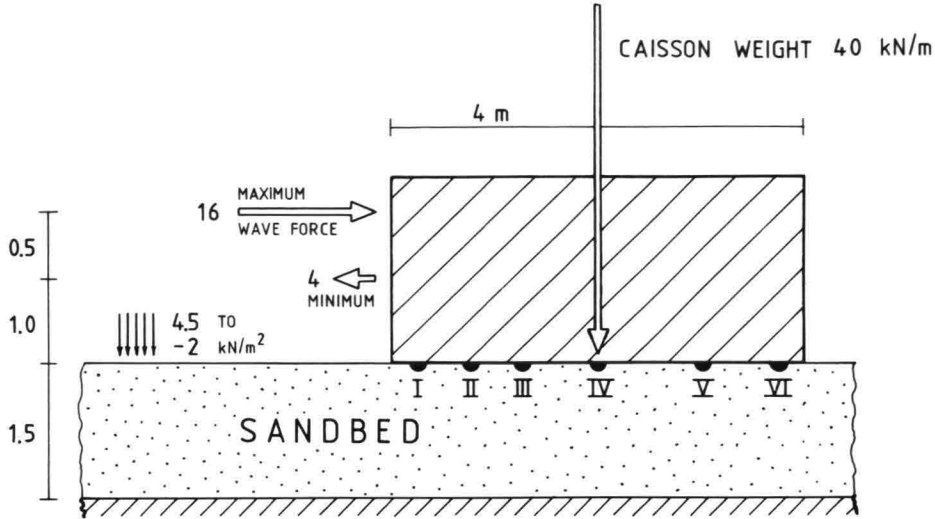


Fig. 6. Schematic cross section of the sand layer and the caisson model in the wave tank at Oregon, U.S.A.; I,II-VI pore pressure meters.

The test was done later and unfortunately not in full agreement with the computations. Moreover the few measurements on the displacements of the caisson were not consistent. It can only be concluded that both the actual and the predicted displacements were small, i.e. a few millimetres. Reasonable agreement was found between the measured and predicted pore water pressures. Values of the pressures just underneath the caisson are shown in figure 7. The predictors had been informed that the aircontent of the pores would be about 2 or 3%. The value 2% was used in the computations giving a compression modulus $K_p = 5000 \text{ kN/m}^2$. This value is obtained from equation (7) using $p_a = 1 \text{ atmosphere}$. It is indicated in figure 7 that far too large pore water pressures are calculated if the compressibility of the pore fluid is neglected. These numerical values demonstrate the importance of the second terms in the equations (4) and (6), i.e. the importance of a computer program that accounts for a compressible pore fluid.

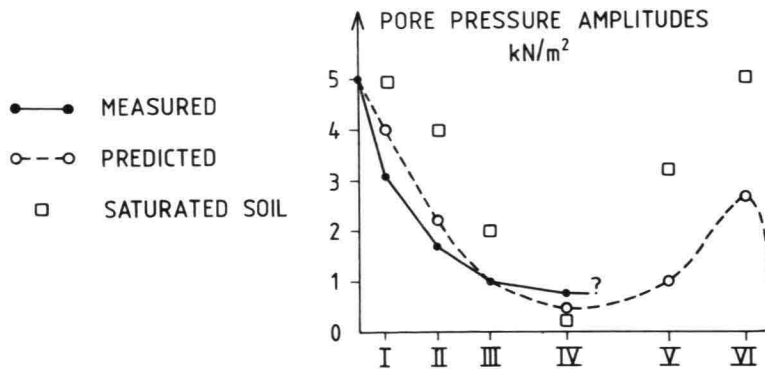


Fig. 7.

2. COMPUTATIONS WITH CONSOL

Most of the F.E. calculations for the Oosterschelde storm surge barrier were made with the F.E. program CONSOL. A description of the stress-strain model of the program is given in [11].

In this section some practical engineering-methods and guidelines will be given, which were developed in order to cope with problems lying beyond the basic possibilities of the program.

An evaluation study was made of a test on a scale 1 : 10 model of the pier in Kats, which showed the value of CONSOL-calculation for the prediction of prototype behaviour. The results of this study will be submitted.

A detailed description of most of the items of this section can be found in ref. [12] and [13].

2.1. Simulation of the building procedure in the calculation of initial stresses

The building procedure can be divided into three stages with regard to the initial stresses in the soil:

- a. initial condition of foundation bed and subsoil
- b. laying down the pier
- c. dumping the sill.

The calculation of the behaviour of the final foundation under headloss and wave forces requires a correct implementation of the initial stresses.

Applying a non linear stress-strain model will give rise to some difficulties in this respect. It is not possible to compute the deadweight-stresses using the normal procedure based on solving equilibrium-equations, because no proper 'starting point' for the non-linear behaviour is defined.

Besides, a procedure, in which the elements of subsoil, foundation bed, pier and sill are given deadweight at the same time, will involve great deformations and yielding in the sill elements next to the pier. The pier will hang on the sill because of its greater deadweight.

The following procedure will give correct results:

- a. Assign initial stresses to the elements of foundation bed and subsoil, which agree with the deadweight and K_0 -values, and which are based on a surface level equal to the top of the sill.
- b. Give the elements of the sill a very low stiffness and give deadweight to the elements of the pier. Pier elements are linear elastic.
- c. Assign initial stresses to the elements of the sill which correspond to the deadweight and the K_0 -values of the sill.

2.2. Mesh-dimensions

The minimal mesh-dimensions in F.E. calculations for the type of foundations, proposed for the Oosterschelde, were determined. The disturbances caused by boundaries at various distances were examined. Criteria were:

- displacement of the construction
- gradient in strains
- rotation of principal stresses
- stress paths of elements near the boundary.

The following guide numbers were found for these types of constructions:

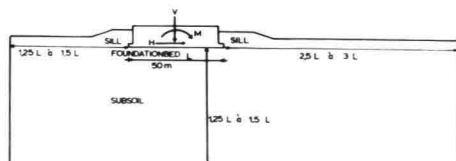


FIG. 8 MINIMAL MESHDIMENSION

- depth below foundation:
1.25 to 1.5 \times length of foundation
- distance of boundary at active side:
1.25 to 1.5 \times length of foundation
- distance of boundary at passive side:
2.5 to 3 \times length of foundation.

2.3. Computation of three dimensional problems with a plane strain program

A row of piers, each 20 m wide and standing 45 m apart from core to core, can not be looked upon as a two dimensional construction. The stresses will spread in the third dimension, which reduces the displacements (see fig. 9).

However, three dimensional F.E. programs are scarce and three dimensional F.E. calculations are extremely expensive.

Hence a method was developed to include the three dimensional effect in a plane strain program. The method is based on an increase of the stiffness to such an extent that strains and displacements approach reality.

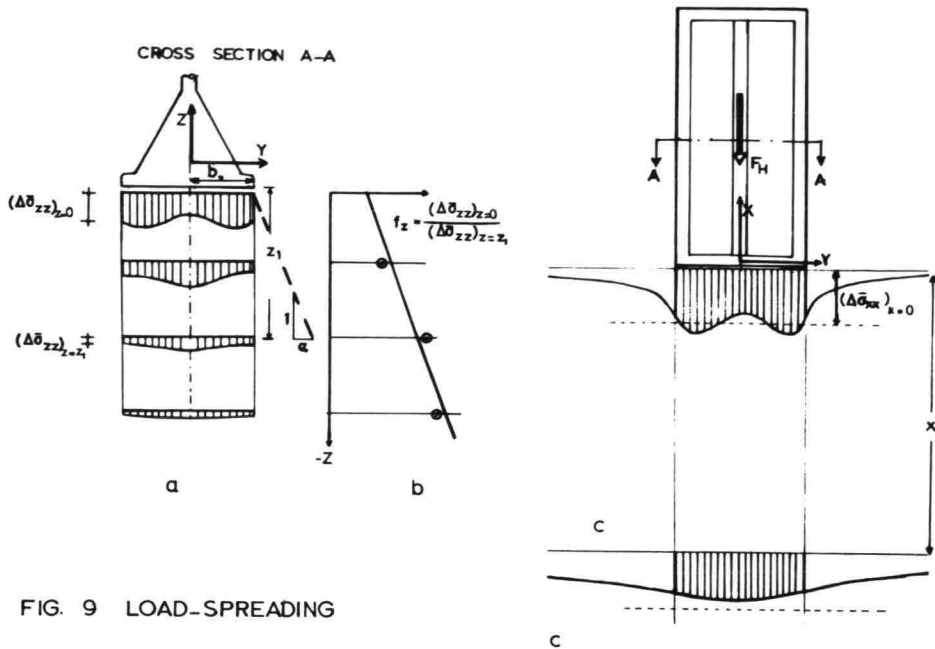


FIG. 9 LOAD-SPREADING

A formulation for the strain (e.g. in z-direction) is:

$$\Delta\epsilon_{zz} = \frac{1}{E} \{ \Delta\sigma_{zz} - \nu (\Delta\sigma_{xx} + \Delta\sigma_{yy}) \} \tag{10}$$

in which E and \$\nu\$ are moduli, valid in a certain increment.

In plane strain conditions \$\epsilon_{yy} = 0\$, (10) becomes:

$$\Delta\epsilon_{zz} = \frac{1}{E} (1 - \nu^2) \Delta\sigma_{zz} - \frac{1}{E} \nu (1 + \nu) \Delta\sigma_{xx} \tag{11}$$

If one considers a cross section at e.g. half of the length of the pier (cross section A-A) the spreading of stresses will be mainly in the Y-Z plane.

In a three dimensional model, \$\sigma_{zz}\$ at \$z = z_1\$, averaged over the width of the pier, will be a factor \$1/f_z\$ smaller than the average value of \$\sigma_{zz}\$ at \$z = 0\$, due to load spreading. A factor \$f_z\$ is defined by the equation:

$$\frac{(\overline{\Delta\sigma_{zz}})_{z=0}}{(\overline{\Delta\sigma_{zz}})_{z=z_1}} = (f_z)_{z=z_1} \tag{13}$$

(three-dimensional)

The assumption is made that:

$$\frac{(\overline{\Delta\sigma_{zz}})_{z=0} - (\overline{\Delta\sigma_{zz}})_{z=z_1}}{(\overline{\Delta\sigma_{zz}})_{z=0}} = \frac{(\overline{\Delta\sigma_{xx}})_{z=0} - (\overline{\Delta\sigma_{xx}})_{z=z_1}}{(\overline{\Delta\sigma_{xx}})_{z=0}} \quad (12)$$

From figure 9-a it can be derived that

$$(fz)_{z=z_1} = 1 + \frac{\alpha_z z_1}{b_0} \quad (14)$$

α_z = angle, indicating the spreading; b_0 = half of the width of the pier.

In a plane strain model σ_{zz} and σ_{xx} will hardly spread.

$$\frac{(\overline{\Delta\sigma_{zz}})_{z=0}}{(\overline{\Delta\sigma_{zz}})_{z=z_1}} = \frac{(\overline{\Delta\sigma_{xx}})_{z=0}}{(\overline{\Delta\sigma_{xx}})_{z=z_1}} = 1 \quad (\text{plane strain}) \quad (15)$$

From (11), (12), (13), (15) it follows that "3-dimensional" strains in a plane strain model may be obtained by multiplying the stiffness E by f_z .

$$\text{So: } (E)_{z=z_1} = E * (f_z)_{z=z_1}$$

The factor f_z , or rather the factor α_z , can be determined with the aid of a plane strain computation, in which X_z is the plane strain direction in stead of Y.

Considering the decrease of $\overline{\Delta\sigma_{zz}}$ in z-direction:

$$(\overline{\Delta\sigma_{zz}})_{z=z_1} = \frac{1}{2b_0} \int_{-b_0}^{b_0} \Delta\sigma_{zz}(y, z_1) dy,$$

one can make a $f_z - z$ diagram and determine α_z . Approximation by a straight line makes α_z independent of z (see figure 9 a, b).

This gives:

$$\alpha_z = (f_z - 1) \frac{b_0}{z}$$

A similar derivation can be given for α_x . (see figure 9 c).

In this case the shear value Φ of the soil has to be adapted, in order to take into account the influence of the third principal stress (vertical stress in the given case).

Further the decrease in width b of the pier has to be taken into account e.g. by multiplication with a factor $\frac{b}{b_0}$.

The final correction factor for the stiffness is in that case:

$$E_{x = x_1} = E * \frac{b + \alpha_x * x_1}{b} * \frac{b}{b_0} = E * \frac{b + \alpha_x * x_1}{b_0}$$

b_0 = half of the width of pier at the bottom.

For a caisson foundation with deep embedment ($H = 20m$, $2l_0 = 46m$, $2b_0 = 16m$) the following factors were determined:

$$\alpha_x = 0.7$$

$$\alpha_z = 0.65$$

Checking the stresses and strains in a computation, in which the loadspreading described above, was introduced, showed, that the stresses were hardly changed whilst the strains had assumed the desired values. Further it was proved, that α will not be influenced seriously by the position of the boundary or mesh dimensions.

Spreading factors determined from the analytical solution of a rigid loaded ellipse and infinite strip on a semi infinite mass are lying in the same range.

Stresses will not decrease according to this method. So the favourable effect of loadspreading on softening and yielding of the soil is not included. That is why the method is only believed to be rather useful for constructions with a safety factor over 1.5.

2.4. Incorporation of seepage forces

In earlier computations seepage forces due to difference in waterlevel at the Northsea- and Oosterschelde side were taken into account by increasing the horizontal force on the construction.

The additional horizontal force was derived from equipotential lines, computed by solving the differential equation for stationary groundwater flow:

$$\sigma_{,ii} = 0 \quad (16)$$

in which: σ = pore pressure.

The comma followed by the index i denotes partial differentiation with respect to the spatial coordinate x_i , and the summation convention applies.

The question arose, if the seepage forces on soil particles might cause additional displacement of the construction.

To solve this question a combined solution of (16) and the equilibrium-equation:

$$\bar{\sigma}_{ij,i} + \sigma_{,j} + K_j = 0 \quad (17)$$

was required.

$\bar{\sigma}_{ij}$ = effective stress tensor

K_j = body force

$\sigma_{,j}$ = seepage forces

Combined computations were made with the consolidation programmes ELPLAST and SPONS [15] solving the storage equation:

$$\frac{\partial e}{\partial t} - \frac{k}{\gamma_w} \sigma_{,ii} = 0 \quad ; \quad \begin{array}{l} e = \text{volumetric strain} \\ k = \text{hydraulic conductivity (m/s)} \\ \gamma_w = \text{specific weight of the porefluid} \end{array} \quad (18)$$

in combination with (2). In linear elastic programs (SPONS) the influence of the additional term $\frac{\partial e}{\partial t}$, compared to (16), may be suppressed by using a penalty-method, or physically by using a very great timestep Δt or k -value, if one is

not interested in the consolidation process. In elasto-plastic programs (ELPLAST) some consolidation steps are required.

In CONSOL, which has poor consolidation facilities, a different method was followed. Equation (16) and (17) are solved decoupled, this is allowed because a permanency is being dealt with. Equation (16) is solved, using the F.E. program for stationary groundwater flow SEEP 16. The pore pressures, now known, are filled in in eq. (17) which can be solved with CONSOL.

Special attention should be given to boundaries where tractions are prescribed. In general form they are:

$$\sigma_{ij} n_i = t_j$$

$$\sigma_{ij} = \text{total stress}$$

$$n_i = \text{components of the normal on the surface}$$

$$t_j = \text{surface traction}$$

with Terzaghi's law, this becomes:

$$(\bar{\sigma}_{ij} + \sigma \delta_{ij}) n_i = t_j \quad ; \quad \delta_{ij} = \text{Kronecker delta}$$

$$\text{or } \bar{\sigma}_{ij} n_i + \sigma n_j = t_j \quad (19)$$

So an additional pressure σ should be placed normal to the surface.

Physically, this stands for the weight of the water above the surface. Without this additional pressure the soil will be blown up by the introduced pore pressures.

The procedure described above leads to the following additional terms in the functional:

$$\int_A \sigma u_{i,i} dA - \int_S \sigma n_i u_i dS$$

u_i = displacement vector

A = surface

S = boundary

These terms end up in load vector after differentiating with respect to the unknown nodal displacements. This gives the following additional load-vector terms for each element:

$$\frac{|A|}{A} \cdot \sigma \cdot b_k + \frac{1}{2} L^j \cdot \sigma \cdot n_x$$

$$\frac{|A|}{A} \cdot \sigma \cdot c_k + \frac{1}{2} L^j \cdot \sigma \cdot n_y$$

b_k and c_k are vectors depending on the nodal coordinates

L^j = length of boundary-segment of element j

By using the same grid in SEEP and CONSOL calculations and automation of data transport, one disposes of a simple and fully correct method to compute the influence of seepage forces on a soil skeleton.

A third, rather elegant, method to include the influence of seepage forces is based on an analogy, described by Engels [17].

Assuming Hooke's law:

$$\bar{\sigma}_{ij} = G (u_{i,j} + u_{j,i}) + (K - 2/3G) u_{k,k} \delta_{ij} \quad (20)$$

K = bulk modules
G = shear modules

the equilibrium equation (17) becomes:

$$G(u_{i,j} + u_{j,i})_{,i} + (K - 2/3 G)u_{k,kj} = 0 \quad (21)$$

if pore pressures and bodyforces are omitted.

By choosing $K \approx -1/3 G$ equation (21) will change into

$$G(u_{j,ii}) = 0 \quad \text{or} \quad u_{j,ii} = 0 \quad (22)$$

which bears great similarity with the equation for stationary groundwater flow

$$\frac{k}{\gamma_w} (\sigma_{,ii}) = 0 \quad \text{or} \quad \sigma_{,ii} = 0 \quad (16)$$

Further elaboration of the equations and boundary conditions gives the following rules for the analogy:

$$u_x = \sigma$$

$$u_y = 0$$

$$\sigma_{xx} = \frac{\partial \sigma}{\partial x}$$

$$\sigma_{yx} = \frac{\partial \sigma}{\partial y}$$

$$G = \frac{k}{\gamma_w}$$

which holds for boundary conditions as well.

u_y should be set zero along the boundary if one chooses u_x for the analogy with σ .

Using the analogy described above, the pore pressures, seepage forces and the influence of these forces on the soil skeleton can be computed in one run, using the same program and grid.

Only the boundary conditions and input parameters for the respective steps have to be changed.

2.5. Computation of modeltest M2 at Kats

The modeltests series in Kats have been covered and supported by many CONSOL-calculations, predictions as well as evaluations. Depending on the type of test they were more or less successful.

The results of a computation of the last modeltest M2 and an impression of the test set-up (see ref [14]) are given in fig. 10.

Comparison of measured pore pressure amplitudes and pore pressure amplitudes computed for an undrained case, showed that the soil behaviour was mainly drained. Static and drained cyclic parameters which were used in this computation were determined from triaxial tests as described in [11].

The angle of internal friction ϕ was increased by 10% and 20% for loose and dense soils respectively, in order to account for the difference between triaxial- and prototype stress conditions. A too low ϕ -value would involve a non-realistic weakening of the soil at certain spots which influences the total mechanism. Stiffness parameters were not increased. The influence of stiffer prototype behaviour is included in a final correction factor, derived from comparison between calculated and measured behaviour.

The 3-dimensional aspect of the construction and seepage forces were taken into account according to the method given in section 2.3 and 2.4. Friction along the side of the pier is ignored. These methods combined with the good stress strain model on which CONSOL is based, are believed to give a rather advanced computation. The agreement between measured and calculated results is reasonable, as one can see in fig. 10.

The mechanism, i.e. the qualitative behaviour, is fairly well computed. The calculated displacements however are too great. A correction factor of about 0,5 has to be applied to get agreement with the measured values. The correction factor will be mainly due to difference between the real and the triaxial stress-strain conditions and the inaccuracy of the stress-strain relation at low stress-levels. The schematization with regard to 3-dimensional aspects also merits discussion.

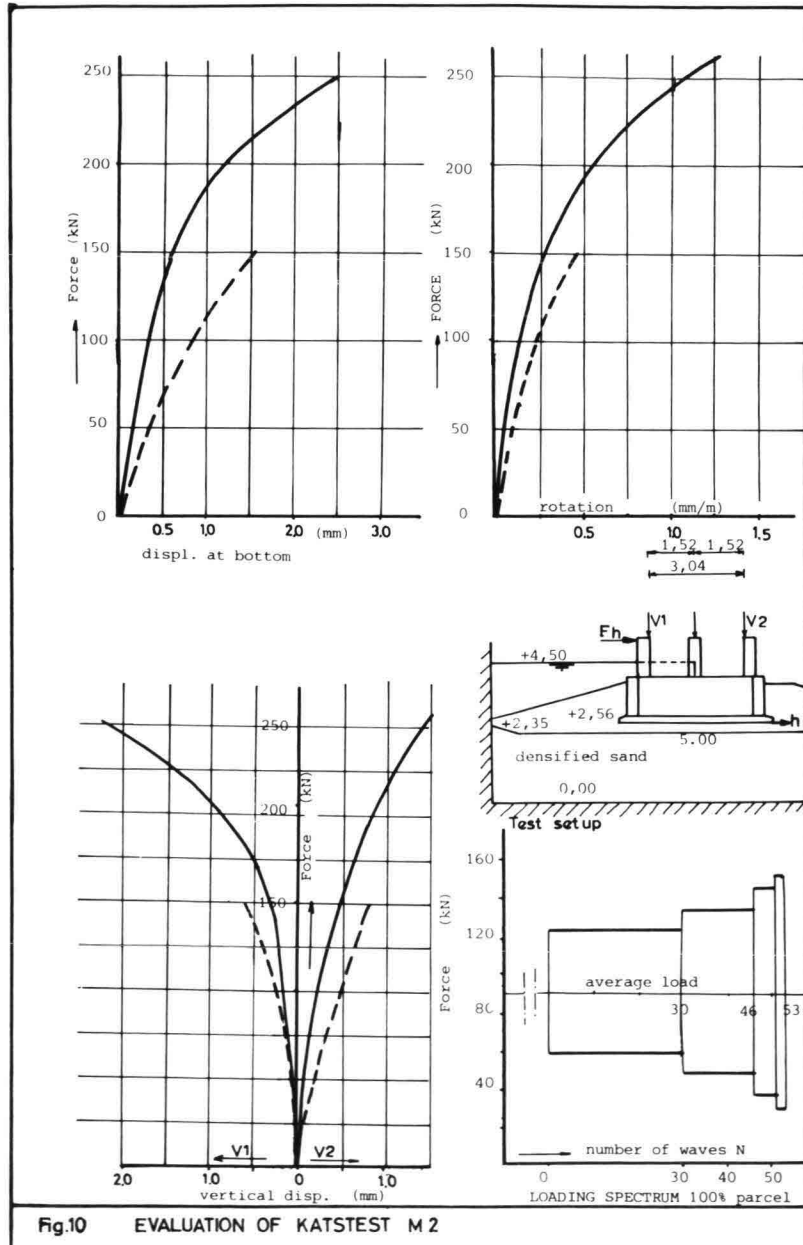


Fig.10 EVALUATION OF KATTEST M 2

3.3 Computations with CASCO

3.1 Introduction

The computerprogram CASCO is a program for the calculation of an almost saturated soil. In the original version (VERRUIJT, 1973, [18]) the basic assumptions regarding the soil behaviour were as follows:

- the soil particles are incompressible,
- the pore water is linearly compressible,
- Terzaghi's effective stress principle is valid,
- the flow of the pore fluid satisfies Darcy's law,
- the deformation of the soil skeleton satisfies Hooke's law.

In later versions [19], [20], the improvements mainly concerned the last assumption, i.e the stress-strain relation.

The resulting model is non-linear elastic: strain increments are coaxial with the incremental stresses instead of the total stresses. This is considered the main imperfection of the program. A set up for the inclusion of a better elasto-plastic behaviour is described in ref [22] but is not implemented yet.

3.2 Description of the model

Differential equations

The resulting model is based on the equilibrium equation (23) and storage equation (24) in an incremental form:

$$G(\Delta u_{i,j} + \Delta u_{j,i})_{,i} + (K - 2/3G) \Delta u_{k,k}{}_{,j} - K \Delta e^d_{,j} + \Delta \sigma_{,j} = 0 \quad (23)$$

$$\Delta u_{i,i} - n\beta \Delta \sigma + \frac{k}{\gamma_w} (1 - \varepsilon) \Delta t \Delta \sigma_{,ii} + \frac{k}{\gamma_w} \Delta t \sigma^t_{,ii} = 0 \quad (24)$$

Boundary conditions:

$$n_i \Delta \sigma_{ij} = \Delta t_j \quad \text{on } A_1 \quad (25)$$

$$u_i = f_i \quad \text{on } A_2 \quad (26)$$

$$\sigma = g \quad \text{on } A_3 \quad (27)$$

$$A_1 + A_2 = A_3 + A_4 = \text{total boundary}$$

$$\frac{k}{\gamma_w} n_i \sigma_{,i} = h \quad \text{on } A_4 \quad (28)$$

f_i , g , h are prescribed boundary values for displacements, pore pressures and discharge.

e^d = dilatancy, i.e. volumetric strain due to shear stresses.

ε = interpolation factor defining the moment in the timestep at which both (23) and (24) are fulfilled. $\varepsilon = 2/3$ gives very good results in general.

n = porosity of the soil

β = compressibility of the pore fluid.

Other symbols are defined in section 2 of this paper.

Stress-strain behaviour

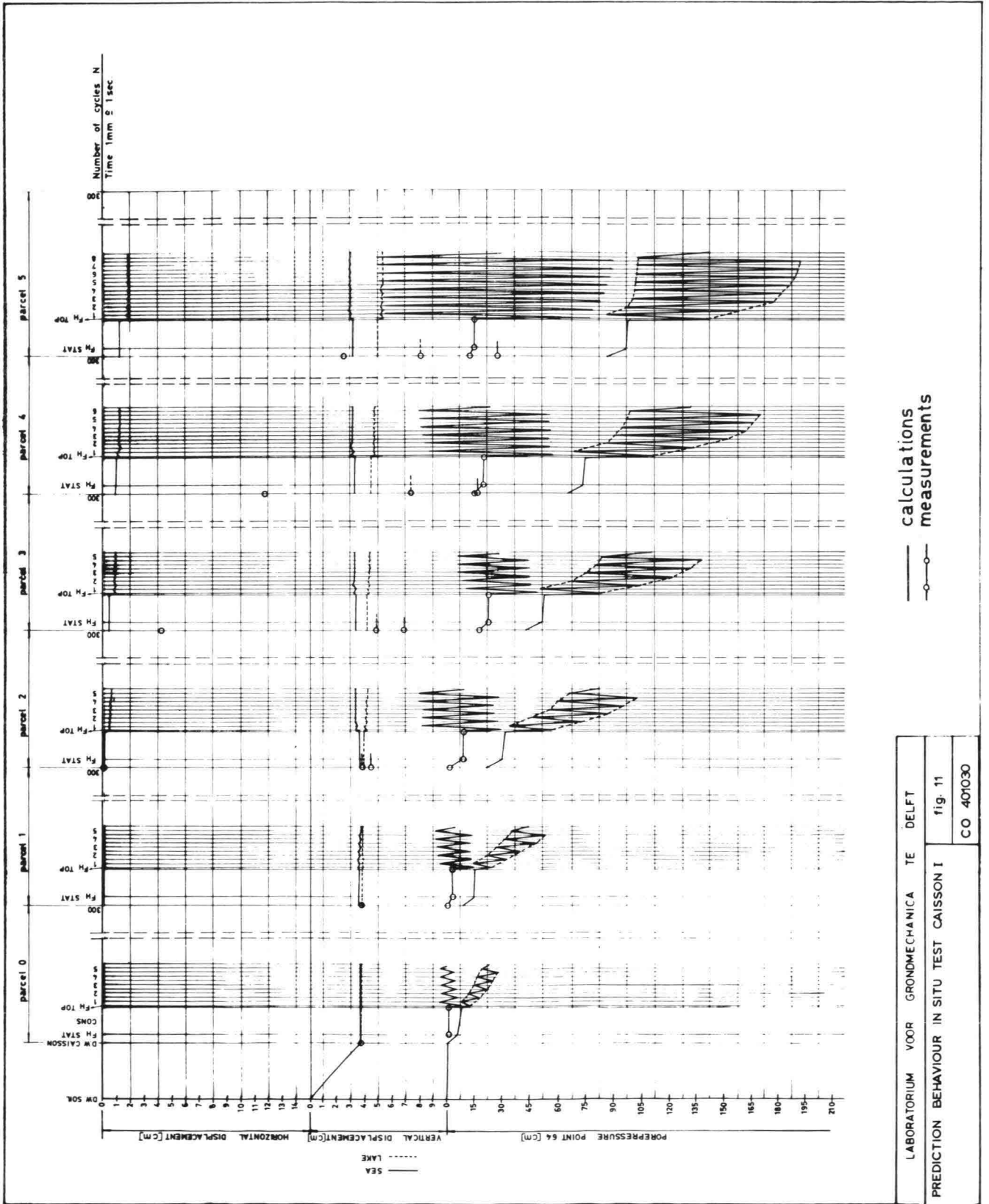
Compression

The value of the bulkmodulus K is governed by the following formulae: loading:

$$K = P_1 \sqrt{S}$$

S = volumetric effective stress

P_1 = reference parameter



LABORATORIUM VOOR GRONDMECHANICA TE DELFT
 PREDICTION BEHAVIOUR IN SITU TEST CAISSON I
 fig. 11
 CO 407030

unloading and reloading:

$$K = .2P_1 \sqrt{S} (1 + A \log N)$$

A = reference parameter

N = number of loadcycles

Shear

The value of the shearmodulus G is governed by the following formulae:
loading:

$$G = P_2 \sqrt{S} \frac{\sin \phi - (q/p)}{\sin \phi}$$

P_2 = a reference parameter

$$q = (\sigma_1 - \sigma_2)/2 \quad \sigma_1, \sigma_2 = \text{principal stresses}$$

$$p = (\sigma_1 + \sigma_2)/2$$

unloading:

$$G = 2P_2 \sqrt{S} (1 + A \log N)$$

reloading:

$$G = 1.75 P_2 \sqrt{S} (1 + A \log N)$$

Dilatancy

Rowe's stress-dilatancy relationship applies:

$$\Delta e^d = \Delta \gamma \frac{q/p - \sin \phi_t}{1 - q/p \sin \phi_t}$$

ϕ_t = parameter, defining the turning point between dilatancy and contraction.

Cyclic loading

Because of the difference between the unloading and reloading shearmodulus, cyclic loading will give incremental plastic shear strain and dilatancy per cycle, which decreases with the number of cycles. In partially drained or undrained conditions this will lead to pore pressure generation, as one can see in fig.11.

Functional

The differential equations (23), (24) and the boundary conditions (25) - (28) may be contained in the following functional, being minimal for the right solution Δu_i and $\Delta \sigma$:

$$U_{\min} = \frac{1}{2} \int_V [G(\Delta u_{i,j} + \Delta u_{j,i}) \Delta u_{i,j} + (K - 2/3 G) \Delta u_{i,i} \Delta u_{j,j} + 2\Delta \sigma \Delta u_{i,i} +$$

$$2K\Delta e^d \Delta u_{i,i} - n\beta(\Delta \sigma)^2 - (1 - \epsilon) \frac{k}{\gamma_w} \Delta t \Delta \sigma_{,i} \Delta \sigma_{,i} +$$

$$- 2 \frac{k}{\gamma_w} \Delta t \sigma_{,i}^t \Delta \sigma_{,i}] \Delta V - \int_{A_1} \Delta t_i \Delta u_i dA - \int_{A_4} (1 - \epsilon) \Delta t \Delta h \Delta \sigma dA$$

Finite Element approximation

Using a finite element approximation one obtains, after differentiating with respect to the unknown nodal displacements u_i and v_i and the unknown nodal pore pressures w_i , a set of linear equations:

$$\begin{aligned} P_{kl} \Delta u_l + Q_{kl} \Delta v_l + S_{kl} \Delta w_l - G_k &= 0 \\ Q_{lk} \Delta u_l + R_{kl} \Delta v_l + T_{kl} \Delta w_l - H_k &= 0 \\ S_{kk} \Delta u_l + T_{lk} \Delta v_l + E_{kl} \Delta w_l + F_{kl} w_l^t - A_k &= 0 \end{aligned}$$

The non-linear shear- and compressionbehaviour is included by varying the stiffnessmatrices P, Q, R, S, T, E, F . An iterationprocedure or a multiple step approach are optional in the program.

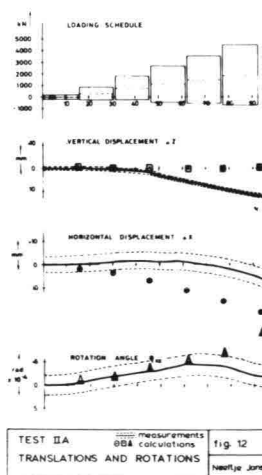
The influence of dilatancy is included in the loadvector terms G_k and H_k , which makes iteration cheap (initial strain method).

3.3 Prediction of Neeltje Jans test I and II

The program CASCO has been used to predict the Neeltje Jans test I and II. A description of these tests is given in ref. [23] and in part 1 of this paper. Soil parameters were determined mainly from drained plane strain tests.

The prediction of Neeltje Jans test I (caisson on undensified soil) is given in fig.11. The pore pressure generation is depicted of a point at 5 m. below the surface at Oosterschelde-side.

As one can see the generation of porepressures starts to faint off but has not vanished yet. This marks the main disadvantage of the method: One has to compute many separate loadcycles when cyclic pore pressure generation is an important aspect. Besides, it is extremely difficult to describe the parameters determining cyclic pore pressure generation, in an effective stress-strain relation. Therefore, a similar method seems to be rather unfit and rather expensive. The agreement between the computation and the measurements is not outstanding. Apart from the reasons mentioned above this will be due to bad contact between soil and caisson during the first three test-parcels.



A computation of Neeltje Jans test II (caisson on densified soil) is given in fig.12. The influence of pore pressures was neglected because of the densification and the gravel that was used.

In the original prediction the influence of cyclic loading was taken into account by multiplying the static deformations with a factor 3. This factor was based on cyclic shear-tests on very loose rip-rap. Later on, cyclic triaxial- and sheartests were performed on densified material, from which a factor 1,3 was derived. The results given in fig. 12 are based on the original prediction modified in respect to this factor.

A reasonable agreement is found between the computation and the measurements.

REFERENCES

1. A. Verruijt. Generation and dissipation of pore-water pressures. Finite elements in Geomechanics, 293-317, (ed. Gudehus). John Wiley & Sons, London (1977).
2. J.R. Booker and J.C. Small. An investigation of the stability of numerical solutions of Biot's equation of consolidation. Res. Report No.R.235 Civil Engineering Laboratories, The University of Sydney, Sydney (1974).
3. P.A. Vermeer. A double hardening model for sand. Delft Progress Report 2, 303-320 (1977).
4. P.A. Vermeer. A double hardening model for sand with reference to experimental studies. Géotechnique 28, No 4 (to be published) (1978).
5. M.A. Stroud. The behaviour of sand at low stress levels in the simple-shear apparatus. Ph.D. Thesis. University of Cambridge (1971).
6. P.W. Rowe. Theoretical meaning and observed values of deformation parameters for soil. Proc. Roscoe Mem.Symp., Cambridge, 143-194 (1971).
7. P.A. Vermeer and E.O.F. Calle. Gegevens-resultaten-plots van de berekeningen voor in situ test I (in Dutch). Report to Delft Soil Mechanics Laboratory (1975).
8. P.A. Vermeer and E.O.F. Calle. Gegevens-resultaten van de berekeningen voor in situ proef II (in Dutch). Report to Delft Soil Mechanics Laboratory (1975).
9. T.W. Lambe, J.W. Boehmer and W.F. Rosenbrand. Caisson tests at Neeltje Jans - The Netherlands. Symp. on Found. Aspects of Coastal Structures, Delft (1978).
10. P.A. Vermeer and S. van Dongen. The prediction of a model test. Report to Delft Soil Mechanics Laboratory (1976).
11. A.W.W.M. Biegstraaten, C.J. Kenter. Stress-strain behaviour for Finite Elements, Proceeding of symposium on Foundation Aspect of Coastal Structures, ch. II.2 (1978).
12. H.L. Jansen. Richtlijnen voor het uitvoeren van CONSOL-Berekeningen ten behoeve van het ontwerp fundering op putten van de stormvloedkering Oosterschelde, Deltadienst, Den Haag, nota DDWT-77-266 (1977).
13. W.J.M. Peperkamp, Onderzoek naar spreiding van belasting, invloed meshafmeting, $\tau - \gamma$ relatie met CONSOL, LGM rapport CO 407003/16 (1978).
14. L. de Quelerij, J.J. Broeze. Model tests on piers, scale 1 : 10, Proceedings of the symposium on Foundation Aspects of Coastal Structures, ch IV.2 (1978).
15. J.J. van Bijsterveld, Application of Numerical Analysis for Two-Dimensional Consolidation, Delft Soil Mechanics Laboratory, LGM mededelingen XVII, no 4 (1976).
16. F.B.J. Barends, SEEP. A finite element code for groundwaterflow, Delft Soil Mechanics Laboratory (1974/680251).
17. C.H. Engels, Verslag van het praktisch werken bij het Laboratorium voor Grondmechanica, University of Technology, Delft (1974).

18. A. Verruijt, A finite element method for plane strain consolidation, University of Technology Delft (1973).
19. C.J. Kenter, Dilatancy of soils, civ. ing. Thesis. University of Technology. Delft (1974). (dutch)
20. A. Verruijt, C.J. Kenter, Stability caissons Oosterschelde. Prediction of performance of first test caisson on the basis of program CASCO, Delft Soil Mechanics Laboratory (1975).
21. A. Verruijt, C.J. Kenter, Stability caissons Oosterschelde. Prediction of performance of test caisson on densified soil on the basis program CASCO, Delft Soil Mechanics Laboratory (1975).
22. C.J. Kenter, Plasticity in CASCO 6, Delft Soil Mechanics Laboratory, rep. CO 40103.0/13 (1976).
23. T.W. Lambe, J.W. Boehmer, W.F. Rosenbrand, Caisson tests at Neeltje Jans, The Netherlands, Proceedings of the Symposium on Foundation Aspects of Coastal Structures ch. IV.1 (1978).

SYMPOSIUM ON FOUNDATION ASPECTS OF COASTAL STRUCTURES

SIMPLE NUMERICAL METHODS TO DETERMINE DISPLACEMENTS AND STABILITY OF PIERS (SPRING CONSTANT AND BRINCH HANSON)

by:

J.B. Sellmeijer, Project Engineer, Delft Soil Mechanics Laboratory
Delft, The Netherlands

LIST OF SYMBOLS

a : height of the structure in the sill
 b : width in the direction of the horizontal load
 b_0 : part of the bottom where the structure has no contact with the soil
 d : width perpendicular to the horizontal force
 e : b_0/b
 f : function indicating the percentage of mobilized shear stress
 g : distribution function
 h : horizontal displacement
 h : index referring to the faces with the normal in horizontal direction
 k : spring constant
 l : center distance between the piers
 u : displacement
 v : vertical displacement
 v : index referring to the bottom with the normal in vertical direction
 w : displacement
 C : coefficient of volume compressibility
 D : diameter
 E : modulus of elasticity
 F : characteristic concerning horizontal spring constant
 G : characteristic concerning vertical spring constant
 H : horizontal hydrodynamic load
 M : moment
 V : vertical dead load of the structure
 α : distribution factor
 β : distribution factor
 γ : unit weight of submerged soil
 δ : distribution factor
 θ : friction angle between soil and structure
 ν : Poisson's constant
 σ : normal stress
 τ : shearing stress
 ϕ : angle of internal friction of soil
 ω : rotation

1. INTRODUCTION

Important design parameters for the piers of the Oosterschelde storm surge barrier are displacement and stability. To gain an insight into the mechanism which controls those parameters, many model types simulating reality can be developed. Most models contain the surrounding soil as an implicit variable (e.g. finite element computer programmes, model tests) and therefore they require time consuming elaboration. The consideration of the problem by this type of model is particularly useful if only one specific case is of interest.

To determine the influence of certain parameters, many computations or tests are required. In order to control costs and time there is need for a more simple model,

which reflects some specific trends in a reliable way. With this purpose in mind the spring constant method has been used for the calculation of the displacements and the Brinch Hansen method for the investigation of the stability.

2. DESCRIPTION OF THE SPRING CONSTANT METHOD

The piers of the barrier are rigid structures compared to the surrounding soil. They are placed parallel to each other, forming a line of foundation for the barrier. If the horizontal loading is perpendicular or parallel to this line, the displacements of the piers are determined by three parameters only, a horizontal and a vertical displacement, and a rotation, provided of course that the construction, the loading and the properties of the soil are symmetrical; see figure 1.

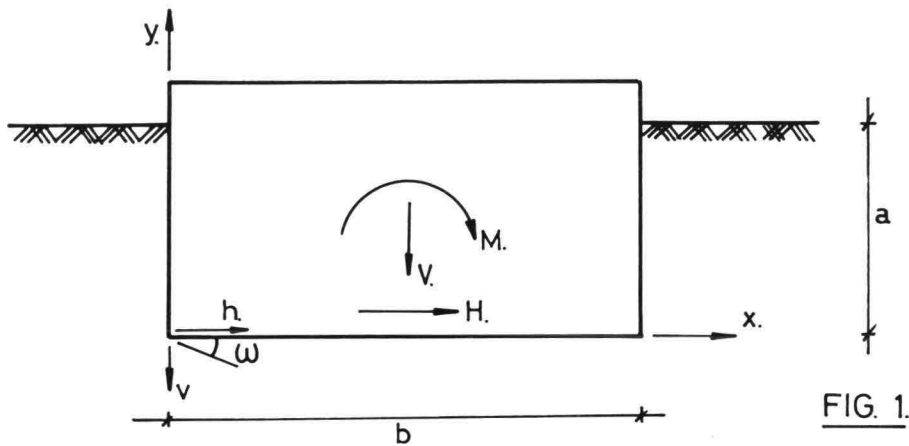


FIG. 1.

The loading consists of a horizontal hydrodynamic force H, a vertical dead weight V and a moment M resulting from the shift of the force H to the bottom of the construction and from a possible eccentricity of the dead weight. The displacements are denoted by a horizontal displacement h, a vertical displacement v and a rotation ω of the origin of the coordinate system. Therefore the displacements of an arbitrary point are:

$$u_x = h + \omega y \text{ horizontal displacement}$$

$$u_y = v + \omega x \text{ vertical displacement}$$

The height of the face is a, the width in the direction of the horizontal force is b and the width perpendicular to the horizontal force is d.

The spring constant method assumes a linear relationship between the normal stress on the construction and the displacement in that direction

$$\sigma_n = k u_n$$

where: σ_n = normal stress
 u_n = displacement in normal direction
 k = spring constant

The term "spring constant" is deceiving. This constant is anything but constant. It depends on the stress level and geometry. Later in this paper it will be shown how the spring constant can be calculated as a function of the geometry and the stress-level.

Besides the normal stresses on the construction the shear stresses play an important role. The maximum shear stress is equal to the product of the normal stress and the tangent of the angle of friction between construction and surrounding soil, denoted by θ . The mobilized shear stress is dependent on the displacement in the direction of the shear stress; see figure 2.

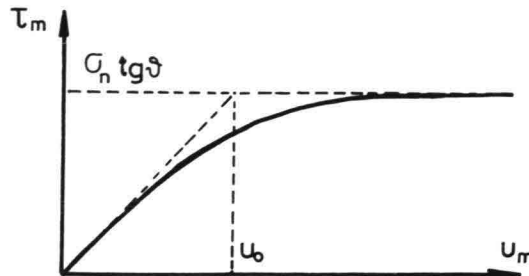


FIG. 2.

τ_m is the shear stress; u_m is the displacement in the direction of the shear stress. A characteristic value for the curve of mobilized shear stress is the parameter u_0 . Its value depends on the geometry, the stress-level and the friction angle θ . It will later be shown how this value can be determined.

Some of the main assumptions of the theory to be presented are the following. Before horizontal loading a neutral soil pressure will act against the vertical faces of the construction. At the side of the loading the soil pressure will diminish until the active pressure is reached. During calculation it is assumed that this active pressure is present. Because it is convenient for the calculation, the soil pressure at the other side will be split up into the active soil pressure and an increase of soil pressure with respect to the active condition. The engineering of the construction is done in such a way that no initial shear stresses are present on the vertical faces. Therefore the initial normal stresses at the bottom are known. Due to the moment the normal stresses at the side of the horizontal loading will decrease. If the size of the moment is relatively large, it is possible that along part of the bottom no normal stresses will occur, as soil cannot provide tension.

3. APPLICATION OF THE SPRING CONSTANT METHOD

In the previous paragraph the relationship between stress and displacement is shown. The displacements could be described by three unknown parameters, a horizontal and a vertical displacement and a rotation.

Since there are three conditions for equilibrium, horizontal, vertical and momental, one is able to determine the unknown parameters.

As has already been noted, the spring constant will be different at any point of the construction. In the direction of the width perpendicular to the horizontal force an average value may be obtained as will be shown when the value of the spring constant is determined.

The three equations of equilibrium now can be written as follows:

$$\frac{H}{d} = \int_0^a (h+\omega y)k_h(y/a)dy + \int_{b_0}^b f(h/u_v)tg \theta_v (v+\omega x)k_v(x/b)dx \quad (3.1)$$

$$\begin{aligned} \frac{V}{d} &= \int_0^a (h+\omega y)k_h(y/a) f((v+\omega b-v_r)/u_h)tg \theta_h dy + \int_{b_0}^b (v+\omega x)k_v(x/b)dx + \\ &+ \int_0^a \lambda \gamma (a-y)tg \theta_h \{ f((v+\omega b-v_r)/u_h) - f((v_1-v)/u_h) \} dy \end{aligned} \quad (3.2)$$

$$\begin{aligned} \frac{M-\frac{1}{2}bV}{d} &= \int_0^a (h+\omega y)k_h(y/a)y dy + \int_{b_0}^b (x-b)(v+\omega x)k_v(x/b)dx + \int_0^a \lambda \gamma (a-y) \\ &tg \theta_h f((v_1-v)/u_h)bdy \end{aligned} \quad (3.3)$$

where the index h refers to the properties of the faces with the normal in horizontal direction and the index v to those of the bottom with the normal in vertical direction. The function $f(u/u_0)$ denotes the percentage of mobilized shear stress. The initial vertical displacement at the left side, being the side of the horizontal loading, is denoted by v_1 , the one at the right side by v_r . In that part of the bottom between $x=0$ and $x=b_0$ it is supposed that there is no contact between structure and soil, so that there acts no stress. λ is the ratio between active horizontal soil pressure and the vertical stress; γ is the submerged unit weight of the soil.

It is convenient to define the following quantities:

$$F_n = \frac{1}{a^{n+1}} \int_0^a y^n k_h(y/a)dy = \int_0^1 \eta^n k_h(\eta)d\eta \quad \eta = y/a \quad n = 0, 1, 2$$

$$G_n = \frac{1}{b^{n+1}} \int_{b_0}^b x^n k_v(x/b)dx = \int_e^1 \xi^n k_v(\xi)d\xi \quad \xi = x/b \quad e = b_0/b$$

$$H_* = \frac{H}{abd} - v_* f(h/u_v)tg \theta_v$$

$$V_* = \left[\frac{v - Hf((v+\omega b-v_r)/u_h)tg \theta_h}{abd} - \frac{1}{2} \lambda \gamma \frac{a}{b} tg \theta_h \{ f((v+\omega b-v_r)/u_h) - f((v_1-v)/u_h) \} \right] / \{ 1 - f((v+\omega b-v_r)/u_h)tg \theta_h f(h/u_v)tg \theta_v \}$$

$$M_* = \frac{M-\frac{1}{2}bV}{ab^2d} - \frac{1}{2} \lambda \gamma \frac{a}{b} tg \theta_h f((v_1-v)/u_h)$$

If one subtracts $f(h/u_v)tg \theta_v$ times equation (3.2) from equation (3.1) and $f((v+\omega b-v_r)/u_v)tg \theta_v$ times equation (3.1) from (3.2) and substitutes the above defined quantities in this result and in equation (3.3) one will obtain the following set of equations in matrix notation:

$$\begin{vmatrix} F_0 & 0 & F_1 a/b \\ 0 & G_0 & G_1 b/a \\ F_1 a/b & G_1 - G_0 & F_2 (a/b)^2 + (G_2 - G_1)b/a \end{vmatrix} \begin{vmatrix} h/b \\ v/a \\ \omega \end{vmatrix} = \begin{vmatrix} H_* \\ V_* \\ M_* \end{vmatrix} \quad (3.4)$$

From these equations it follows:

$$\begin{aligned} \frac{h}{b} - \frac{H^*}{F_0} &= - \frac{F_1}{F_0} \frac{a}{b} \omega \\ \frac{v}{a} - \frac{V^*}{G_0} &= - \frac{G_1}{G_0} \frac{b}{a} \omega \\ \left\{ \frac{F_2 F_0 - F_1^2}{F_0} \left(\frac{a}{b}\right)^2 + \frac{G_2 G_0 - G_1^2}{G_0} \frac{b}{a} \right\} \omega &= M^* - \frac{G_1 - G_0}{G_0} V^* - \frac{F_1}{F_0} \frac{a}{b} H^* \end{aligned} \quad (3.5)$$

The quantities H^* , V^* and M^* contain the parameters h , v and ω , and the quantity G_0 contains the parameter e , being a function of h , v and ω . Accordingly the displacements of the pier have to be determined by an iteration process. This process is carried out by computer and takes only a fraction of a second. The displacements due to the hydrodynamic force are calculated. The initial displacements v_1 and v_r have no practical importance. They only indicate the vertical displacement of the construction by the dead weight in case the soil has the present stiffness.

An example of the output of a computation is shown in appendix 1. It is noted that the influence of initial inclination is considered, due to eccentricity of the dead weight and/or non-homogeneous subsoil. Moreover the consequences of a possible negative value for h are taken into account.

4. DETERMINATION OF THE SPRING CONSTANTS

As already mentioned, the value of the "spring constant" depends on geometry and stress level. This means that first of all in any specific case values of the soil characteristics have to be determined. As an example the case will be considered where all piers are loaded perpendicular to the barrier. For the calculation of the parameters needed a linear stress distribution into the subsoil will be presumed. For the determination of the vertical spring constant the parameter indicating this distribution will be denoted by β ; see figure 3.

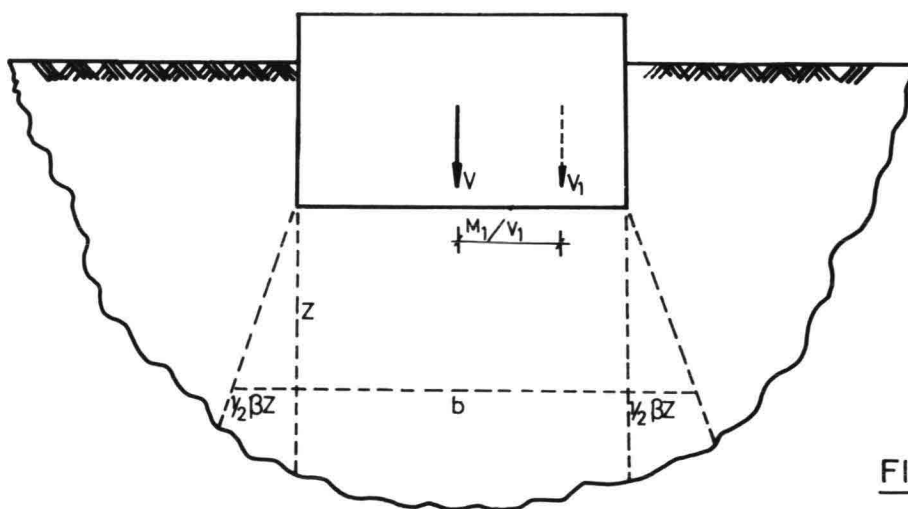


FIG. 3.

From more advanced calculations by computer it followed that the value of β is about unity; V_1 is the total vertical reaction and M_1 the moment, resulting from the stresses along the bottom after applying the horizontal hydrodynamic load. The value of V_1 is smaller than the one of the dead weight V , due to the influence of the shear stresses on the faces. The average effective stress level at a depth z now is outlined by

$$\sigma_t = \frac{V - (V - V_1)t}{(b - 2t M_1/V_1 + \beta z)d} + \gamma z \quad (4.1)$$

The value $t = 0$ yields the initial stress-level; $t = 1$ the final one. The stress concentration by the moment is simulated by a decreasing width with the resulting load V_1 acting in the center. The stress-strain relationship formulated by Terzaghi is,

$$d\sigma_t = C \sigma_t d\left(\frac{w_z}{dz}\right) \quad (4.2)$$

where: C = the coefficient of volume compressibility of Terzaghi

w_z = the vertical displacement

Integration of formula (4.2) from $t = 0$ until $t = 1$ yields

$$\frac{dw_z}{dz} = \frac{1}{C} \left[\ln \left\{ \frac{V_1}{(b - 2M_1/V_1 + \beta z)d} + \gamma z \right\} - \ln \left\{ \frac{V}{(b + \beta z)d} + \gamma z \right\} \right] \quad (4.3)$$

The vertical displacement w_z is now obtained by integration of equation (4.3) with respect to z . It has to be noted that the coefficient C is a function of z since the subsoil is not homogeneous. However, it is sufficient to consider an average value \bar{C} to be derived later in this section. The vertical spring constant is equal to the quotient of the increase of stress along the bottom and the vertical displacement. This results in the formula,

$$\frac{1/4 \gamma \bar{C}}{k_v} = \frac{\kappa \sqrt{|\mu_1 - 1|} \operatorname{arctg}(h) \sqrt{|\mu_1 - 1|} - \sqrt{|\mu - 1|} \operatorname{arctg}(h) \sqrt{|\mu - 1|} - \kappa \ln(\frac{1}{2} \sqrt{\mu_1}) + \ln(\frac{1}{2} \sqrt{\mu})}{\kappa \mu_1^{-\mu}} \quad (4.4)$$

where: k_v = average value of the spring constant along the bottom

κ = $1 - 2 M_1/bV_1$

$\operatorname{arctg}(h)$ = arctg if $\mu > 1$ or $\mu_1 > 1$

$-\operatorname{arctgh}$ if $\mu < 1$ or $\mu_1 < 1$

μ = $4\beta V/\gamma b^2 d$

μ_1 = $4\beta V_1/\gamma \kappa^2 b^2 d$

The values of V and V_1 are not very much different; the one for V_1 is always slightly smaller than the one for V . This means that the stress decreases by the decreasing vertical load, but increases by the moment. Therefore there exists a value for M_1 such that the increase in stress is zero and such that the vertical displacement is zero, resulting in a spring constant zero and infinite respectively; see appendix 2. If $V_1 = V$ the value of k_v increases gradually with increasing values of M_1 . If $M_1 = 0$ the value of k_v increases gradually with increasing values of V_1 . However, the last values of k_v are smaller than the ones with variable M_1 . This fact is also found in practice. Because a discontinuity in the values for k_v is not realistic and because in our case change in moment prevails over change in vertical load the vertical spring constant will be determined from equation (4.4) under the condition $V = V_1$.

The average value for the coefficient of volume compressibility can be determined as follows. From appendix 2 it is clear that the value for k_v increases rather slowly for increasing values of M_1 . Therefore consider equation (4.3) for the limit $M_1 \rightarrow 0$ and the condition $V = V_1$. The average value C will be defined as,

$$\frac{1}{\bar{C}} \int_0^\infty \lim_{M_1 \rightarrow 0} \ln \left[\frac{\frac{V}{(b-2M_1/V+\beta z)d} + \gamma z}{\frac{V}{(b+\beta z)d} + \gamma z} \right] dz = \int_0^\infty \frac{1}{C} \lim_{M_1 \rightarrow 0} \ln \left[\frac{\frac{V}{(b-2M_1/V+\beta z)d} + \gamma z}{\frac{V}{(b+\beta z)d} + \gamma z} \right] dz$$

or with $\zeta = \beta z/b$,

$$\frac{1}{\bar{C}} \int_0^\infty \frac{\mu}{\mu+4\zeta(\zeta+1)} \frac{d\zeta}{\zeta+1} = \int_0^\infty \frac{1}{C} \frac{\mu}{\mu+4\zeta(\zeta+1)} \frac{d\zeta}{\zeta+1} \tag{4.5}$$

In case the subsoil consists of a number of more or less homogeneous layers equation (4.5) may be outlined by:

$$\frac{1}{\bar{C}} = \frac{\sum_{m=1}^n \frac{1}{C_m} \frac{4}{\mu+(\zeta_m+\zeta_{m-1})(2+\zeta_m+\zeta_{m-1})} \cdot \frac{\zeta_m-\zeta_{m-1}}{2+\zeta_m+\zeta_{m-1}} + \frac{1}{C_{n+1}} \frac{1}{(2\zeta_{n+1})^2}}{n \frac{\sum_{m=1}^n \frac{4}{\mu+(\zeta_m+\zeta_{m-1})(2+\zeta_m+\zeta_{m-1})} \cdot \frac{\zeta_m-\zeta_{m-1}}{2+\zeta_m+\zeta_{m-1}} + \frac{1}{(2\zeta_{n+1})^2}}}} \tag{4.6}$$

where ζ_m is the distance of the m^{th} layer until the bottom of the pier; see figure 4. The value of ζ_n must be large enough, for example $\zeta_n > 2$ and $\zeta_n > \frac{1}{2}\sqrt{\mu}$.

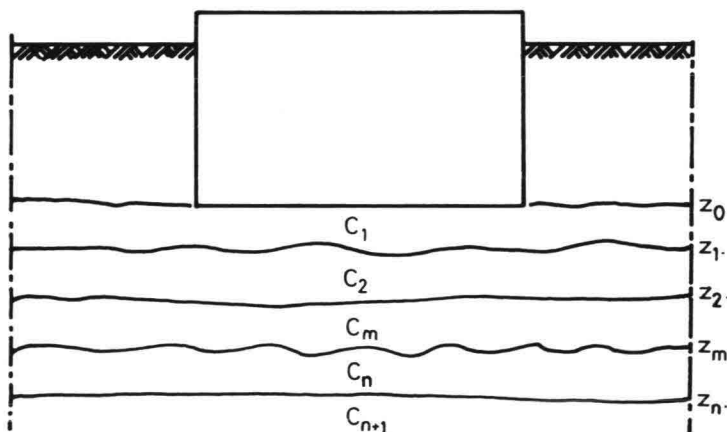


FIG. 4.

In the direction parallel to the barrier no distribution of stress was presumed. This is not completely according to reality since partial stress distribution is possible; see figure 5.

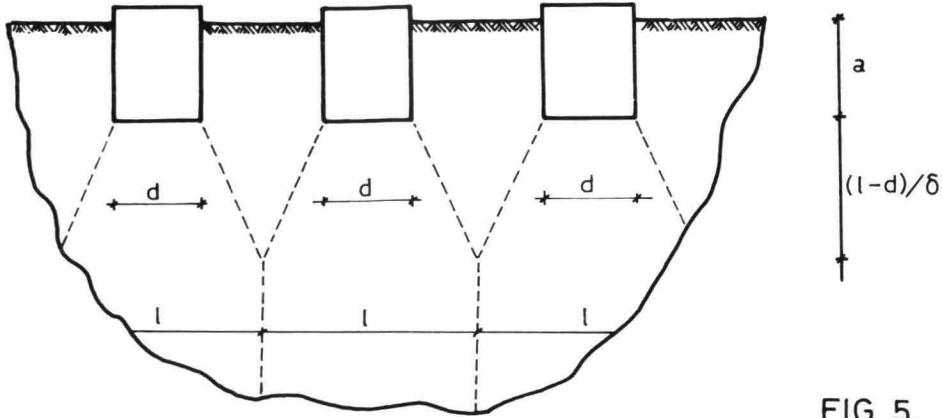


FIG. 5.

δ indicates the normal stress distribution in the direction parallel to the barrier. Over a depth of $(l - d)/\delta$ stress distribution will appear. After this level the stresses of the adjacent piers interfere so that distribution no longer takes place. This fact can be taken into account by multiplying the factor $4\zeta(1+\zeta)$ in formula (4.5) by $(1 + \frac{\delta}{\beta} \frac{b}{d} \zeta)$ for values of z until $(l - d)/\delta$ and by $\frac{1}{d}$ for values of z larger than $(l - d)/\delta$. This results in a larger value of \bar{C} . Generally the value for δ is equal to the one for β .

The value for u_v can be determined in an analogous way. One assumes for the normal as well as the shear stress a linear stress distribution,

$$\tau = \frac{-H_s}{(b+\beta'z)d} \quad \sigma = \frac{V}{(b+\beta z)d} + \gamma z$$

where H_s is the total shearing force along the bottom. However, shear stress decreases with depth faster than normal stress. This means that the value for β' is larger than the one for β . The linear relationship between the shear stress and the shearing strain γ_{xz} is:

$$\tau = G \gamma_{xz} = \frac{E}{2(1+\nu)} \gamma_{xz} = \frac{C\sigma}{2(1+\nu)} \gamma_{xz}$$

where: G = shear modulus of soil
 ν = Poisson's ratio
 E = elasticity modulus of soil

The shearing strain can be written as:

$$\gamma_{xz} = \frac{\partial w_z}{\partial x} + \frac{\partial w_x}{\partial z}$$

where: w_x = horizontal displacement.

The value of $\partial w_z / \partial x$ at $z = 0$ is equal to the value of $-\omega$ to be calculated. If one assumes that $\partial w_z / \partial x$ is the same type of function of z as $\partial w_x / \partial z$ then, since γ_{xz} is a function of τ / σ ,

$$\frac{\partial w_z}{\partial x} = -\omega \frac{\tau}{\sigma} \frac{V}{H_s}$$

and it follows for the horizontal displacement,

$$\frac{\partial w_x}{\partial z} = \left\{ \frac{2(1+\nu)}{C} \frac{H_s}{V} + \omega \right\} \frac{V}{H_s} \frac{\tau}{\sigma} \tag{4.7}$$

Integration with respect to z between $z \rightarrow \infty$ and $z = 0$ provides the horizontal displacement w . Since a linear stress-strain relationship was assumed u_v can be determined from w_x ; see figure 6.

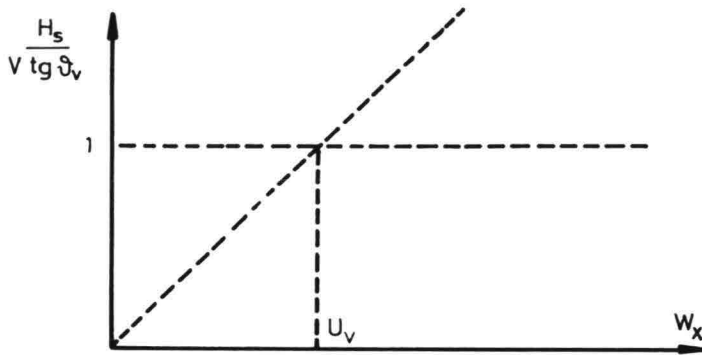


FIG. 6.

u_v is the value for w_x in order that $H = V \operatorname{tg} \theta_v$. Therefore,

$$\frac{u_v}{w_x} = \frac{V}{H_s} \operatorname{tg} \theta_v$$

Equation (4.7) now yields after integration and multiplication with u_v / w_x

$$\frac{1 - \beta' / \beta + \mu / 4 (\beta' / \beta)^2}{2(1+\nu) \operatorname{tg} \theta_v \sqrt{C + \omega / f(h/u_v)}} \cdot \frac{4\beta}{\mu} \frac{u_v}{b} = \left\{ 1 - \frac{\beta'}{\beta} + \frac{\mu}{2} \frac{\beta'}{\beta} \right\} \frac{\sqrt{|\mu-1|}}{\mu-1} \operatorname{arctg}(h) \sqrt{|\mu-1|} - \left(1 - \frac{\beta'}{\beta} \right) \ln \left(\frac{1}{2} \frac{\beta'}{\beta} \sqrt{\mu} \right) \tag{4.8}$$

In this formula $H/V \operatorname{tg} \theta_v$ is replaced by $f(h/u_v)$.

The average value of the coefficient of volume compressibility differs slightly from the one used for the vertical spring constant. In formula (4.5) one has to replace the term $1/(1 + \zeta)$ by $(1 + \zeta)/(1 + \zeta\beta'/\beta)$.

For the determination of the horizontal spring constant at the sides of the structure several methods can be applied. The most direct one is a pressiometer test. However, from point of engineering the barrier, in situ data cannot be achieved. From the results of pressiometer tests, Menard (1) derived a formula by which the spring constant can be calculated as a function of geometry and soil characteristics,

$$\frac{1}{k_h} = \frac{1.3}{6E_p} D_o \left(\frac{D}{D_o} \lambda_m \right)^{\alpha_m} + \frac{\alpha_m D}{6E_p} \quad (4.9)$$

where: D = diameter of the construction
 D_o = reference diameter being 0.6 m
 λ_m = geometry factor being 1.12 in the case that the vertical cross section is square and 2.65 in the case of a strip
 α_m = soil characteristic having the value 1/3 for sand
 E_p = modulus of elasticity following from pressiometer tests being fairly equal to the cone resistance of a penetrometer test

Menard considered a critical depth about 3 or 4 times the diameter D above which the spring constant decreases to zero at ground level. Since the value of E_p cannot be measured beforehand, the values to be expected have to be carefully selected.

Besides this more practical approach, the method of stress distribution used by the vertical spring constant can be used.

In order to introduce a spring constant increasing with depth, the following will be assumed; see figure 7.

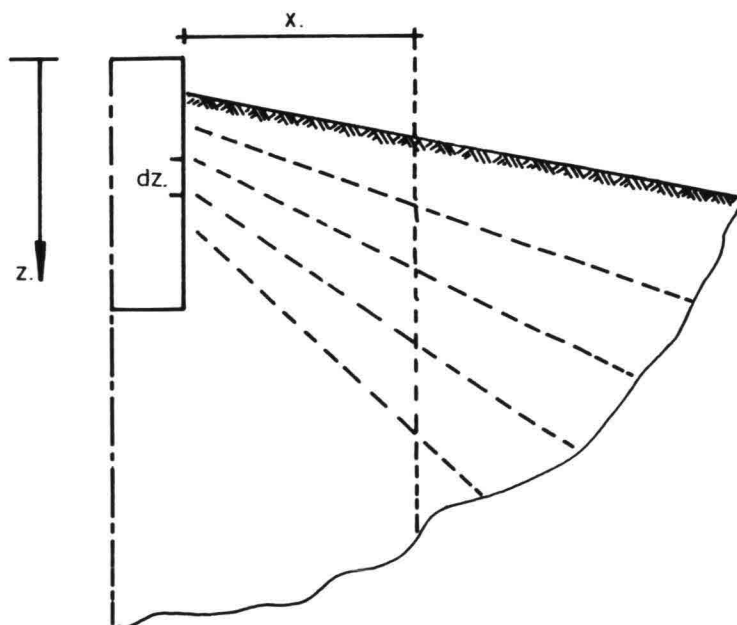


FIG. 7

Every area dz has a stress distribution $\alpha' \left(\frac{z}{a}\right) \frac{dz}{a}$ between the dotted lines. The total horizontal stress along such a dotted line can be reflected by:

$$\sigma = \frac{H_n g_n(z/a)}{(a + \alpha'(z/a)x)d} + \lambda\gamma(z + \alpha xz/a) \quad (4.10)$$

H_n is the total horizontal reaction provided by the face; $\int_0^a g_n(z/a) dz = a$, $g_n(z/a)$ being an arbitrary function of z . It is not necessary that α equals:

$\frac{1}{z} \int_0^z \alpha' \left(\frac{z}{a}\right) dz$. This parameter may be chosen independent of z which results in a linear fan-shape of the dotted lines. Every area between two dotted lines has its own value of $\alpha'(z/a)$ dependent on the mechanism of transmission of shear stresses. Applying Terzaghi's stress-strain relationship one obtains:

$$\frac{dw_x}{dx} = \frac{1}{C(z/a)} \ln \left[1 + \frac{H_n g_n(z/a)}{\lambda\gamma z a (1 + \alpha x/a) (1 + \alpha' x/a)} \right] \quad (4.11)$$

where the coefficient of volume compressibility is assumed to be constant on a dotted line. Integration of (4.11) provides the horizontal displacement. The quotient of stress increase and this displacement is the horizontal spring constant; the result is:

$$\begin{aligned} \frac{\alpha' \lambda \gamma z/a}{\frac{1}{2}(1 + \alpha/\alpha')} \frac{C(z/a)}{k_h} \frac{\alpha}{\alpha'} \mu &= 2 \sqrt{\frac{\left| \frac{\alpha}{\alpha'} \mu^{-\frac{1}{2}} \left(1 - \frac{\alpha}{\alpha'}\right)^2 \right|}{\frac{1}{4} \left(1 + \frac{\alpha}{\alpha'}\right)^2}} \operatorname{arctg}(h) \sqrt{\frac{\left| \frac{\alpha}{\alpha'} \mu^{-\frac{1}{2}} \left(1 - \frac{\alpha}{\alpha'}\right)^2 \right|}{\frac{1}{4} \left(1 + \frac{\alpha}{\alpha'}\right)^2}} + \\ &+ \frac{\frac{\alpha}{\alpha'} \ln \frac{\alpha}{\alpha'}}{\frac{1}{2}(1 + \alpha/\alpha')} - \ln \left(\frac{\alpha}{\alpha'} \mu + \frac{\alpha}{\alpha'} \right) \end{aligned} \quad (4.12)$$

where $\mu = H_n g_n(z/a) / \lambda\gamma z a$

If $\alpha/\alpha' \mu$ has a small value one may approximate this result by

$$\frac{\alpha \lambda \gamma z/a}{k_h} \frac{C(z/a)}{\frac{\alpha}{\alpha'} - 1} \sim \frac{\frac{\alpha}{\alpha'} \ln \frac{\alpha}{\alpha'}}{\frac{\alpha}{\alpha'} - 1} \sim \sqrt{\frac{\alpha}{\alpha'}} \quad 0 < \frac{\alpha}{\alpha'} < 2 \quad \text{or} \quad k_h \sim \alpha \lambda \gamma C(z/a) z/a \sqrt{\alpha'/\alpha}$$

If $\alpha/\alpha' \mu$ has a large value the following approximation may be used,

$$\frac{\alpha' \lambda \gamma z/a}{k_h} \frac{C(z/a)}{\sqrt{\frac{\alpha}{\alpha'} \mu}} \quad \text{or} \quad k_h \sim \frac{\alpha^2 \lambda \gamma C^2(z/a)}{\pi^2} \frac{\alpha'}{\alpha} \frac{z}{a} \frac{w_x}{a}$$

where use is made of the relation

$$H_n g_n(z/a) / a d = k_h w_x$$

w_x is the horizontal displacement of the face. Since horizontal displacement does not vary very much with depth, the influence of rotation on the spring constant is not concerned.

From calculations by more advanced computer programmes and experiments it followed that the horizontal spring constant increases with depth more or less like a square root function. This means that in this model the distribution factor α/α' increases linear with depth for very small values of the horizontal loading, gradually becoming proportional to a square root relation for large values of the horizontal loading. This result is rather satisfactory since the stiffness at smaller depths increases relatively more than at larger depths.

To simplify the result (4.12) one will assume that at $z = a_0$ $\alpha' = \alpha$, a_0 indicating the place of the resultant force H_n on the face.

If k_h is a square root function of depth, the value of $g_n(z/a)$ at $z = a_0$ is $\frac{3}{2}\sqrt{\frac{3}{5}} \sim 1$. Therefore the horizontal spring constant can now be outlined by,

$$\frac{\frac{1}{2}\alpha\lambda\gamma\sqrt{z/a} \sqrt{a_0/a} C(z/a)}{k_h} = \frac{1}{\sqrt{\mu}} \operatorname{arctg} \sqrt{\mu} - \frac{1}{\mu} \ln \sqrt{\mu + 1} \quad (4.13)$$

where $\mu = \frac{H_n}{\lambda\gamma a_0 a d}$

If α has the value 1 the result of the horizontal spring constant calculated by this method is very close to the one calculated by Menard's formula (4.9). By the equation of (4.13) it is possible to introduce the influence of the slope beside the pier by reducing the value of α .

The value controlling the mobilizing of shear stress for the faces can be determined using the same assumptions as mentioned before. The shearing stress will be outlined by

$$\tau = \frac{P g_s(z/a)}{(a + \alpha'' x) d}$$

where the distribution function $g_s(z/a)$ has to satisfy $\int_0^a g_s(z/a) dz = a$ and

$\alpha'' = \alpha''(z/a)$ reflects the stress distribution. P is the total shearing force. From the formulae

$$\tau = \frac{C\sigma}{2(1+\nu)} \gamma_{zx} \quad \gamma_{zx} = \frac{\partial w_z}{\partial x} + \frac{\partial w_x}{\partial z}$$

$$\sigma = \frac{H_n g_n(z/a)}{(a + \alpha' x) d} + \lambda\gamma \frac{z}{a} (a + \alpha x)$$

and with the assumption

$$\frac{\partial w_x}{\partial z} = -\omega \frac{\tau}{\sigma} \frac{H_n g_n(z/a) + \lambda\gamma z a d}{P g_s(z/a)}$$

it follows

$$\frac{\partial w_z}{\partial x} = \left\{ \frac{2(1+\nu)}{C(z/a)} \frac{P g_s(z/a)}{H_n g_n(z/a)} - \omega \left(1 + \frac{\lambda\gamma z a d}{H_n g_n(z/a)} \right) \right\} \frac{H_n g_n(z/a)}{P g_s(z/a)} \frac{\tau}{\sigma} \quad (4.14)$$

The factor controlling the mobilizing of shearing stress, u_h , is related to the forces P and H_n as follows:

$$\frac{u_h}{w_z} = \frac{H_n f(z/a) + \lambda\gamma z a d}{P g(z/a)} \operatorname{tg} \theta_h$$

Therefore after integration of (4.14) one obtains for the parameter u_h , with $\xi = \alpha x/a$.

$$\alpha \frac{u_h}{a} = \left\{ \frac{2(1+\nu)}{C(z/a)} \operatorname{tg} \theta_h - \omega \frac{H_n g_n(z/a) + \lambda \gamma z a d}{P g_s(z/a)} \operatorname{tg} \theta_h \right\} \int_0^\infty \frac{\mu+1}{\mu+(1+\xi)(1+\xi\alpha'/\alpha)} \cdot \frac{1+\xi\alpha'/\alpha}{1+\xi\alpha''/\alpha} d\xi \quad (4.15)$$

In this formula the factor $P g_s(z/a)/\{H_n g_n(z/a) + \lambda \gamma z a d\} \operatorname{tg} \theta_h$ will be replaced by $f((v+\omega b-v_r)/u_h)$.

Since u_h is independent of z , assuming there is no slip between soil and construction, one may average equation (4.15) over the height a . Roughly this can be done by

$$\frac{1}{C} = \frac{1}{a} \int_0^a \frac{dz}{C(z/a)} \quad (4.16)$$

For small values of ξ this is correct and for large values of ξ an exact average is arbitrary since the fan-shaped distribution of the areas with equal C -values is arbitrary. Equation (4.15) can now be rewritten for $\alpha'/\alpha = 1$.

$$\frac{(\alpha''/\alpha)^2 \mu + (1-\alpha''/\alpha)^2}{2(1+\nu) \operatorname{tg} \theta_h / C - \omega/f((v+\omega b-v_r)/u_h)} \cdot \frac{\alpha}{\mu+1} \frac{u_h}{a} = \frac{\alpha''}{\alpha} \sqrt{\mu} \operatorname{arctg} \sqrt{\mu} - (1 - \frac{\alpha''}{\alpha}) \ln \left\{ \frac{\alpha''}{\alpha} \sqrt{\mu+1} \right\} \quad (4.17)$$

The derivations of parameters, carried out in this paragraph are examples of how spring constant values can be determined. In other cases, for example loading parallel to the barrier of only one pier, other equations are derived because the stress distribution is two-dimensional in this case.

4. STABILITY

Besides the displacements of the piers an important design factor is the stability. Calculations are carried out by formulae given by J. Brinch Hansen (2). The bearing capacity of the foundation was compared with the loading and expressed in a safety factor.

In the spring constant programme discussed in the previous paragraphs, a stability calculation is also enclosed. The following model is considered. It is assumed that failure occurs by slipping of the structure pushing the soil beside the structure along the slip lines, to be determined from the Mohr circle; see figure 8.

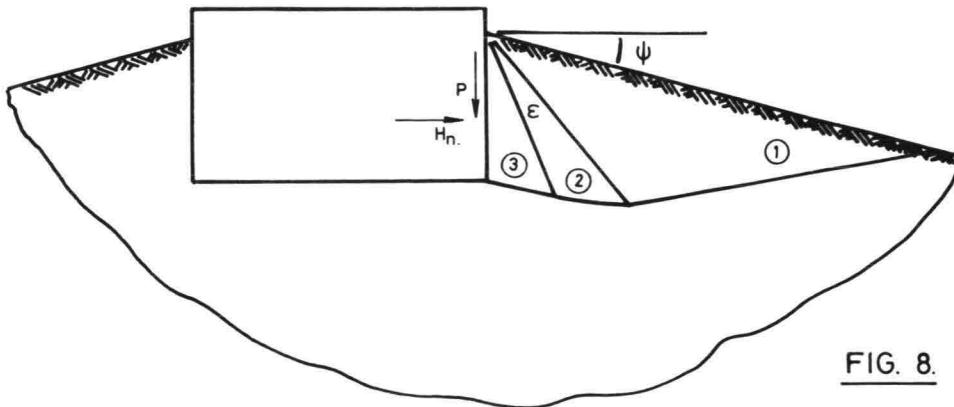


FIG. 8.

The angle of the slope with the horizontal plane is denoted by ψ . Three areas are distinguished, area 1, 2 and 3. In the first stage of the calculation, the bearing capacity of the construction for arbitrary loads P and H_n with the condition $P/H_n > \text{tg } \psi$ is compared with the one for loading parallel to the slope, $P/H_n = \text{tg } \psi$. In this calculation no dead load of the soil is considered, but a constant load on the slope. The stress situation in area 1 follows from the Mohr circle; see figure 9.

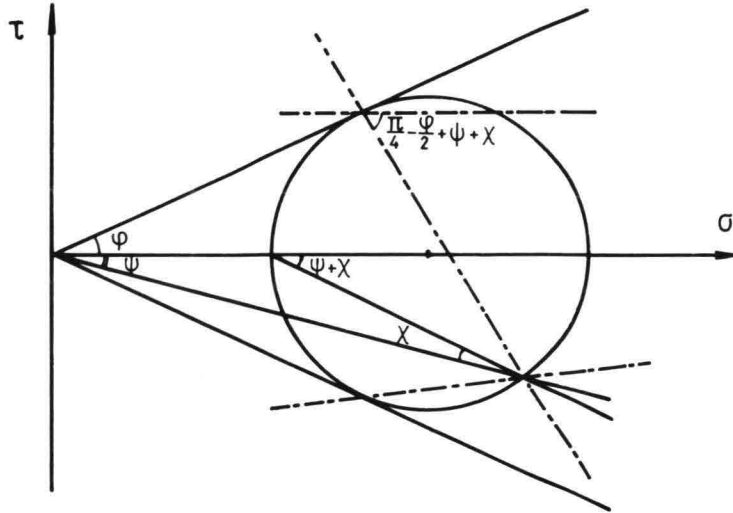


FIG. 9.

ϕ is the angle of internal friction of the soil. The relation between ψ and χ is,

$$\sin(2\chi + \psi) = \sin \psi / \sin \phi$$

The stress situation in area 3 depends also on ϵ ; see figure 10.

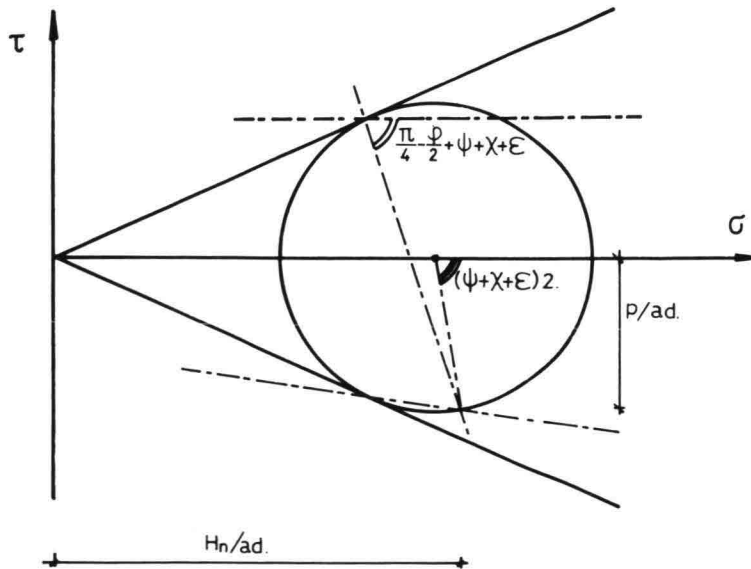


FIG. 10.

From the equations of Kötter (3) it follows that the quotient of bearing capacity for arbitrary ε and the one for $\varepsilon = 0$ equals

$$\Theta = \frac{1 + \sin \phi \cos \{2(\psi + \chi + \varepsilon)\}}{1 + \sin \phi \cos \{2(\psi + \chi)\}} \exp (2\varepsilon \operatorname{tg} \phi)$$

The value for ε depends on the quotient $P/H_n = f \operatorname{tg} \theta_h$, where f stands for $f((v + \omega b - v_r)/u_h)$

$$\frac{H_n}{P} = \frac{1 + \sin \phi \cos \{2(\psi + \chi + \varepsilon)\}}{\sin \phi \sin \{2(\psi + \chi + \varepsilon)\}} = \frac{1}{f \operatorname{tg} \delta_h}$$

Or after rewriting

$$2(\psi + \chi + \varepsilon) = \theta' + \arcsin\left(\frac{\sin \theta'}{\sin \phi}\right)$$

where

$$\operatorname{tg} \theta' = f \operatorname{tg} \delta_h$$

In case $\varepsilon = 0$ the bearing capacity due to dead load of the soil is known and equals

$$H'_{n \max} = \frac{1}{2} \gamma a^2 d \frac{1 + \sin \phi \cos(\chi + \psi)}{1 - \sin \phi \cos(2\chi)}$$

The maximum load $H_{n \max}$ which can be sustained by the construction is then

$$H_{n \max} = \Theta H'_{n \max}$$

Or after rewriting,

$$H_{n \max} = \frac{1}{2} \gamma a^2 d \frac{1 + \sin \phi \sqrt{1 - (\operatorname{tg} \psi / \operatorname{tg} \phi)^2}}{1 - \sin \phi \sqrt{1 - (f \operatorname{tg} \theta_h / \operatorname{tg} \phi)^2}} \exp \left[\left\{ \arctg(f \operatorname{tg} \theta_h) - \psi + \arcsin\left(\frac{1}{\sin \phi} \frac{f \operatorname{tg} \theta_h}{\sqrt{1 + (f \operatorname{tg} \theta_h)^2}}\right) - \arcsin\left(\frac{\sin \psi}{\sin \phi}\right) \right\} \operatorname{tg} \phi \right]$$

The value of f can be taken as unity because during collapse total mobilization of shear stresses can be expected.

The calculated $H_{n \max}$ is expressed together with the maximum possible shear force along the bottom in a safety factor dividing their sum by the horizontal hydrodynamic force.

5. RESULTS AND CONCLUSIONS

A parametric study is carried out with the results of the described theory. Five typical locations of piers in the Oosterschelde were considered. The horizontal cross section of the piers was varied; 50 x 20 m, 50 x 25 m and 60 x 25 m. Moreover those fifteen standard cases were investigated on the influence of the amount of compaction of the sill, the size of the height of the sill, the presence of a thin slip layer under the foundation plate, the value of the friction angle of the faces, the amount of dead weight. The results of these calculations are summarized in tables. An example of such a table is given in appendix 3. In figure 11 the geometry and some specific parameters are indicated.

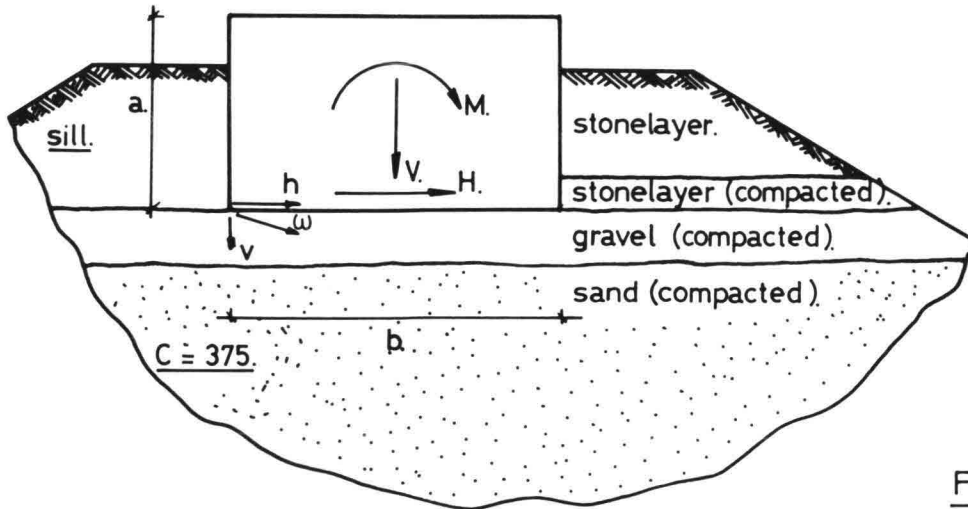


FIG. 11.

The rotation depends for the most on the size of the cross section. The horizontal displacement is very sensitive for the presence of a thin slip layer under the bottom. From the results of all the calculations one carefully selected the dimensions and dead weight of the piers and desired soil conditions in order to meet the design criteria.

It is interesting to compare the result of a calculation by the present theory with the one by a more advanced theory. This is carried out with the aid of the finite element computer programme "CONSOL" (Christian, Boehmer, Biegstraaten). Two examples are presented with cross section 50 x 25 m. The size of the height "a" of the sill is 7.5 m and 10 m.

a = 7.5 m	Spring Constant	CONSOL	a = 10 m	Spring Constant	CONSOL
h	13.22 cm	9.67 cm	h	9.19 cm	7.96 cm
h + ωa	14.36 cm	10.67 cm	h = ωa	10.82 cm	9.35 cm
ω	0.00152	0.00134	ω	0.00163	0.00139
v	-4.23 cm	-4.61 cm	v	-4.46 cm	-4.66 cm
v + ωb	3.38 cm	2.07 cm	v + ωb	3.69 cm	2.29 cm

The values for the rotation are rather close. The compared cases showed a difference of 10 to 20 percent. The values for the horizontal displacement differ in the compared cases much more. However, it is not yet clear if the programme CONSOL simulates the same severe slip condition between bottom and soil as the spring constant programme.

Besides the displacements, also the values for the safety coefficients are compared with the ones obtained by formulae formulated by Brinch Hansen (2). Those results are rather close.

	Spring Constant	Brinch Hansen
a = 7.5 m	0.89	0.87
a = 10 m	1.17	1.10

Those values also agree very well with the ones obtained from centrifuge experiments by Rowe.

The Spring Constant programme is a very cheap and fast device to calculate displacements and the safety of structures exposed to loading.

It is especially very useful to determine specific trends by the influence of certain parameters. However, comparison with more advanced, time-consuming models is necessary in order to determine the parameters which reflect the influence of the subsoil.

6. REFERENCES

- (1) Ménard, L., 1973
Règles d'utilisation des techniques pressiometriques et d'exploitation des resultats obtenus pour le calcul des fondations; III - notice speciale no. 2. Centre d'études géotechniques, Paris.
- (2) Brinch Hansen, J., 1970
A revised and extended formula for bearing capacity; bulletin no. 28 Geotechnisk Institut, Copenhagen.
- (3) Kötter, F., 1903
Die Bestimmung des Druckes an gekrümmten Gleitflächen, eine Aufgabe aus der Lehre vom Erddruck.
Monatsber. Akad. Wiss. Berlin, 1903: 229-233.

BCBR-BER ** ROOMPOT 13 ** 78-08-01 **

APPENDIX 1.

INPUT:

GEOMETRY:

A = 11.0 M
B = 50.0 M
D = 25.0 M
LO = 10.0 M
TAL = 0.25

LOADINGS:

H = 116.6 MN
V = 254.0 MN
M = 2274.5 MNM
EXC = 0.0 M
VERH = 1.00

SOIL CHARACTERISTICS:

DELTA H = 33.00 DGR
FI H = 33.00 DGR
DELTA V = 29.00 DGR
SRT.MAS. = 0.01 MN/M3

CONE RESISTANCE:

QCD = 8.0 MN/M2
QC(2) = 9.0 MN/M2
QC(1) = 10.0 MN/M2
KH/QC = 0.1957 1/MHNAP(2) = 21.00 M
HNAP(1) = 27.50 M
HNAP(0) = 30.00 M

SPRING CONSTANT VALUES:

UH = 4.12 CM
UV = 8.09 CM
KV = 4.75 MN/M3

OUTPUT:

DISPLACEMENTS DUE TO DEAD LOAD:

INIT V-N.Z. = 4.28 CM
INIT V-O.S. = 4.28 CM
INIT ROTATIE = -0.00000

DISPLACEMENTS DUE TO HORIZONTAL LOAD:

H-TRANSL = 6.79 CM h
H-TPV MV = 8.39 CM h + ωa
V-N.Z. = -3.82 CM v
V-O.S. = 3.46 CM v + ωb
ROTATIE = 0.00146 ω

DISTRIBUTION HORIZONTAL LOAD:

H-VOORZIJDE = 24.11 MN FACE
H-ONDERZIJDE = 92.49 MN BOTTOM
MEEW. BREEDTE = 50.00 M b-b_o

MOBILIZED SHEAR STRESS:

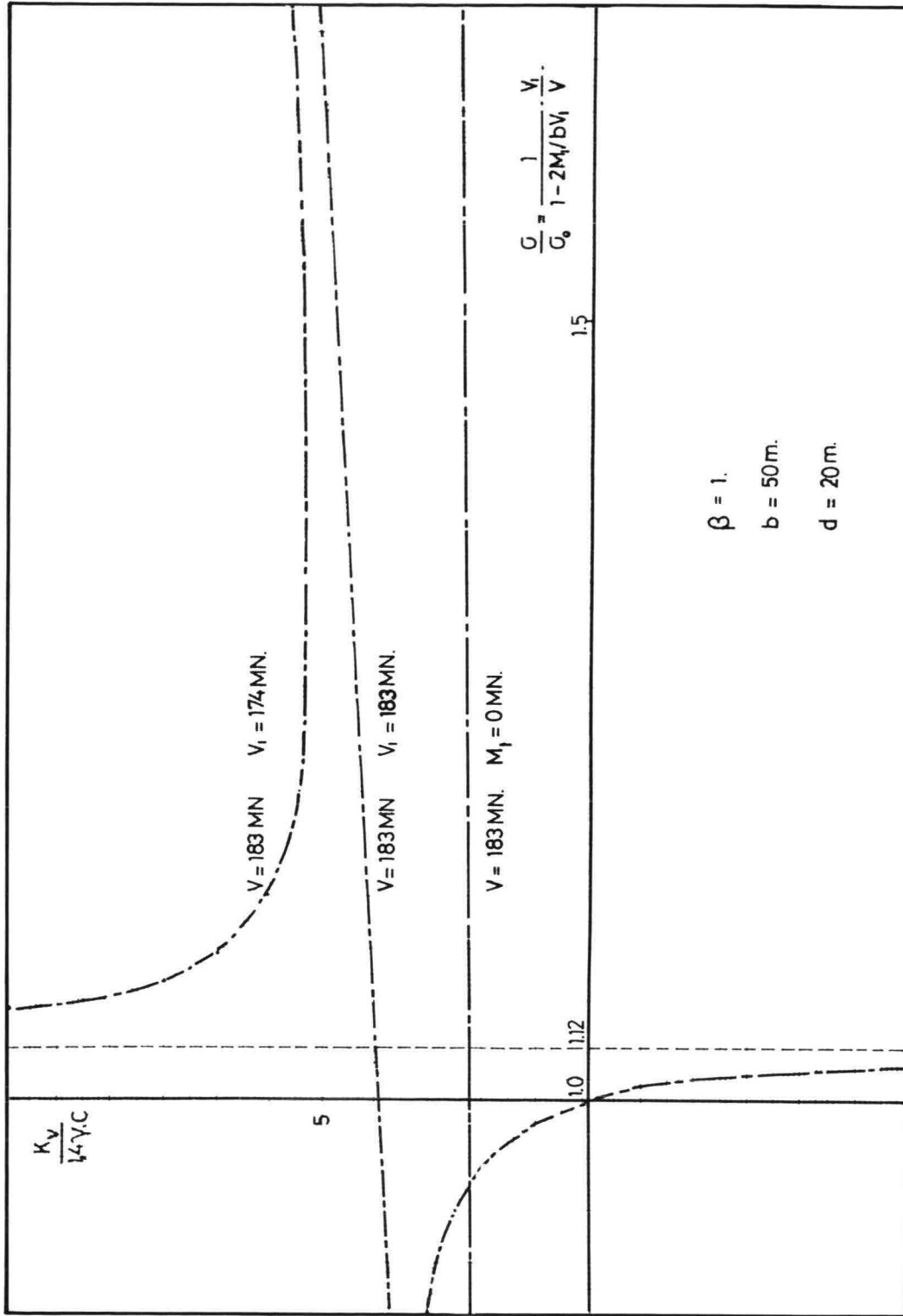
LANGS ACHTERZIJDE 72.89 % RIGHT FACE
LANGS VOORZIJDE 68.56 % LEFT FACE
LANGS ONDERZIJDE 68.55 % BOTTOM

HORIZONTAL FAILURE:

RESERVE H-VOORZ = 38.57 MN SPARE LOAD FACE
RESERVE H-ONDERZ = 42.43 MN SPARE LOAD BOTTOM
MAX H-VOORZ = 62.69 MN MAXIMUM LOAD FACE
MAX H-ONDERZ = 134.91 MN MAXIMUM LOAD BOTTOM

VEILIGH. FACTOR = 1.69 SAFETY FACTOR

**** OOSTERSCHELDE-VERSIE D.D. 78-02; LGM-DELFT ****



RELATIONSHIP OF VERTICAL SPRING CONSTANT- AND STRESS LEVEL.

APP. 2.

LOCATION I	cross section d * b (m ²)	height sill a (m)	LOADINGS			DISPLACEMENTS					HORIZONTAL LOAD DISTRIBUTION				FRICTION ANGLES				
			H (MN)	V (MN)	M (MNm)	h (cm)	h ^{+ua} gl. (cm)	V (cm)	V ^{+ub} (cm)	u ¹ x 10 ⁻³	superstorm		collapse		safety coeff.	structure bottom		faces	
										H faces %	H structure bottom %	H faces %	H structure bottom %		δ _v (°)	k _v (°)	δ _h (°)	φ _h (°)	
standard	25 x 50	8	95	208	1200	4.4	5.6	- 4.0	3.5	1.5	17.5	82.5	27.2	72.8	1.82	29.0	2.34	37	37
sill not compacted	25 x 50	8	95	208	1200	4.8	6.1	- 4.2	3.9	1.6	11.6	88.4	22	78	1.71	29	2.34	37	33
sill compacted	25 x 50	8	95	208	1200	4.0	5.0	- 3.7	3.0	1.4	23.9	76.1	31.3	68.7	1.91	29	2.34	40	40
height sill 2 m more	25 x 50	10	100	224.0	1395	4.1	5.6	- 4.0	3.5	1.5	20.1	79.9	32.8	67.2	2.03	29	2.65	36	36
height sill 2 m less	25 x 50	6	90	192	1005	4.8	5.7	- 3.8	3.4	1.4	14.6	85.4	20.2	79.8	1.02	29	2.15	38	38
slip layer	25 x 50	8	95	208	1200	5.9	7.0	- 3.9	3.2	1.4	23	77	31.5	68.5	1.53	24	2.34	37	37
no slip layer	25 x 50	8	95	208	1200	3.6	4.9	- 4.1	3.7	1.6	14.7	85.3	24.3	75.6	2.08	33	2.34	37	37
smooth face	25 x 50	8	95	208	1200	4.3	5.6	- 4.3	3.9	1.6	17.4	82.6	24.2	75.8	1.76	29	2.34	25	37
increased dead weight	25 x 50	8	95	248	1200	3.5	4.7	- 3.7	3.4	1.4	14.3	85.7	23.4	76.6	2.10	29	2.64	37	37

SYMPOSIUM ON FOUNDATION ASPECTS OF COASTAL STRUCTURES

EXCESS PORE PRESSURES AND DISPLACEMENTS DUE TO WAVE INDUCED LOADING
OF A CAISSON FOUNDATION AS PREDICTED BY PLASTICITY ANALYSIS

by:

Frans P. Smits, Research Engineer, Delft Soil Mechanics Laboratory
Delft, The Netherlands

SUMMARY

The paper deals with an analytical plasticity method to compute excess pore pressures and displacements for a caisson type foundation structure exposed to repeated wave load action, as it has been applied to predict Neeltje Jans test I. It allows for the capacity of the soil to improve its resistance against liquefaction by preshearing during the rise time of a major storm or during prior moderate storms.

The material model of a strain-hardening plastic soil which relates mobilized strength to shear strain is used. Constant mobilization of strength is assumed for the stress field to balance the external load and a simplified procedure is adopted to calculate increments of displacement from the accumulated shear strain and a flow rule.

The selection of relevant cyclic stress ratios, $\bar{\tau}_c/\bar{\sigma}'_0$ and $\bar{\tau}_a/\bar{\tau}_c$, for calculation of pore pressure generation by cyclic loading is outlined. A procedure is described to calculate the net excess pore pressures which allows for the decreasing liquefaction potential of the soil by periodical updating of the rate of pore pressure generation. Results of calculations are presented and discussed in relation to field measurement.

1. INTRODUCTION

In October 1975 a large scale liquefaction test has been carried out at the Neeltje Jans site in the Oosterschelde to investigate the feasibility of a gated caisson type storm-surge barrier (De Leeuw, 1976). A test caisson, 15 m wide and 27.7 m long, with a height of 10 m, has been placed in 7 metres deep water and cyclically loaded by hydraulic jacks. The submerged weight of the caisson was approximately 13.5 MN. The loading program for the horizontal forces consisted of 6 parcels of 300 load cycles each, with a cycle period of 3 seconds. Within each parcel all cycles had a constant cyclic amplitude, simulating the wave action, superimposed on a constant static force, simulating the loading from a tidal decay. Both the static and cyclic components of the horizontal force increased in every next parcel, following the loading program indicated in the table of figure 1.

The foundation soil consisted of medium-fine sand with a porosity of 41 - 42% and with average CPT-values of 10 MN/m² over the top 10 m depth.

The present paper reports a prediction of the above test by an analytical plasticity method.

The foundation problem with directional variable but periodical recurring boundary loading is difficult to solve primarily due to the lack of knowledge on the onloading-reloading characteristics of the soil. This has contributed to the experience with a special approach by which the response of the soil to the external load within cycles is separated from the macro-response to successive peak cycle conditions. In such an approach the primary outcome of the events within a cycle searched for is the change of effective stresses. As in general the effective stresses decrease, at least under loading conditions which give us cause for

concern, it is expected that the response in the large to a continuous peak cycle loading condition is similar as that to monotonic loading. However, adequate stress-strain relations will then be required which may have to be obtained from cyclic loading tests.

The method outlined in this paper follows the above approach, but no special attention is paid to stress-strain relations.

2. MATERIAL MODEL

The cohesionless foundation soil is considered to behave as a strain-hardening plastic material, such that the applied boundary load is balanced by an equilibrium stress field for which holds the stress limiting condition:

$$\frac{\tau}{\sigma'} \leq \sin \phi_m = f(\gamma) \quad \phi_m < \phi_f \quad (1)$$

where τ = maximum shear stress

σ' = effective mean normal stress

ϕ_m = mobilized angle of internal friction, which is a function of shear strain γ

ϕ_f = internal friction angle at failure

Boundary displacements are considered to be related to a plastic strain field which follows a flow rule:

$$\frac{\delta \epsilon}{\delta \gamma} = \sin \nu_m = g\left(\frac{\tau}{\sigma'}\right) \quad (2)$$

where $\delta \epsilon$ = volumetric strain increment

$\delta \gamma$ = shear strain increment

ν_m = mobilized angle of dilatancy

Elastic behaviour of the soil is disregarded except in as far as it effects the dissipation of pore pressures generated by cyclic loading (cf. Sec.5).

The above relations, such as shown in figure 2 and figure 3, suffice to calculate displacements for monotonic boundary loading under fully drained condition in which case $\tau/\sigma' = \sin \phi_m$. In a partially drained loading condition an additional pore fluid storage relation is required, e.g. $\nabla^2 u = \frac{\gamma w}{k} \frac{\partial \epsilon}{\partial t}$ in conjunction with plastic stress-strain behaviour.

In the present analysis where the pore pressure production by cyclic loading and the simultaneous dissipation are determined by an uncoupled calculation a slightly different equation for the pore pressure is used (cf. Sec. 5, Equ.(16)).

The displacements of the caisson, i.c. the cumulative lateral displacement in the direction of the static tidal force and the settlement, are calculated as those arising from a continuously acting maximum wave plus tidal force. At peak cycle loading the effective stress ratio or mobilized strength, τ/σ' , may increase gradually due to generation of pore pressures by successive cycles. This increasing effective stress ratio is accompanied by plastic volumetric strains, contraction or dilation, which in turn induce changes of pore pressure. For the present analysis it is assumed that these pore pressure changes are negligible as compared with those arising from shear stress reversals in successive cycles. In other words, the loading condition to estimate cumulative displacements is considered to be fully drained.

3. CALCULATION OF CUMULATIVE DISPLACEMENTS

A numerical procedure to solve a boundary value problem based on plastic stress-strain behaviour according to Equ. (1) and Equ. (2) is the so-called associated field method. It used the method of characteristics to calculate compatible stress and strain fields alternately, until at convergence the specified stress-strain relationship is satisfied in all elements. However, the method is extremely complicated, and although some progress is made we have as yet not been able to solve the caisson problem. Instead, a simplified analytical procedure for calculating the caisson displacements is developed, which is described below.

Consider the caisson problem as a strip footing of width B_o , placed upon the horizontal surface of a cohesionless foundation soil. It is subjected to an inclined eccentric load, composed of a vertical component F_V due to the caisson weight and a horizontal component F_H which equals the sum of a tidal force, F_{Ha} , and the maximum wave force in the direction of the tidal forces, F_{Hc} . The horizontal force acts above the foundation level thus causing a moment $M = M_a + M_c$ and a load eccentricity $e = \frac{M}{F_V}$.

Provided that the actual distribution of mobilized friction and excess pore pressure may be approximated by constant average values $\bar{\phi}_m$ and \bar{u} throughout the plastic stress field, the external load causes a critical equilibrium state in the soil expressed by the equation:

$$\bar{\sigma}_V = \frac{F_V}{A} = \frac{1}{2} \gamma' B N_\gamma - \bar{u} N_u \quad (3)$$

where B = effective foundation width, $B = B_o - 2e$

A = effective foundation area, $A = B \cdot L$

γ' = effective unit weight of the soil

$\bar{\sigma}_V$ = average total vertical stress

N_γ, N_u = bearing capacity factors

$$N_u = \frac{1 + \sin \phi \cos 2\Delta}{1 - \sin \phi} e^{(\pi - 2\Delta) \tan \phi} - 1 \quad (4)$$

$$N_\gamma \approx \frac{N_\gamma(+)}{N_\gamma(+)} \cdot \frac{N_\gamma(-)}{N_\gamma(+)} \quad (5)$$

$$\begin{aligned} N_\gamma(+)\approx & \frac{1 + \sin \phi \cos 2\Delta}{\cos^2 \phi} \cos(\mu \pm \Delta) \cdot \left| \frac{\sin \phi \cos \phi}{\cos(\mu \pm \Delta)} + \right. \\ & - \cos(\phi - \mu \pm \Delta) + \frac{\cos \phi_o}{\cos \phi} \cos(\phi_o - \mu \pm \Delta) + \\ & \left. \left(\frac{\cos \phi_o}{\cos \phi} \sin(\phi_o - \mu) + \cos \mu \right) e^{3\left(\frac{\pi}{2} \pm \Delta\right) \tan \phi} \right| \quad (6) \end{aligned}$$

where $\phi = \bar{\phi}_m$

$2\mu = \frac{\pi}{2} - \bar{\phi}_m$

$\phi_o = \arctan(3 \tan \bar{\phi}_m)$

$2\Delta = \delta + \arcsin\left(\frac{\sin \delta}{\sin \phi_m}\right)$

$\tan \delta = \frac{F_H}{F_V - \bar{u}BL}$, angle reflecting boundary load inclination

Equ. (5) is an approximate solution for N_γ , which has been obtained by integrating one of the characteristic equations based on the characteristics field for a weightless soil (Smits, 1973).

Equ. (3) may now be used to calculate the mobilized friction angle \bar{v}_m for increasing values of the external load and of the excess pore pressure generated by cyclic loading. A pore pressure $\bar{u} > 0$ cannot exist close to the free boundary aside the caisson without surcharge, however, a deviation from $\bar{u} = \text{constant}$ in this low stress level zone has only a minor effect on the value of the mobilized friction angle.

Supposed that a constant average value of the mobilized angle of dilatancy, \bar{v}_m , may be assumed at least below the center and the edges of the caisson, the direction of increments of boundary displacement as established from the plastic velocity field is expressed by the equation:

$$\Delta S_V = \Delta S_H \cdot \tan(\kappa - \Delta) \quad (7)$$

where ΔS_V and ΔS_H = increments of vertical and horizontal displacement

$$2\kappa = \frac{\pi}{2} - \bar{v}_m$$

The values of \bar{v}_m and $\bar{\phi}_m$ are linked by Eqs. (1) and (2).

To estimate the magnitude of incremental displacements it is now hypothesized that an average shear strain $\bar{\gamma}$ may be defined as if simple shear like deformation were taking place over the depth of the plastic stress zone $d = B \cos(\Delta + \mu) \exp((\frac{\pi}{2} - \Delta - \mu) \tan \phi_m)$. Then increments of horizontal displacements are expressed:

$$\Delta S_H = B \Delta \bar{\gamma} \cos(\Delta + \mu) \exp((\frac{\pi}{2} - \Delta - \mu) \tan \phi_m) \quad (8)$$

and ΔS_V is obtained by substituting ΔS_H in Equ. (7).

The cumulative displacements in successive load parcels have been calculated as outlined below.

Denote the maximum horizontal load in previous parcels by F_{HO} , average values of excess pore pressure, shear strain and mobilized friction angle at the end of the last parcel respectively by \bar{u}_O , $\bar{\gamma}_O$ and $\bar{\phi}_{mO}$, the maximum horizontal load in the present parcel by $F_H (= F_{Ha} + F_{Hc})$ and the maximum average excess pore pressure in the present parcel by $\bar{u}(\text{max})$. The increase of horizontal load, $F_H - F_{HO}$, is divided into a number of small load increments ΔF_H .

First $\bar{\phi}_m$ is determined by means of Equ. (3) for external loading by F_V and $F_{HO} + \Delta F_H$ with $\bar{u} = \bar{u}_O$. Next $\bar{\gamma}$ and \bar{v}_m are selected from Eqs. (1) and (2) as depicted by figures 2 and 3. Finally displacement increments ΔS_H and ΔS_V are calculated from Eqs. (7) and (8) with $\Delta \bar{\gamma} = \bar{\gamma} - \bar{\gamma}_O$. This procedure is repeated for successive load

steps $F_{HO} + n \cdot \Delta F_H$ with $\Delta \bar{\gamma}(n) = \bar{\gamma} - \bar{\gamma}_O - \sum_{i=1}^{n-1} \Delta \bar{\gamma}(i)$ until the maximum value F_H is

reached. If \bar{u}_O is smaller than the maximum average excess pore pressure during the previous parcel, the mobilized friction $\bar{\phi}_m$ calculated in the first load steps will remain smaller than $\bar{\phi}_{mO}$. In this case the displacement increments remain zero until $\bar{\phi}_m > \bar{\phi}_{mO}$ is reached. The cumulative displacements obtained from the above calculations may be considered to occur immediately or in a short time interval after the rise of the tidal force and the wave force in the new parcel.

Next the effect of the rise of pore pressures due to cyclic loading is evaluated. Therefore, the maximum increase within the parcel, $\bar{u}(\text{max}) - \bar{u}_O$, is divided into

a number of small increments $\Delta\bar{u}$. Now $\bar{\phi}_m$ is determined by Equ. (3) under constant external loading by F_V and F_H ($= F_{Ha} + F_{Hc}$) for successive excess pore pressures $\bar{u} = \bar{u}_0 + n \cdot \Delta\bar{u}$ until the maximum value $\bar{u}(\max)$ is reached. Displacement increments are calculated again as described previously for increasing external load. Increments $\Delta\bar{u}$ are selected so as to yield approximately constant increments of shear strain. The cumulative displacements due to the excess pore pressure advance in time simultaneously with the rise of the pore pressure as it is calculated in Sec. 5 of this report. If the pore pressure reaches a maximum within the parcel displacements tend to become stationary afterwards.

The relation $\sin v_m = g\left(\frac{\tau}{\sigma'}\right)$ as shown by figure 3 has been obtained from drained triaxial tests with octahedral stress constant at initial porosity of the sand $n_0 = 41.5\%$. The relation $\sin \phi_m = f(\gamma)$ as shown by figure 2 has been obtained from simple shear tests to cope with the somewhat heuristic determination of shear strain and the displacements resulting from it (Equ. (8)).

4. SELECTION OF CYCLIC STRESS RATIOS

To establish excess pore pressures by cyclic loading, which is the subject of the next section, first the relevant stresses have to be determined. Among the most important stress parameters are the cyclic shear stress amplitude, τ_c , the average shear stress level, τ_a , and the initial effective mean normal stress, σ'_0 . Pore pressure generation may effectively be expressed as a function of the cyclic stress ratio, τ_c/σ'_0 , and the ratio of average versus cyclic shear stress, τ_a/τ_c .

Although the procedure outlined below allows to define these stress ratios throughout the plastic stress field, equivalent average values are required to calculate pore pressure generation by the analytical procedure described in Sec. 5. As the effect of cyclic stresses on the net excess pore pressure increases with increasing distance from the stress free boundary aside the caisson, the stress variations in the central plastic zone below the caisson are likely to be most important. The cyclic stress ratio τ_c/σ'_0 is considered to be the primary stress parameter. For individual elements both the maximum shear stress and the direction of the planes on which it acts vary within a load cycle. This causes a problem for selection of the significant cyclic shear stress amplitude τ_c . It is recommended by the author that τ_c is selected as half the total change of shear stress on the plane where this change reaches a maximum. The shear stresses are to be calculated in undrained loading.

The average shear stress level τ_a may be selected as the shear stress on the same plane due to drained loading by the mid-cycle value of the external load. In the present example this is the load by the weight of the caisson and by the tidal force. In general the average shear stress τ_a thus calculated is somewhat different from the average value of the above undrained loading process. However, as the average shear stress level τ_a is a secondary parameter the cyclic loading may well be approximated as symmetric around τ_a .

The effective mean normal stress σ'_0 at the beginning of a new parcel may be determined from drained loading under the action of the caisson weight and the tidal force as for calculation of τ_a , however, with excess pore pressures due to cyclic loading in previous parcels fully dissipated.

Loading within a load cycle may be considered to occur under virtually undrained condition. Each soil element is capable to resist a maximum shear stress $\tau = \tau_f$ which is a function of the effective mean normal stress σ' resulting from previous cycles ($\tau_f = \sigma' \sin \phi_f$ in case of a non-dilating soil). The stress distribution

in the soil becomes quite similar to that for a cohesive soil, however, with variable undrained shear strength c_u due to the actual distribution of effective mean normal stress σ' . If only partial loading to failure occurs a mobilized strength c_m may be defined which for a constant shear strength material is expressed approximately:

$$\bar{c}_m = \frac{\bar{\sigma}_V / N_C}{1 - \frac{|\bar{\tau}_H|}{\bar{\sigma}_V} \frac{N_C}{4}} \quad (9)$$

where: $N_C = \pi + 2$

$$\bar{\sigma}_V = F_V / BL, \quad \bar{\tau}_H = F_H / BL$$

Let average shear stresses, $\bar{\tau}_{H1}$ and $\bar{\tau}_{H2}$, at peak-cycle loading be defined as:

$$\bar{\tau}_{H1} = \frac{F_{Ha} + F_{Hc}}{BL}, \quad \bar{\tau}_{H2} = \frac{F_{Ha} - F_{Hc}}{BL} \quad (10)$$

and corresponding values of mobilized strength, \bar{c}_{m1} and \bar{c}_{m2} , according to Equ. (9). Also define angles ϵ_1 and ϵ_2 by:

$$\sin \epsilon_1 = \frac{\bar{\tau}_{H1}}{\bar{c}_{m1}}, \quad \sin \epsilon_2 = \frac{\bar{\tau}_{H2}}{\bar{c}_{m2}} \quad (11)$$

and an angle θ by:

$$\tan \theta = \frac{\sqrt{\bar{c}_{m1}^2 - \bar{\tau}_{H1}^2} - \sqrt{\bar{c}_{m2}^2 - \bar{\tau}_{H2}^2}}{\bar{\tau}_{H1} - \bar{\tau}_{H2}} \quad (12)$$

where θ refers to the direction of maximum change of shear stress. Then a cyclic shear stress amplitude $\bar{\tau}_c$, is calculated from the equation:

$$2\bar{\tau}_c = \bar{c}_{m1} \sin(\epsilon_1 + \theta) - \bar{c}_{m2} \sin(\epsilon_2 + \theta) \quad (13)$$

(In the case of symmetric loading with no tidal force, $F_H = \pm F_{Hc}$, θ becomes zero and $\bar{\tau}_c = \bar{\tau}_H$).

For a uniform cohesive soil $\bar{\tau}_c$ as calculated by Equ. (13) would apply to a wedge-shaped central zone below the caisson, to the extent as the plastic stress fields due to the peak-cycle loading conditions overlap. In a first approximation it may be assumed that the effective stress distribution in sand does not cause a non-uniform strength mobilization in partial loading to failure, and that the cyclic shear stress amplitude $\bar{\tau}_c$ is fairly uniform in the central zone.

The average effective mean normal stress $\bar{\sigma}'_0$ at base level below the caisson is determined for each parcel by the equation:

$$\bar{\sigma}'_0 = \frac{\bar{\sigma}_V}{1 + \sin \phi_m \cos 2\Delta} \quad (14)$$

where ϕ_m and Δ are calculated by Eqs. (3), (5) and (6) with $\bar{u} = 0$ and $\tan \delta = \frac{F_{Ha}}{F_V}$.

The average shear stress $\bar{\tau}_a$ at base level below the caisson and on the plane with maximum change of shear stress within a cycle is determined by the equation:

$$\bar{\tau}_a = \frac{\sin \phi_m \sin(2\Delta + \theta)}{1 + \sin \phi_m \cos 2\Delta} (\bar{\sigma}_V - \bar{u}) \quad (15)$$

where θ is calculated by Equ. (12) and ϕ_m and Δ by Equ. (3), (4), (5) and (6), with \bar{u} the instantaneous average excess pore pressure generated by previous cycles and with $\tan \delta = \frac{F_{Ha}}{F_V - \bar{u}BL}$.

In the present calculations the average shear stress $\bar{\tau}_a$ has been kept constant within a parcel and has been determined with $\bar{u} = \bar{u}_O$, the average excess pore pressure at the end of the previous parcel.

In first approximation it may be assumed that the average shear stress and the effective mean normal stress increase with depth below base level with the ratios $(\bar{\sigma}_V - \bar{u} + \gamma z)/(\bar{\sigma}_V - \bar{u})$ and $(\bar{\sigma}_V + \gamma z)/\bar{\sigma}_V$ respectively.

5. DETERMINATION OF EXCESS PORE PRESSURES

Within each parcel a rate of pore pressure generation \dot{w} is calculated as if loading by individual cycles was undrained and as if this rate was a constant. Next the net excess pore pressure is calculated by allowing simultaneous dissipation, which is achieved by solving a pore fluid storage equation that contains the rate of generation as a pumping term:

$$\nabla^2 u = \frac{\gamma w}{kD} \left(\frac{\partial u}{\partial t} - \dot{w} \right) \quad (16)$$

This generation-consolidation process is allowed to continue over a time interval Δt of 10 cycle periods, after which the rate of generation \dot{w} is adjusted and the process is continued for the next time interval with new initial conditions.

The rate of pore pressure generation \dot{w} is calculated by means of the equation:

$$\dot{w} = \sigma'_O f \cdot \beta \left(\frac{\tau_c}{\sigma'_O}, \frac{\tau_a}{\tau_c}, n_O, n_O - \Delta n \right) \quad (17)$$

where f = frequency of wave cycles

$$\beta = \frac{\Delta u}{\sigma'_O \Delta n} = \text{normalized pore pressure generation per cycle}$$

n_O = initial porosity

Δn = change of porosity in cyclic loading

In the case of storm loading with varying wave heights and wave periods \dot{w} may be calculated by:

$$\dot{w} = \frac{\sigma'_O}{t} \sum \beta_i N_i \quad (18)$$

where t = duration of the storm

The pore pressure parameter β is obtained from undrained cyclic laboratory tests. For the present analysis triaxial test data have been used with the re-

sult shown by figure 4 for Neeltje Jans sand of $d_{50} = 160 \mu$: β versus $\frac{\tau_c}{\sigma'_0}$ relations for $\frac{\tau_a}{\tau_c} = 0.8$ at initial porosity $n_0 = 41.5\%$ and changes of

porosity $\Delta n = 0.1 - 0.3\%$. These data have been obtained from undrained tests with intermittent drainage stages.

To estimate the net excess pore pressure it has been assumed that pore pressure is produced at a constant rate \dot{w} over the extent of a rectangular cilinder, whose cross sectional area equals the caisson base area $L \cdot B_0$, and that dissipation occurs by horizontal drainage only with a boundary condition of zero excess pressure at the circumferential surface of the rectangular cilinder. Solving Equ. (16) yields for the average excess pore pressure:

$$\bar{u} = \bar{u}_\infty \cdot (1 - \exp(-At)), \quad \text{if } \bar{u}_0 = 0 \quad (19)$$

$$\text{with } A = \frac{\pi^2 kD}{\gamma_w} \cdot \frac{B_0^2 + L^2}{B_0^2 L^2} \quad (20)$$

\bar{u}_∞ = average steady state pressure

$$\bar{u}_\infty = \frac{\gamma_w}{kD} \dot{w} \left(\frac{2}{\pi}\right)^6 \cdot \frac{B_0^2 L^2}{B_0^2 + L^2} \quad (21)$$

k = horizontal permeability

D = constrained modulus of recompression, $D = K + \frac{4}{3} G$

Horizontal drainage has been assumed as the permeability in lateral direction may be 5 to 10 times larger than in vertical direction due to the formation process of the soil. The permeability has been measured in situ by a mono-source constant head test. The average value measured, which is assumed to represent approximately the horizontal permeability, is $k = 5 \cdot 10^{-5}$ m/s.

The constrained modulus of recompression has been obtained from K_0 -consolidation test with preloading to $\sigma'_V = 100$ kN/m², which yielded an average value $D = 17.5$ MN/m² for Neeltje Jans sand at initial porosity $n_0 = 41.5\%$. It might be more appropriate to determine a stiffness modulus in the drainage stages of the undrained cyclic tests.

Actually the rate of pore pressure generation \dot{w} does not remain constant during the progress of storm loading. The soil improves its resistance against liquefaction with number of cycles. This is the so-called preshearing effect which is discussed in a contribution to this symposium by Smits, Andersen and Gudehus. The rate of generation \dot{w} also changes due to redistribution of stresses caused by the build-up of pore pressures.

The effect of preshearing has been taken into account in the present analysis by selecting new β values after each time interval Δt according to the porosity reduction caused by the consolidation process. The rate of average change of porosity is expressed by:

$$\frac{d\bar{n}}{dt} = 4(n - 1) \frac{\dot{w}}{D} \left(\frac{2}{\pi}\right)^4 (1 - \exp(-At)) \quad (22)$$

The buildup of pore pressure in time within each parcel has been determined by accumulating the increments Δu over the duration Δt of each time 10 cycles, calculated as:

$$\Delta \bar{u} \Big|_{t_N \rightarrow t_{N+10}} = (\bar{u}_\infty(t_N) - \bar{u}(t_N)) \cdot (1 - \exp(-A \Delta t)) \quad (23)$$

where $\bar{u}(t_N)$ = the accumulated pore pressure at time t_N or at the end of the previous parcel if $N = 0$

$\bar{u}_\infty(t_N)$ = the steady state pressure if \dot{w} would remain constant on its updated value at time t_N , as calculated by Equ. (21)

The change of porosity during each 10 cycles has been calculated as:

$$\Delta \bar{n} \Big|_{t_N \rightarrow t_{N+10}} = (\bar{n}(t_N) - 1) \frac{4}{D} \dot{w}(t_N) \cdot \left(\frac{2}{\pi}\right)^4 \cdot \left(\Delta t - \frac{\Delta \bar{u}}{A \cdot \bar{u}_\infty(t_N)}\right) \quad (24)$$

where $\bar{n}(t_N)$ = instantaneous porosity at time t_N

$\dot{w}(t_N)$ = the rate of pore pressure generation according to the updated value of β at time t_N

$\Delta \bar{u}$ and $\bar{u}_\infty(t_N)$ as in Equ. (23).

6. RESULTS OF CALCULATIONS

The following stress ratios have been calculated by the procedure described in Sec. 4:

Parcel	$\bar{\tau}_c / \bar{\sigma}'_o$	$\bar{\tau}_a / \bar{\tau}_c$	
0	0.02	1.6	
1	0.04	1.05	
2	0.08	0.80	
3	0.11	0.73	$(\bar{u}_o = 0.5 \text{ kN/m}^2)$
4	0.15	0.68	$(\bar{u}_o = 2.8 \text{ kN/m}^2)$

These are average values at base level below the caisson. Based on the above cyclic stress ratios $\bar{\tau}_c / \bar{\sigma}'_o$ and on a ratio of average versus cyclic shear stress $\bar{\tau}_a / \bar{\tau}_c = 0.8$ the buildup of average excess pore pressure in time has been calculated according to the procedure described in Sec. 5. The result is shown in figure 5. Pore pressures start to develop after parcel 2. In parcels 3 and 4 the excess pore pressure decreases after having reached a maximum at about 130 and 80 cycles respectively. This is due to the decreasing response to shear stress reversals with number of cycles. The calculated decrease of porosity $\Delta \bar{n}$ and the corresponding decrease of β is shown in figure 6 in plots of β versus $\Delta \bar{n}$ for successive cyclic stress ratios.

Once having established the change of excess pore pressure in time within each parcel, the caisson displacements have been calculated by the procedure described in Sec. 3. Figures 7 and 8 show the horizontal and vertical displacements of the caisson centre as predicted by the analysis (P) and as actually measured (M).

7. DISCUSSION

Comparison of measured and predicted displacements shows that the agreement is very close for the horizontal displacement, but less for the settlement.

According to figure 5 excess pore pressures start to become significant in parcel 3, which is reflected by the increased rate of predicted displacements and very

likely also by the increased rate of measured displacements shown by figures 7 and 8. Once the maximum excess pore pressure has been reached in parcels 3 and 4, the predicted lateral displacement starts to slow down. It may be that this effect is also observed with the actual horizontal displacements in parcel 4 and with the actual settlements in parcels 2 and 3.

The dissipation of excess pore pressure tends to add some cyclic loading settlement in parcels 3 and 4, which has been neglected in the settlement calculations. Nevertheless, this settlement contribution is insufficient to explain the difference between measured and predicted values in parcels 3 and 4.

Due to the small weight of the caisson the cyclic stress level $\bar{\tau}_c/\bar{\sigma}'_0$ tends to decrease rapidly with depth: at 1 m depth it is approximately 75% of its value at the caisson base level. Accordingly the generation of pore pressure in parcels 3 and 4 at 1 m depth is about the same as in parcels 2 and 3 at caisson base level. Equalization of these generated pressures is opposed by a small vertical compared to horizontal permeability. Consequently, the average excess pore pressure at 1 m depth might be about 3.5 kN/m² in parcel 4, which in order of magnitude corresponds to the measured value at that depth. Pore pressures at base level have not been measured.

As the average excess pore pressure at base level in the calculations has been assumed as the average value throughout the plastic zone, the calculations tend to over-estimate the displacements in view of the actual strong gradient of pore pressure in vertical direction.

On the other hand, with high pore pressures the plastic stress zone becomes very shallow which limits again the over-estimation.

The plasticity method outlined in this paper uses very much the same equations and calculating procedures as for a stability analysis of a wave loading problem. The calculation process terminates with loss of stability as soon as the strains are insufficiently controlled by the hardening relation. A conventional stability analysis based on the concepts of plasticity and including the evaluation of the cyclic loading action would have predicted loss of stability in parcel 4, where the excess pore pressures and the horizontal displacement become large according to the present calculations. This relation to a stability calculation process may be considered as a strong argument in favour of the method.

On the other hand, it suffers very much under the condition that stresses, strains and strength parameters have to be averaged for the analytical calculations, which in the first place affects the determination of the displacements but to a less extent also the calculation of pore pressures. Determination of excess pore pressures can easily be improved by numerical stress field and consolidation calculations. However, to calculate strains and displacements associated with stresses will always remain complicated by the method of characteristics.

REFERENCES

- De Leeuw, E.H., 1976, Results of large scale liquefaction tests, International Conference on Behaviour of Offshore Structures, Boss'76, Trondheim, Vol. II, pp. 65-84.
- Smits, F.P., 1973, Boundary value problems in soil mechanics as related to soil cutting, Delft.

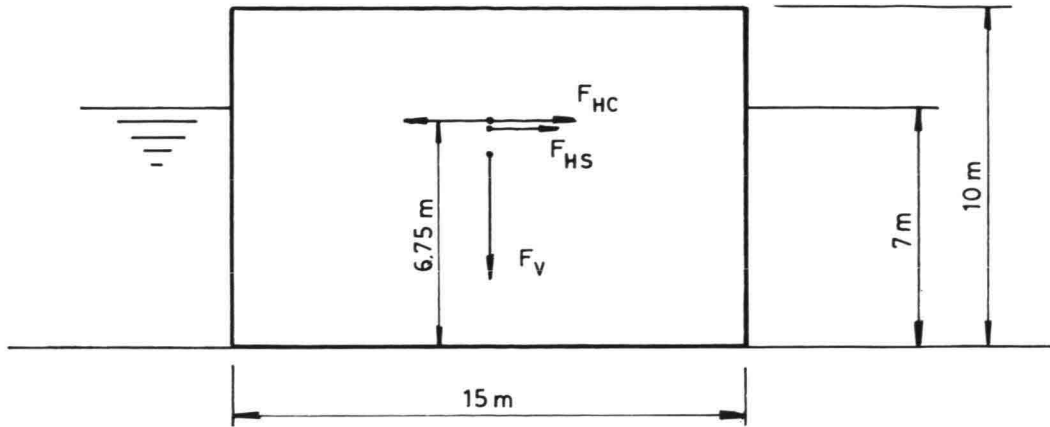


Fig. 1: Neeltje Jans caisson test

Storm loading scheme

Parcel number	Tidal force F_{HS} [kN]	Wave force F_{HC} [kN]	Duration [min]
0	200	+ 250	15
1	400	+ 500	15
2	800	+ 1000	15
3	1200	+ 1500	15
4	1600	+ 2000	15
5	2000	+ 2500	until stationary performance or failure

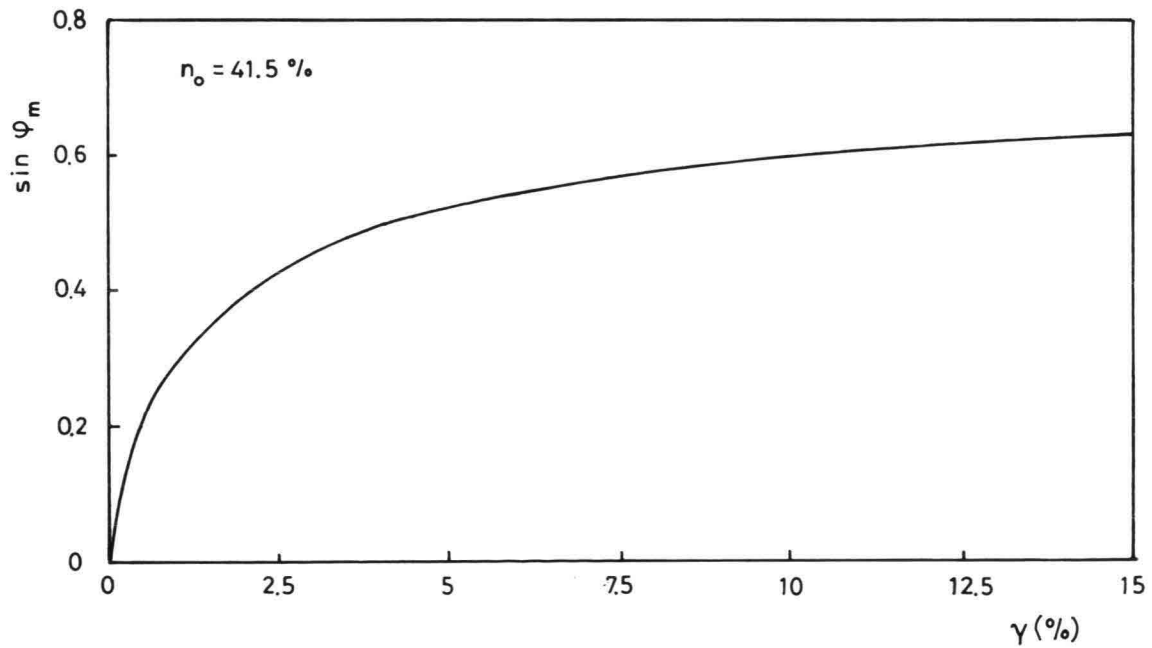


Fig. 2: Mobilized strength as a function of shear strain.

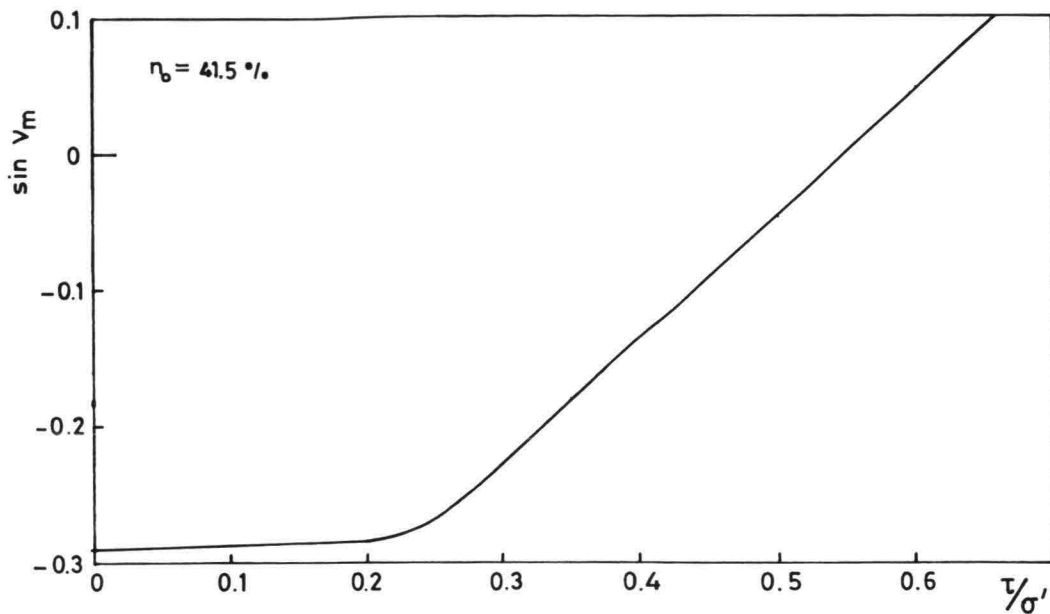


Fig. 3: Mobilized angle of dilatancy as a function of effective stress ratio.

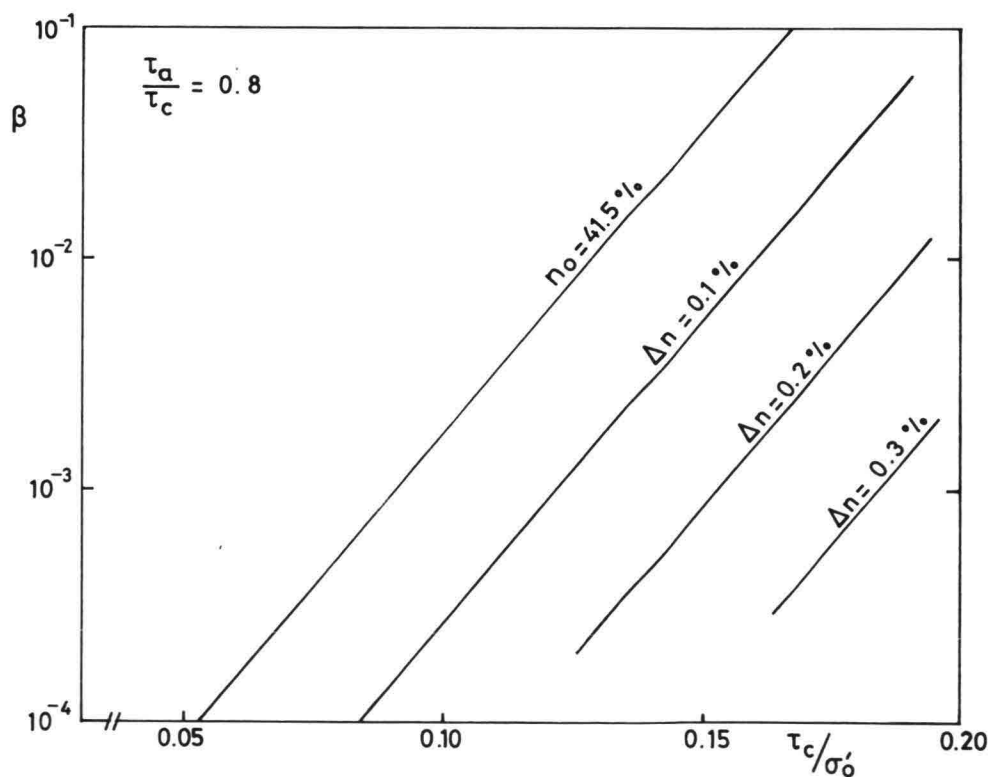


Fig. 4: Pore pressure generation per cyclic versus cyclic shear stress ratio for various degrees of porosity reduction.

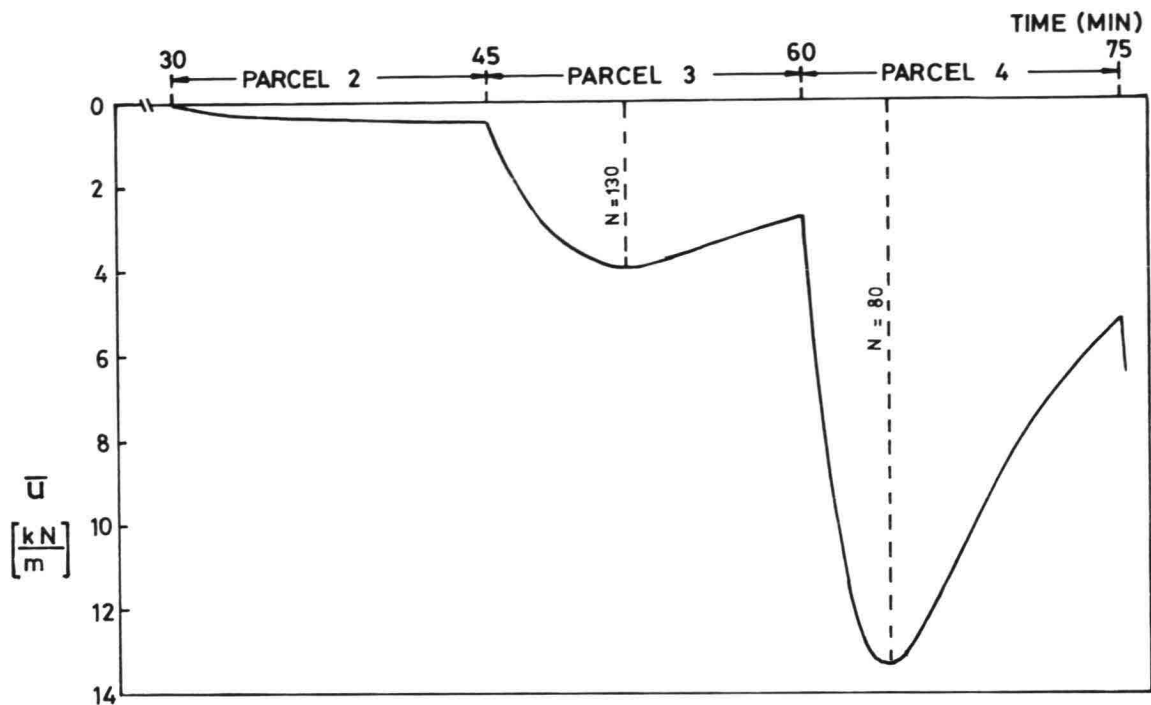


Fig. 5: Calculated average excess pore pressures.

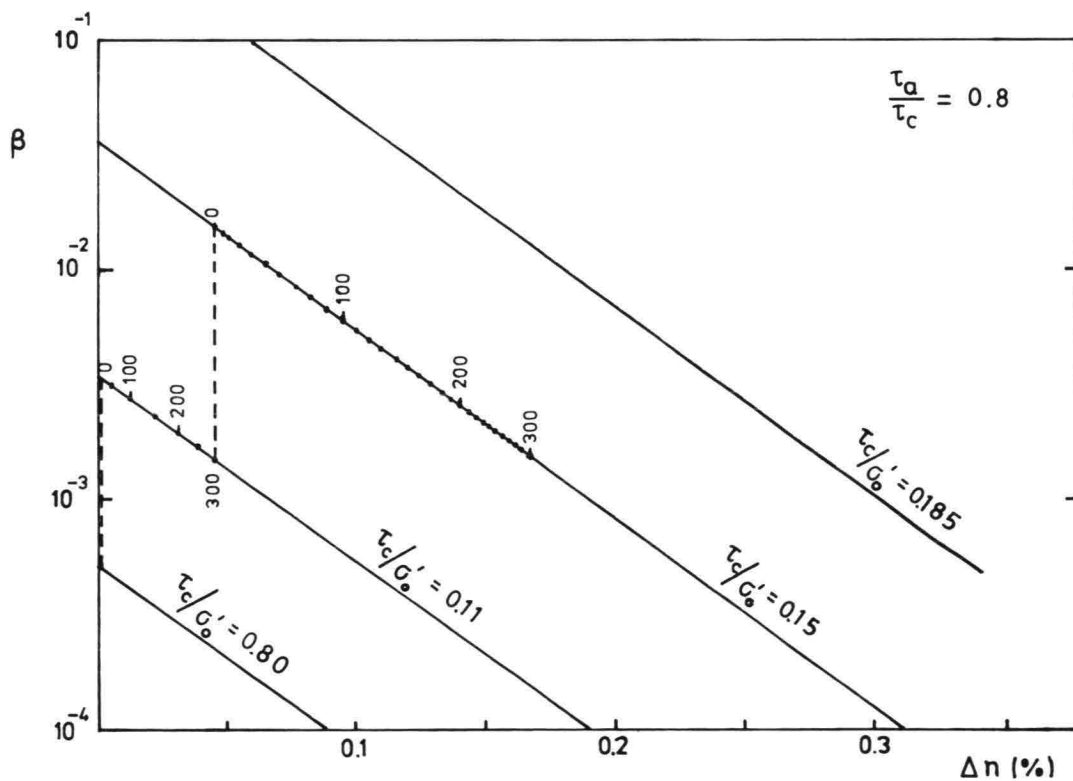


Fig. 6: Calculated changes of porosity and corresponding β -values.

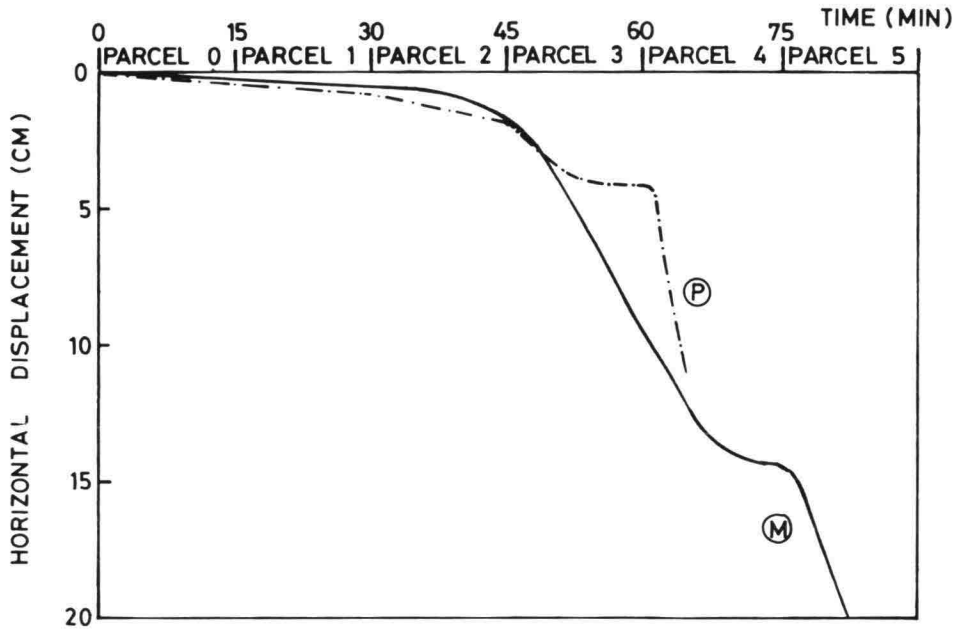


Fig. 7: Calculated (P) and measured (M) horizontal displacement.

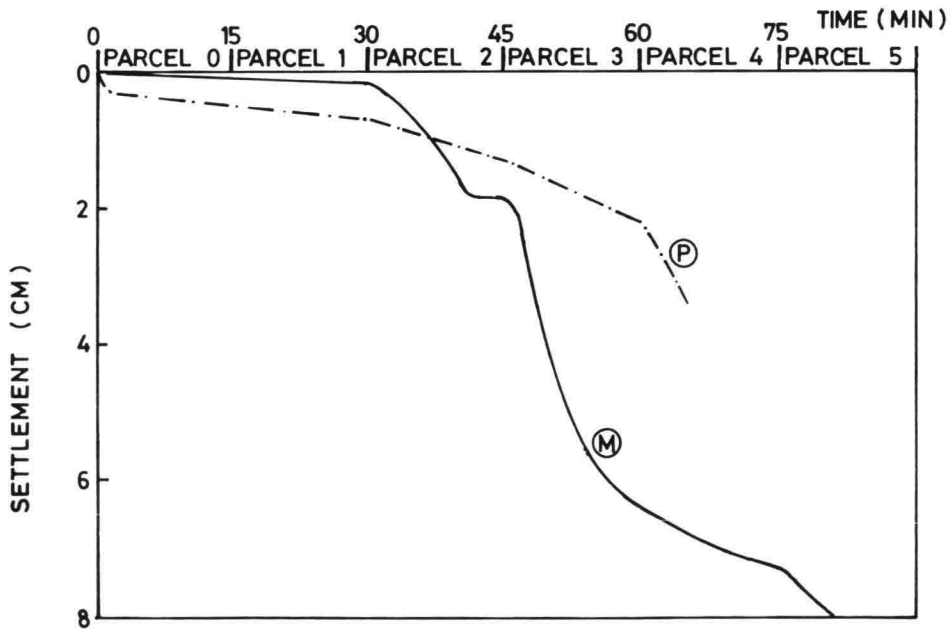


Fig. 8: Calculated (P) and measured (M) settlement.

